

Decant Calculations and Groundwater – Surface Water Interaction in an Opencast Coal Mining Environment

By

Johannes Lodewiekus du Plessis

THESIS

Submitted in fulfilment of the requirement for the degree of

Master of Science

Faculty of Natural and Agricultural Science

Institute for Groundwater Studies, Bloemfontein

University of the Free State

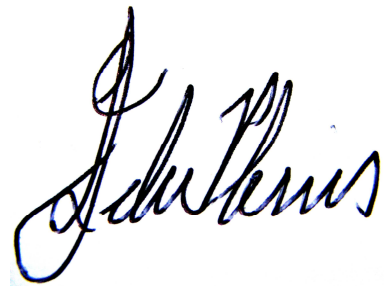
November 2010

Supervisor:

Dr I. Dennis

Declaration of Own Words

I, Johannes Lodewiekus du Plessis, hereby declare that this dissertation submitted for the degree Magister Scientiae in the Faculty of Science, Institute for Groundwater Studies, University of the Free State, Bloemfontein, South Africa, is my own work and have not been submitted to any other institution of higher education. I further declare that all sources cited are indicated in references.



J.L du Plessis

2010/11/30

Key Words

Acid Mine Drainage

Analytical Calculations

Correlation

Decant

Decant Volumes

Groundwater

Numerical Groundwater Flow Model

Time-To-Decant

Acknowledgements

I would like to use this opportunity to thank everybody who has helped me in the completion of this thesis. It would not have been possible without your assistance. The following people deserve mentioning:

- My supervisor, doctor Ingrid Dennis for your expert guidance throughout the past three years,
- Doctor Danie Vermeulen for all your time and guidance,
- Pierre Coetzer of Delta Mining Consolidated for providing me with the data necessary for the completion of this thesis,
- Delta Mining Consolidated for giving me permission to use your data,
- Gerhard Steenekamp for giving me the opportunity to further my studies and for your undivided support and guidance,
- My family, and in particular my wife for your loving support.

I want to thank God Almighty, as it is His grace which has guided me to where I am today.

Contents

Declaration of Own Words	I
Key Words.....	II
Acknowledgements	III
1. Introduction	1
1.1 Background.....	1
1.2 Objectives	4
1.3 Structure of Thesis.....	4
2. Methodology	6
2.1 Data gathering.....	6
2.2 Data processing	6
2.3 Aquifer testing	7
2.4 Construction of the numerical groundwater flow model.....	8
2.5 Decant calculations	9
2.5.1 Numerical groundwater flow model	9
2.5.2 Mathematical volume calculations	11
2.6 Groundwater – surface water interaction	12
2.6.1 Numerical groundwater flow model	12
2.6.2 Analytical calculations.....	12
3. Literature Review	14
3.1 Groundwater recharge	14
3.2 Groundwater – surface water interaction	17
3.3 Backfill material porosity	21
3.4 Review of geohydrological case studies	23
4. General Description of the Study Area.....	28
4.1 Geology.....	28
4.2 Climate.....	34

4.3	Surface topography and drainage	34
4.4	Land use, vegetation, and soil types	36
5.	General Description of the Geohydrology	38
5.1	Hydrocensus Results	38
5.2	Depth to Water Level and Flow Gradients/Velocities/Directions	41
5.3	Aquifer Types, Thickness, and Yields	46
5.4	Aquifer Parameters	48
5.5	Aquifer Delineation and Recharge	50
5.6	Generalised Conceptual Model	52
5.7	Groundwater Quality Evaluation.....	57
6.	Numerical Decant Calculations and Groundwater Discharge	71
6.1	Pre-mining numerical groundwater flow model	71
6.2	Post-closure numerical groundwater flow model.....	77
7.	Analytical Decant Calculations and Groundwater Discharge	98
8.	Discussion.....	103
8.1	Numerical groundwater flow model results	103
8.1.1	Pre-mining numerical groundwater flow model results	104
8.1.2	Post-closure numerical groundwater flow model results.....	104
8.2	Analytical and volume calculations results	116
8.3	Numerical and analytical correlation	118
9.	Conclusions	133
10.	References	136
11.	Appendix A: Monitoring Boreholes Logs.....	141
12.	Appendix B: Pump test Sheets.....	155
13.	Appendix C: Hydrocensus Report	175
14.	Summary	195
15.	Opsomming	197

List of Figures

Figure 1.1-1:	Site location	3
Figure 3.3-1:	Sorting of sediments	21
Figure 4.1-1:	Simplified geological map of the study area	28
Figure 4.1-2:	Extent of Karoo Groups and Formations	29
Figure 4.1-3:	Cross sections of mine lease area	30
Figure 4.1-4:	Floor contours of the base of coal seam 2	31
Figure 4.3-1:	Surface contour map of study area	35
Figure 5.1-1:	Positions of hydrocensus boreholes	39
Figure 5.2-1:	Thematic water level map of the study area	42
Figure 5.2-2:	Water level elevation vs. borehole elevation	43
Figure 5.2-3:	Limitation of Bayesian interpolation	43
Figure 5.2-4:	Bayesian interpolated water level elevation contour map	45
Figure 5.5-1:	Aquifer delineation	51
Figure 5.6-1:	Conceptual model of study area	56
Figure 5.7-1:	Layout of the EDD	61
Figure 5.7-2:	Regional and site specific borehole distribution	65
Figure 5.7-3:	Thematic TDS concentration map of the mine lease area	66
Figure 5.7-4:	Expanded Durov diagram of site specific monitoring boreholes	68
Figure 5.7-5:	Stiff diagrams of site specific groundwater qualities	69
Figure 5.7-6:	Stiff diagrams of site specific groundwater qualities	69
Figure 6.1-1:	Model grid with river nodes and no-flow boundaries	71
Figure 6.1-2:	Model parameters and parameter values	72
Figure 6.1-3:	Numerical groundwater flow model calibration	74
Figure 6.1-4:	Water budget zones	76
Figure 6.2-1:	Concept of decanting groundwater	79
Figure 6.2-2:	Opencast pits and decant positions	80
Figure 6.2-3:	Maximum groundwater drawdown at mine closure	81
Figure 6.2-4:	Scenario 1 model simulated water level elevation-time graph	89
Figure 6.2-5:	Scenario 2 model simulated water level elevation-time graph	90
Figure 6.2-6:	Scenario 3 model simulated water level elevation-time graph	91
Figure 6.2-7:	Scenario 4 model simulated water level elevation-time graph	92

Figure 6.2-8:	Scenario 5 model simulated water level elevation-time graph	93
Figure 6.2-9:	Scenario 6 model simulated water level elevation-time graph	94
Figure 6.2-10:	Scenario 7 model simulated water level elevation-time graph	95
Figure 6.2-11:	Scenario 8 model simulated water level elevation-time graph	96
Figure 6.2-12:	Scenario 9 model simulated water level elevation-time graph	97
Figure 8.1.2-1:	Subdivision of opencast pits	105
Figure 8.3-1:	Time-to-decant correlation graph – Scenario 1	119
Figure 8.3-2:	Decant volume correlation graph – Scenario 1	119
Figure 8.3-3:	Time-to-decant correlation graph – Scenario 2	121
Figure 8.3-4:	Decant volume correlation graph – Scenario 2	121
Figure 8.3-5:	Time-to-decant correlation graph – Scenario 3	122
Figure 8.3-6:	Decant volume correlation graph – Scenario 3	122
Figure 8.3-7:	Time-to-decant correlation graph – Scenario 4	123
Figure 8.3-8:	Decant volume correlation graph – Scenario 4	124
Figure 8.3-9:	Time-to-decant correlation graph – Scenario 5	125
Figure 8.3-10:	Decant volume correlation graph – Scenario 5	125
Figure 8.3-11:	Time-to-decant correlation graph – Scenario 6	126
Figure 8.3-12:	Decant volume correlation graph – Scenario 6	126
Figure 8.3-13:	Time-to-decant correlation graph – Scenario 7	127
Figure 8.3-14:	Decant volume correlation graph – Scenario 7	128
Figure 8.3-15:	Time-to-decant correlation graph – Scenario 8	129
Figure 8.3-16:	Decant volume correlation graph – Scenario 8	129
Figure 8.3-17:	Time-to-decant correlation graph – Scenario 9	130
Figure 8.3-18:	Decant volume correlation graph – Scenario 9	131

List of Tables

Table 3.1-1:	Water recharge characteristics for opencast mining	16
Table 3.3-1:	Porosities of Karoo rocks	22
Table 4.1-1:	Lithologies of exploration boreholes	32
Table 4.1-2:	Simplified stratigraphy of the Karoo Supergroup	33
Table 4.1-3:	Simplified stratigraphy of the Transvaal Supergroup	33
Table 4.2-1:	Mean annual precipitation measured at rainfall stations present within the B20A quaternary catchment	34
Table 4.3-1:	Surface water drainage directions and gradients	36
Table 4.4-1:	Estimated evapotranspiration rates for the Olifants Catchment	37
Table 5.1-1:	Summary of hydrocensus survey	39
Table 5.2-1:	Groundwater flow directions, gradients, and velocities	46
Table 5.4-1:	Aquifer parameters	49
Table 5.7-1:	Thickness of unsaturated zone	60
Table 5.7-2:	South African Drinking Water Standards – SANS: 241 (2005)	65
Table 6.1-1:	Model stress periods and simulations	75
Table 6.2-1:	Post-closure model simulations	77
Table 6.2-2:	Simulated post closure baseflow	78
Table 6.2-3:	Results of post closure model simulations – Scenarios 1 and 2	84
Table 6.2-4:	Results of post closure model simulations – Scenarios 3 and 4	85
Table 6.2-5:	Results of post closure model simulations – Scenarios 5 and 6	86
Table 6.2-6:	Results of post closure model simulations – Scenarios 7 and 8	87
Table 6.2-7:	Results of post closure model simulations – Scenarios 9	88
Table 7-1:	Volume calculations	100
Table 7-2:	Time-to-decant calculations	101
Table 7-3:	Decant volume calculations	102
Table 8.1.2-1:	Transmissivity sensitivity analysis ($T = 2 \text{ m}^2/\text{d}$)	114
Table 8.1.2-2:	Transmissivity sensitivity analysis ($T = 4 \text{ m}^2/\text{d}$)	115

List of Equations

Equation 3.1-1: Chloride mass balance method	15
Equation 3.2-1: Surface water discharge into surrounding aquifer	19
Equation 3.2-3: Groundwater discharge into surface water bodies	19
Equation 3.2-2: Groundwater hydraulic gradient	19
Equation 5.2-1: Groundwater seepage velocity	44

List of Abbreviations

Abbreviation	Definition
AMD	Acid Mine Drainage
EDD	Expanded Durov Diagram
ET	Evapotranspiration
FC	Fracture Characteristic
GW	Groundwater
IGS	Institute for Groundwater Studies
MAMSL	Meters Above Mean Sea Level
MAP	Mean Annual Precipitation
MBGL	Meters Below Ground Level
NGDB	National Groundwater Database
Rch	Recharge
S	Storage Coefficient
S _y	Specific Yield
T	Transmissivity
TDS	Total Dissolved Solids
WISH	Windows Interpretation System for the Hydrogeologist

1. Introduction

1.1 Background

This study was carried out at a greenfields opencast coal mine situated approximately 13 kilometres south-east of Delmas along the R 50 road. Bituminous coal is the target mineral and will be mined using the conventional Truck and Shovel method. Two coal seams (coal seams 2 and 4) will be mined concurrently with backfill material being replaced as soon as an area is mined out. Coal seam 2 varies in depth between 6 and 83 meters below ground level (mbgl), while the depth of coal seam 4 varies between 2 and 70 mbgl. Due to the varying depth of the coal seams, opencast mining of coal seam 2 will not take place within all of the proposed opencast pits. The position of the mine (mine lease) is indicated in **Figure 1.1-1**. The mine lease covers an area of approximately 27 km².

Groundwater within a coal mining environment is exposed to **Acid Mine Drainage Reactions (AMD)**, which ultimately leads to the production of sulphuric acid and the subsequent lowering of the groundwater pH. Groundwater that is affected by AMD is more often than not characterised by elevated sulphate, iron, aluminium and manganese concentrations (*Akcil & Koldas, 2006*). Decant of AMD affected groundwater from abandoned mine workings is a global problem affecting all mines in which sulphide minerals are abundant and the conditions are favourable (*Banks et al, 1997 & Pulles et al, 2005*).

In extreme cases the quality of the groundwater is reduced far below the recommended standards for drinking water. The generation of acidic water will continue for as long as the conditions remain favourable and sulphide bearing minerals are available - which may last for decades (*Younger, 1997*). These reactions and their consequences are discussed in more detail in **Section 5.7** of the thesis.

An estimated volume of 50 Ml/d of AMD affected groundwater discharges into the Olifants River Catchment, which originates from old, inactive coal mine workings (*Maree et al, 2004*). By roughly estimating the mass load, the extent of the problem becomes even clearer. Given a conservative total dissolved solids concentration of 1 500 mg/l, an estimated 75 000 kg of dissolved salts are being discharged on a daily basis into aquatic ecosystems and the highly sensitive weathered zone aquifer.

On average, an opencast coal mining operation produces between 4 and 12 Mt of coal per annum (*Hodgson & Krantz, 1998*). Opencast mining, which is predominantly conducted by conventional truck and shovel methods or by draglines, involves the continuous backfilling of the voids after the coal has been extracted. It was estimated that for every ton of coal removed, an average of eight tons of rock, or spoils is generated and subsequently used as backfill material. The backfilling of the voids will lead to (*Hodgson et al, 2007*):

- A drastic increase in the hydraulic conductivity of the pits,
- An increase in the effective recharge to the pits (up to approximately 20% of the annual rainfall),
- An increase in the availability of oxygen,
- A decrease in the pit water quality, as sulphate is initially produced at an average rate of approximately 5 – 10 kg/ha/d at the time of flooding with water, after which sulphate production will decrease to approximately 0.3 kg/ha/d (*Hodgson & Krantz, 1998*).

The most adverse and prolonged impacts on the groundwater quality are therefore expected to be caused by the following:

- The decant of AMD affected groundwater onto the surface and into the shallow weathered zone, and
- The discharge of AMD affected groundwater into surface water bodies and natural wetlands.

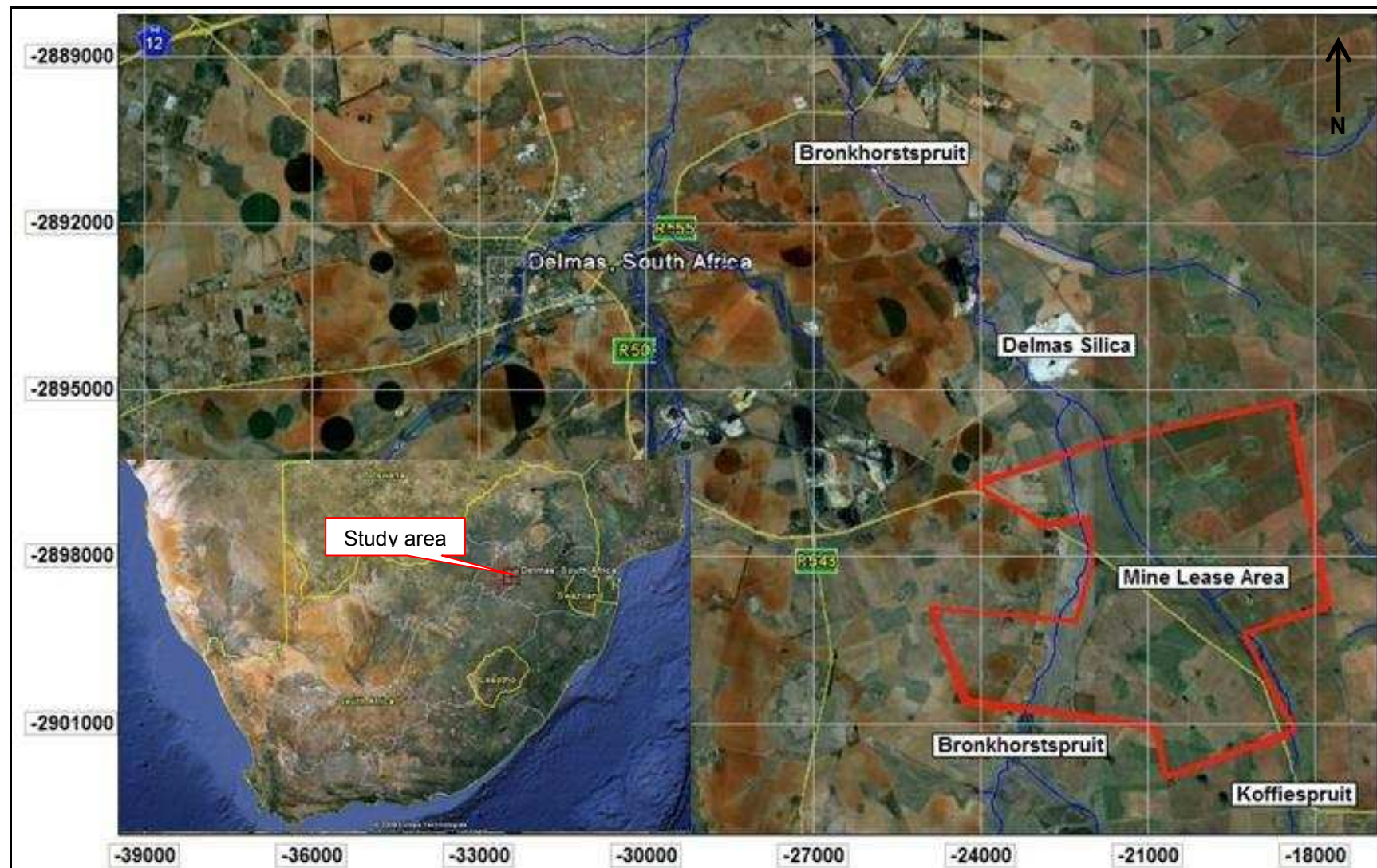


Figure 1.1-1: Site location

1.2 Objectives

Based on the foregoing statements the main objectives of the thesis are as follow:

- Determining decant volumes of each individual opencast pit within the proposed mine lease area,
- Determining the time of decant with varying degrees of backfill material porosity and recharge percentages,
- Determining the volume of groundwater discharge to both the Bronkhorstspuit and Koffiespruit, as indicated in **Figure 1.1-1**.

Numerical groundwater flow models as well as analytical calculations were used to meet the above mentioned objectives. The correlation between the above mentioned methods are discussed in detail in **Section 8** of the thesis. At the end of the day a **toolbox of models** are presented for decant volume and time-to-decant estimations and the **aquifer conditions** under which these models can be used.

1.3 Structure of Thesis

The thesis is structured in such a manner as to allow for easy reading and understanding of the process that was followed to meet the above stated objectives. The thesis is structured as follows:

Chapter 2 provides a comprehensive discussion on the methodology that was followed throughout the study to comply with the objectives as stated in **Section 1.2** of the thesis.

Chapter 3 provides a literature review during which relative groundwater concepts such as groundwater recharge, groundwater – surface water interaction and backfill material properties are discussed. A short discussion is also provided which focuses on both local and international geohydrological studies which are of relevance to the study.

Chapter 4 provides a general discussion of the study area during which the geology, climate, surface topography and drainage, land use, vegetation and soil types are discussed.

Chapter 5 provides a full description of the geohydrology of the study area. The results of a hydrocensus that was conducted in and around the study area are discussed in full. From the results of the hydrocensus the depth to water level, groundwater flow directions and gradients could be determined and are discussed in detail. Field work conducted including the drilling of exploration and monitoring boreholes, pumping tests and groundwater sampling made it possible to develop a sound conceptual model for the study area.

Chapter 6 provides the numerical decant and groundwater discharge calculations, while the analytical decant and groundwater discharge calculations are provided in **Chapter 7**.

Chapter 8 provides a comprehensive discussion on the results of both the numerical and analytical calculations. The results of numerous statistical analyses are provided and discussed in order to determine whether there exists a correlation between the numerical and analytical calculations.

Chapter 9 provides the conclusions and recommendations drawn from the results of the numerical and analytical calculations and subsequent analyses, while the references that were used are listed in **Chapter 10**.

The following three chapters are included in the thesis as Appendices. **Chapter 11** provides the logs of the monitoring/exploration boreholes, while the pumptest sheets are provided in **Chapter 12**. **Chapter 13** provides the report of the hydrocensus that was conducted in and around the study area.

Lastly, **Chapters 14** and **15** provide a short summary in both English and Afrikaans respectively.

2. Methodology

In order for the objectives, as stated in **Section 1.2** of the thesis, to be completed successfully the following methodology was followed:

2.1 Data gathering

Data were gathered from the following sources:

- A hydrocensus that was conducted within a ± 2 kilometre radius of the mine lease area, of which a full discussion is provided in **Section 5.1** of the thesis,
- Groundwater level and quality data were requested from the National Groundwater Database (NGDB),
- Groundwater data collected from surrounding mining activities which include coal as well as silica mines,
- All required maps indicating mine infrastructure, opencast pits and mining schedule, geology and geological structures were collected from the mine personnel,
- A comprehensive desktop study of available and relevant academic material, of which the references are included in **Section 10** the thesis.

2.2 Data processing

Both the hydrocensus and NGDB data were arranged in such a format so that it could be imported and used in the *Windows Interpretation System for the Hydrogeologist (WISH)*. *WISH* was used extensively throughout the study. *WISH* was developed by the *Institute for Groundwater Studies* (herein referred to as IGS) as a tool which can be used by Hydrogeologists to view and edit field data and numerous maps. *WISH* was also used to generate surface contours, which were in turn used in the construction of a numerical groundwater flow model. The *Kriging Interpolation* method was used during the interpolation process of the surface contours.

Due to the limited amount of accurate water levels measured in the vicinity of the study area, some areas were left with data gaps. Groundwater level interpolation was therefore conducted with the use of the *Bayesian Interpolation* method in order to obtain accurate estimates of water levels within these areas.

The *Bayesian Interpolation* method can only be used if there exist a strong correlation between the surface topography and groundwater level elevation of the study area. In most areas ($\pm 90\%$ of South Africa) there do exist a high correlation between the static groundwater levels and surface topography, as is the case in the study area (**Figure 5.2-2**).

A correlation between surface topography and groundwater level elevation will not exist in areas where the static groundwater levels have been disturbed by groundwater abstraction and/or artificial aquifer recharge.

The constant discharge pumping tests were analysed using the *Flow Characteristic Method* (herein referred to as the FC – Program), which was specifically developed by the IGS for the determination of aquifer parameters and sustainable yield estimations in fractured rock environments. The pumping test data were also analysed with the use of *Aquifer Test*, which was developed by *Waterloo Hydrogeologic Inc.* The results of both methods are provided in **Table 5.4-1**.

WISH was used extensively in the generation of surface contours and other relevant images for the purpose of importing into the numerical groundwater flow model.

2.3 Aquifer testing

No boreholes were drilled for the purpose of groundwater level and quality monitoring, as the distribution and quantity of exploration boreholes were considered to be sufficient. Due to the nature of the study and generally low blowout yields measured during the drilling of exploration boreholes, the pumping tests were conducted at an average abstraction rate of 0.1 l/s for a maximum time period of 15 minutes after which recovery was measured.

The results of the pumping tests are provided in **Table 5.4-1**, and the log sheets are available in **Appendix B**.

2.4 Construction of the numerical groundwater flow model

The following steps were followed in the construction of the numerical groundwater flow model:

- The *Processing Modflow Pro* (PMWIN Pro, Version 7.0.0) software was chosen as the appropriate software for the specific task at hand. The software is based on the original work that was done by Wen-Hsing Chiang and Wolfgang Kinzelbach,
- A mesh size was determined and assigned to the model,
- Flux boundaries were assigned to the perimeter of the flow model,
- Two layers were assigned to the model,
- The contour file that was created with the use of *WISH* was used to create a grid/matrix with the use of the model *Field Interpolator*, and was assigned to the model as the elevation of the first, or top layer,
- The elevation of the second layer, or bottom layer was assigned to the model by simply subtracting 15 meters from the elevation of the first/top layer,
- Water levels were interpolated with the use of the *Bayesian Interpolation* method, after which a water level grid was generated with the use of the model *Field Interpolator*,
- The water level grid was assigned to the model as the initial water levels,
- The required aquifer parameters were assigned to the model as discussed in **Section 6**,
- River nodes were assigned to the flow model for the simulation of both the Bronkhorstspuit and Koffiespruit,
- River nodes were used rather than constant head nodes, as the assigning of the riverbed hydraulic conductance, head in river, and elevation of riverbed bottom is more representative of real world conditions,
- Boreholes together with their measured head observations were entered into the model,

- The flow model was calibrated in steady state using the measured water level elevations and the results are presented in **Figure 6.1-3**.
- After the model was calibrated, 28 stress periods (**Table 6.1-1**) were assigned to the model,
- Because there exist areas where only coal seam 4 will be mined, a drain grid was generated which contained a combination of elevations for both coal seams 2 and 4 within the appropriate pit areas, which was used as drain elevations,
- Drains with a hydraulic conductance of $5.5 \text{ m}^2/\text{d}$ were assigned to the model stress periods according to the mine layout and schedule,
- A conductance of $5.5 \text{ m}^2/\text{d}$ was considered to be sufficient, as groundwater flow towards the drain is primarily controlled by the hydraulic conductivity and hydraulic gradient of the surrounding undisturbed aquifer/s (**Section 8.1.2**),
- The model was run in transient state.

2.5 Decant calculations

The following decant calculations were done with both the numerical groundwater flow model and mathematical volume calculations:

- The time it will take each individual backfilled opencast pit to fill with water to the decant elevation,
- The volumes of water that will decant from the rehabilitated opencast pits.

2.5.1 Numerical groundwater flow model

The following steps were followed in determining the **time-to-decant** for each individual backfilled opencast pit:

- End-of-mine water levels of both the upper and lower model layers were exported from stress period 28,

- A post closure flow model was constructed in order to simulate the effects of the increased transmissivity, specific yield, storage coefficient, and recharge of the backfilled pits,
- The end-of-mine water levels exported from stress period 28 were assigned to the post closure model as initial water levels,
- Increased transmissivity, specific yield, storage coefficient, and recharge were assigned to the backfilled opencast pits of the post closure flow model,
- The post closure model was assigned 50 stress periods of 5 years each,
- Artificial observation boreholes were assigned to the post closure model at the decant positions of each individual pit (**Figure 6.2-2**),
- A total of nine different model scenarios were simulated, as illustrated in **Table 6.2-1**,
- The model scenarios were run in transient state, after which head-time data were exported from the model for the purpose of constructing head-time graphs for each rehabilitated opencast pit (**Figures 6.2-4 to 6.2-12**),
- The estimated time-to-decant for each individual pit was then deduced from the graphs (**Tables 6.2-3 to 6.2-7**).

In determining the **decant volumes** for each pit during each model scenario the following steps were followed:

- The post closure model, as discussed above, was used,
- Drain cells were inserted at the surface of the top model layer, at the decant positions of each opencast pit,
- The drain cells were assigned a hydraulic conductance of $25 \text{ m}^2/\text{d}$,
- Each pit was assigned a subregion,
- A water budget was run for each individual opencast pit at the end of stress period 50 (after a time elapse of 250 years), after which the volumes of groundwater entering the drain cells were calculated for each model scenario,
- Decant volumes were calculated at the end of stress period 50, rather than at the time-of-decant, in order for the decant volumes to represent “steady state”, or average volumes (**Tables 6.2-3 to 6.2-7**).

2.5.2 Mathematical volume calculations

Surfer 8 was used to calculate the mined-volume for each individual opencast pit and the following steps were followed:

- A grid file of the floor of both coal seams 2 and 4 was created,
- A .bln file of the boundary of each individual opencast pit was exported from *Wish*,
- Boundary files were created from the .bln files,
- Blanked grids were created for each opencast pit,
- Decant elevations for each pit were identified (**Table 6.2-2**),
- By selecting a blanked grid as the lower surface and the decant elevation as a constant upper surface, the volume between the grid and decant elevation was calculated (**Table 7-1**),
- The procedure was repeated for each individual opencast pit.

After the mined-volumes were calculated the following steps were followed in determining the **time-to-decant**:

- A sensitivity analysis was conducted during which the total mined volume of each opencast pit was multiplied with a range of backfill material porosities in order to determine the volume of voids (**Table 7-1**),
- Average annual rainfall to the study area is considered to be in the order of 680 to 700 mm,
- Recharge to the rehabilitated opencast pits were calculated by multiplying the pits areas with a range of recharge percentages,
- In order to determine an average time-to-decant, a sensitivity analysis was conducted during which the calculated void volume of each opencast pit was divided between a range of recharge values (**Table 7-2**).

The following steps were followed in calculating the **decant volumes** of each rehabilitated opencast pit:

- During the analytical decant volume calculations, groundwater seepage into the rehabilitated opencast pits was not taken into account,
- The lateral groundwater seepage component is considered to be far less than the actual seepage of water from recharge (**Table 3.1-1**),
- A sensitivity analysis was conducted during which the decant volumes were calculated by multiplying the pit surface area with a range of recharge percentages (**Table 7-3**).

2.6 Groundwater – surface water interaction

Groundwater discharge to surface water bodies was calculated with the use of a numerical groundwater flow model and analytical calculations.

2.6.1 Numerical groundwater flow model

The following steps were followed in calculating the volumes of groundwater discharge to both the Bronkhorstspuit and Koffiespruit:

- Groundwater discharge to surface water bodies was calculated by conducting a water budget,
- Both the Bronkhorstspuit and Koffiespruit were assigned a subregion, which is illustrated in **Figure 6.1-4**,
- The volumes of groundwater leaving the model area through river nodes were calculated and the results are provided in **Section 6** of the thesis.

2.6.2 Analytical calculations

Equation 3.2.3 was used to calculate the volumes of groundwater discharge to surface water bodies. The following steps were followed:

- An average aquifer transmissivity was calculated (**Table 5.4-1**),

- Average hydraulic gradients between the surrounding aquifer and surface water streams were calculated by calculating the average gradient of a number of points along the length of the streams,
- Hydraulic gradients were calculated with the use of **Equation 3.2-2**,
- The length of the surface water streams were measured with the use of *Wish*.

3. Literature Review

3.1 Groundwater recharge

Numerous studies have been conducted to determine the effective recharge of an aquifer. Effective recharge in a geohydrological sense refers to the volume of rainfall that enters the aquifer system and is indicated as a percentage of the mean annual rainfall.

Recharge and annual precipitation maps were developed by *Vegter (2001)*, which indicates aquifer recharge throughout the entire South Africa. One must however be very careful when using these maps, as they only provide ballpark figures. Aquifer recharge is a very complex and sensitive parameter and is more often than not oversimplified.

Factors that may influence aquifer recharge include (*Bredenkamp et al, 1995*):

- Thickness of unsaturated zone – recharge will be higher in areas where the geology outcrops and precipitation can move freely into fractures,
- Composition of unsaturated zone – determines rate at which precipitation moves through the unsaturated zone,
- Rainfall events – heavy rainfall contributes more to surface runoff than to aquifer recharge,
- Topography – steep topographies contribute more to surface runoff, while gentle slopes favour aquifer recharge,
- Land surface cover – a surface densely covered by vegetation will favour evapotranspiration, while poorly covered land surfaces will favour aquifer recharge (assuming a flat topography),
- Evapotranspiration – areas with high evapotranspiration rates will receive less recharge because of a loss of water due to evaporation and transpiration. The riparian zones along river banks are largely affected by evapotranspiration due to lush vegetation growth and shallow groundwater levels,

- Annual rainfall – areas that receive high annual rainfall will receive high recharge (if above mentioned factors are favourable).

Numerous methods exist for determining aquifer recharge. Probably the most frequently used and well known method is the *Chloride Mass Balance Method*. The chloride mass balance method was first proposed by *Eriksson and Khunakasem* in 1969 and is defined by the following equation (*Van Tonder & Bean, 2003*):

Equation 3.1-1: Chloride mass balance method

$$R = (P \text{ Cl}_p + D) / \text{Cl}_w$$

Where

P	=	precipitation (mm/a)
Cl _p	=	chloride in rain (mg/l)
D	=	dry chloride deposition (mg/m ² /a)
Cl _w	=	Cl in soil water below root zone or Cl in groundwater (harmonic mean)

The chloride mass balance method does have its limitations and uncertainties especially in areas where sufficient data are scarce. When using the method to determine groundwater recharge the following assumptions are made: chloride is conservative in the aquifer system and therefore do not participate in chemical reactions; chloride concentrations in rainwater remain relatively constant as do the mean annual rainfall; there exist no alternative source of chloride and all chloride is derived from rainfall.

When a groundwater sample is taken from a borehole that was drilled in a fault zone one must remember that the recharge determined from the sample will only be representative of the preferred flow path and not of the entire aquifer. When sampling a borehole the sample must be taken close to the surface. Samples taken at greater depths will contain diluted chloride concentrations and will therefore contribute to inaccurate recharge calculations. Accurate chloride concentrations are vital for accurate recharge calculations, which may cause problems since many laboratories can only measure concentrations greater than a certain amount and with up to a 10 percent error range (*Van Tonder & Bean, 2003*).

Other methods of determining groundwater recharge include the *Isotope Method*, *Saturated Volume Fluctuation Method*, *Cumulative Rainfall Departure Method*, *EARTH-Method*, and *Spring Flow Method* to name a few.

Recharge to typical Karoo aquifers vary between 1 and 3% of the mean annual rainfall, while recharge to aquifers of the Table Mountain Group vary between 7 and 23%. Higher recharge percentages varying between 8 and 14% can be expected for dolomitic aquifers, while recharge to primary aquifers can be as high as 20 to 30% of the mean annual precipitation (*Parsons, 2004*).

During the backfilling of opencast pits material is placed systematically back into the pits in an effort to return the post-mining environment to its pre-mining conditions. Despite all these efforts the hydraulic conductivity or transmissivity of pit areas is significantly higher than the surrounding undisturbed aquifer/s. The increased transmissivity will lead to an increase in the vertical hydraulic conductivity, which ultimately results in an increase in recharge to the backfilled opencast pit/s. Recharge was calculated to be in the order of 20% (12% runoff, and 8% spoil infiltration) of the mean annual precipitation (*Hodgson & Krantz, 1998*).

Table 3.1-1: Water recharge characteristics for opencast mining (*Hodgson & Krantz, 1998*)

Sources which contribute water	Water sources into opencast pits	Suggested average values
Rain onto ramps and voids	20 - 100% of rainfall	70% of rainfall
Rain onto unrehabilitated spoils (run-off and seepage)	30 - 80% of rainfall	60% of rainfall
Rain onto levelled spoils (run-off)	3 - 7% of rainfall	5% of rainfall
Rain onto levelled spoils (seepage)	15 - 30% of rainfall	20% of rainfall
Rain onto rehabilitated spoils (run-off)	5 - 15% of rainfall	10% of rainfall
Rain onto rehabilitated spoils (seepage)	5 - 10% of rainfall	8% of rainfall
Surface run-off from pit surroundings into pits	5 - 15% of total pit water	6% of total pit water
Groundwater seepage	2 - 15% of total pit water	10% of total pit water

3.2 Groundwater – surface water interaction

Groundwater always moves from higher to lower hydraulic gradients, and under natural/steady state conditions will more or less follow the surface topography. This means that an increase in surface elevation will cause an increase in the groundwater hydraulic gradient. Groundwater will therefore move from high elevations to lower elevations where it will discharge into surface water bodies such as dams, rivers/streams, or wetlands.

Springs and fountains are also areas where groundwater is discharged at the surface, but under different hydraulic conditions. According to *Kotze (2001)* springs can be divided into three distinct groups:

- Type 1 – shallow seasonal springs and seeps emanating from perched water tables. Springs represent discharge of interflow rather than groundwater.
- Type 2 – lithologically controlled springs, often discharges at lithological contacts. Flow is more permanent and plays an important role in sustaining baseflow. Susceptible to the impacts of localised groundwater abstraction.
- Type 3 – fault controlled springs that are perennial. May discharge either hot or cold water depending on the depth from where the groundwater originates and the presence of heat producing chemical reactions. Only potentially impacted by large scale regional abstraction.

Streams and rivers can be divided into two main groups, namely influent and effluent streams. Influent streams/rivers feed the surrounding aquifers due to the hydraulic head in the stream/river being higher than that of the surrounding aquifers. Effluent streams/rivers, on the other hand, are fed by the surrounding aquifers due to the hydraulic head of the stream/river being lower than that of the surrounding aquifers (*Parsons, 2004*).

In the drier parts of South Africa a third type of stream/river occurs, namely a detached stream. These streams are created when low recharge, and/or high groundwater abstraction cause the groundwater level to decrease below the base of the stream. In these areas very little or no interaction occurs between the surface water and groundwater. Only after heavy rainfalls will the regional groundwater level rise above the hydraulic head of the stream and will the stream become effluent. As the groundwater level recedes again, the stream will change from being effluent, to influent, and once again detached as soon as the groundwater level decrease to below the base on the stream.

The process whereby groundwater contributes to streamflow is known as baseflow and is influenced by the following factors (*Hughes, Parsons & Conrad, 2007*):

- Transmissivity,
- Storativity,
- Groundwater recharge,
- Drainage density,
- Regional groundwater drainage slope,
- Rest water level, and
- Evapotranspiration.

According to a study done by *Le Maitre and Colvin (2008)*, catchments dominated by carbonates have the greatest proportion of baseflow (37%), followed by basement complex (31%) and extrusive aquifer types (31%). The reason why the Karoo Supergroup isn't even mentioned is because of the low transmissivities of the rocks that form part of the Supergroup.

The rate at which **groundwater is discharged into a stream**, or **surface water is discharged into surrounding aquifers** can be calculated with the use of Darcy's Law:

Equation 3.2-1: Surface water discharge into surrounding aquifer

$$Q = K L W i$$

Where:	Q	=	rate at which water flows from stream to aquifer (L^3/T)
	K	=	vertical hydraulic conductivity of stream bed (L/T)
	L	=	length over which discharge is calculated (L)
	W	=	width of stream over which discharge is calculated
	i	=	hydraulic gradient between stream and aquifer

To determine the hydraulic gradient (i) between the stream and the surrounding aquifer the following equation can be used:

Equation 3.2-2: Groundwater hydraulic gradient

$$i = (h_{\text{aquifer}} - h_{\text{stream}})/M$$

Where:	h_{aquifer}	=	hydraulic head of aquifer (mamsl)
	h_{stream}	=	hydraulic head of stream (mamsl)
	M	=	thickness of stream bed (L)

Equation 3.2-3: Groundwater discharge into surface water bodies

$$Q = T i 2L$$

Where:	T	=	transmissivity of aquifer (L^2/T)
	i	=	hydraulic gradient between aquifer and stream
	L	=	length over which discharge is calculated (L)

Notes: Due to aquifer heterogeneity, the above calculation was modified in an attempt to calculate a more representative groundwater discharge volume. Groundwater discharge was calculated separately for both river banks in order to obtain an overall average.

According to *Parsons (2004)*, the following activities could potentially impact groundwater – surface water interaction:

Groundwater abstraction

In a South African context, the agricultural and mining sectors are the two biggest groundwater abstractors (*Parsons, 2004*). In the mining industry groundwater is abstracted for two reasons: mine dewatering if mining occurs below the regional groundwater level; and for the use in various ore enrichment processes. In the agricultural industry groundwater is abstracted on a large scale for irrigation purposes.

The lowering of the regional groundwater level may cause streams to change from being effluent to influent and ultimately detached.

Unlined storage dams

Groundwater levels within the direct vicinity of storage dams may increase, due to increased infiltration of surface water into the underlying aquifers. This process is known as artificial recharge and may cause streams to change from being detached to influent, and ultimately effluent if artificial recharge to the aquifers continues over a long enough period.

Forestry

In a study conducted by *Scott and le Maitre (1997)*, a decrease in baseflow, or a reduction in groundwater discharge into surface water bodies, was observed for areas utilised for extensive plantation.

Removal of vegetation

A process known as evapotranspiration (evaporation and transpiration) plays a major role in groundwater – surface water interaction. Evapotranspiration is a major groundwater sink and is especially influential along watercourses where dense vegetation and shallow groundwater levels lead to an increase in evapotranspiration. The removal of vegetation along watercourses (riparian zones) will thus cause an increase in aquifer recharge and will consequently lead to increased groundwater levels.

3.3 Backfill material porosity

Because the study is conducted on secondary/fractured rock aquifers, the porosity of primary aquifers will not be discussed.

Porosity in geological and geohydrological terms refers to the percentage of voids relative to the percentage of rock mass. To be more specific, the effective porosity of a rock mass refers to the volume of water that is capable of draining from the mass under the force of gravity.

Factors such as the shape and size, as well as the degree of sorting of the consolidated sediments play a major role in porosity. **Figure 3.3-1** (Nichols, 1999) clearly illustrates the difference in porosity between well and poorly sorted sediments. In the case of a poorly sorted sedimentary rock, the pores are filled with smaller sediments, which cause a decrease in the porosity of the rock. A sedimentary rock composed of poorly sorted sediments will also have a lower hydraulic conductivity than one composed of well sorted sediments, as the smaller sediments will obstruct the movement of groundwater through the porous medium.

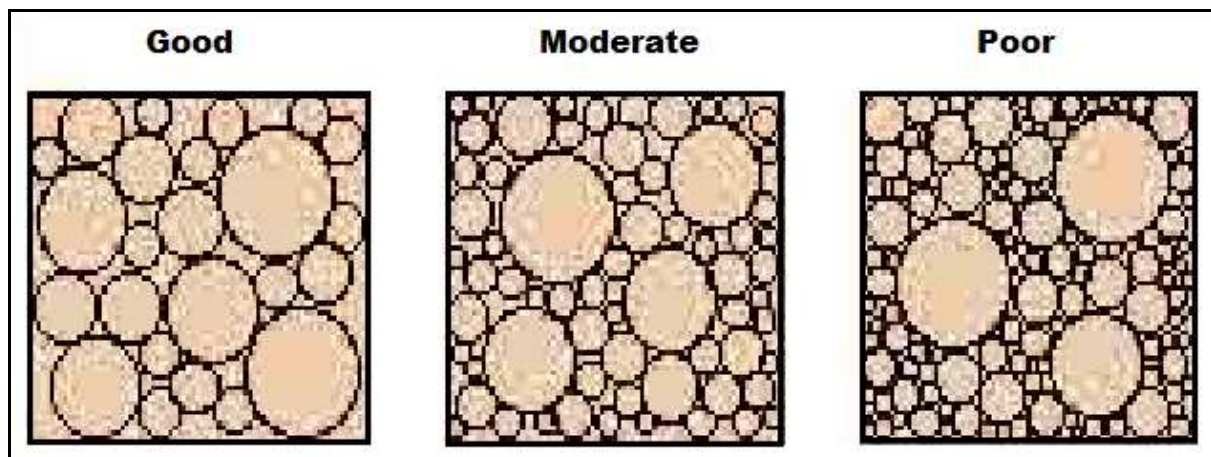


Figure 3.3-1: Sorting of sediments

Numerous studies have been conducted to determine the porosity of the Karoo type aquifers.

One such a study was conducted by *Kirchner and Van Tonder (1991)* during which the average porosity for Karoo type aquifers was determined to vary between 0.003 and 0.01. The results of earlier studies conducted by *Beukes (1969)*, *Van Wyk (1963)*, and *Roswell and De Swardt (1976)* are presented in **Table 3.3-1**.

Due to backfilling techniques and the irregular shapes and sizes of the backfill material the porosity of a backfilled opencast pit area may vary significantly.

The increased porosity of a backfilled mine void may have the following effects on the geohydrological regime:

- An increase in porosity will more often than not lead to an increase in transmissivity and specific yield, given that the pores are interconnected,
- The backfilled mine void will act as a preferred flow path for groundwater and contamination as a result of the increased transmissivity,
- The porosity of the backfill material (as a whole) will influence the time-to-decant, as illustrated in **Table 7.2** of the thesis,
- The time-to-decant will ultimately have an effect on the quality of the decanting groundwater. Acid mine drainage reactions require oxygen to take place, which means that the longer it takes a backfilled mine void to decant, the longer oxygen is available for acid mine drainage reactions to occur.

Table 3.3-1: Porosities of Karoo rocks (*Woodford and Chevallier, 2002*)

Rock Type	Group/Formation	Porosity %
Very fine Sandstone1	Clarens	6.2 – 9.8
Cross-bedded Sandstone1	Clarens	8.9 – 10.8
Sandstone3 **	Clarens	4.7 – 21.0
Sandstone4	Clarens	6.19 – 10.75
Mudstone2	Beaufort	25.4 – 26.9
Sandstone2	Beaufort	5.4 – 6.8
Sandstone3	Beaufort	1.9
Shale2	Upper Ecca	2.5 – 2.7

Rock Type	Group/Formation	Porosity %
Shale2	Middle Eccu	1.8 – 2.5
Sandstone2	Middle Eccu	4.0 – 12.9
Shale2	Lower Eccu	1.5 – 3.1
Shale3 *	Eccu	1.5 – 12.5
Diamictite2	Dwyka	0.5 – 1.3

Notes: 1 - after Beukes (1969).

2 - samples from Natal, after Van Wyk (1963).

3 - after Rowsell & De Swardt (1976).

4 - after Beukes (1969)

* - boreholes in the Welkom-Virginia area

** - SOEKOR borehole at Barkly East

3.4 Review of geohydrological case studies

From a study conducted by *Straskraba* (1986) on opencast coal mining within the western United States the following groundwater related impacts were emphasised:

- The destruction of the physical characteristics of the aquifers as a result of coal extraction,
- A change in aquifer porosity and hydraulic conductivity after the opencast pits have been backfilled,
- A change in the chemical environment of the backfilled opencast pits, as minerals are exposed to an oxidising environment.

According to *Straskraba's* findings, the prediction of groundwater impacts is based on geohydrological studies and the proposed mining and rehabilitation methods. The prediction of the quality of water within backfilled opencast pits is further based on the pre-mining groundwater quality and the chemical composition of the material used to backfill the mine voids. It is for this reason why most of the states in the western United States require, by law, groundwater monitoring data of at least one year before mining can commence.

The chemical composition of the backfill material is determined with the use of the *Saturated Paste Method (Straskraba, 1986)*. The method involves the crushing of a representative sample of the backfill material and saturating it with distilled water. The water is then removed from the paste and analysed to determine the dissolved chemical composition thereof. Saturated paste tests of backfill material within western Colorado indicated that calcium, magnesium, and sulphate are the major contaminants.

The hydraulic conductivity of the backfilled opencast pits depends on the following factors (*Straskraba, 1986*):

- The variations in the size of the backfill material,
- The mining method, and
- The backfill method, as studies have shown that spoils handled by a dragline have higher transmissivity than those replaced by the conventional truck and shovel method.

Within the Wyoming, Edna, and Colowyo coal mines it was found that the total dissolved solids content within backfilled opencast pits were 2 to 3 times higher than that of pre-mining groundwater concentrations (*Straskraba, 1986*).

During a study conducted by *Buck & Winegar (2003)* on an opencast phosphate mine located in south-eastern Idaho, the potential groundwater quality impacts associated with phosphate overburden being used as backfill material were determined with the use of *Column Leach Tests*.

Column Leach Tests are commonly used to determine the desorption or dissolution rates of contaminants from potential sources of groundwater contamination such as backfill material (*Susset & Grathwohl, 2001*).

During the *Buck & Winegar* study, infiltrations into the opencast pits were simulated with the use of the *HELP3.07* infiltration model. The model was developed by the U.S. Corps of Engineers to assess seepage of precipitation through solid waste fills. Mass transport simulations were however conducted with the use of *MODFLOW* and *MT3D*.

A study was conducted by *Terry Braun (2002)* on the prediction of post-mining opencast pit water quality within the south-western United States. Throughout the study the importance of a comprehensive post-closure monitoring program was emphasized. Such monitoring programs are necessary to determine whether model predictions of pit water quality are accurate and legitimate.

In 2009 a study was conducted by *Michael Paul, Delf Baacke, Thomas Metschies, and Werner Kuhn*. The study was conducted on Europe's formerly largest uranium mine which is situated in Germany. The aim of the study was to compare water flow rates and water quality model predictions with real life post-closure monitoring data.

The following preventative measures were taken to prevent the contamination of groundwater and surface water as a result of poor quality decant water:

- A subsurface pumping system was installed downstream of the decant area,
- A water collection system was installed along the edge of the opencast pit,
- A pumping well was drilled into the old mine workings in an effort to keep the water level within the underground workings below the decant elevation.

The study came to the following conclusions (*Paul et al, 2009*):

- The model predicted groundwater recovery, decant, and mine water quality (concentration loads) were not always correct when compared to real life monitoring information,
- The main reason for the discrepancies was thought to be the underestimation of contributions from near surface contaminant storage.

Once again the importance of a comprehensive post-closure monitoring program is brought to light.

A geohydrological investigation was conducted by *Adams and Younger (2000)*, which was prompted by concerns that the closure of a tin mine, located in Cornwall, South West England, would have negative impacts on the environment.

The objectives of the investigation were to determine the recharge volumes to the underground voids, and the time it would take the voids to fill with water and for the groundwater levels to rebound.

Meteorological data were gathered in order to determine whether there existed any relationship between the likely recharge to the mining voids and the volumes of water pumped from the workings. The relationship between the estimated recharge to the voids and the annual precipitation was examined in order to determine whether the water pumped from the mine workings originated from groundwater seepage or recharge from rainfall. The results indicated that the water pumped from the underground workings originated from groundwater seepage rather than seepage from rainfall.

Infiltration into the mine was calculated by subtracting the estimated evapotranspiration rate and surface runoff from the average precipitation, as no infiltration is expected if evapotranspiration and runoff exceeds the annual rainfall. A numerical model, namely the *SHETRAN/VSS-NET* model was however used to determine the time it would take the groundwater levels to rebound.

Similar to the thesis, a groundwater investigation was conducted by the *Institute for Groundwater Studies (IGS)* in 2005 during which areas were identified where intermine flow was expected to occur. The purpose of the study was to predict groundwater flow directions, filling times of mining voids and flow volumes with the use of both numerical groundwater flow models and analytical techniques.

During the IGS numerical model simulations, the model sensitivity with respect to aquifer hydraulic conductivity and recharge were tested. Similar sensitivity analyses were conducted for the purpose of the thesis regarding aquifer transmissivity, recharge, specific yield, and storage coefficient. During the IGS sensitivity analyses it was found that an increase in hydraulic conductivity leads to a decrease in the filling times of mine voids. The same phenomenon was encountered during the sensitivity analyses that were conducted for the purpose of the thesis (**Section 8.1.2**). An increase in hydraulic conductivity does lead to accelerated inflow of water to the pit, but it also leads to an accelerated outflow of water from the pit.

This results in more water leaving the pit than actually entering it (given that the groundwater hydraulic gradient allows it), which explains the decrease in filling times (*Hodgson et al, 2005*).

During the IGS study, a hydraulic conductivity of 0.864 – 0.000864 and recharge of 14 to 20% were assigned to the pit areas during model simulations. These values correlate well with those assigned to the model parameters during model simulations for the purpose of the thesis (**Section 8.1.2**).

The IGS study is of relevance to the thesis, as it further confirms that there does exist a good correlation between numerical groundwater flow models and analytical techniques. During the IGS study, the time it would take opencast pits to fill was calculated with both a numerical groundwater flow model and analytically. The same was done for the thesis, except that the time-of-decant was calculated, which is virtually the same. The IGS study concluded that both the numerical and analytical volume calculations were in the same order, except for the time-to-decant, or filling times. The exact same conclusion can be drawn from the thesis, as is illustrated by the numerous correlation graphs in **Section 8.3**.

4. General Description of the Study Area

4.1 Geology

The geology of the study area is somewhat different compared to the majority of the Mpumalanga coal mines. The study area contains rocks of the Karoo Supergroup, as well as rocks that form part of the Transvaal Supergroup. Both of these Supergroups are thick sedimentary successions, where the different sedimentary rocks represent different depositional environments. The Karoo Supergroup covers approximately two thirds of the surface area of South Africa and range in age from Late Carboniferous to Early Jurassic. The extent and occurrence of the different Groups and Formations of the Karoo Supergroup is indicated in **Figure 4.1-2** (Woodford & Chevallier, 2002). **Figure 4.1-1** is a simplified geological map of the study area, while **Tables 4.1-2** and **4.1-3** illustrates the simplified stratigraphy of the Karoo and Transvaal Supergroups.

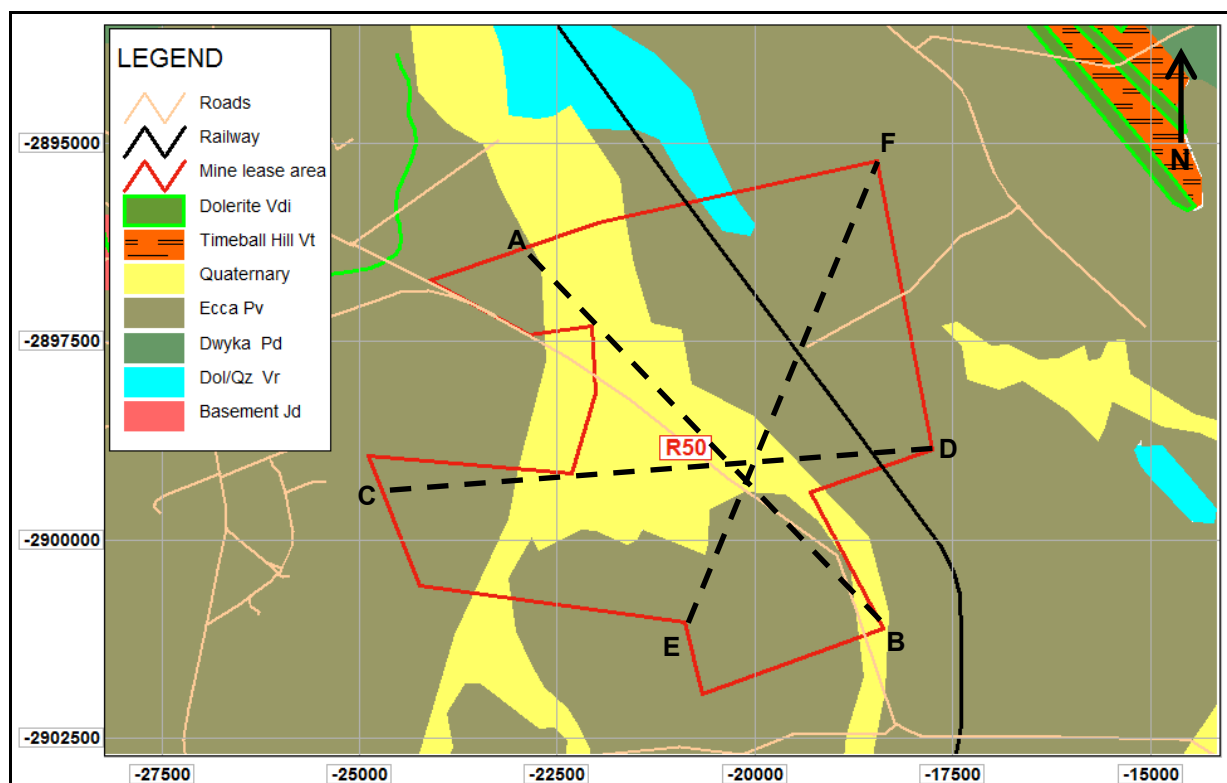


Figure 4.1-1: Simplified geological map of the study area

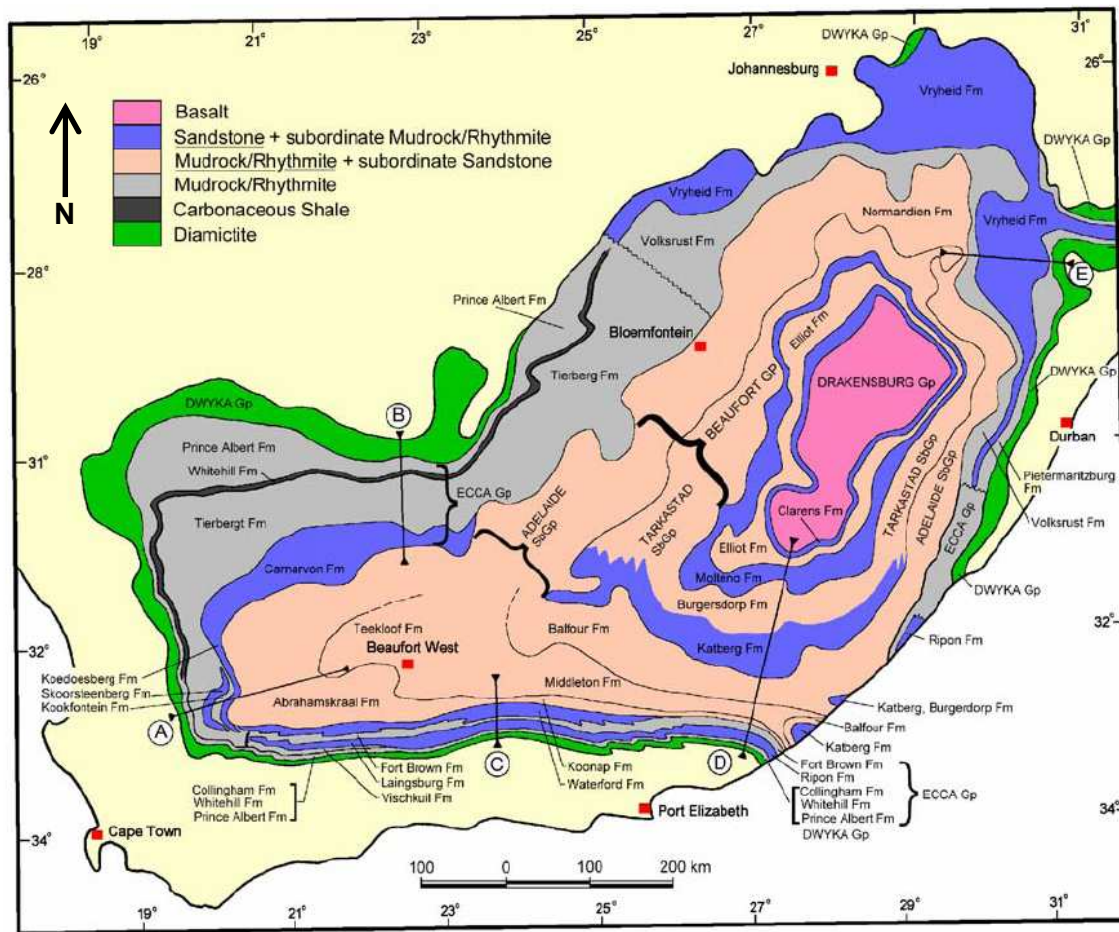


Figure 4.1-2: Extent of Karoo Groups and Formations (Woodford & Chevallier, 2002)

Even though dolomite is not indicated throughout the mine lease area (**Figure 4.1-1**), it was intersected in a number of the exploration boreholes. Cross sections were generated with the use of surface and coal seams elevations and their positions are indicated in **Figure 4.1-1** with the use of dashed black lines. **Figure 4.1-3** clearly indicates the positions of the coal seams in relation to the surface topography, and the gently undulating nature of both coal seams 2 and 4. Irregularities in either the exploration borehole data or the data interpolation process have lead to some discrepancies in the cross sections of **Figure 4.1-3**, as it is unlikely for the roof of coal seam 2 to exceed the elevation of coal seam 4.

The average thickness of coal seam 2 is 3.7 meters, while coal seam 4 has an average thickness of 4.7 meters.

The coal seams are at their deepest in the north-eastern corner of the mine lease with a maximum depth varying between 75 and 95 meters below surface. Due to the depth of coal seam 2, mining of only coal seam 4 will take place in some areas.

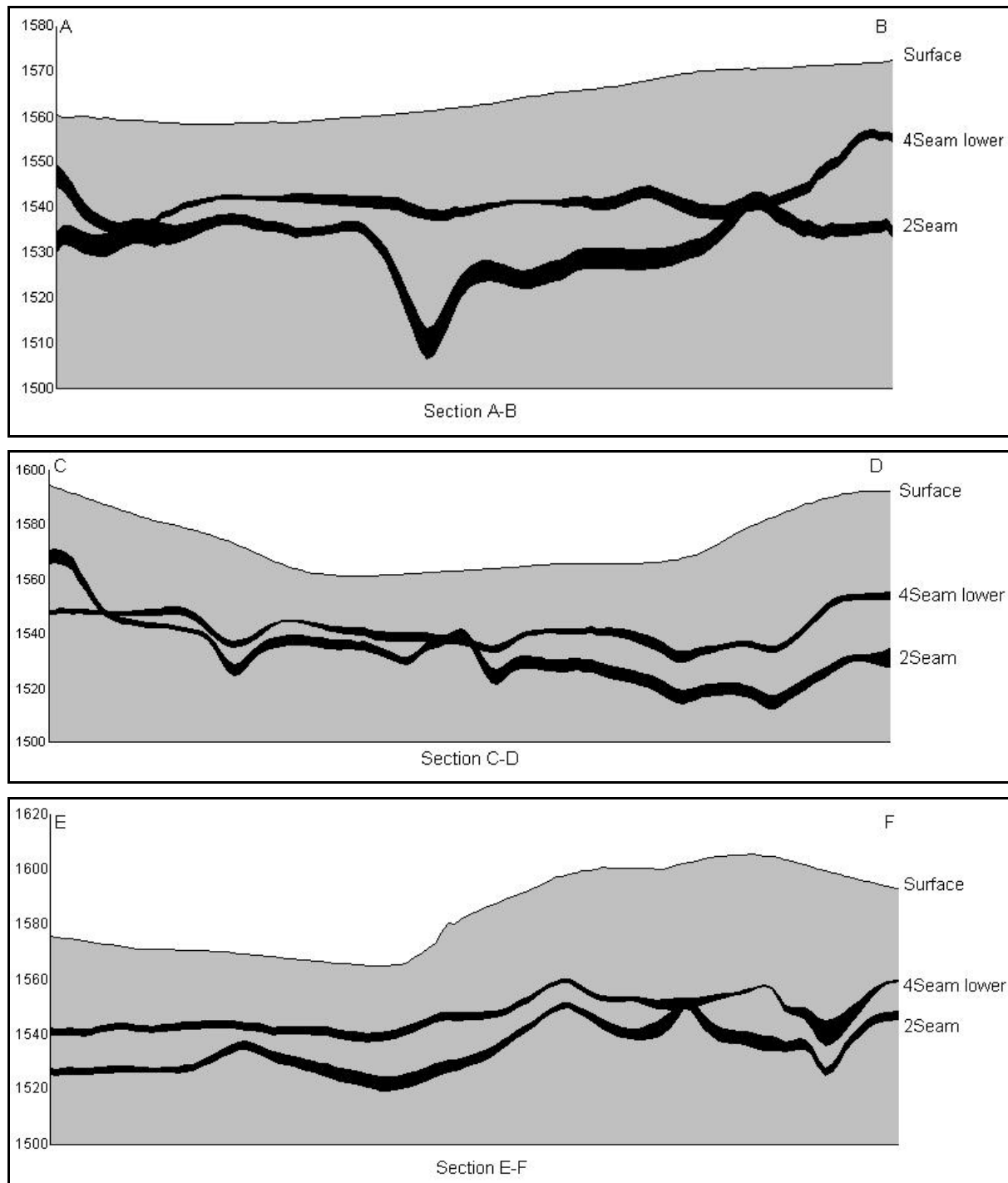


Figure 4.1-3: Cross sections of mine lease area

Notes: Cross sections are shown on Figure 4.1-1.

Due to the sheer number of exploration boreholes, borehole logs of only the monitoring boreholes are provided in **Appendix A**. The distribution and quantity of exploration boreholes is considered to be sufficient to allow for a general interpretation of the site specific geology.

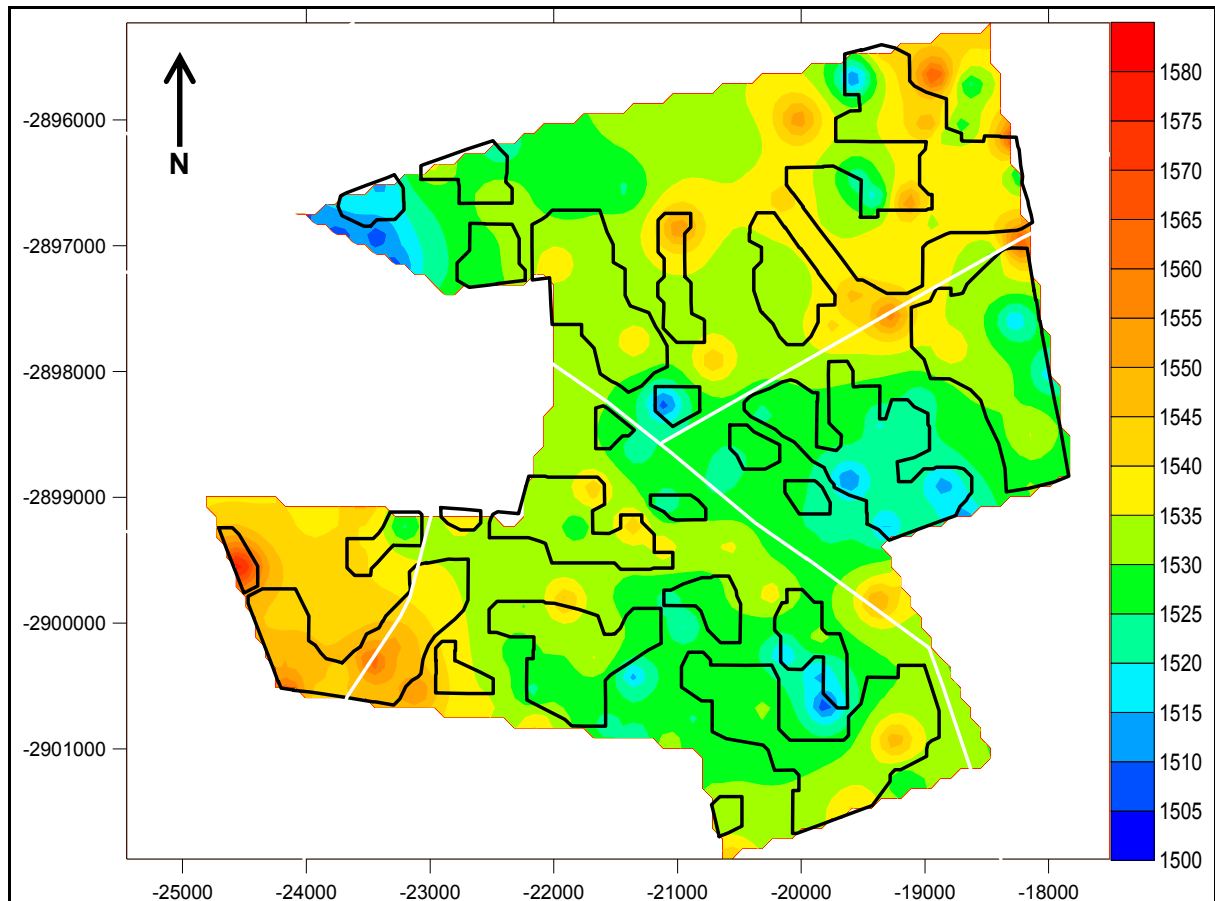


Figure 4.1-4: Floor contours of the base of coal seam 2

Figure 4.1-4 further confirms the undulating nature of the coal seam. The highest floor elevation is at approximately 1 570 meters above mean sea level, which occurs in the north-eastern and south-western corners of the mine lease. The lowest coal elevation occurs at approximately 1 500 meters above mean sea level, which is found within the north-western corner of the mine lease, as indicated in **Figure 4.1-4**.

Figure 4.1-4 was generated through the interpolation of all available coal seam data with the use of the *Inverse Distance Method*.

A short summary indicating the intersected lithologies is provided in **Table 4.1-1**. The depths at which the individual lithologies were intersected are provided in **Appendix A**.

Table 4.1-1: Lithologies of exploration boreholes

BH	Lithology	BH depth (m)
R060	SOIL, SHLE, SNDS, COAL, DLRT, TLLT	41
R133	SOIL, SNDS, SHLE, DLRT, COAL, TLLT	58
R142	SOIL, CLAY, DLRT, SNDS, SHLE	36
R149	SOIL, DLRT, SNDS, COAL, SHLE, MDSN, TLLT	33
R171	SOIL, MDSN, SNDS, DLRT, SHLE, COAL, TLLT	53
R184	SOIL, SLSN, SNDS, COAL, MDSN, SHLE, TLLT, VNQZ	32
R196	SOIL, MDSN, SLSN, SNDS, COAL, SHLE, TLLT	80
R199	SOIL, SLSN, SNDS, COAL, MDSN, SHLE, TLLT	32
R206	SOIL, SNDS, MDSN, SLSN, SHLE, COAL, TLLT	23
R210	SOIL, DLRT, MDSN, SNDS, SLSN, DLRT, TLLT, VNQZ	68
R216	SOIL, DLRT, SLSN, SNDS, COAL, TLLT, DLMT	83
R222	SOIL, SNDS, SHLE, SLSN, COAL, TLLT	41
R265	SOIL, SNDS, MDSN, SLSN, SHLE, COAL, TLLT	59
R274	SOIL, CLAY, MDSN, SLSN, COAL, SHLE, TLLT	25

Notes: SHLE - Shale
 SNSN - Siltstone
 SNDS - Sandstone
 DLMT - Dolomite
 DLRT - Dolerite
 TLLT - Tillite
 MDSN - Mudstone
 VNQZ - Quartz vein

From **Table 4.1-1** and **Appendix A** it is made clear that the mine lease is predominantly underlain by carbonaceous shale, sandstone, siltstone, mudstone, coal, and tillite. Dolomite was intersected at depths varying between 26 and 87 meters below surface with an average depth of 50 meters below surface. Igneous intrusions (dolerite dykes) are also a prominent feature of the geology of the mine lease. The depths at which the above mentioned lithologies were intersected are provided in **Appendix A**.

Table 4.1-2: Simplified stratigraphy of the Karoo Supergroup

Supergroup	Group	Formation
Karoo	Stormberg	Drakensberg
		Clarens
		Elliot
		Molteno
		Burgersdorp
		Katberg
	Beaufort	
	Ecca	
	Dwyka	

Table 4.1-3: Simplified stratigraphy of the Transvaal Supergroup

Transvaal Supergroup (Western Transvaal)		
Group	Formation	Lithology
Rooiberg		
Pretoria	Magaliesberg Quartzite	Quartzite
	Silverton Shale	Hornfels and Graphitic Shale
	Daspoort Quartzite	Orthoquartzite
		Shale and Quartzite
		Orthoquartzite
	Strubenkop Shale	Iron-rich Shale and Siltstone
		Conglomerate
	Hekpoort Andesite	Amygdaloidal Andesitic Lava
	Timeball Hill	Shale
		Quartzite
		Shale and Siltstone
	Rooihoogte	Quartzite
		Shale
		Bevets Conglomerate Member
Chuniespoort	Penge	Iron Formation
	Frisco (Malmani Sub-G)	Chert-free Dolomite
	Eccles (Malmani Sub-G)	Chert-rich Dolomite
	Lyttleton (Malmani Sub-G)	Chert-free Dolomite
	Monte Christo (Malmani Sub-G)	Chert-rich Dolomite
	Oaktree (Malmani Sub-G)	Dark coloured Dolomite
Wolkberg	Black Reef Quartzite	Feldspathic Quartzite and Shale
		Conglomerate
	Sadowa Shale	
	Mabin Quartzite	
	Selati Shale	
	Schelem	
	Abel Erasmus Basalt	
	Sekororo	

4.2 Climate

The study area falls within a summer rainfall region. Rainfall is measured at seven rainfall stations within the B20A quaternary catchment area (**Table 4.2-1**). The area receives a mean annual precipitation (MAP) of approximately 680 mm (*Middleton et al, 1990*). The annual mean maximum temperature varies between 27 and 29 degrees Celsius, while the annual mean minimum temperatures vary between 0.1 and 2 degrees Celsius (*Low & Rebelo, 1996*).

Table 4.2-1: Mean annual precipitation measured at rainfall stations present within the B20A quaternary catchment

Details of rainfall stations used		
Number	Name	MAP (mm)
0477191	Droogefontein	674
0477309	Delmas - POL	719
0477404	Weilaagte	645
0477459	Moabsvelden	702
0477494	Vlakplaas	697
0477501	Devon - POL	666
0477555	Madjiesgoedkuil	673
Average MAP:		682

The mine lease area falls within the 4A Evaporation Zone, with an evaporation rate varying between 1 600 and 1 700 mm/a, which far exceeds the mean annual precipitation (*Middleton et al, 1994*).

4.3 Surface topography and drainage

The main topographical features of the study area are indicated in **Figure 4.3-1**.

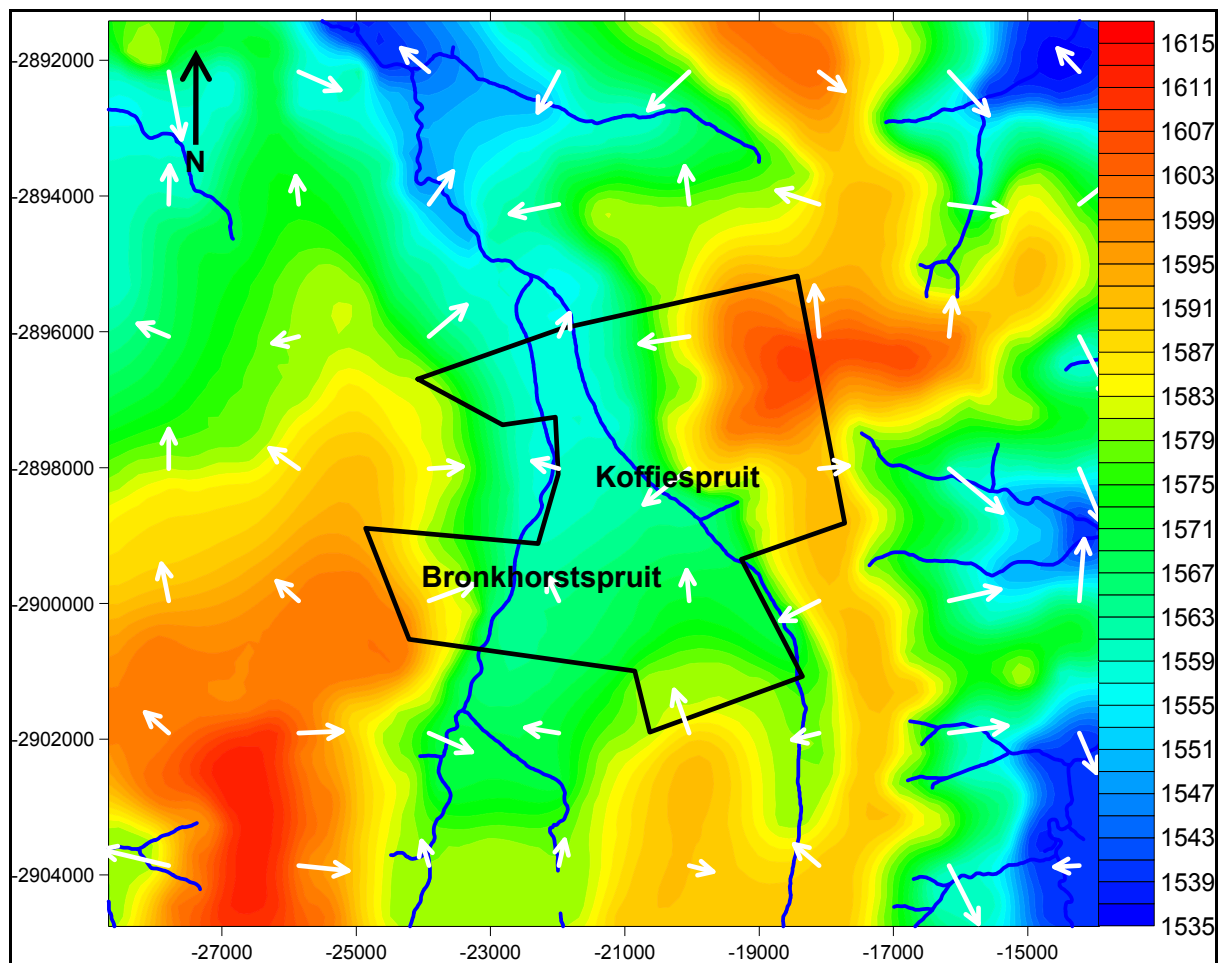


Figure 4.3-1: Surface contour map of study area (mamsi)

The topography of the mine lease area is gently undulating with a vertical difference of approximately 50 meters between the highest and lowest elevations. The highest elevation occurs in the north-eastern corner of the mine lease area, while the lowest elevation occurs in the north, north-western corner.

Two water courses occur within the mine lease area that are of interest to the study namely the Bronkhorstspruit and Koffiespruit. Both the water courses together with a number of pans within the study area form part of the B20A quaternary catchment area, which forms part of the wider Olifants River catchment. Local surface water drainage is towards the watercourses, while the regional drainage direction of the watercourses is towards the north/north-west.

A number of watersheds are located within the study area and the following surface water drainage directions can be deduced from **Figure 4.3-1**:

Table 4.3-1: Surface water drainage directions and gradients

Area	Drainage directions	Surface gradient
West of study area	East	0.9%
	North-west	0.5%
East of study area	West	0.7%
	East	1.2%
North-east corner of lease area	North	0.9%
	South	1.0%
	West	1.4%

4.4 Land use, vegetation, and soil types

The entire mine lease area is classified as high potential arable land with a high agricultural potential. No large scale irrigation takes place within the mine lease area as dryland agriculture is practised.

Approximately 68% of the mine lease area is cultivated, while 32% can be viewed as natural wetland. According to *Acocks' Veld Type Groups* the mine lease area is classified as pure grassveld. The area is covered with red, yellow, and/or greyish soils with low to medium base status (*Van der Watt & Van Rooyen, 1995*).

Evapotranspiration refers to the loss of groundwater recharge through processes such as evaporation and the transpiration of vegetation. Based on this definition, the conclusion can be drawn that evapotranspiration is concentrated along the riparian zones where dense vegetation is often present together with a shallow groundwater table.

Typical evapotranspiration rates for the Olifants catchment area are provided in **Table 4.4-1** (*Ahmad et al, 2005*).

Table 4.4-1: Estimated evapotranspiration rates for the Olifants Catchment

Land Cover	Area (ha)	Mean ET _a (mm/day)	ET _a Volume (m ³)	% ET _a
Cultivated Commercial Dryland				
-Temporal	275026	2.78	7,645,841	15.04
-Permanent	2781	3.19	88,622	0.17
Cultivated Commercial Irrigated				
-Temporal	56065	3.67	2,057,092	4.05
-Permanent	4927	3.64	179,186	0.35
Cultivated Semi-commercial / subsistence dryland	73276	3.04	2,225,593	4.38
Forest and Woodlands	847328	3.51	29,729,685	58.47
Forest Plantations	913	3.82	34,822	0.07
Grasslands	64338	3.48	2,238,421	4.40
Thicket & bushlands	127373	3.49	4,439,428	8.73
Mines and Quarries	900	2.49	22,436	0.04
Urban / built-up land	52197	2.88	1,503,704	2.96
Dongas & sheet erosion scars	1468	4.57	67,088	0.13
Waterbodies	7784	7.92	616,149	1.21

According to **Table 4.4-1** an evapotranspiration rate of 3.2 mm/d can be expected for $\pm 68\%$ of the mine lease covered by dryland agriculture. Even though natural wetlands are not included in the above table, an evapotranspiration rate of ± 6 mm/d can be expected to occur within approximately 32% of the mine lease.

Given the size of the mine lease area, a total volume of ± 40.4 million m³/y, or 110 760 m³/d, is expected to be lost through evapotranspiration.

5. General Description of the Geohydrology

5.1 Hydrocensus Results

A hydrocensus survey was conducted in and around the mine lease area. The objectives of the hydrocensus were as follow:

- Locate and identify all groundwater users,
- Determine all groundwater uses,
- Locate and log boreholes for inclusion into a comprehensive database,
- Measure groundwater levels and sampling of groundwater for the purpose of an inorganic chemical analysis.

During the hydrocensus survey a total of approximately 87 boreholes were located. The positions of the hydrocensus boreholes are indicated in **Figure 5.1-1**, and a short summary is provided in **Table 5.1-1**. A hydrocensus report is included in **Appendix C**.

From the results of the hydrocensus survey it followed that groundwater within the vicinity of the study area is mainly used for domestic purposes, and watering of gardens and livestock. A total of 41 boreholes were sampled during the initial and follow-up hydrocensus surveys. The results of the analyses are discussed in **Section 5.7** of the thesis.

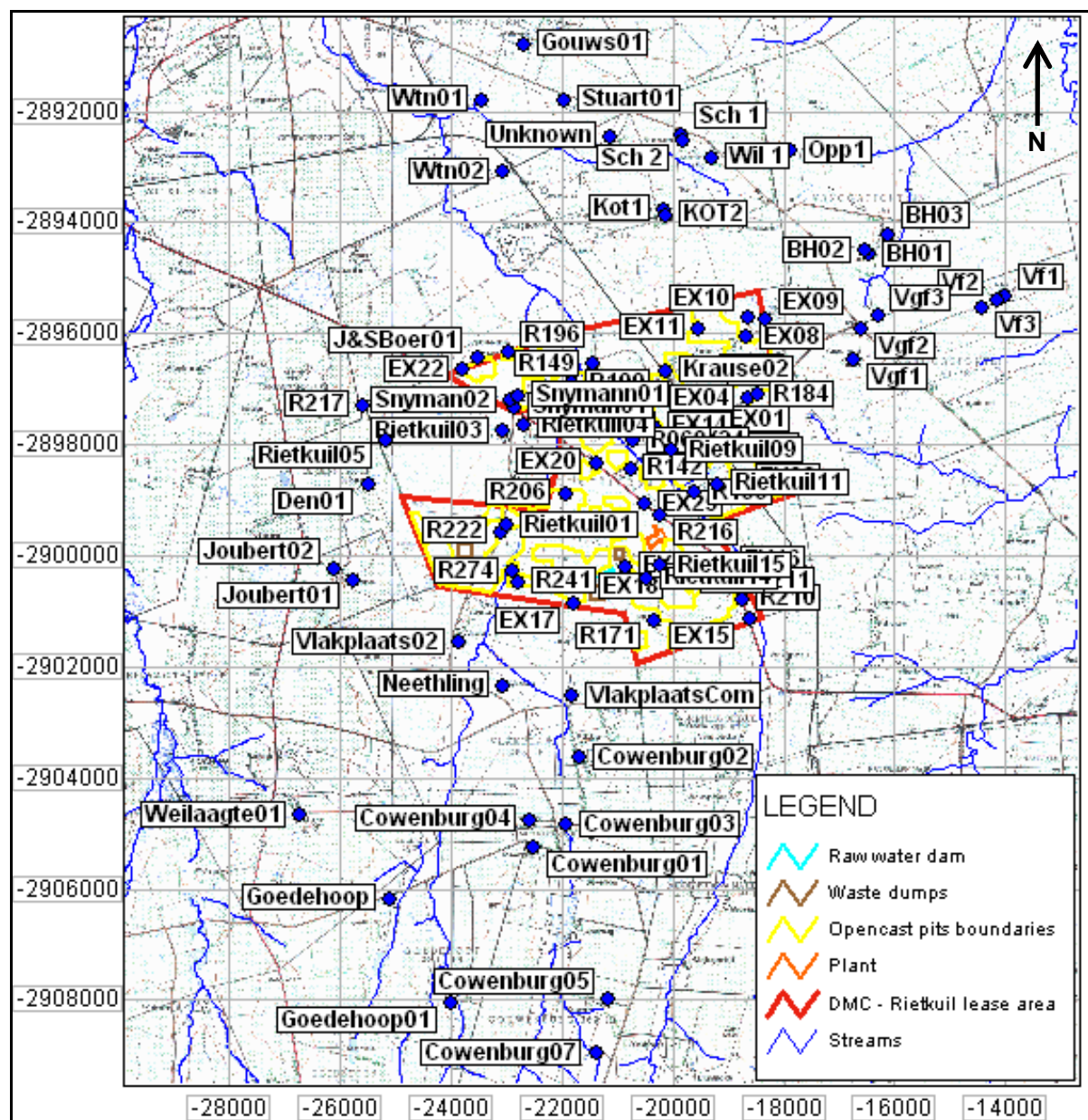


Figure 5.1-1: Positions of hydrocensus boreholes

Table 5.1-1: Summary of hydrocensus survey (Coordinates: WGS84, LO29)

Site Name	Ycoord	Xcoord	Zcoord
BH01	-26.160	28.835	1591
BH02	-26.159	28.835	1593
BH03	-26.157	28.839	1583
Cla 1	-26.108	28.842	1540
Cowenburg01	-26.256	28.775	1602
Cowenburg02	-26.242	28.783	1585
Cowenburg03	-26.253	28.780	1590
Cowenburg04	-26.252	28.774	1602

Site Name	Ycoord	Xcoord	Zcoord
R133	-26.199	28.804	1566
R142	-26.195	28.792	1562
R149	-26.178	28.786	1556
R171	-26.219	28.796	1580
R184	-26.183	28.815	1604
R196	-26.176	28.770	1561
R199	-26.181	28.782	1558
R206	-26.199	28.781	1560

Site Name	Ycoord	Xcoord	Zcoord
Cowenburg05	-26.281	28.788	1630
Cowenburg07	-26.290	28.786	1625
Den01	-26.197	28.745	1600
EX01	-26.187	28.807	1599
EX02	-26.191	28.809	1584
EX03	-26.196	28.813	1583
EX04	-26.183	28.814	1602
EX05	-26.183	28.815	1602
EX06	-26.179	28.807	1599
EX07	-26.178	28.806	1597
EX08	-26.173	28.813	1605
EX09	-26.171	28.817	1598
EX10	-26.170	28.814	1598
EX11	-26.172	28.805	1599
EX12	-26.181	28.782	1558
EX13	-26.178	28.786	1559
EX14	-26.188	28.796	1579
EX15	-26.219	28.814	1577
EX16	-26.210	28.810	1572
EX17	-26.217	28.782	1570
EX18	-26.214	28.784	1570
EX19	-26.211	28.791	1570
EX20	-26.194	28.786	1561
EX21	-26.205	28.769	1574
EX22	-26.179	28.762	1578
EX23	-26.199	28.781	1562
EX24	-26.191	28.800	1584
EX25	-26.200	28.795	1566
Goedehoop	-26.265	28.749	1594
Goedehoop01	-26.282	28.760	1568
Gouws01	-26.126	28.773	1577
J&SBoer01	-26.177	28.765	1579
Joubert01	-26.213	28.742	1607
Joubert02	-26.211	28.739	1605
Kot1	-26.153	28.798	1588
KOT2	-26.154	28.799	1586
Krause02	-26.179	28.799	1585
Morgan01	-26.219	28.796	1593
Neethling	-26.230	28.769	1580
Opp1	-26.143	28.821	1616
R060	-26.190	28.793	1560

Site Name	Ycoord	Xcoord	Zcoord
R210	-26.216	28.812	1573
R211	-26.213	28.811	1576
R216	-26.202	28.798	1566
R217	-26.185	28.744	1587
R222	-26.205	28.769	1573
R241	-26.213	28.772	1564
R265	-26.213	28.803	1574
R274	-26.211	28.771	1566
Rietkuil01	-26.204	28.770	1583
Rietkuil03	-26.189	28.769	1581
Rietkuil04	-26.188	28.773	1574
Rietkuil05	-26.190	28.748	1602
Rietkuil09	-26.192	28.800	1589
Rietkuil11	-26.198	28.808	1581
Rietkuil14	-26.213	28.795	1578
Rietkuil15	-26.211	28.797	1577
RKL01	-26.185	28.744	1587
RKL02	-26.183	28.767	1581
Sch 1	-26.141	28.801	1584
Sch 2	-26.141	28.802	1583
Schalenkamp01	-26.173	28.786	1568
Snyman01	-26.185	28.771	1577
Snyman02	-26.184	28.771	1578
Snymann01	-26.183	28.772	1577
Stuart01	-26.135	28.780	1580
Unknown	-26.141	28.789	1581
Van Rensburg01	-26.155	28.797	1583
Vf1	-26.167	28.860	1594
Vf2	-26.168	28.858	1596
Vf3	-26.169	28.856	1593
Vg1	-26.158	28.839	1580
Vg3	-26.151	28.842	1560
Vgf1	-26.177	28.832	1621
Vgf2	-26.172	28.834	1605
Vgf3	-26.170	28.837	1598
Vlakplaats02	-26.223	28.761	1591
VlakplaatsCom	-26.232	28.782	1588
Weilaagte01	-26.251	28.733	1611
Wil 1	-26.144	28.807	1585
Wtn01	-26.135	28.766	1555
Wtn02	-26.146	28.769	1558

5.2 Depth to Water Level and Flow Gradients/Velocities/Directions

Very few water levels could be measured in boreholes of surrounding farmers, as the boreholes were equipped either with submersible pumps or windpumps. The water levels that could be measured varied between 1.3 and 13 meters below ground level (mbgl). A thematic water level map of the study area is provided in **Figure 5.2-1**.

Water levels exceeding 15 mbgl were also measured within the study area but are not representative of ambient groundwater level conditions, as these water levels are affected by groundwater abstraction. Groundwater levels are of great importance to the thesis as they are used in the calibration of numerical groundwater flow models. In order for the modelling process to be as accurate as possible only those water levels that are not affected by groundwater abstraction are considered.

Under natural/steady state groundwater conditions water levels will more or less follow the surface topography, meaning that higher groundwater level elevations are expected to occur in topographically higher areas than in the lower areas. Under these conditions where there exist a good correlation between water level elevations and the surface topography the *Bayesian Interpolation* method can be used to determine the water levels in areas where no water level information exist.

A statistical analysis was conducted to determine the correlation between the water level elevations and surface topography of the study area and a correlation coefficient/ R^2 of 0.97 was calculated (**Figure 5.2-2**). The result is that there do exist a good correlation between the surface topography and groundwater level elevations of the study area. In such a situation the accuracy of interpolation methods, such as the *Bayesian Interpolation* method increases significantly.

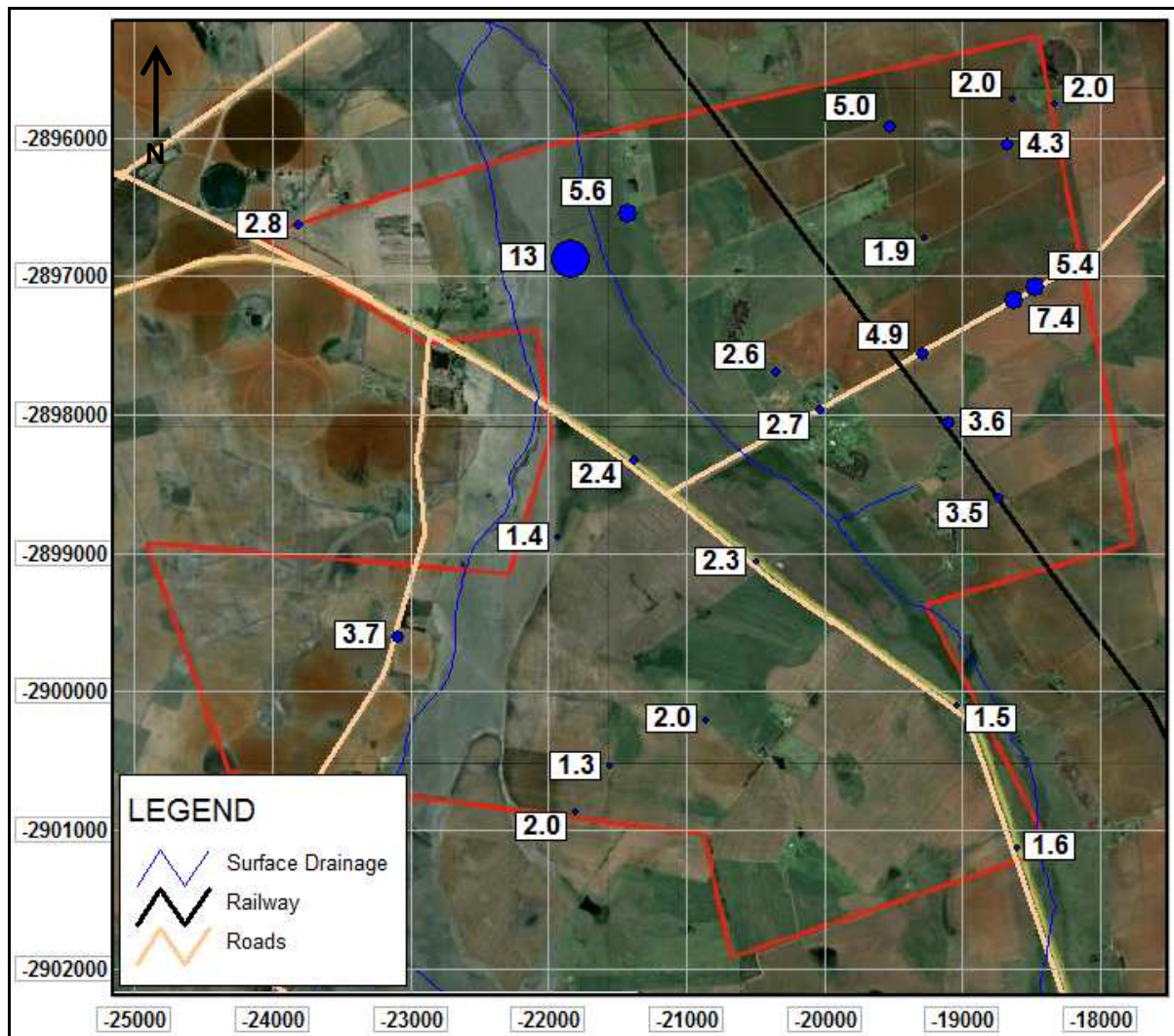


Figure 5.2-1: Thematic water level map of the study area

As mentioned previously, the *Bayesian Interpolation* method is only accurate in areas where there exists a good correlation between the surface topography and water level elevations. In order to do the interpolation one needs the coordinates of a number of boreholes (x, y, and z - axes) as well as their water level elevations (mamsl). Secondly, one needs the coordinates of a number of points within the study area of which the water level elevations are not known.

Assuming a near perfect water level/topography correlation, the *Bayesian Interpolation* method will then determine the correlation that exist between the input topography and water level elevations and assume the same correlation for the second set of coordinates that were required.

Because of this 'assumption', over and under estimations of water level elevations may occur.

Abrupt variations in the surface topography, low aquifer recharge, as well as groundwater abstraction and artificial aquifer recharge may also lead to over and under estimations of the water level elevations when using the *Bayesian Interpolation* method.

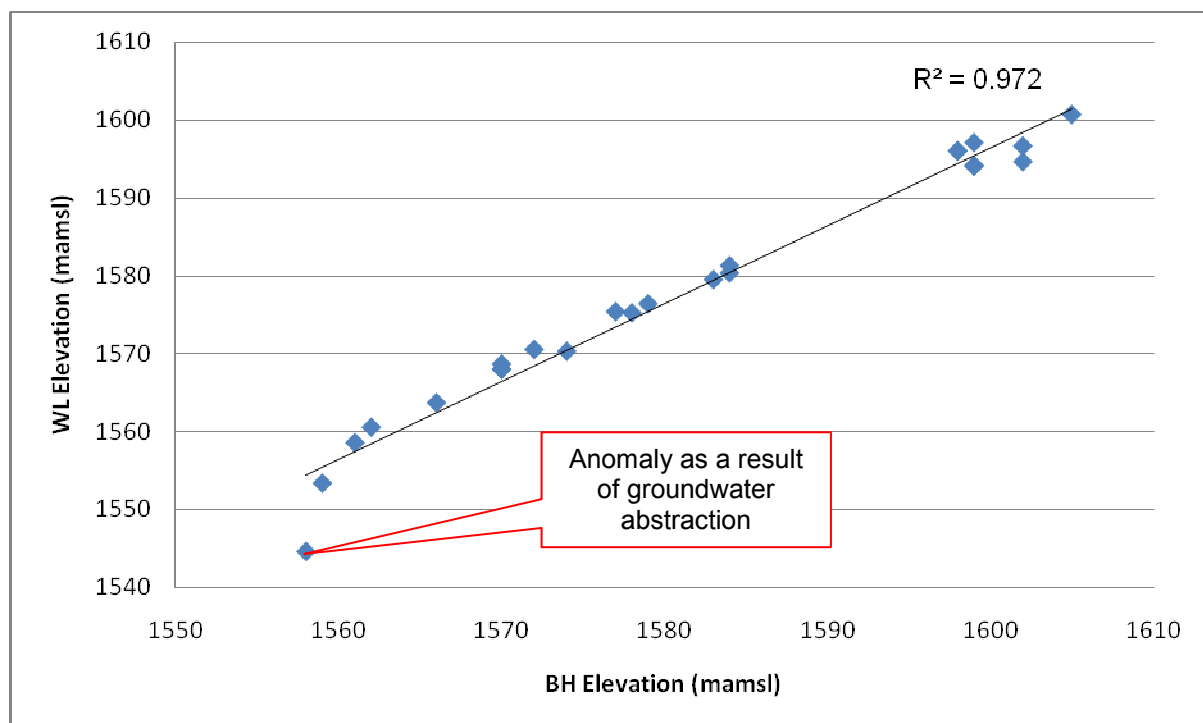


Figure 5.2-2: Water level elevation vs. borehole elevation

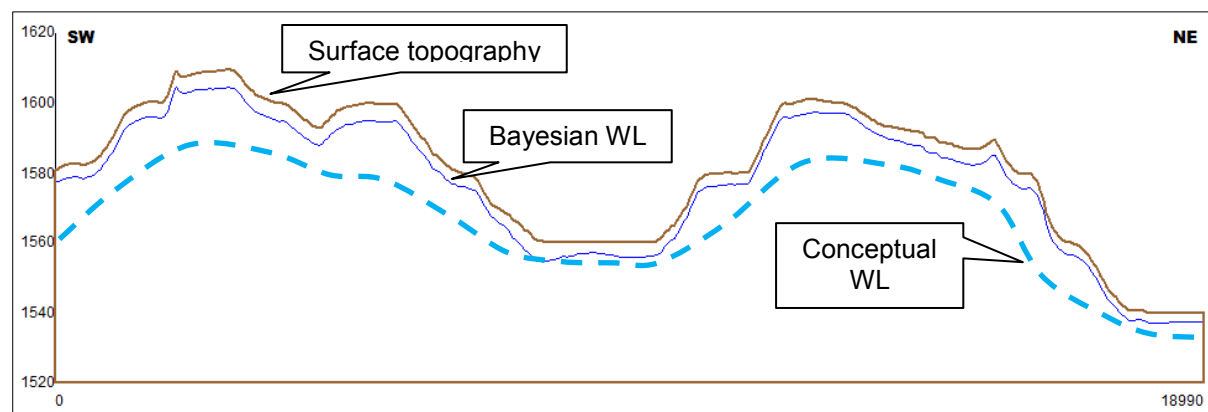


Figure 5.2-3: Limitation of Bayesian interpolation

Bayesian interpolated groundwater levels are indicated in **Figure 5.2-3** in a cross section stretching from the south-western to the north-eastern corner of the study area. The Bayesian water level is represented by a solid blue line, while the surface topography is represented by the solid brown line.

Figure 5.2-3 clearly illustrates how the *Bayesian Interpolation* technique utilises the correlation that exists between the surface topography and groundwater level elevations. It also points out the limitation of the *Bayesian Interpolation* technique. In order to achieve accurate groundwater level elevation estimations with the use of the *Bayesian Interpolation* technique, a **good distribution** of measured groundwater level elevations throughout the study area are required. Even though groundwater levels increase with an increase in the surface elevation, in reality, groundwater levels are closer to the surface along the valley bottoms and lower lying areas. A more realistic representation of groundwater levels is depicted by a dashed blue line.

Figure 5.2-4 represents Bayesian interpolated groundwater elevations of the modelled area, as well as groundwater flow directions as indicated with vectors. The direction of groundwater flow is perpendicular to the groundwater elevation contour lines as indicated in **Figure 5.2-4**. Along hills where groundwater contour lines are concentrated, greater groundwater flow velocities are expected than along flat lying areas where the groundwater contour lines are spaced far between.

Groundwater gradients were calculated using **Equation 3.2-2**. After the groundwater gradients were calculated the groundwater flow velocities were calculated with the following equation:

Equation 5.2-1: Groundwater seepage velocity

$$V = Ki / \alpha$$

Where V	=	Darcy velocity (m/d)
K	=	groundwater hydraulic conductivity (m/d)
i	=	groundwater hydraulic gradient
α	=	effective porosity

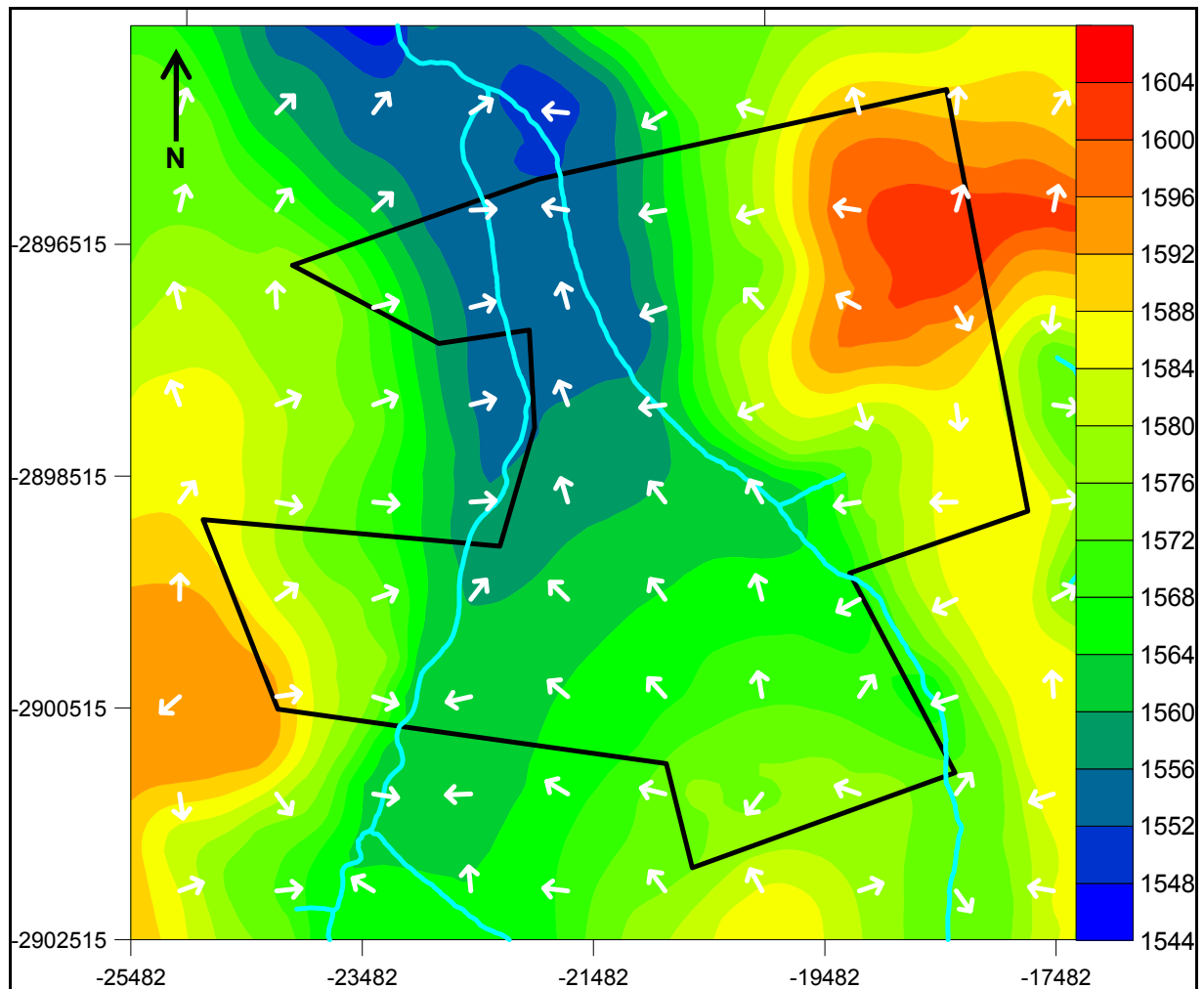


Figure 5.2-4: Bayesian interpolated water level elevation contour map (mamsl)

The groundwater hydraulic conductivity was calculated by dividing the average aquifer transmissivity as provided in **Section 5.4** of the thesis with an average aquifer thickness of 25 meters. Given the porosity information provided in **Table 3.3-1**, a representative Karoo rock porosity of 6% was used in the calculations.

Due to the complex stratigraphy underlying the mine lease area, as indicated in **Appendix A** with the use of exploration borehole logs, an immense amount of porosity tests are necessary to calculate an average aquifer porosity. Porosity tests were therefore not conducted and an educated and representative aquifer porosity was deduced from **Table 3.3-1**.

From the water level elevations depicted in **Figure 5.2-4** the following main groundwater flow directions, gradients, and seepage velocities were identified and calculated:

Table 5.2-1: Groundwater flow directions, gradients, and velocities

Area	GW flow direction	GW gradient	Seepage velocity (m/d)	Seepage velocity (m/y)
West of mine lease	East	1.2%	0.013	4.7
	West	1.3%	0.014	5.1
South-east of mine lease	North-west	0.3%	0.003	1.2
North-east corner of lease area	North	1.5%	0.016	5.8
	South	0.9%	0.009	3.5
	West	1.7%	0.018	6.6
	East	1.4%	0.015	5.5

Overall greater groundwater flow velocities occur in the north-eastern corner of the mine lease, while slower groundwater flow velocities occur south-east of the mine lease.

5.3 Aquifer Types, Thickness, and Yields

An aquifer is defined as a geological formation, or a group of formations that are capable of storing and yielding economical volumes of groundwater (*Vegter, 2001*). The thickness and extent of an aquifer is difficult to define accurately, as it is influenced by fracture extent, orientation, aperture, as well as the thickness of the geological layers.

Three possible aquifers were intersected during the drilling of exploration boreholes:

- Weathered zone aquifer

The aquifer occurs at depths varying between 1 and 25 mbgl. The aquifer is composed of highly weathered Eccca Group rocks and is characterised by relatively high transmissivity values. The unconfined nature of the aquifer and high transmissivity values (compared to the matrix of the fractured rock aquifer) resembles a primary aquifer rather than a secondary aquifer. The aquifer is poorly developed within the study area with yields varying between 0.1 and approximately 1.5 l/s in the dry and wet seasons respectively. Aquifer transmissivity typically varies between 1 and 5 m²/d.

Due to the unreliable nature of the aquifer it is only utilised for the watering of gardens and livestock.

- Fractured rock aquifer

The aquifer is composed of solid/fresh Eccca and Dwyka group rocks and is characterised by low matrix transmissivities, which may be as low as 0.1 m²/d, and large fracture transmissivities varying approximately from 1 to as high as 50 m²/d and higher.

Fracture transmissivity is a highly heterogeneous aquifer parameter and may be influenced by fracture extent and aperture as well as the groundwater level within the aquifer. The movement of groundwater is almost fully restricted to open fractures and fissures. Water level elevations exceeding the elevation of the water strike/s is a common occurrence, due to the semi-confined nature of the aquifer. The yields of boreholes intersecting water yielding fractures vary between 0.1 and 3 l/s. The fractured rock aquifer is considered to be a more reliable source of groundwater compared to the weathered zone aquifer.

- Dolomitic aquifer

Dolomite was intersected at depths varying between 26 and 87 meters below surface with an average depth of 50 meters below surface (**Appendix A**). The aquifer is composed of dolomite, which forms part of the Malmani sub-group of the Transvaal Supergroup. Yields within dolomitic aquifers may vary significantly, as it is determined by the degree of chemical weathering and void formation. One characteristic that separates the dolomitic aquifer from the Karoo rock aquifers is its ability to form large dissolution cavities, which may contain vast volumes of groundwater. The flow of groundwater is fully restricted to open fractures and voids. The yields of boreholes intersecting water bearing dissolution cavities within dolomites may vary from 0 to as high as 40 l/s.

No piezometers were installed, neither in the exploration boreholes nor the monitoring boreholes. Piezometers are installed in areas where multiple aquifer systems are present, in an effort to determine whether any interaction between the different aquifer systems is expected to occur. The installation of piezometers in exploration boreholes (for the purpose of measuring representative piezometric levels in the dolomitic aquifer) are not possible, as the drilling of exploration boreholes were ceased as soon as dolomite was intersected.

5.4 Aquifer Parameters

Only seepage water on the weathered/fresh contacts was intersected during the drilling of the exploration boreholes, which lead to low blow yields. For this reason low rate pumping tests were conducted on 19 boreholes at an average rate of 0.1 l/s. Each borehole was tested for a time period of approximately 15 minutes after which recovery was measured until the borehole recovered to $\pm 90\%$ of its original starting water level. Conventional slug tests are commonly performed on boreholes, but due to the improved accuracy of pumping tests analyses software, much more reliable aquifer parameters are calculated by conducting low rate, short duration pumping tests. The pump tests were analysed with both the *FC-Program* and *Aquitest* and the results of both were compared to one another (**Table 5.4-1**).

Storage coefficient cannot be accurately determined with the use of conventional pumping test analysis techniques because aquifer storativity is dependent on the distance of the observation borehole from the abstraction borehole (*Van Tonder et al, 2004*).

Because of the heterogeneity of the aquifer system the geometric and harmonic mean of the aquifer parameters were calculated. The average of the geometric and harmonic means was then calculated, which gives a good overall indication of the transmissivity of both the fractures and matrix of the study area. There exists a near perfect correlation between the transmissivities calculated with the above mentioned methods.

According to the results of both *Aquitest* and the *FC-Program*, fracture transmissivity within the study area was calculated to be $\pm 1.6 \text{ m}^2/\text{d}$, while the matrix transmissivity was calculated at approximately $0.3 \text{ m}^2/\text{d}$. The T-late values are representative of the matrix flow regime, while the T-early values represent fracture flow – hence lower T-late values.

Table 5.4-1: Aquifer parameters (m^2/d)

Aquitest			FC - Method		
BH	T-early	T-late	BH	T-early	T-late
EX17	0.6	0.3	EX17	0.8	0.3
EX21	1.3	0.7	EX21	2.2	0.7
EX22	1.4	0.4	EX22	1.8	0.4
EX23	4.4	1.2	EX23	4.9	1.4
EX02	2.4	0.2	EX02	2.3	0.2
EX03	1.8	0.4	EX03	2.7	0.3
EX05	3	0.3	EX05	3	0.3
EX12	0.7	0.2	EX12	0.9	0.2
EX13	0.8	0.1	EX13	0.7	0.1
R 60	0.3	0.2	R 60	0.3	0.1
R 133	161	5.1	R 133	98	5.1
R 142	0.5	0.2	R 142	0.5	0.2
R 149	0.6	0.2	R 149	0.6	0.2
R 171	4.6	1.1	R 171	3.9	1.2

Aquitest			FC - Method		
BH	T-early	T-late	BH	T-early	T-late
R 184	4	0.6	R 184	4	0.6
R 199	0.7	0.1	R 199	0.8	0.1
R 216	3.6	1.4	R 216	22.5	1.5
R 241	45.4	0.6	R 241	3.9	0.6
R 265	1.7	0.7	R 265	1.7	0.7
GeoMean:	2.1	0.4	GeoMean:	2.2	0.4
HarMean:	1.1	0.3	HarMean:	1.2	0.3
Average:	1.6	0.3	Average:	1.7	0.3

Notes:

T-early – Transmissivity fracture

T-late – Transmissivity matrix

Geomean – Geometric Mean

Harmean – Harmonic Mean

5.5 Aquifer Delineation and Recharge

Recharge to typical Karoo rocks vary between 1 and 3% of the mean annual rainfall (*Parsons, 2004*). In order to determine the total volume of recharge to the aquifer, the aquifer catchment area must first be defined. The aquifer catchment area is defined as the area towards which rainfall will drain to. Aquifer boundaries are used to define the catchment area and include the following:

- No-flow boundary (Neuman boundary)

No-flow boundaries, or groundwater divides are areas over which the movement of groundwater is not possible. No-flow boundaries may include low transmissivity zones such as dykes or any low transmissivity geological unit, or areas of low or high elevations such as valleys or hills.

- Constant head boundary (Dirichlet boundary)

Constant head boundaries are areas such as perennial rivers or dams where the hydraulic head remains constant, regardless of groundwater abstraction or recharge.

- General head boundary (Cauchy boundary)

General head boundaries are only used in the construction of numerical groundwater flow and mass transport models. These boundaries allow the movement of groundwater through it, according to the hydraulic conductance and hydraulic gradient assigned to the boundary.

The aquifer catchment of the modelled study area is indicated in **Figure 5.5-1** and was defined using groundwater divides.

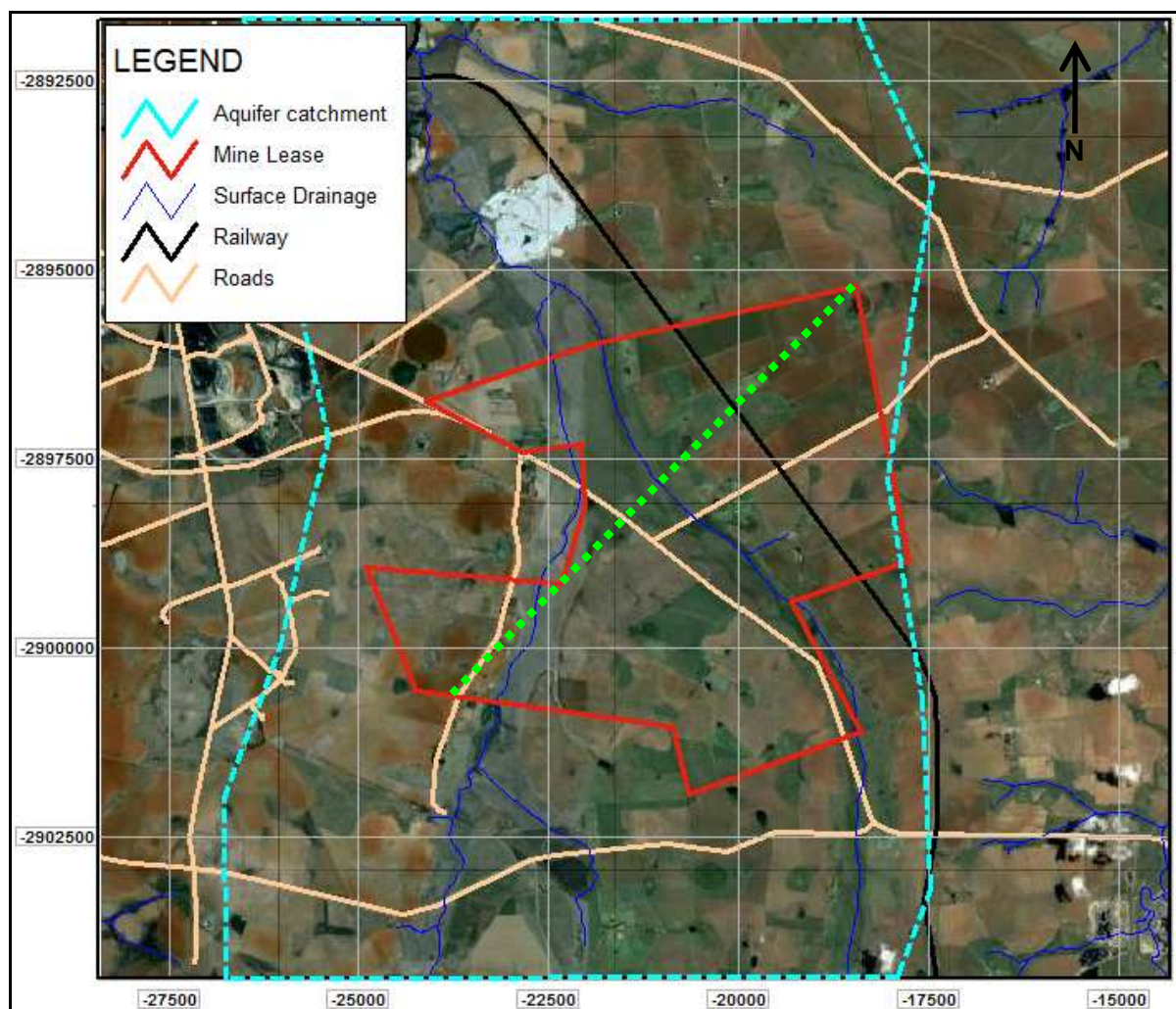


Figure 5.5-1: Aquifer delineation

Notes: The dotted green line indicates the position of the cross section as provided in Figure 5.6-1.

The area of the aquifer catchment, as indicated in **Figure 5.5-1**, is approximately 106 346 000 m². Using an effective aquifer recharge percentage of 3% (*Parsons, 2004*) and an average annual rainfall of approximately 680 mm (*Middleton et al, 1994*), recharge to the aquifer catchment was calculated by multiplying the effective aquifer recharge (3% of MAP) with the catchment surface area. A volume of $\pm 2\,169\,460\text{ m}^3/\text{y}$ ($5\,940\text{ m}^3/\text{d}$) was calculated for the aquifer catchment.

5.6 Generalised Conceptual Model

In order to increase ones understanding of the geohydrological environment, a conceptual model is constructed, which is a simplified, visual representation of real world situations.

A conceptual model is also important as it may emphasize any areas which lack field data. Because an aquifer system is highly heterogeneous, one must be careful not to oversimplify the construction thereof.

Recharge to the aquifer, as defined in **Figure 5.5-1**, will be slightly higher in the higher elevated areas or where rocky outcrops occur. Valleys or lower elevated areas will receive less recharge due to the accumulation and deposition of clayey material. This phenomenon is better known as a catena, or toposequence. A catena is defined as “a sequence of soils with similar age and parent material, but which have differences in properties caused by their relative topographical positions on a hillslope” (*Fox & Rowntree, 2000*). Clayey material, due to its weight and size relative to the surrounding material, will therefore be flushed out of the soils found on ridges and will be transported to the valley bottoms due to the forces of gravity. The result is an accumulation of clayey material within the valley bottoms, which will ultimately lead to a decrease in aquifer recharge.

As have already been mentioned in **Section 5.3** of the thesis, three aquifers are likely to occur within the study area. The first, the weathered zone aquifer is poorly developed throughout the study area – more so in the higher elevated areas and rocky outcrops.

Along valley bottoms where weathering is more intense the aquifer thickness may increase. Reasonable yields only occur during the wetter summer months of the geohydrological year.

Recharge will seep through the soil profile and weathered zone until a more impermeable layer is encountered to form a perched aquifer. The water will then seep on the contact of the impermeable layer in the downgradient direction.

No perched aquifer was intersected during the drilling of the exploration boreholes, which means that recharge will seep through the unsaturated zone until it reaches the saturated zone from where it will flow in the downgradient direction. The groundwater will then ultimately flow into a groundwater compartment or be discharged in surface water bodies such as rivers and dams/pans.

Dolerite dykes are prominent geological features throughout the Mpumalanga coal fields. Dykes are more often than not preferred flow paths for groundwater, which is the result of fracture formation along the sides of the structure. Despite the high transmissivity zones along the sides of dykes, their overall low transmissivity enables them to form groundwater compartments. Groundwater intersecting a dyke will cause an anomaly within the local groundwater level, with groundwater upwelling occurring in the upstream direction of the structure.

The direction and rate of groundwater flow is determined by the groundwater gradients and aquifer transmissivity. Under natural/steady state conditions groundwater will flow from higher to lower hydraulic gradients. Steep hydraulic gradients and high aquifer transmissivity will allow for greater groundwater seepage velocities. Groundwater flow directions, gradient, and Darcy velocities were calculated and are provided in **Table 5.2-1**.

Groundwater flow within the second, the fractured rock aquifer is mostly restricted to open fractures and joints due to the low matrix transmissivity of the Karoo type aquifers. The geometry of the Karoo rocks are undulating, and weathering along rivers and streams have caused thin aquifers in some areas, and very thick Karoo aquifers in areas where weathering of the rocks were less intense.

As with the Karoo aquifers, flow within the third, the dolomitic aquifer is also restricted to open fractures, joints and cavities. The main difference between the Karoo type aquifer and Transvaal dolomitic aquifer is the ability of the dolomitic aquifer to form large dissolution cavities. These cavities within the dolomitic aquifer may have infinitely high transmissivity and high storativity values and could therefore store vast volumes of groundwater.

The process by which dissolution cavities are created is known as chemical weathering. The chemical weathering of rocks that are composed of carbonaceous minerals (such as dolomite and limestone) creates very prominent structures that are known as “karst” structures. The following components all play a role in the rate and direction of the chemical weathering process (*Nichols, 1999*):

- Water

Water, and in the context of this study, groundwater, is the medium in which all chemical reactions occur. In the absence of groundwater, the formation of dissolution cavities cannot take place. In order for a dissolution cavity to form, fractures must intersect the carbonaceous rock, which will act as preferred flow paths for groundwater. The flow of groundwater through these pathways will lead to an increase in the rate and extent of the chemical reactions/weathering.

- Climate

Temperature plays a very important role in specifically the rate at which chemical reactions take place. An increase in temperature will cause a significant increase in the rate of chemical reactions. Calcium carbonates are interestingly the exception to the rule, as they are more soluble in cold water.

- Chemistry of groundwater

Groundwater pH is an important factor, as the presence of acids greatly increases the rate of chemical reactions. A decrease in groundwater pH will therefore lead to an increase in the rate of chemical weathering.

Groundwater will move towards dissolution cavities, as water tends to follow the route of least resistance. Excessive groundwater abstraction from water bearing dissolution cavities may cause the roof to become unstable, and will ultimately lead to a collapse in the roof of the subsurface cavity – thus forming a sinkhole.

Figure 5.6-1 is a south-west to north-east cross section of the mine lease area. Due to the limited amount and distribution of coal seam data, local over- and under estimations of the elevations of the coal seams and Dwyka tillite is most likely to occur during the interpolation process (as indicated in **Figure 5.6-1**).

Unfortunately no piezometers were installed, neither in the exploration boreholes nor the monitoring boreholes. Groundwater level differences and interaction between the three aquifer systems could therefore not be discussed in full detail. The underlying dolomite was not included in **Figure 5.6-1** because of the lack of available data.

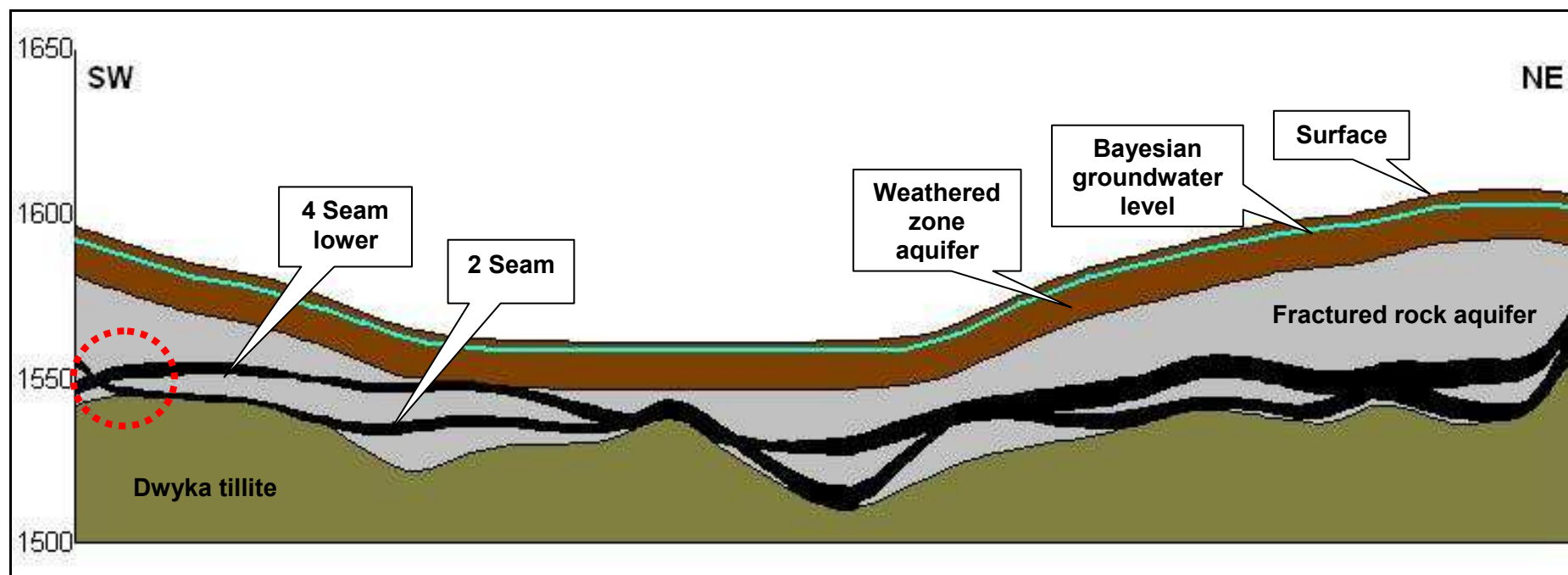


Figure 5.6-1: Conceptual model of study area

Notes:

- The limited amount and distribution of coal seam data have lead to some anomalies in the interpolation process, as pointed out in **Figure 5.6-1** with the use of a dotted red circle.
- The position of the cross section is indicated in **Figure 5.5-1**.

5.7 Groundwater Quality Evaluation

Groundwater quality information was obtained from the following sources:

- A hydrocensus that was conducted within the study area and its surroundings,
- The National Groundwater Data Base, and
- Surrounding coal and silica mines.

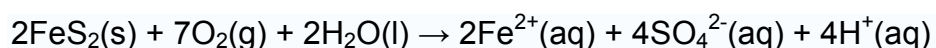
Due to the fact that the study was carried out at a greenfields coal mining operation and the majority of the groundwater quality information is only available from once-off measured hydrocensus boreholes, the construction of time-series graphs and interpretations thereof is not possible. Groundwater samples collected during the hydrocensus were analysed by a SANAS Accredited Testing Laboratory and the results are provided in **Appendix C**.

The following factors may influence groundwater quality:

- Geology of the area

The geology of an area plays an important role in groundwater quality. Many sedimentary and igneous rocks contain reactive minerals that may create acidic conditions when in contact with oxygen and water. These reactions are collectively referred to as *Acid Mine Drainage* reactions (AMD).

Sulfide bearing minerals, of which pyrite (FeS_2) is the most abundant, will react with water in an oxidising environment to form sulphuric acid, H_2SO_4 (Manahan, 1991):



Sulphuric acid is a strong acid and will mobilise most heavy metals, which will lead to widespread contamination of the aquifer system. AMD is specifically associated with coal mines as pyrite is abundant in most carbonaceous material.

Many sedimentary rocks contain water that was trapped within pores during their deposition. This water is known as pore or connate water, and is usually brine as a result of extensive ion exchange reactions.

As the pressure and temperature steadily increase (as more material is deposited), the connate water will be released from the pores and will cause an increase in the salinity of the surrounding groundwater.

Geological structures such as dykes are known to create separate groundwater compartments of which the groundwater chemistry differs from the surrounding aquifer. Groundwater compartments may receive less recharge than the surrounding aquifer, which will ultimately lead to an increase in the groundwater salinity.

- Aquifer recharge and groundwater residence time

The residence time of groundwater refers to the time that groundwater remains within an aquifer before it is discharged into surface water bodies. An increase in the residence time of groundwater will lead to an increase in groundwater salinity, given that the aquifer is composed of reactive minerals. When groundwater is in contact with reactive minerals ion exchange will cause the groundwater to become progressively more saline.

Under natural geohydrological conditions, one can distinguish between groundwater within higher elevated areas and groundwater found within valley bottoms or lower elevated areas. Groundwater found within the higher elevated areas will plot within field one or two of the Expanded Durov diagram, which represents fresh, recently recharged groundwater that has undergone a minimum degree of ion exchange. The groundwater chemistry will therefore closely resemble the chemical composition of fresh rainwater due to the limited degree of ion exchange.

As the groundwater migrate in the downgradient direction, an increase in aquifer residence time will lead to an increase in the degree of ion exchange, which will ultimately lead to higher salinity groundwater found within the lower elevated areas or valley bottoms.

A high hydraulic conductivity, good aquifer recharge, and sufficient groundwater gradients will mobilise groundwater, which will minimise the amount of time that groundwater spends within an aquifer and will lead to improved groundwater quality.

- Unsaturated zone

The unsaturated zone is defined as the area between the water table and the land surface. The unsaturated zone is of great importance, as it plays a role in the recharge of an aquifer as well as the quality of the groundwater. The unsaturated zone acts as a filter that will filter out any solids in the water before it enters the aquifer.

The volume of water that will filter through the unsaturated zone is determined by its composition and thickness. If the unsaturated zone is composed of clayey or other impermeable material only a small volume of water will filter through it and enter the aquifer. Because hydrogeology focuses on the saturated zone rather than the unsaturated zone, very little is known of the unsaturated zone regarding chemical reactions, infiltration rates, etc.

The thickness of the unsaturated zone is determined by subtracting the surface elevation from the groundwater level elevation. As evident from **Table 5.7-1**, the unsaturated zone within the study area varies between 1.3 and 13.4 meters, with an average thickness of 3.7 meters.

The above mentioned factors are all natural factors, or inherent aquifer characteristics.

Table 5.7-1: Thickness of unsaturated zone

BH	BH elevation (mamsl)	WL elevation (mamsl)	Unsaturated thickness (m)
EX01	1599	1594.13	4.9
EX02	1584	1580.35	3.7
EX03	1583	1579.51	3.5
EX04	1602	1594.60	7.4
EX05	1602	1596.62	5.4
EX06	1599	1597.06	1.9
EX08	1605	1600.66	4.3
EX09	1598	1595.97	2.0
EX10	1598	1596.02	2.0
EX11	1599	1594.03	5.0
EX12	1558	1544.65	13.4
EX13	1559	1553.41	5.6
EX14	1579	1576.40	2.6
EX15	1577	1575.40	1.6
EX16	1572	1570.55	1.5
EX17	1570	1568.03	2.0
EX18	1570	1568.69	1.3
EX19	1570	1568.00	2.0
EX20	1561	1558.60	2.4
EX21	1574	1570.32	3.7
EX22	1578	1575.25	2.8
EX23	1562	1560.59	1.4
EX24	1584	1581.29	2.7
EX25	1566	1563.73	2.3
RKL01	1584	1574.95	9.1
RKL02	1574	1568.78	5.2
R211	1570	1571.69	1.7

*Notes: The thickness of the unsaturated zone is directly proportional to the depth of the groundwater level below surface. A thematic map the groundwater level depth below surface, or thickness of the unsaturated zone is provided in **Figure 5.2-1**.*

There are numerous methods of displaying and defining the type of groundwater that occurs within an area. Two of the most frequently used methods are the Expanded Durov diagram (EDD) and Stiff diagrams. Each field of the EDD represents groundwater dominated by different anions and cations, which in turn represents groundwater that is at different stages of the hydrogeological cycle.

The different fields of the EDD are indicated in **Figure 5.7-1**, after which a short description of each field follows (*Freeze & Cherry, 1979*).

A Stiff diagram on the other hand plots major cations and anions on opposite sides of a y-axis, with the x-axis representing the concentration of the ions in meq/l. By plotting the ions in this manner, each different type of groundwater will have its own unique geometry.

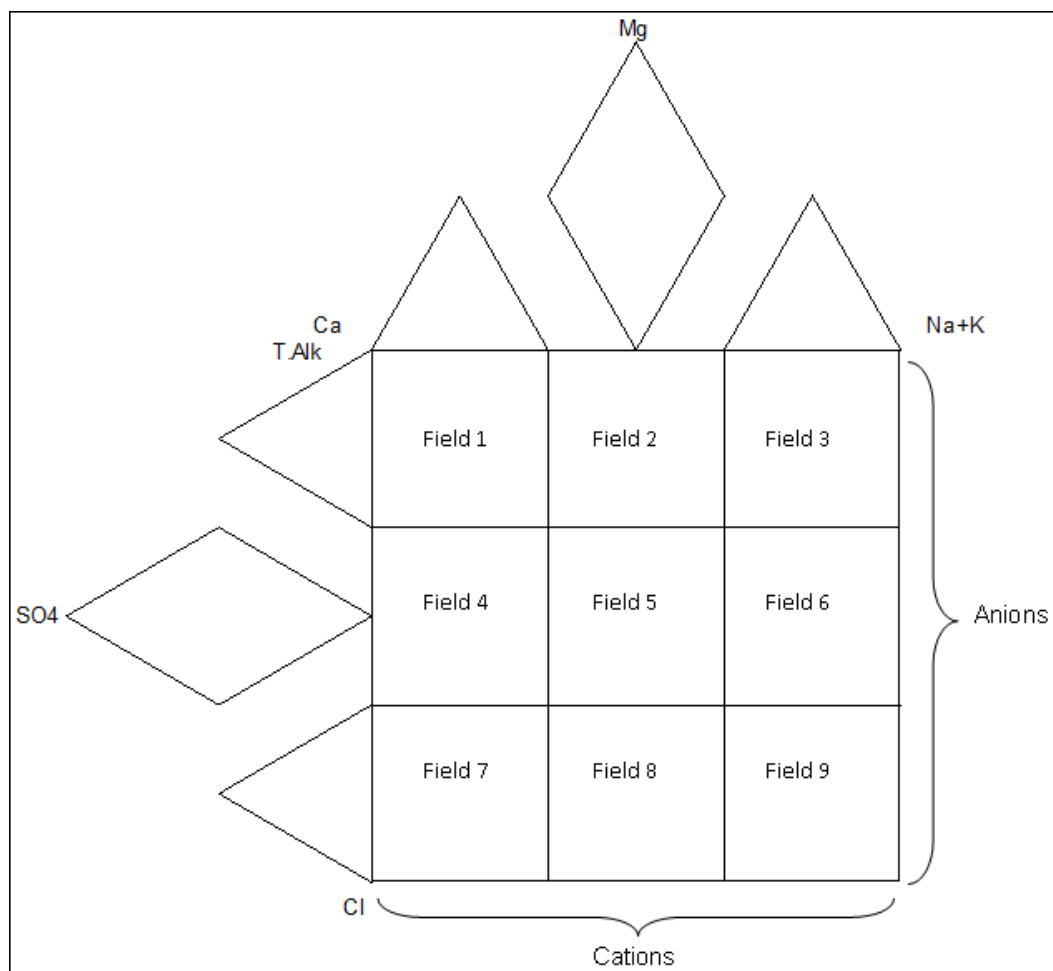


Figure 5.7-1: Layout of the EDD

The fields of the EDD represent the following:

Field 1

Fresh, very clean, recently recharged groundwater with alkalinity and calcium dominated ions.

Field 2

Fresh, clean, relatively young groundwater that has started to undergo magnesium ion exchange, often found in dolomitic terrain.

Field 3

Fresh, clean, relatively young groundwater that has undergone sodium ion exchange (sometimes in sodium enriched granites or other felsic rocks). The dominance in sodium may also be as a result of sodium enriched pollution.

Field 4

Fresh, recently recharged groundwater that is dominated by calcium cations and sulphate anions. The sulphate enrichment may be as a result of acid mine drainage reactions.

Field 5

Groundwater that is usually a mix of different types – either clean water from fields 1 and 2 that has undergone SO_4 and NaCl mixing/contamination or old stagnant NaCl dominated water that has mixed with clean water.

Field 6

Groundwater from field 5 that has been in contact with a source rich in Na or old stagnant NaCl dominated water that resides in Na rich host rock/material.

Field 7

Water rarely plots in this field that indicates NO_3 or Cl enrichment or dissolution.

Field 8

Groundwater that is usually a mix of different types – either clean water from fields 1 and 2 that has undergone SO_4 , but especially Cl mixing/contamination or old stagnant NaCl dominated water that has mixed with water richer in Mg.

Field 9

Old or stagnant water that has reached the end of the geohydrological cycle (deserts, salty pans etc) or water that has moved a long time and/or distance through the aquifer or on surface and has undergone significant ion exchange because of the long distance or residence time in the aquifer.

Although all major macro elements were analysed for, only the elements that are expected to show concentration increases within a coal mining environment will be discussed. All analysed elements were however studied and discussed where anomalies did occur.

The following chemical parameters are discussed in the thesis:

- pH – pH is an important parameter as it determines the solubility of metals within groundwater. Most metals are immobile in groundwater of which the pH varies between 5 and 9 units. pH decreases are also a good indication of the presence of acid mine drainage reactions (AMD), which occur when sulphide bearing minerals such as pyrite is exposed to an oxidizing environment in the presence of groundwater and microbial organisms.
- Total Dissolved Solids (TDS) – the TDS of groundwater is a good overall indication of the quality of groundwater, as it is a measurement of the total volume of salts in solution. TDS increases are generally linked to pH decreases.
- Sodium and Potassium – sodium and potassium are found in high concentrations in groundwater which has undergone a high degree of sodium, or potassium ion exchange.

- Sulphate – sulphate contamination is associated with the oxidation of sulphide bearing minerals such as pyrite (acid mine drainage reactions – AMD). As mentioned previously, sulphate contamination will under most conditions lead to a decrease in the pH of groundwater due to the formation of sulphuric acid.
- Nitrate – nitrate contamination is predominantly associated with nitrate based explosives within a mining environment, which is commonly used in South African mines. Another major source of nitrate contamination includes raw, untreated sewage.
- Chloride – elevated chloride concentrations are generally due to the inherent high chloride concentrations that exist in some sedimentary rocks. High chloride concentrations are also associated with old, stagnant groundwater that has undergone a reasonable degree of ion exchange.
- Iron – elevated iron concentrations is a good indication of the presence of acid mine drainage reactions. As previously discussed, AMD reactions will more often than not lead to a decrease in groundwater pH, and the subsequent mobilisation of metals.

The positions of the boreholes of which groundwater chemistry data are available are indicated in **Figure 5.7-2**. Groundwater quality information was obtained for a total of 106 boreholes. Borehole names are not included in the figure, as name tags would clutter the image.

All chemical parameters will be compared to the South African Drinking Water Standards, as provided in **Table 5.7-2**. Because only once off monitoring data are available, no increasing or decreasing concentration trends could be identified, nor can explanations be given for anomalies with a high degree confidence.

Table 5.7-2: South African Drinking Water Standards – SANS: 241 (2005)

Parameter	Ideal	Recommended	Absolute Maximum
mg/l			
TDS	0 – 1000	1000 – 2400	>2400
pH	5 – 9.5	4.5 – 5, 9.5 – 10	<4.5, >10
Sodium	0 – 200	200 – 400	>400
Potassium	0 – 50	50 – 100	>100
Sulphate	0 – 400	400 – 600	>600
Nitrate	0 – 6	6 – 20	>20
Magnesium	0 – 70	70 – 100	>100
Chloride	0 – 200	200 – 600	>600
Calcium	0 – 150	150 – 300	>300

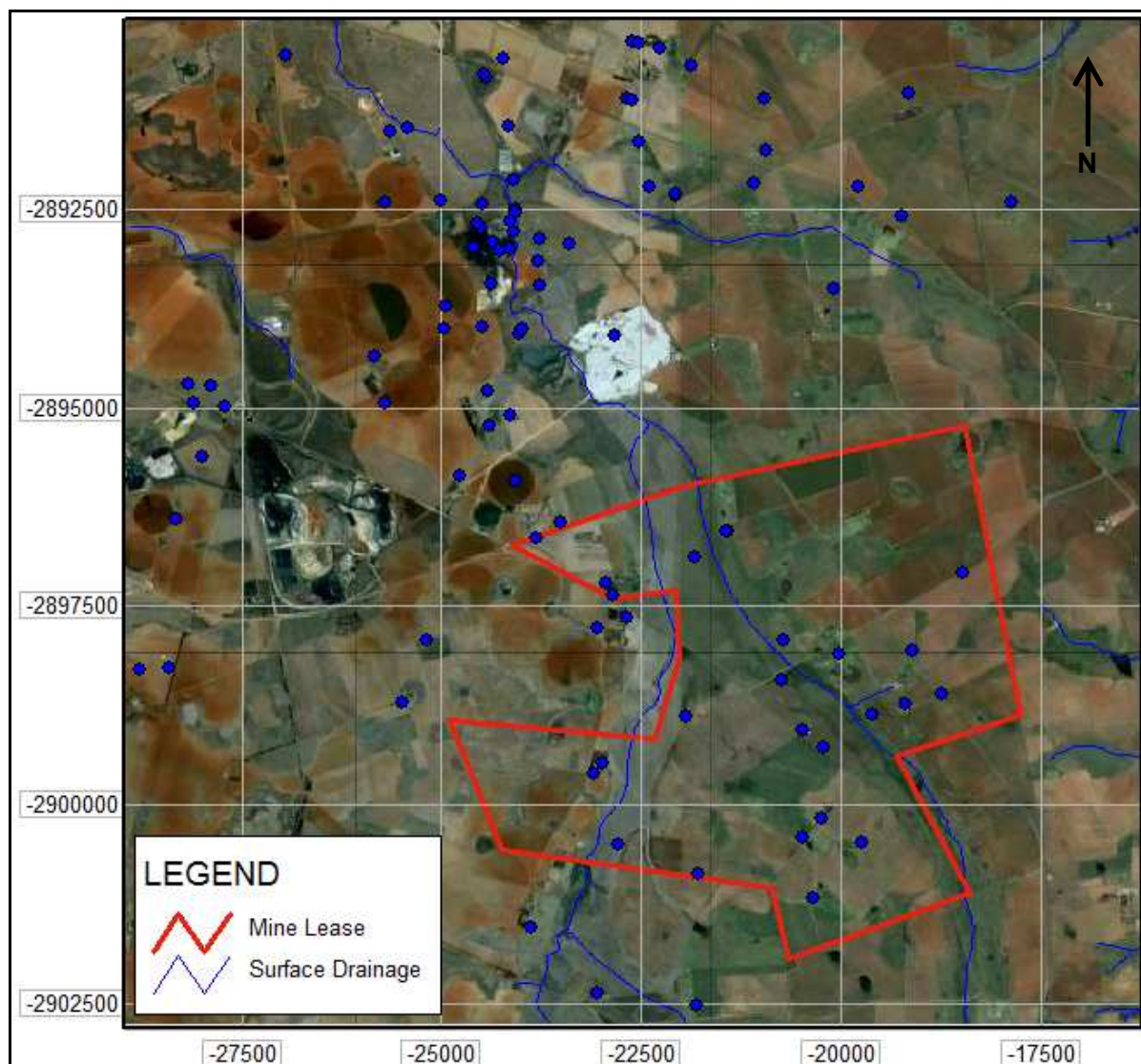


Figure 5.7-2: Regional and site specific borehole distribution

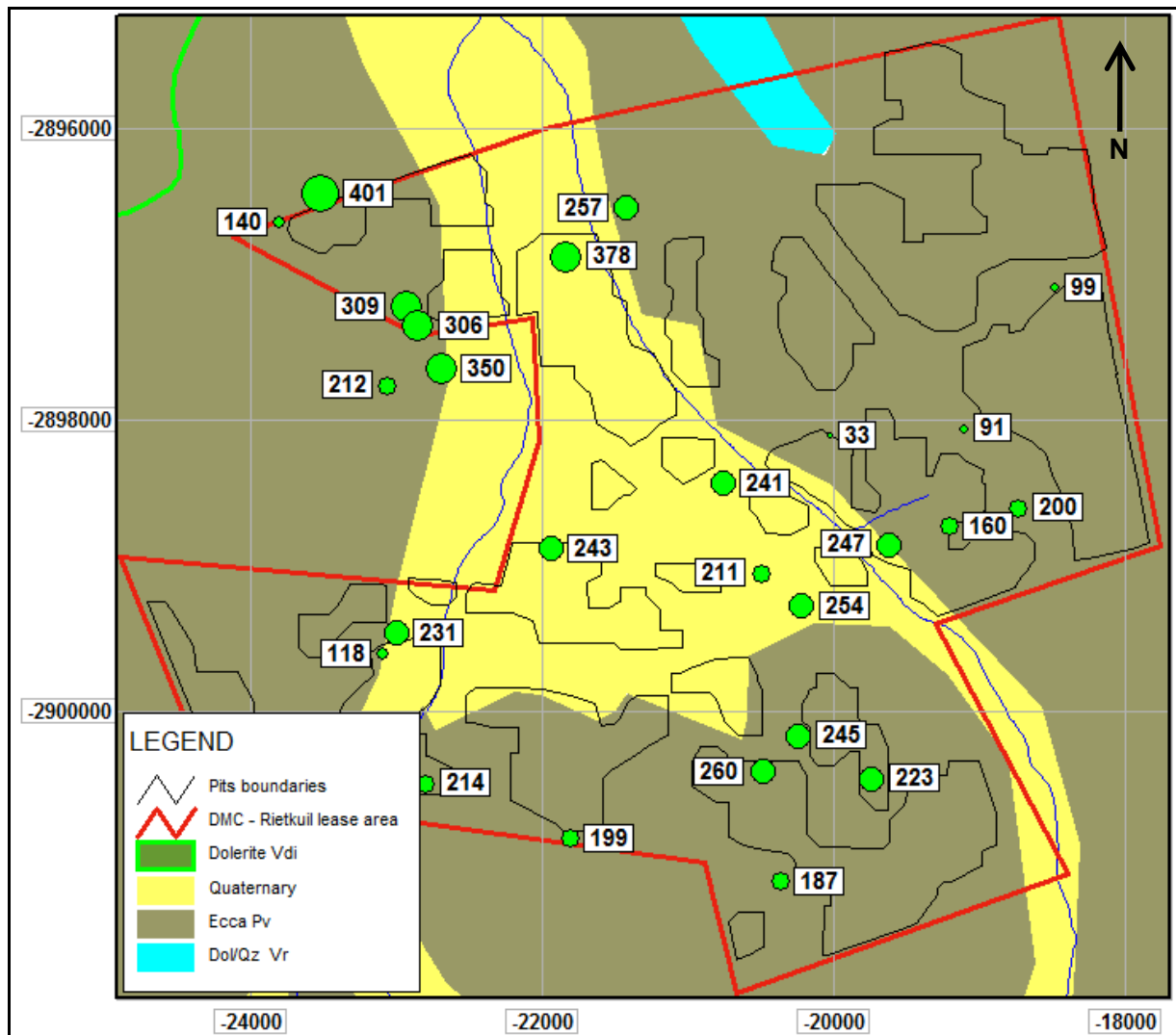


Figure 5.7-3: Thematic TDS concentration map of the mine lease area (mg/l)

TDS is a good indicator of the overall groundwater quality. TDS concentrations of both site specific and regional groundwater monitoring boreholes vary between 20 and 760 mg/l, which are within the ideal limits for domestic use. Groundwater salinity does appear to increase from the higher elevated areas towards the valley bottoms as a result of increased ion exchange reactions.

When plotting groundwater TDS concentrations against the underlying geology of the mine lease area (**Figure 5.7-3**), it becomes clear that there exists no clear-cut correlation. The conclusion can therefore be drawn that the groundwater within the mine lease is unaffected by the underlying geology.

Groundwater pH conditions are more or less neutral throughout the entire study area and vary between 6.4 and 9. Neutral groundwater pH conditions is a good indication of the absence of acid mine drainage reactions. AMD reactions require oxygen and water to occur and will therefore not take place within a reducing environment. The carbonaceous material underlying the study area is therefore likely to be located below the local groundwater level where oxygen concentrations are subsequently low.

Most metals are insoluble under such neutral groundwater conditions, which is why the majority of metal concentrations are within the ideal and recommended ranges for domestic use (**Table 5.7-2**). Elevated iron concentrations do however occur to the north-west (downstream) of the mine lease area where coal mining has been ongoing for an extensive time period.

Sulphide concentrations vary between 1 and 390 mg/l, which is within the ideal ranges (**Appendix C**). Sulphide concentrations increase towards the north-western downstream direction from the mine lease where mining activities are concentrated and have been ongoing for an extensive time period.

Magnesium, sodium and potassium concentrations are all well within the ideal ranges for domestic use. Chloride concentrations show the same trend and are all within the ideal ranges according to the South African Drinking Water Standards.

Because of the sheer number of monitoring boreholes, only those within the mine lease area were selected for the Expanded Durov diagram provided in **Figure 5.7-4** and the Stiff diagrams in **Figures 5.7-5** and **5.7-6**.

According to the EDD the following types of groundwater occur within the mine lease area:

- Groundwater dominated by magnesium cations and bicarbonate alkalinity. The groundwater plot within **Field 2** of the EDD, which represents recently recharged, fresh groundwater of which calcium was replaced with magnesium in the geohydrological cycle,

- Groundwater that is dominated by sodium/potassium cations and bicarbonate alkalinity. **Field 3** of the EDD represents groundwater that is relatively fresh and has undergone sodium/potassium cation exchange,
- Groundwater dominated by magnesium cations and sulphate anions. **Field 5** represents a dominance in sulphate, which may indicate contamination from a sulphate rich source or the presence of acid mine drainage reactions.

The Stiff diagrams (**Figures 5.7-5 and 5.7-6**) further confirm the presence of three main types of groundwater, as indicated in **Figure 5.7-4**. Boreholes Rietkuil04 and EX22 are the exceptions with their chemistries plotting in field 8 of the EDD. Field 8 represents groundwater dominated by magnesium cations and chloride anions. Such groundwater is typically found within groundwater compartments of which low aquifer recharge and low groundwater gradients cause increased groundwater residence time, which ultimately leads to a high degree of ion exchange within the geohydrological cycle.

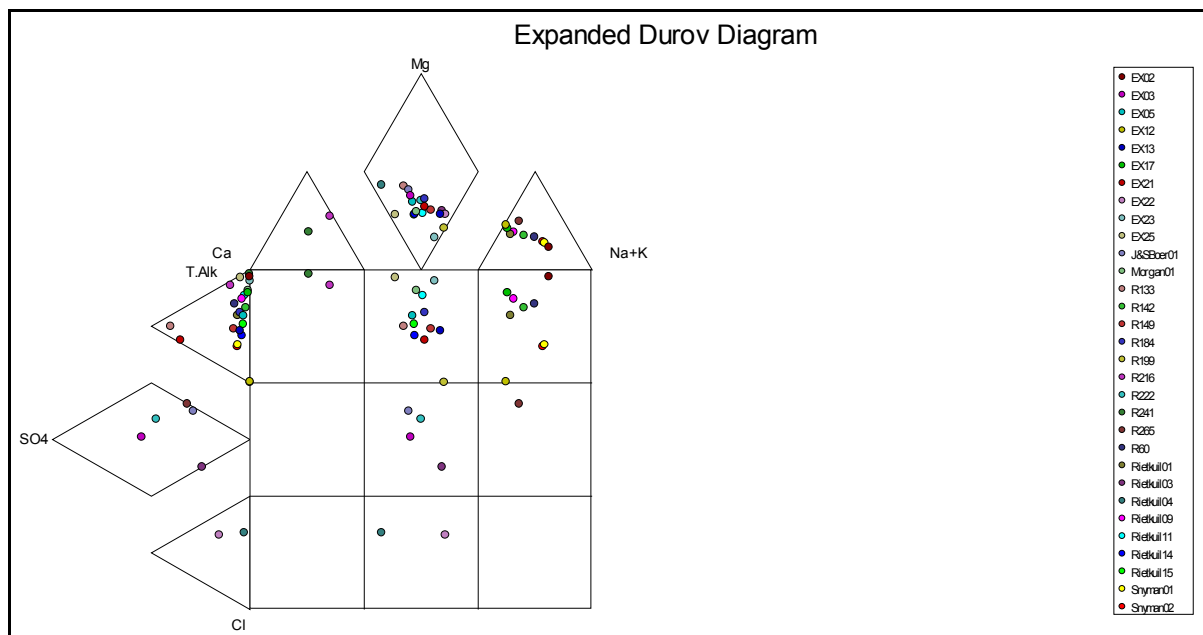


Figure 5.7-4: Expanded Durov diagram of site specific monitoring boreholes

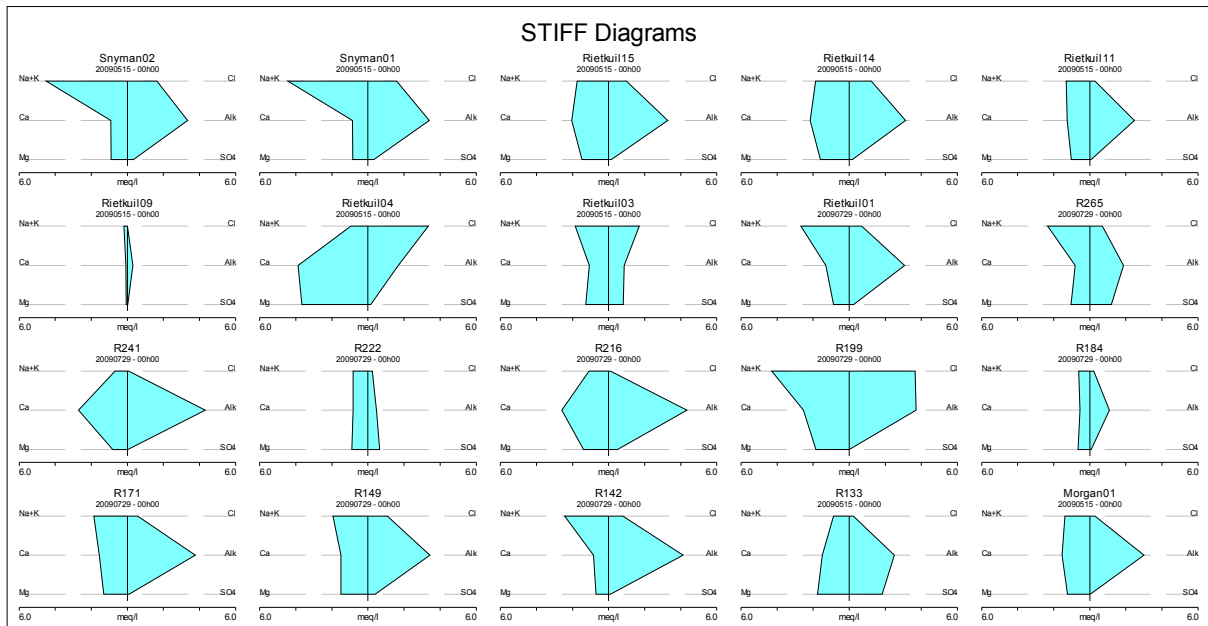


Figure 5.7-5: Stiff diagrams of site specific groundwater qualities

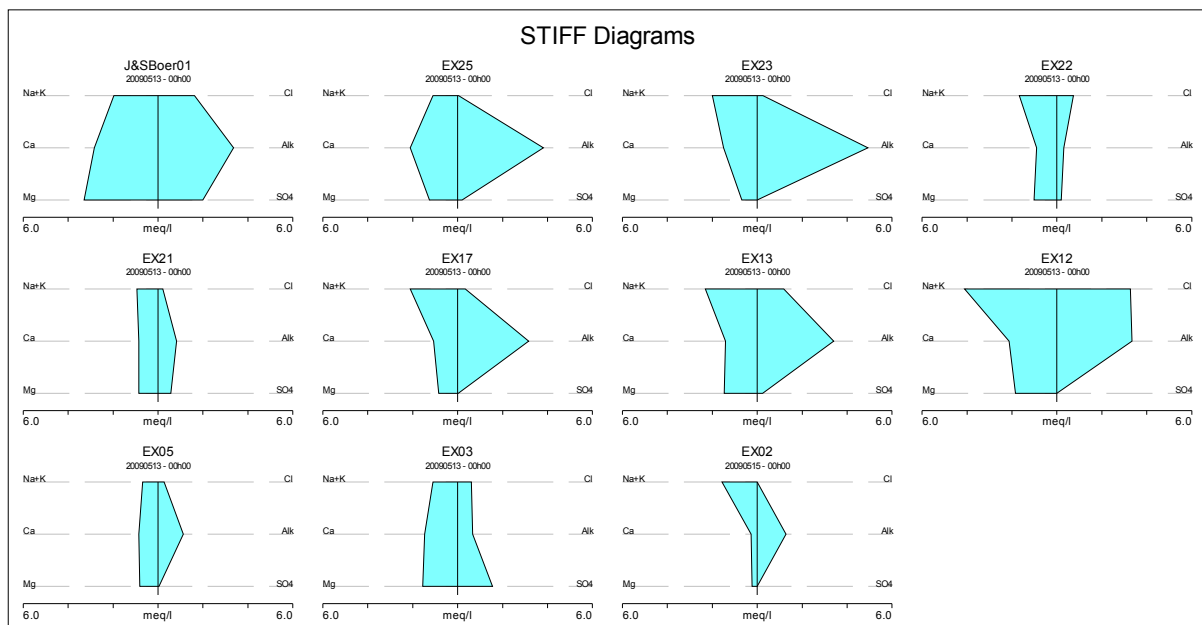


Figure 5.7-6: Stiff diagrams of site specific groundwater qualities

Summary:

- The majority of chemical parameters are within the ideal and recommended ranges for domestic use according to the South African Drinking Water Standards,
- Groundwater quality seems to deteriorate towards the north-western downstream direction where coal mining activities are concentrated and have been ongoing for an extensive time period,
- A slight increase in groundwater salinity occurs along the valley bottoms due to increased residence time,
- No clear correlation exists between groundwater quality and the underlying geology of the mine lease area,
- Groundwater within the mine lease area is of good quality and is suitable for human consumption,
- Three main types of groundwater occur within the mine lease area, namely:
 - groundwater dominated by magnesium cations and bicarbonate alkalinity,
 - groundwater dominated by magnesium cations and sulphate anions,
 - groundwater dominated by sodium/potassium cations and bicarbonate alkalinity.
- The neutral pH conditions and low iron and sulphate concentrations all point towards the absence of acid mine drainage reactions within the mine lease area.

6. Numerical Decant Calculations and Groundwater Discharge

6.1 Pre-mining numerical groundwater flow model

In order to meet the objectives as stated in **Section 1.2** of the thesis a numerical groundwater flow model was constructed using *Processing Modflow Pro*. Due to the size of the area under investigation the model area was not defined using any groundwater boundaries as discussed in **Section 5.5**. The modelled area is indicated in **Figure 6.1-1**, which also indicates the general head boundaries and river nodes that were used in the construction of the numerical groundwater flow model.

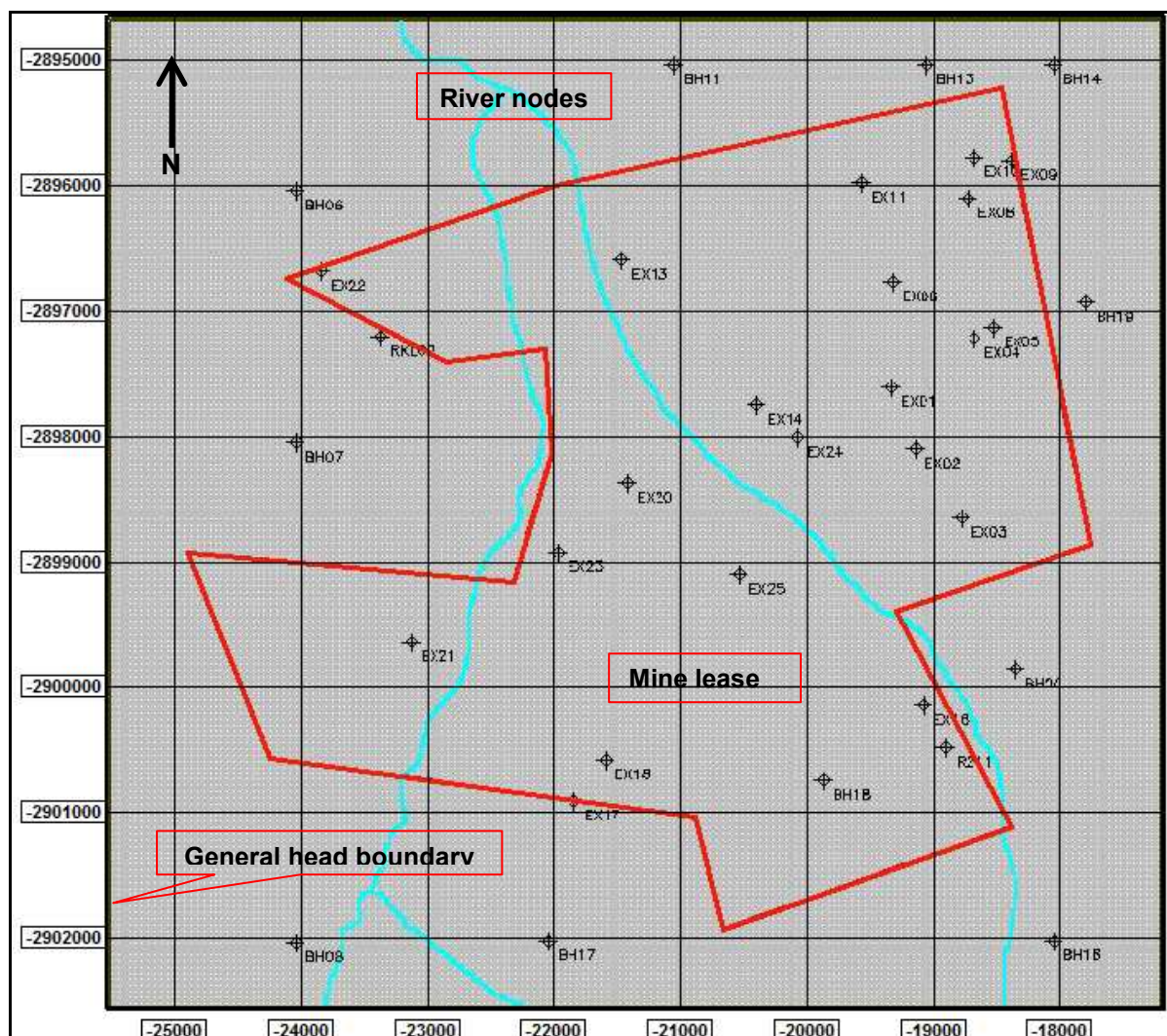


Figure 6.1-1: Model grid with river nodes and no-flow boundaries

The model consists of 227 850 cells (17 x 17 meters each) and covers an area of approximately 66 km² (7.9 x 8.3 kilometres).

The numerical groundwater flow model was constructed using two layers, thus a three dimensional model. The dolomitic aquifer was not included as a third layer in the numerical groundwater flow model, because of a lack of sufficient data.

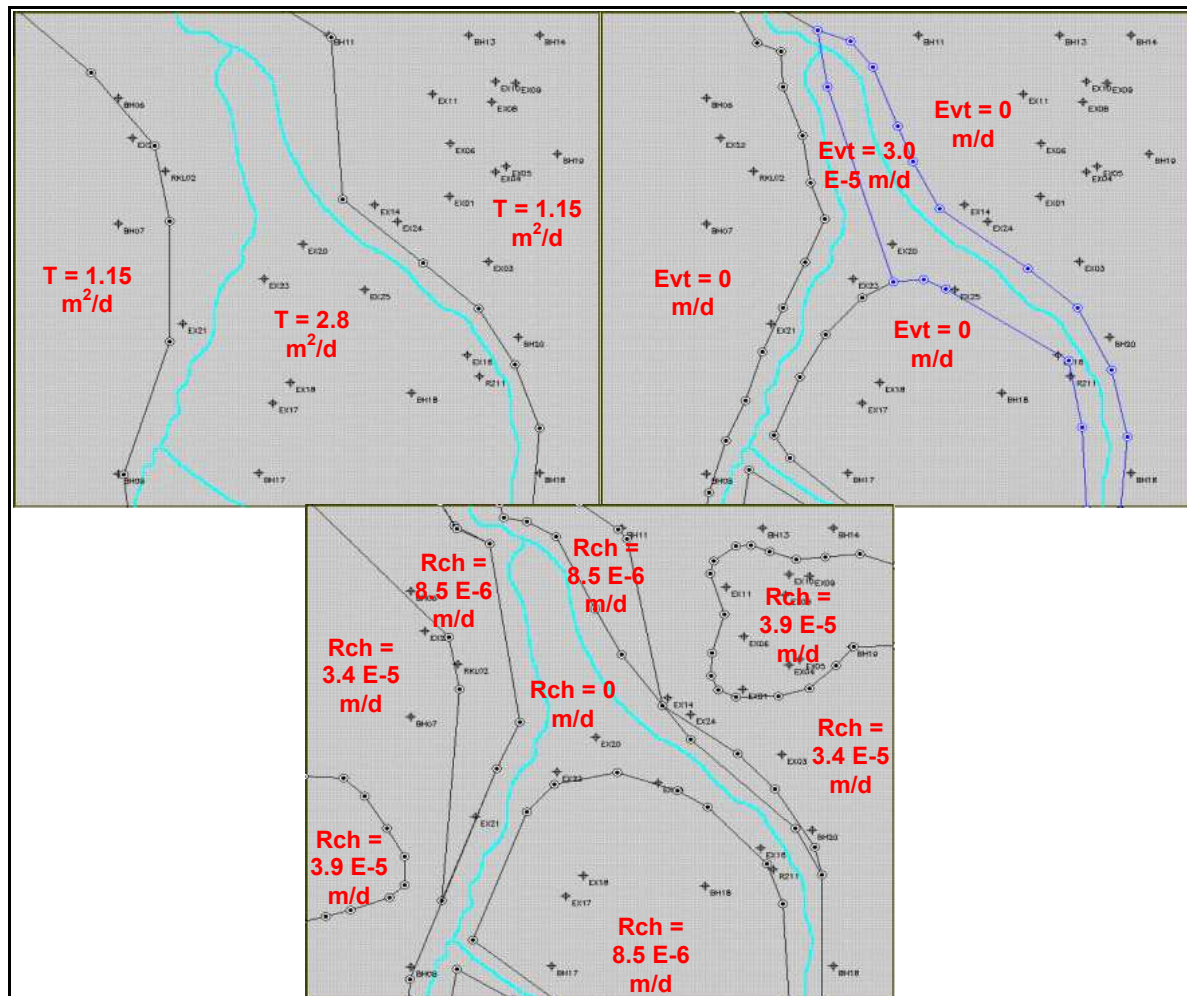


Figure 6.1-2: Model parameters and parameter values

Notes:

T - Aquifer transmissivity (m²/d)

Evt - Evapotranspiration (m/d)

Rch - Effective aquifer recharge (% of Mean Annual Precipitation)

- Layer 1

Layer 1 represents the weathered zone aquifer and is unconfined, as discussed in **Section 5.3** of the thesis. The layer is 15 meters thick with a vertical difference of approximately 56 meters between the highest and lowest elevations. **Figure 6.1-2** illustrates the parameters that were used to construct the model as well as the values assigned to the parameters.

According to the simplified geological map of the study area (**Figure 4.1-1**), significant quaternary deposits occur within the immediate vicinity of both the Bronkhorstspuit and Koffiespruit. A slightly higher aquifer transmissivity was therefore assigned to these areas (**Figure 6.1-2**).

As discussed in **Section 3.2** of the thesis, significant volumes of groundwater are lost within the riparian zones as a result of evapotranspiration. For this reason, evapotranspiration was assigned to the areas within close proximity of the Bronkhorstspuit and Koffiespruit (**Figure 6.1-2**). As a result of evapotranspiration, no recharge was assigned to those areas located within the riparian zone.

The topographically lower lying areas were assigned lower recharge compared to the higher lying areas. This was done in an effort to simulate the effects of a catena or toposequence, as discussed in **Section 5.6** of the thesis.

- Layer 2

Layer two of the model represents the fractured Karoo rock aquifer and is confined, as discussed in **Section 5.3** of the thesis. The layer was assigned a transmissivity of $0.55 \text{ m}^2/\text{d}$.

Groundwater elevations obtained from surrounding mines and hydrocensus boreholes were used to calibrate the numerical groundwater flow model. The parameters and parameters values assigned to the model during calibration are indicated in **Figure 6.1-2**.

During the calibration process, the groundwater hydraulic head for each model cell is calculated with mathematical equations. The calculated heads are then compared to the actual measured heads. The model parameters are adjusted until an acceptable correlation is obtained between the calculated and measured hydraulic heads.

A correlation of 97% (**Figure 6.1-3**) was achieved during calibration of the numerical groundwater flow model in steady state. Model calibration is of utmost importance as it will greatly influence the accuracy of the model simulations – the quality of the numerical simulations are thus completely dependent upon the quality of the field data used for model calibration.

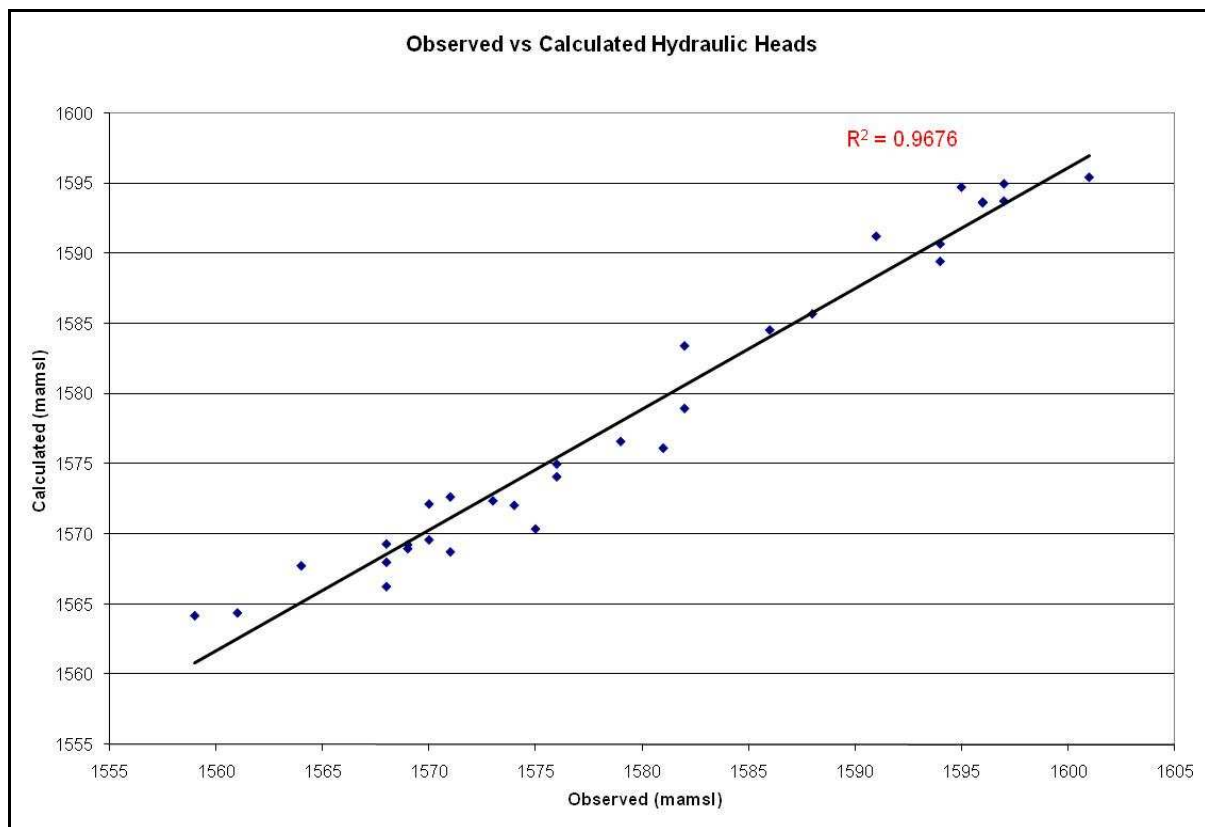


Figure 6.1-3: Numerical groundwater flow model calibration

Stress periods were assigned to the numerical groundwater flow model according to the mine schedule and are provided in **Table 6.1-1**. A model stress period is a given time within the model during which the model parameters remain unchanged.

Table 6.1-1: Model stress periods and simulations

Stress period	Time (years)	Simulation
1 - 2	2	Active mining of opencast pits 2 and 3; mining of pit 2 ceases at the end of stress period 2.
3	1	Active mining of opencast pits 3 and 4; mining of pits 3 and 4 ceases at the end of stress period 3.
4	1	Active mining of opencast pits 5 and 6; mining of pit 5 ceases at the end of stress period 4.
5 - 6	2	Active mining of opencast pits 1 and 6.
7	1	Active mining of opencast pits 1, 6, and 7; mining of pits 1 and 6 ceases at the end of stress period 7.
8	1	Active mining of opencast pits 7, 8, 9, and 10; mining of pits 8, 9, and 10 ceases at the end of stress period 8.
9	1	Active mining of opencast pits 7, 11, and 12; mining of pits 11 and 12 ceases at the end of stress period 9.
10	1	Active mining of opencast pits 7, 13, and 14; mining of pit 13 ceases at the end of stress period 10.
11 - 15	5	Active mining of opencast pits 7 and 14; mining of pit 14 ceases at the end of stress period 15.
16	1	Active mining of opencast pits 7 and 15; mining of opencast pits 7 and 15 ceases at the end of stress period 16.
17	1	Active mining of opencast pits 16 and 17; mining of pit 16 ceases at the end of stress period 17.
18	1	Active mining of opencast pits 17 and 18; mining of pit 18 ceases at the end of stress period 18.
19	1	Active mining of opencast pits 17, 19, 20, and 21; mining of pits 17 and 19 ceases at the end of stress period 19.
20	1	Active mining of opencast pits 20, 21, and 22; mining of pits 20 and 22 ceases at the end of stress period 19.
21 - 22	2	Active mining of opencast pits 21 and 23; mining of pit 23 ceases at the end of stress period 22.
23	1	Active mining of opencast pits 21 and 24; mining of pit 24 ceases at the end of stress period 23.
24 - 28	5	Active mining of opencast pit 21; all mining activities cease at the end of stress period 28.

According to **steady state** flow model simulations both the Koffiespruit and Bronkhorstspruit are gaining streams, which were determined by conducting a water budget. The zones around which the water budget was conducted are indicated in **Figure 6.1-4**.

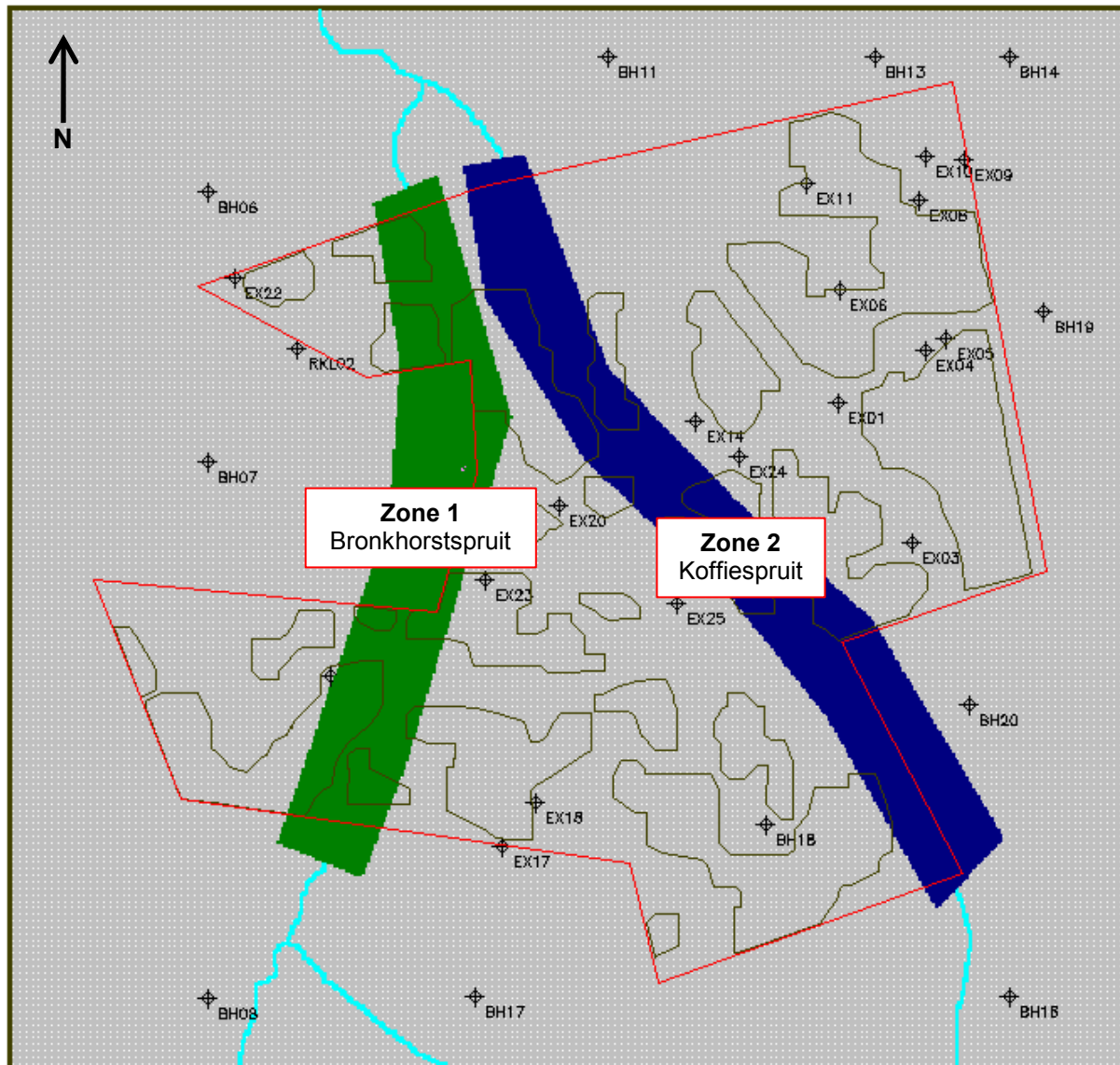


Figure 6.1-4: Water budget zones

The implication is that groundwater is discharged from the surrounding aquifer into the two streams. A groundwater discharge of **90 m³/d into the Bronkhorstspuit**, and **130 m³/d into the Koffiespruit** were calculated during model simulations.

Groundwater discharge (baseflow) to surface water bodies is reduced during active mining, as a result of mine dewatering and the lowering of local groundwater levels.

According to transient state model simulations, as discussed in **Table 6.1-1**, groundwater discharge into the **Bronkhorstspruit** was reduced to 30 m³/d, while discharge into the **Koffiespruit** was reduced to only 20 m³/d at the end of stress period 28.

6.2 Post-closure numerical groundwater flow model

Because aquifer hydraulic conductivity, specific yield, and storage coefficient are time-independent model parameters, a post-closure model was generated in order to simulate the effects of the increased transmissivity, specific yield, storage coefficient, as well as recharge of the **backfilled opencast pits**. Affected groundwater level contours exported from stress period 28 were used as an initial or starting water level, and the model was assigned 50 stress periods (5 years each).

A total of 9 different model scenarios were run with regards to the backfilled opencast pits and are explained in **Table 6.2-1**.

Table 6-2-1: Post-closure model simulations

Scenario	Recharge	T	Pit S _y	Aquifer S
1	10%	1.15, 2.8	0.06	0.008
2	10%	25	0.12	0.01
3	10%	50	0.18	0.012
4	13%	1.15, 2.8	0.06	0.008
5	13%	25	0.12	0.01
6	13%	50	0.18	0.012
7	16%	1.15, 2.8	0.06	0.008
8	16%	25	0.12	0.01
9	16%	50	0.18	0.012

Notes:

T - Transmissivity (m²/d)

S_y - Specific yield; May be as high as 0.20 – 0.25, depending on nature of backfill material and process

S - Storage coefficient of bottom layer

From **Table 6.2-1** it is clear that scenarios 1, 4, and 7 simulates pre-mining aquifer conditions with varying degrees of aquifer recharge, while the remainder of the model scenarios simulates increases in transmissivity, specific yield, and storage coefficient as a result of backfilling of the opencast pits.

During post closure model simulations (Scenario 5 of **Table 6.2-1**) the following discharges to the surface water streams were simulated:

Table 6.2-2: Simulated post closure baseflow (m³/d)

Years (post closure)	Bronkhorstspuit	Koffiespruit
5	140	50
10	230	90
15	330	130
20	420	150
25	510	200
50	700	570

According to post closure model simulations (**Table 6.2-2**), a steady increase in groundwater discharge to both the Bronkhorstspuit and Koffiespruit takes place as soon as active mining ceases. The increase in groundwater baseflow is the direct result of increased recharge and transmissivity of the backfilled opencast pits.

Groundwater decant occurs when a mine void, or a backfilled mine void is filled with groundwater to the decant elevation where the groundwater will discharge onto the surface, or into the high transmissivity weathered zone. In an opencast coal mining environment decanting will occur at the lowest surface elevation that is intersected by mining. Groundwater levels depicted in **Figure 6.2-1** are merely theoretical and are used to illustrate the concept of a decanting opencast pit.

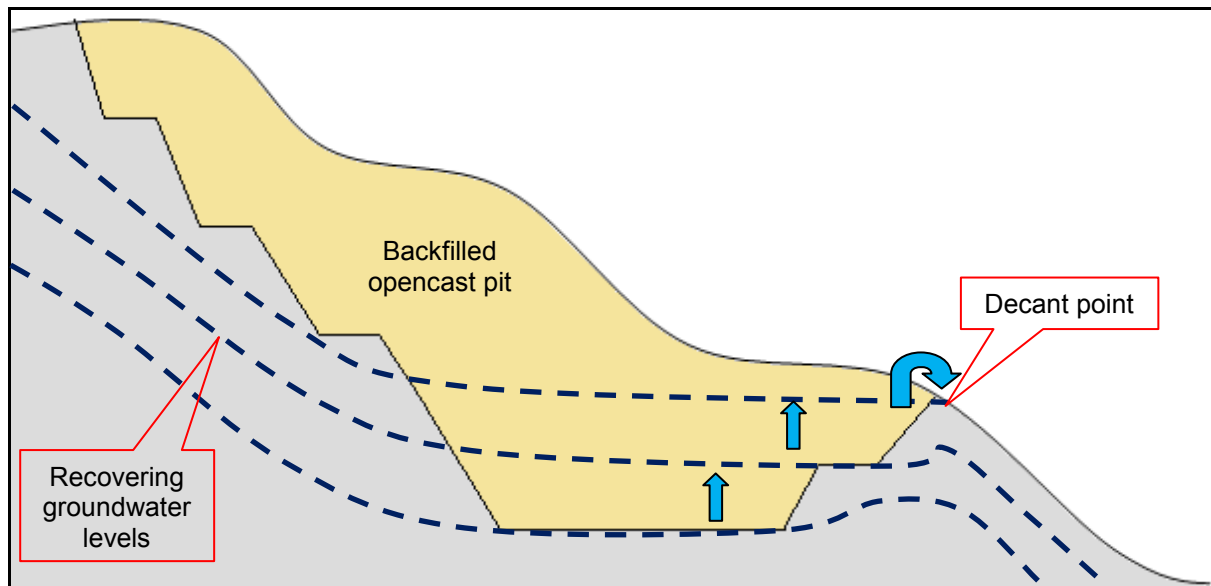


Figure 6.2-1: Concept of decanting groundwater

During active mining, a cone of depression is created more or less radially around the opencast pit. The shape and extent of the cone of depression is determined by the following factors:

- Transmissivity of the surrounding aquifer/s,
- The presence of geological structures such as dykes and faults that could act as preferred flow paths for groundwater,
- Depth of mining below the static groundwater level,
- Aquifer recharge rate, and
- Rate of mining, and the size of the opencast pit.

During active mining the groundwater level is lowered to below the base of the lowest mineable elevation, and the mine void will effectively act as a groundwater sink. The mine void will continue to act as a groundwater sink until a new groundwater level equilibrium has been reached, well after closure.

As soon as mining and mine dewatering has ceased, the groundwater levels will tend to recover to pre-mining conditions. Due to the high transmissivity and porosity of the backfill material, the mine void will act as a preferred flow path for groundwater. The natural groundwater flow direction will therefore be influenced.

Figure 6.2-2 indicates the opencast pits, as well as the expected decant positions that were simulated in the numerical groundwater flow model.

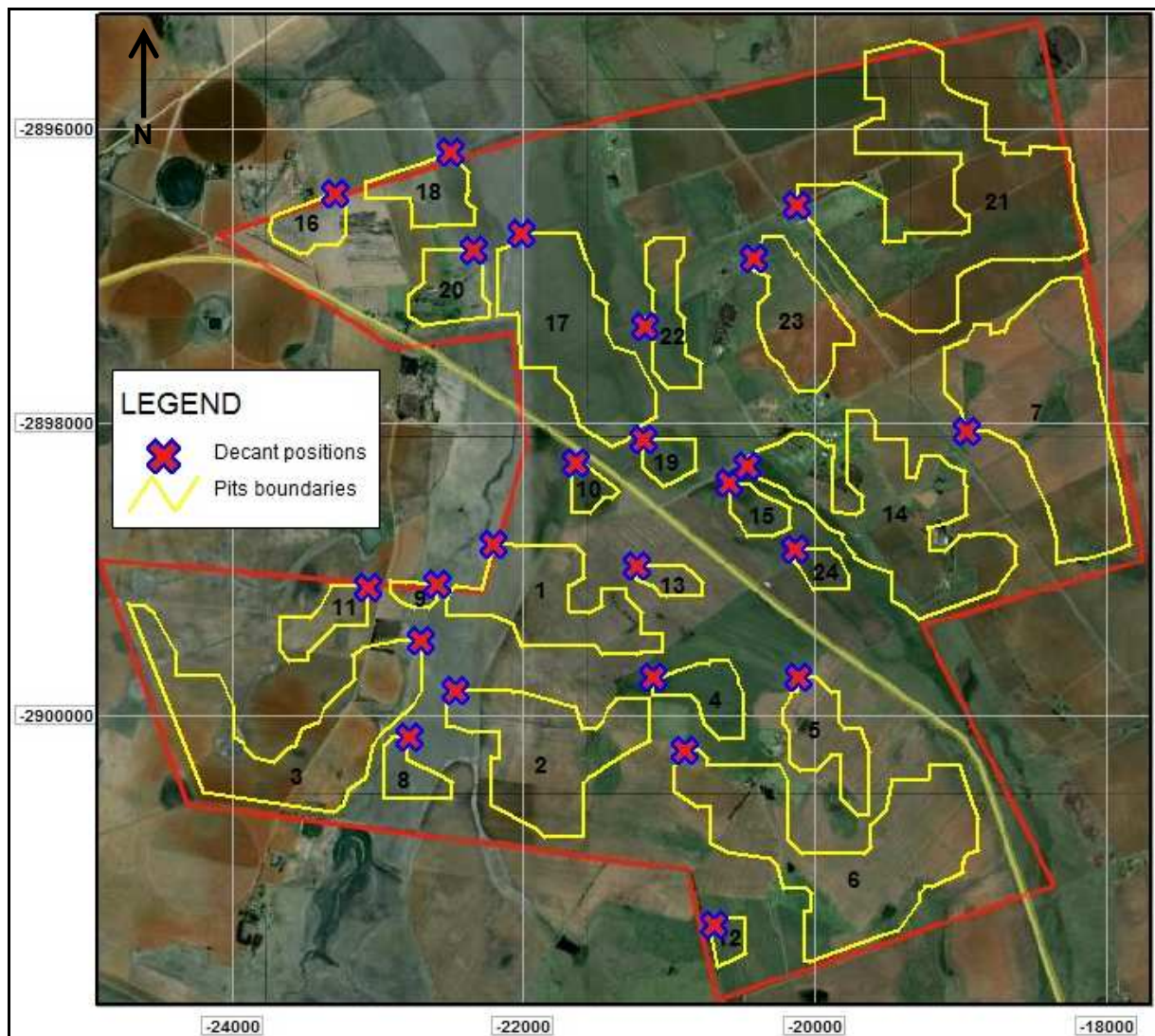


Figure 6.2-2: Opencast pits and decant positions

Figure 6.2-3 is a model simulated groundwater level contour map indicating the cone of depression at mine closure. The most severe water level impacts are towards the north-east of the mine lease area, as this is where large opencast pits are located, and the coal seams are at their deepest. At mine closure, groundwater levels towards the south and south-west have already started to recover. Until a new groundwater level equilibrium has been reached, local groundwater flow directions will be towards the opencast pit areas.

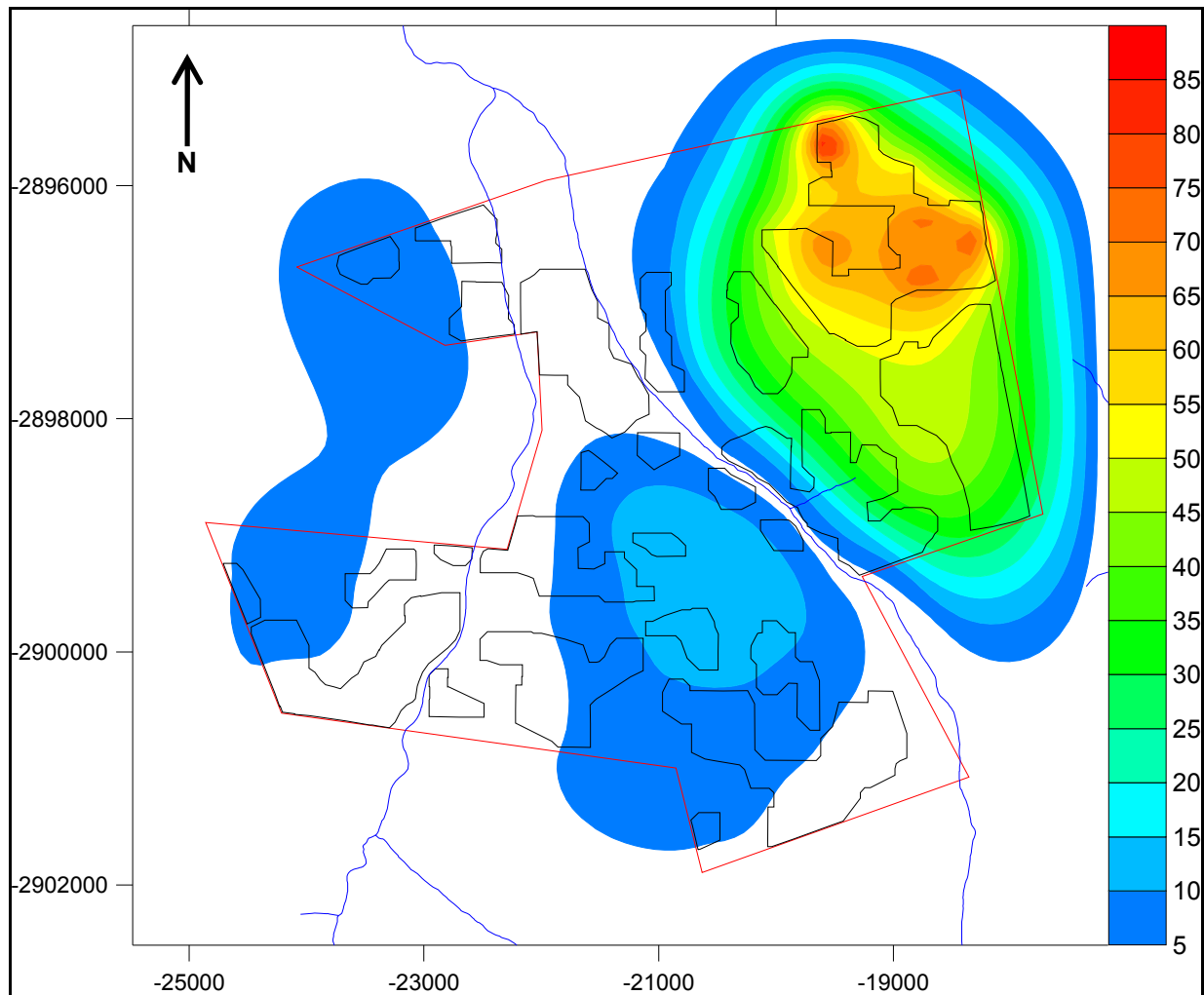


Figure 6.2-3: Maximum groundwater drawdown at mine closure (m)

At mine closure a maximum groundwater level drawdown of approximately 85 meters were simulated. As have already been mentioned in **Section 3.1** of the thesis, recharge to backfilled opencast pits is higher than to the surrounding undisturbed aquifer/s. As have already been discussed, river nodes were used for the simulation of the Bronkhorstspuit and Koffiespruit, instead of conventional constant head nodes. The effect of the river nodes on the local groundwater levels is made clear in **Figure 6.2-3**. The cones of depression are elongated along the streams and do not exceed them, as they provide a constant flow of groundwater to the model – thus acting in the same way a constant head boundary would have.

In order to determine the time-of-decant, monitoring boreholes were placed in the post closure model at the decant positions as indicated in **Figure 6.2-2**. The model was then used to construct water level-time graphs for each model scenario, as illustrated in **Table 6.2-1**. Because the decant elevations of the opencast pits are all known, the time-of-decant were deduced from the X-axis as soon as the individual graphs reached their decant elevations.

The water level-time graphs are provided in **Figures 6.2-4 to 6.2-12**, and the results are provided in **Tables 6.2-3 to 6.2-7**. The results are however discussed in more detail in **Section 8** of the thesis.

The **time-to-decant** of a backfilled opencast pit will depend on the following factors:

- The total mined volume – the larger the mine void, the more water is required to fill the pit to the decant elevation, which will lead to an increase in the time-to-decant of a backfilled mine void,
- The porosity of the backfill material – an increase in the porosity of the backfill material will lead to an increase in the void space, which will ultimately lead to an increase in the volume of water required to fill the pit to its decant elevation,
- Recharge to the backfilled mine void – an increase in recharge will lead to a decrease in the time-to-decant of a mine void,
- Geometry of the surface – as illustrated in **Figure 6.2-1**, decant will always occur at the lowest surface elevation. The distance between the lowest surface elevation and the pit floor elevation will therefore influence the time-to-decant, as a decrease in the distance will lead to a decrease in the time-to-decant and vice-versa.

The **decant volume** of a backfilled opencast pit depend on the following factors:

- Mean annual rainfall – an increase in the annual rainfall will lead to an increase in decant volumes, simply because more water is available for decanting,
- The recharge percentage to a backfilled opencast pit – an increase in the effective recharge to a backfilled opencast pit will lead to an increase in decant volumes,
- The size of the disturbed surface area – an increase in the size of the surface area disturbed by opencast mining will lead to an increase in the effective recharge to the backfilled opencast pit.

The results of the post closure model simulations, as exemplified in **Table 6.2-1**, are provided in **Tables 6.2-3 to 6.2-7**, while the model simulated time-water level elevation graphs are provided in **Figures 6.2-4 to 6.2.12**.

Section 8 of the thesis provides a full discussion of the results of both the numerical groundwater flow model simulations and analytical calculations.

Table 6.2-3: Results of post closure model simulations – Scenarios 1 and 2

Scenario 1					Scenario 2				
Pit	Decant elevation (mamsl)	Time-to-decant (days)	Time-to-decant (years)	Decant volumes (m ³ /d)	Pit	Decant elevation (mamsl)	Time-to-decant (days)	Time-to-decant (years)	Decant volumes (m ³ /d)
Pit01	1561	12775	35	104	Pit01	1561	10037	27	117
Pit02	1564	7300	20	158	Pit02	1564	8212	22	157
Pit03	1563	11862	32	101	Pit03	1563	10950	30	142
Pit04	1566	8212	22	31	Pit04	1566	11862	32	34
Pit05	1569	11862	32	54	Pit05	1569	16425	45	50
Pit06	1568	8212	22	171	Pit06	1568	12775	35	189
Pit07	1585	21900	60	212	Pit07	1585	44712	122	165
Pit08	1563	1825	5	35	Pit08	1563	3650	10	48
Pit09	1562	17337	47	8	Pit09	1562	18250	50	12
Pit10	1560	14600	40	6	Pit10	1560	18250	50	7
Pit11	1569	19162	52	17	Pit11	1569	31025	85	0
Pit12	1580	43800	120	0	Pit12	1580	>91250	>250	0
Pit13	1564	10037	27	12	Pit13	1564	17337	47	13
Pit14	1565	30112	82	165	Pit14	1565	42887	117	238
Pit15	1565	31025	85	12	Pit15	1565	42887	117	14
Pit16	1567	41062	112	0.5	Pit16	1567	86687	237	4
Pit17	1557	11862	32	93	Pit17	1557	12775	35	91
Pit18	1556	1825	5	46	Pit18	1556	1825	5	32
Pit19	1562	22812	62	14	Pit19	1562	33762	92	13
Pit20	1557	10037	27	39	Pit20	1557	10037	27	18
Pit21	1581	25550	70	252	Pit21	1581	40150	110	254
Pit22	1559	22812	62	55	Pit22	1559	25550	70	75
Pit23	1578	27375	75	52	Pit23	1578	42887	117	46
Pit24	1566	27375	75	5	Pit24	1566	39237	107	8

Table 6.2-4: Results of post closure model simulations – Scenarios 3 and 4

Scenario 3					Scenario 4				
Pit	Decant elevation (mamsl)	Time-to-decant (days)	Time-to-decant (years)	Decant volumes (m ³ /d)	Pit	Decant elevation (mamsl)	Time-to-decant (days)	Time-to-decant (years)	Decant volumes (m ³ /d)
Pit01	1561	10950	30	128	Pit01	1561	10037	27	136
Pit02	1564	9125	25	156	Pit02	1564	5475	15	200
Pit03	1563	9125	25	172	Pit03	1563	10037	27	152
Pit04	1566	14600	40	34	Pit04	1566	6387	17	42
Pit05	1569	19162	52	43	Pit05	1569	8212	22	70
Pit06	1568	15512	42	204	Pit06	1568	6387	17	242
Pit07	1585	59312	162	149	Pit07	1585	17337	47	283
Pit08	1563	3650	10	51	Pit08	1563	1825	5	42
Pit09	1562	19162	52	14	Pit09	1562	15512	42	11
Pit10	1560	19162	52	7	Pit10	1560	10037	27	10
Pit11	1569	36500	100	0	Pit11	1569	14600	40	26
Pit12	1580	>91250	>250	0	Pit12	1580	22812	62	0
Pit13	1564	19162	52	12	Pit13	1564	8212	22	16
Pit14	1565	47450	130	254	Pit14	1565	25550	70	222
Pit15	1565	50187	137	14	Pit15	1565	25550	70	18
Pit16	1567	>91250	>250	2	Pit16	1567	29200	80	5
Pit17	1557	13687	37	101	Pit17	1557	9125	25	137
Pit18	1556	1825	5	34	Pit18	1556	1825	5	57
Pit19	1562	39237	107	12	Pit19	1562	18250	50	19
Pit20	1557	10950	30	19	Pit20	1557	9125	25	50
Pit21	1581	52012	142	271	Pit21	1581	20987	57	343
Pit22	1559	29200	80	81	Pit22	1559	20075	55	67
Pit23	1578	54750	150	47	Pit23	1578	21900	60	76
Pit24	1566	45625	125	10	Pit24	1566	21900	60	10

Table 6.2-5: Results of post closure model simulations – Scenarios 5 and 6

Scenario 5					Scenario 6				
Pit	Decant elevation (mamsl)	Time-to-decant (days)	Time-to-decant (years)	Decant volumes (m ³ /d)	Pit	Decant elevation (mamsl)	Time-to-decant (days)	Time-to-decant (years)	Decant volumes (m ³ /d)
Pit01	1561	8212	22	149	Pit01	1561	9125	25	159
Pit02	1564	6387	17	201	Pit02	1564	7300	20	200
Pit03	1563	9125	25	188	Pit03	1563	7300	20	224
Pit04	1566	9125	25	49	Pit04	1566	10950	30	46
Pit05	1569	1186	3	72	Pit05	1569	14600	40	64
Pit06	1568	9125	25	254	Pit06	1568	11862	32	270
Pit07	1585	33762	92	248	Pit07	1585	44712	122	227
Pit08	1563	2737	7	55	Pit08	1563	3650	10	58
Pit09	1562	15512	42	15	Pit09	1562	16425	45	18
Pit10	1560	14600	40	12	Pit10	1560	16425	45	11
Pit11	1569	22812	62	8	Pit11	1569	25550	70	1
Pit12	1580	57487	157	0	Pit12	1580	77562	212	0
Pit13	1564	12775	35	18	Pit13	1564	15512	42	17
Pit14	1565	35587	97	299	Pit14	1565	41975	115	316
Pit15	1565	36500	100	20	Pit15	1565	42887	117	20
Pit16	1567	62962	172	11	Pit16	1567	79387	217	9
Pit17	1557	10950	30	131	Pit17	1557	10950	30	142
Pit18	1556	1825	5	44	Pit18	1556	1825	5	46
Pit19	1562	29200	80	20	Pit19	1562	33762	92	18
Pit20	1557	9125	25	30	Pit20	1557	10037	27	30
Pit21	1581	31937	87	335	Pit21	1581	41975	115	360
Pit22	1559	22812	62	89	Pit22	1559	26462	72	95
Pit23	1578	33762	92	67	Pit23	1578	42887	117	69
Pit24	1566	32850	90	12	Pit24	1566	39237	107	14

Table 6.2-6: Results of post closure model simulations – Scenarios 7 and 8

Scenario 7					Scenario 8				
Pit	Decant elevation (mamsl)	Time-to-decant (days)	Time-to-decant (years)	Decant volumes (m ³ /d)	Pit	Decant elevation (mamsl)	Time-to-decant (days)	Time-to-decant (years)	Decant volumes (m ³ /d)
Pit01	1561	7300	20	176	Pit01	1561	6387	17	184
Pit02	1564	3650	10	253	Pit02	1564	4562	12	250
Pit03	1563	8212	22	210	Pit03	1563	7300	20	235
Pit04	1566	5475	15	55	Pit04	1566	7300	20	55
Pit05	1569	6387	17	90	Pit05	1569	9125	25	93
Pit06	1568	5475	15	328	Pit06	1568	7300	20	324
Pit07	1585	13687	37	371	Pit07	1585	27375	75	334
Pit08	1563	912	2	50	Pit08	1563	2737	7	62
Pit09	1562	13687	37	14	Pit09	1562	13687	37	18
Pit10	1560	7300	20	15	Pit10	1560	10950	30	16
Pit11	1569	10037	27	37	Pit11	1569	16425	45	18
Pit12	1580	13687	37	0	Pit12	1580	31937	87	0
Pit13	1564	6387	17	21	Pit13	1564	9125	25	23
Pit14	1565	21900	60	289	Pit14	1565	31025	85	363
Pit15	1565	21900	60	25	Pit15	1565	31025	85	27
Pit16	1567	20075	55	12	Pit16	1567	46537	127	19
Pit17	1557	7300	20	189	Pit17	1557	8212	22	180
Pit18	1556	1825	5	70	Pit18	1556	1825	5	58
Pit19	1562	14600	40	25	Pit19	1562	24637	67	25
Pit20	1557	8212	22	63	Pit20	1557	8212	22	43
Pit21	1581	17337	47	455	Pit21	1581	26462	72	418
Pit22	1559	17337	47	82	Pit22	1559	20075	55	103
Pit23	1578	17337	47	103	Pit23	1578	26462	72	91
Pit24	1566	18250	50	14	Pit24	1566	28287	77	16

Table 6.2-7: Results of post closure model simulations – Scenarios 9

Scenario 9				
Pit	Decant elevation (mamsl)	Time-to-decant (days)	Time-to-decant (years)	Decant volumes (m ³ /d)
Pit01	1561	7300	20	194
Pit02	1564	5475	15	248
Pit03	1563	5475	15	275
Pit04	1566	8212	22	57
Pit05	1569	10950	30	87
Pit06	1568	9125	25	339
Pit07	1585	35587	97	307
Pit08	1563	2737	7	66
Pit09	1562	13687	37	21
Pit10	1560	12775	35	16
Pit11	1569	18250	50	10
Pit12	1580	41975	115	0
Pit13	1564	11862	32	22
Pit14	1565	36500	100	381
Pit15	1565	37412	102	27
Pit16	1567	59312	162	17
Pit17	1557	9125	25	188
Pit18	1556	1825	5	58
Pit19	1562	29200	80	24
Pit20	1557	9125	25	42
Pit21	1581	35587	97	449
Pit22	1559	23775	65	109
Pit23	1578	34675	95	91
Pit24	1566	33762	92	19

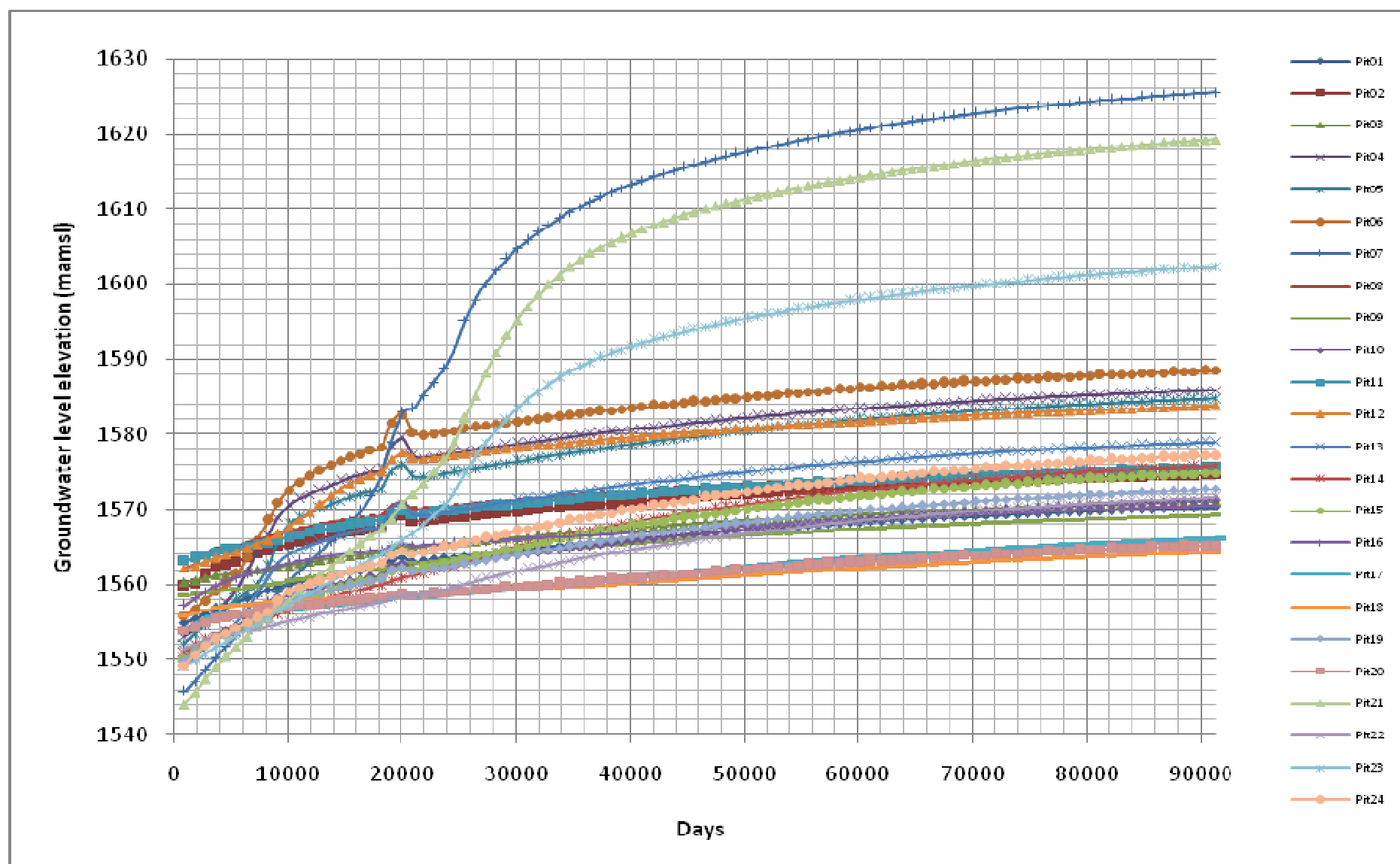


Figure 6.2-4: Scenario 1 model simulated water level elevation-time graph

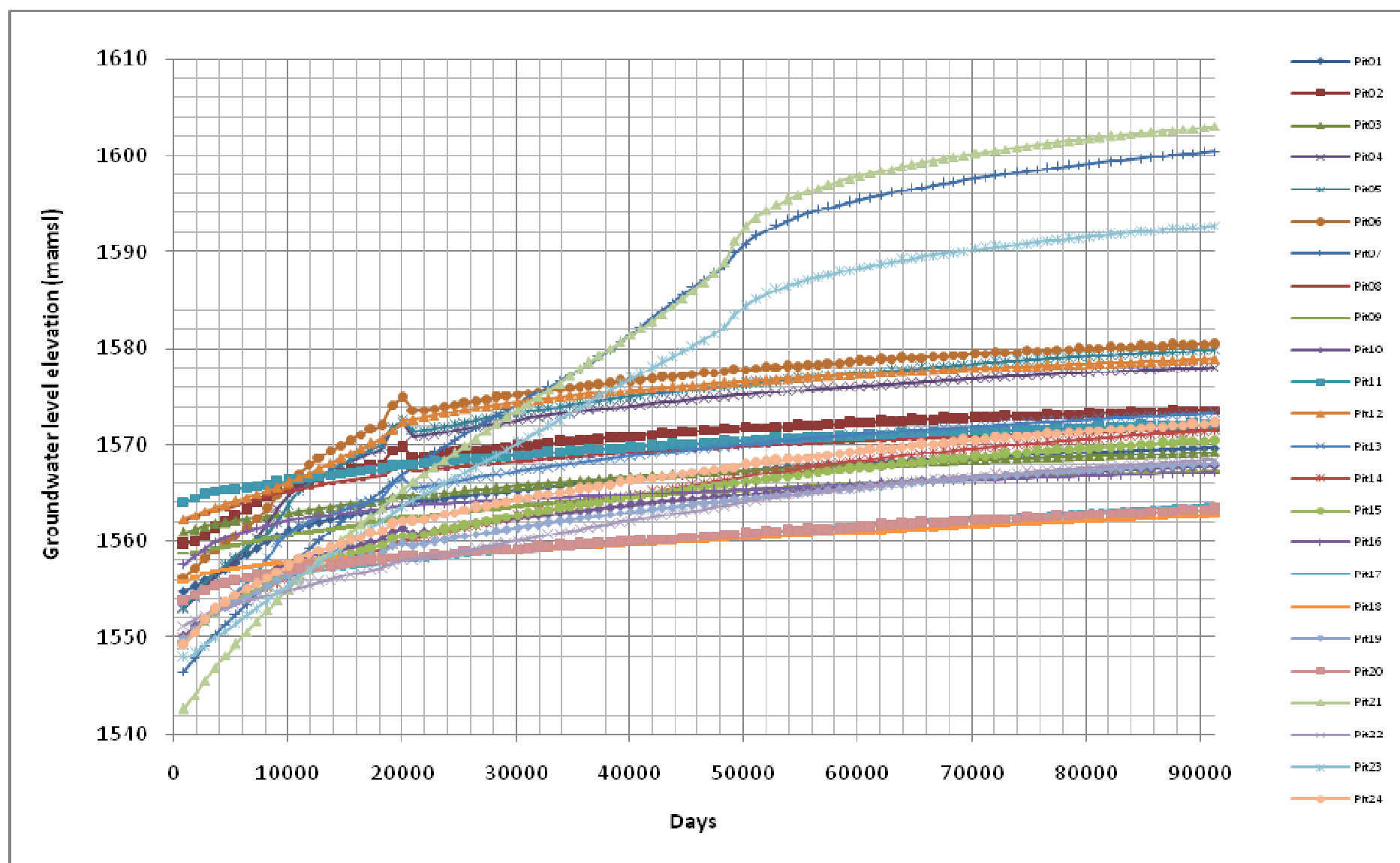


Figure 6.2-5: Scenario 2 model simulated water level elevation-time graph

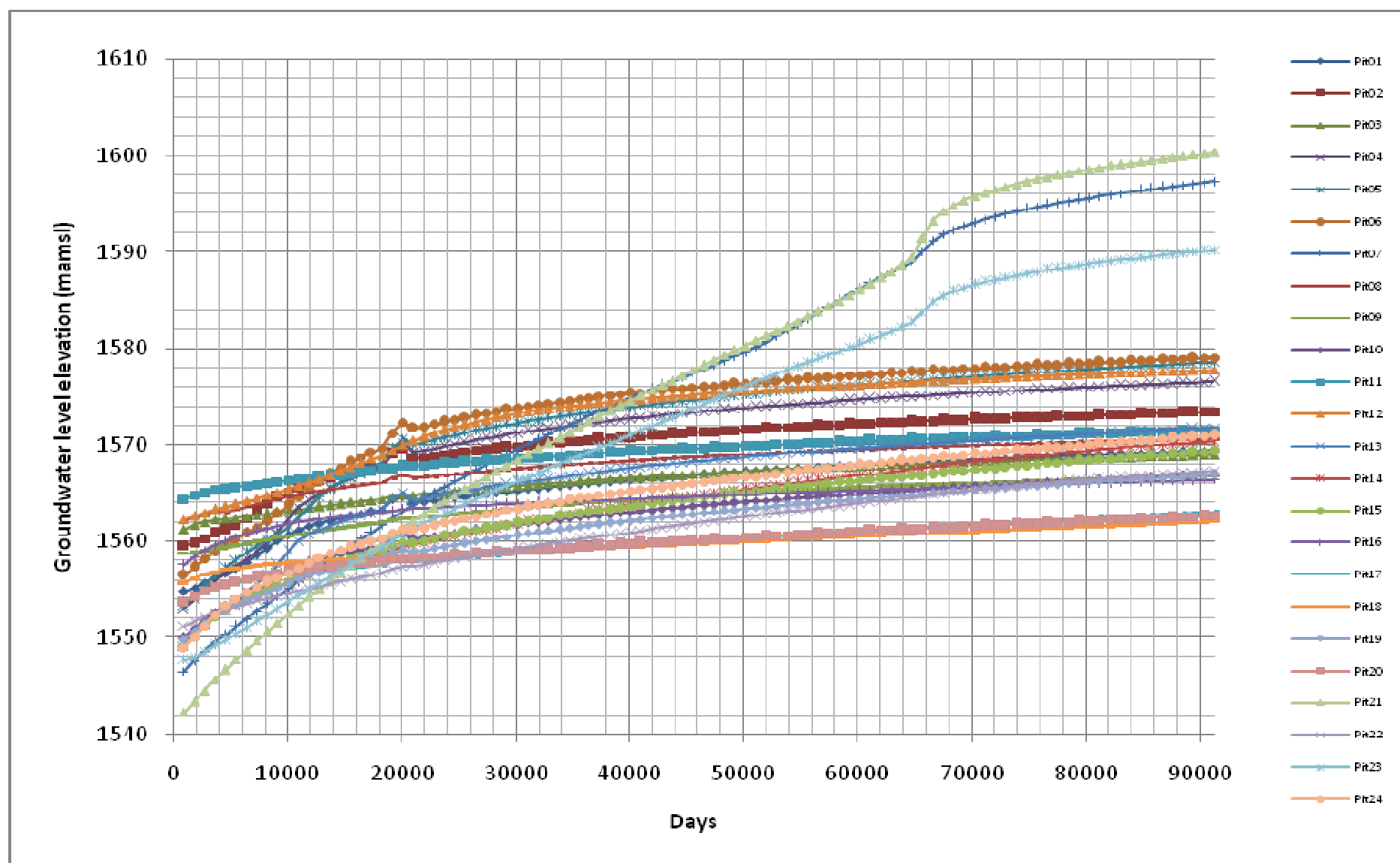


Figure 6.2-6: Scenario 3 model simulated water level elevation-time graph

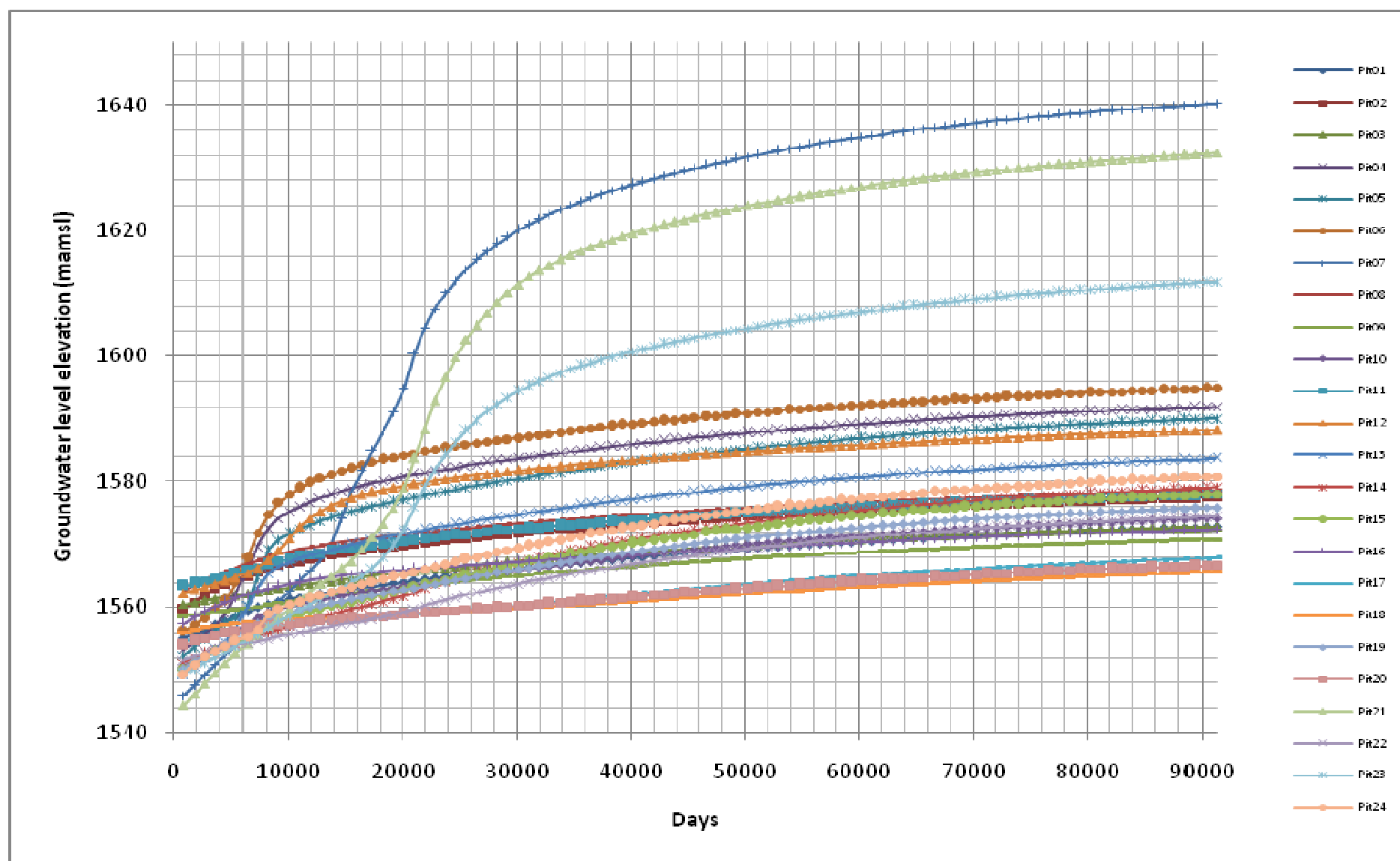


Figure 6.2-7: Scenario 4 model simulated water level elevation-time graph

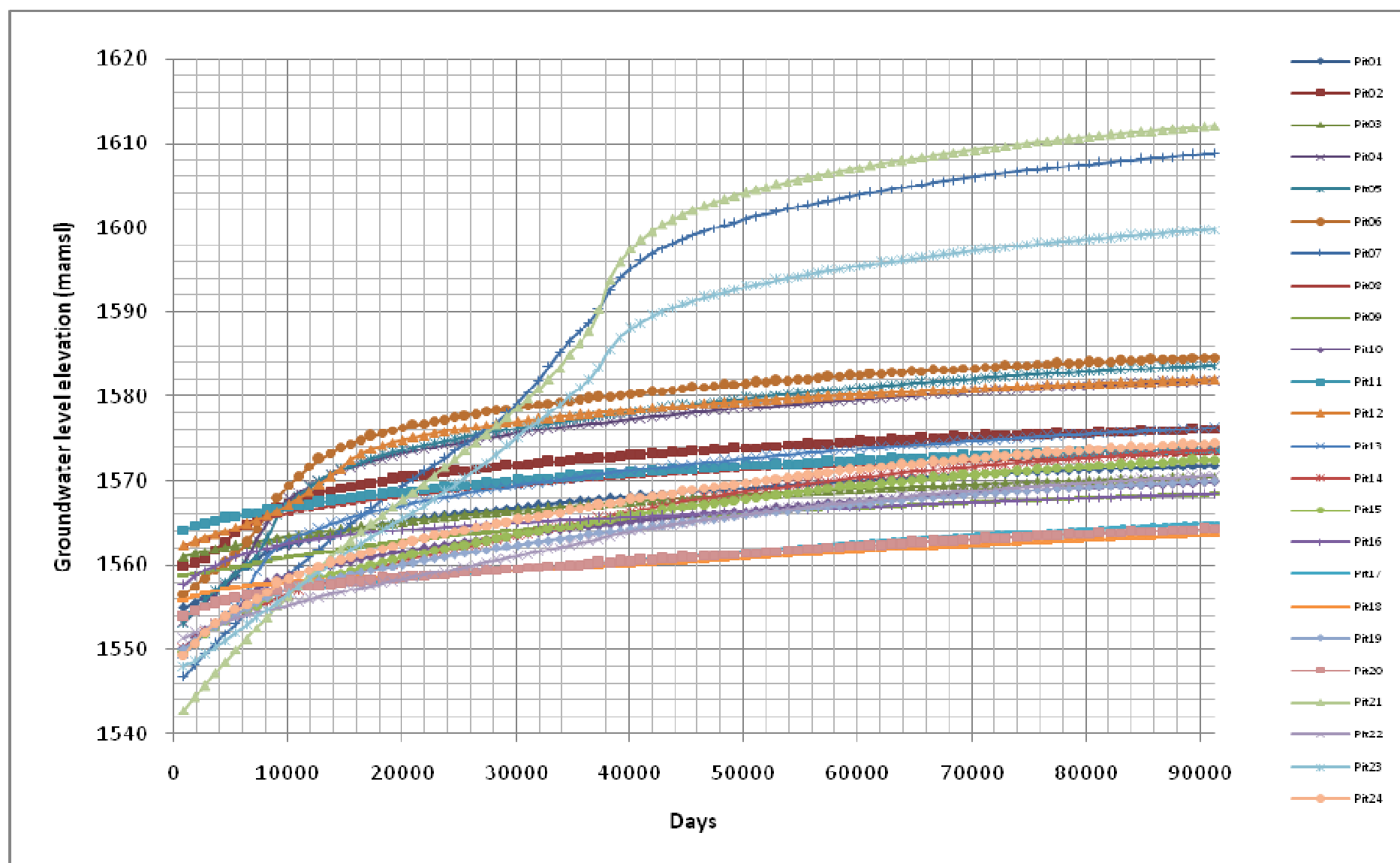


Figure 6.2-8: Scenario 5 model simulated water level elevation-time graph

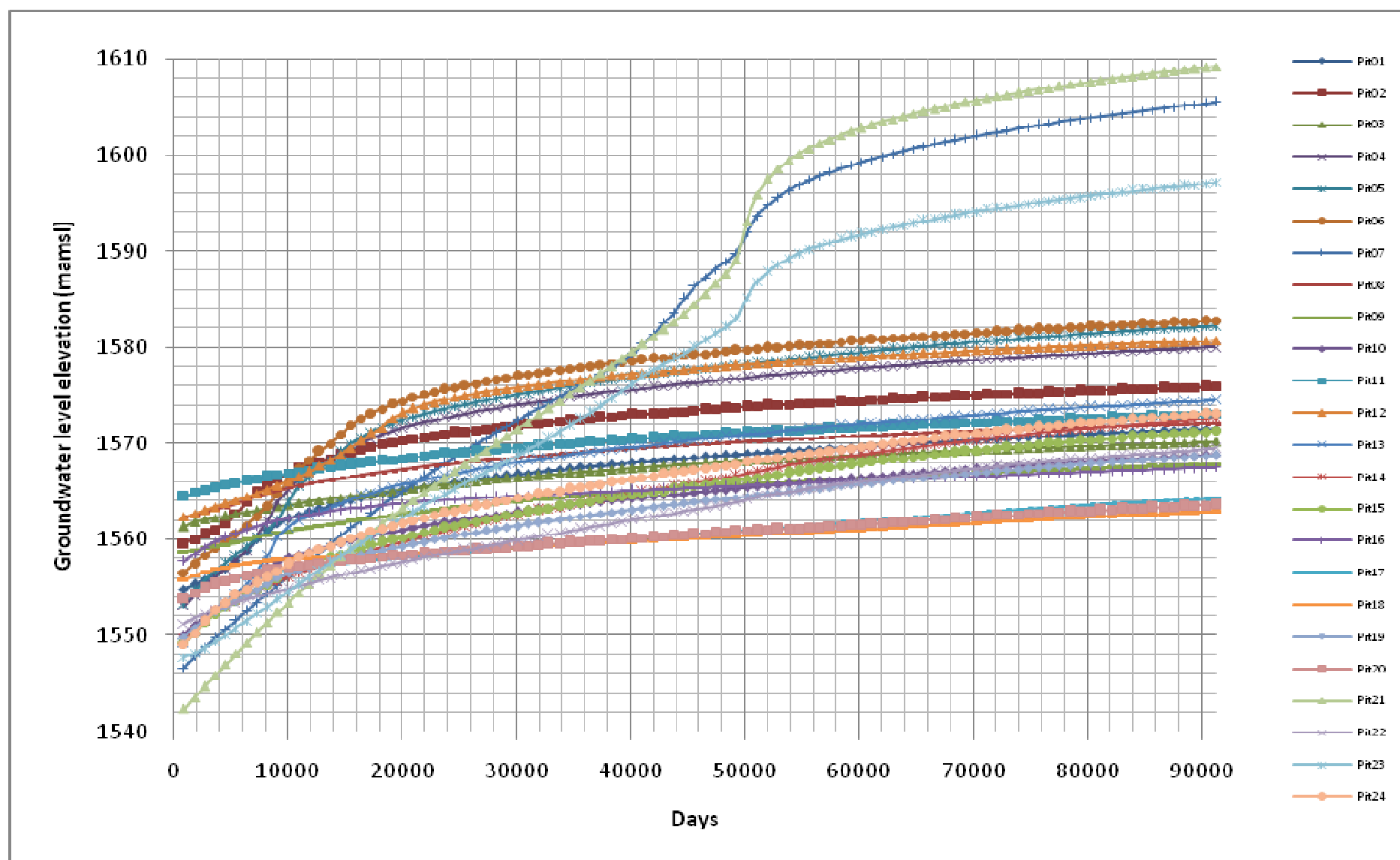


Figure 6.2-9: Scenario 6 model simulated water level elevation-time graph

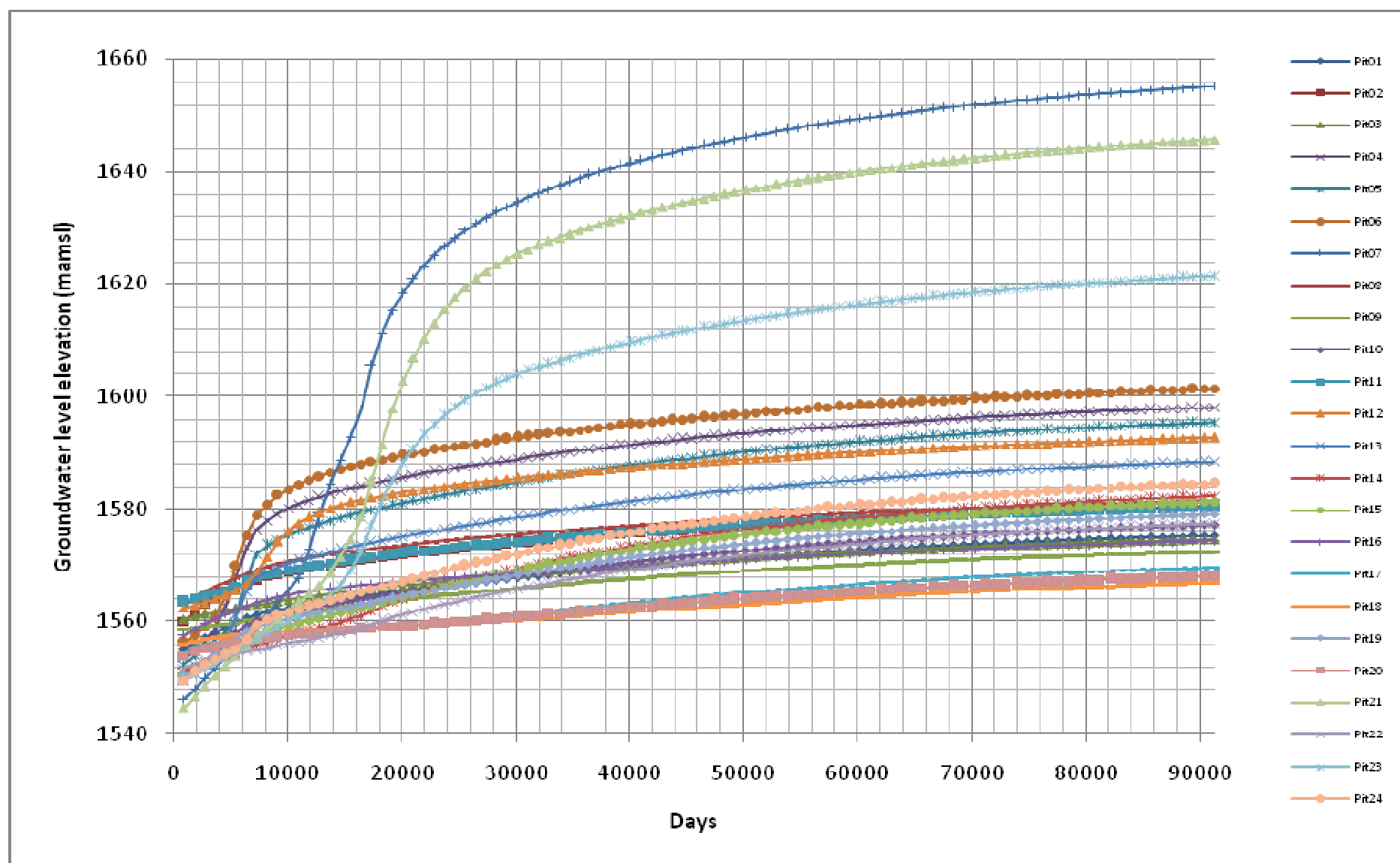


Figure 6.2-10: Scenario 7 model simulated water level elevation-time graph

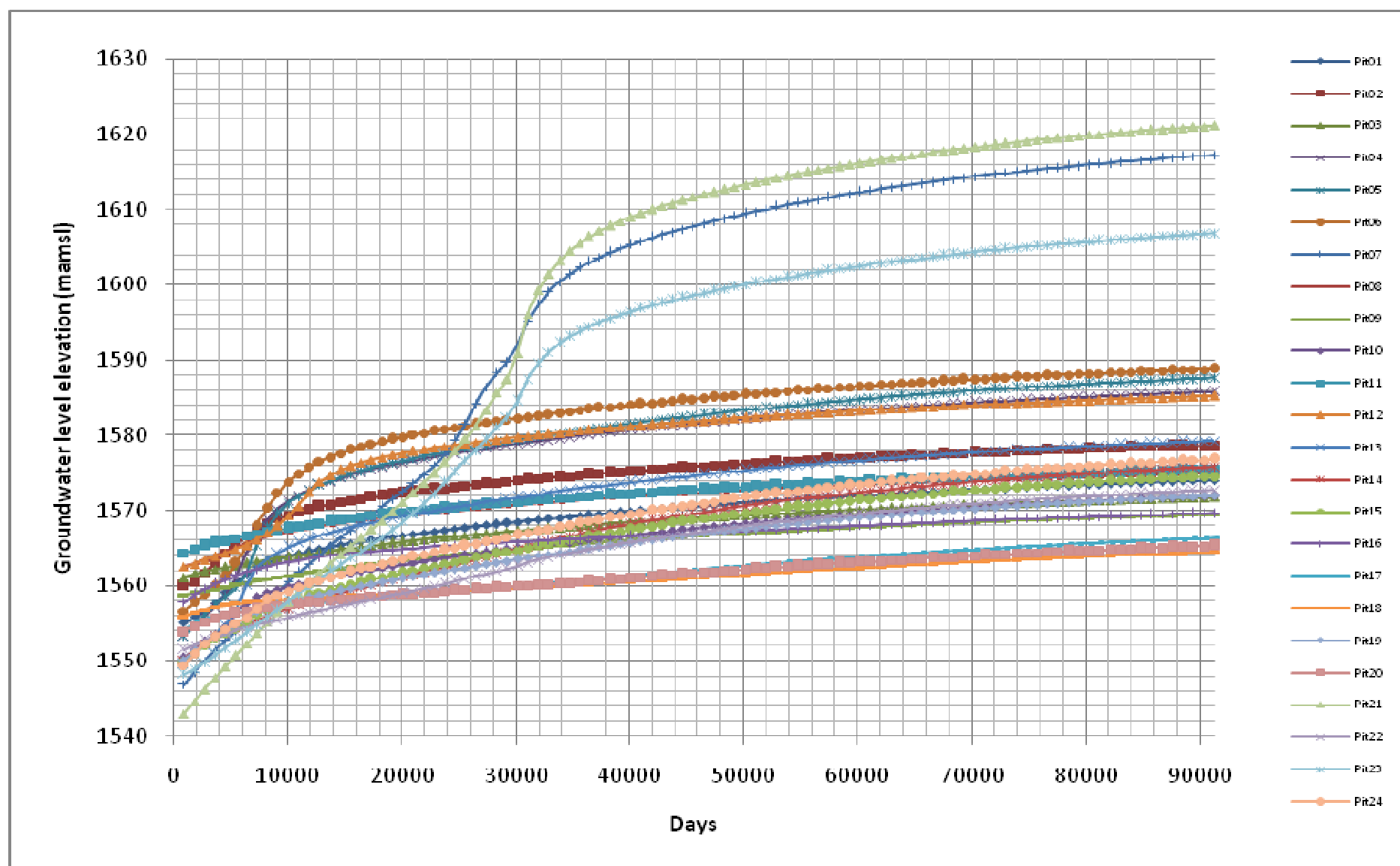


Figure 6.2-11: Scenario 8 model simulated water level elevation-time graph

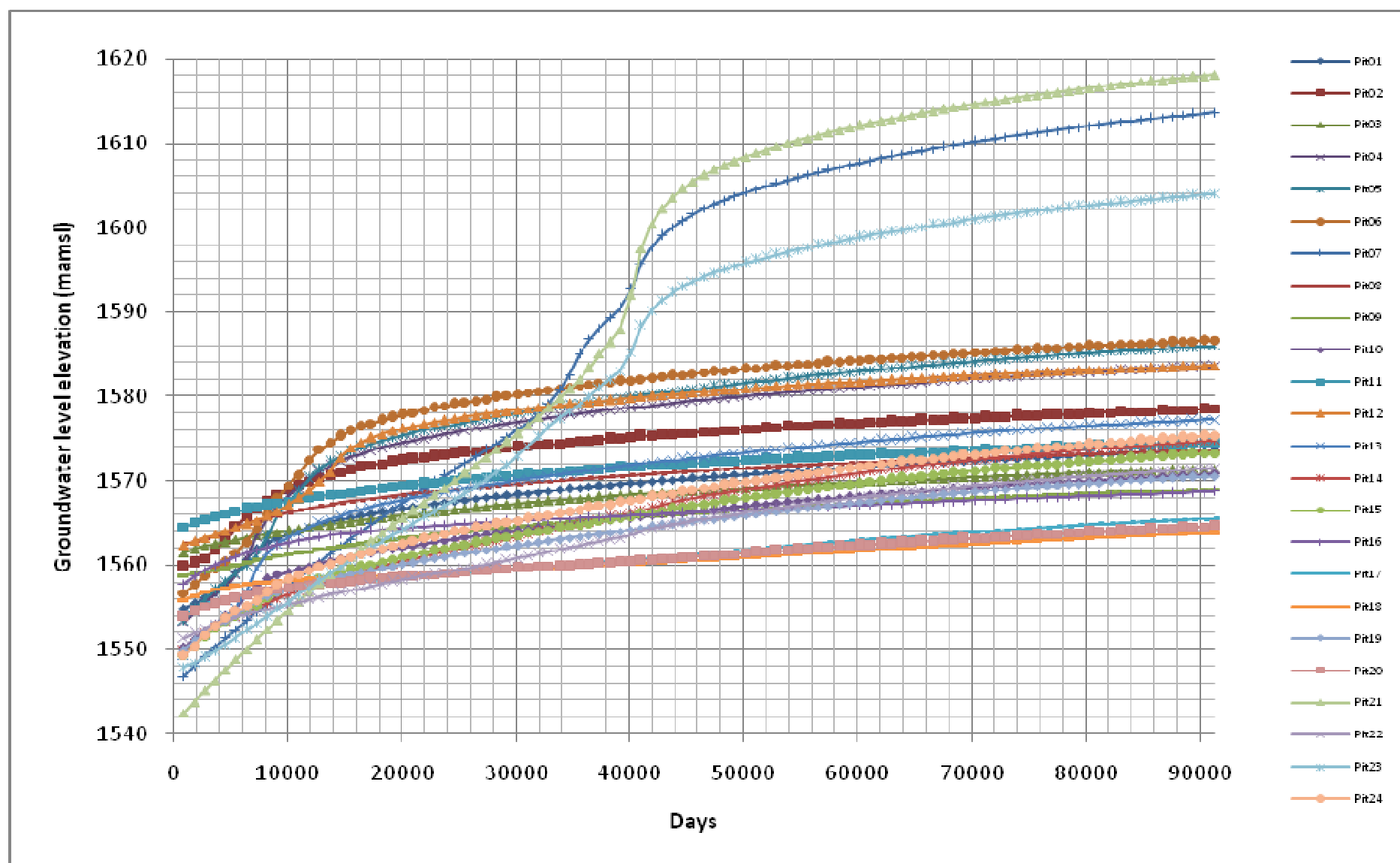


Figure 6.2-12: Scenario 9 model simulated water level elevation-time graph

7. Analytical Decant Calculations and Groundwater Discharge

Analytical calculations, also known as mathematical or hand calculations are the foundations on which numerical models are built. Modern numerical models replaced hand calculations and are extensively being used by geohydrologists. However, hand calculations are still an important factor in geohydrology as will the following advantages point out:

- Once mathematical formulas are understood correctly, answers can be delivered in a relatively short time period and with limited field data, and
- Expensive computers and modelling software are not required.

An aquifer system is however a very complex and heterogeneous system, which restricts the use of mathematical hand calculations.

Equation 3.2-3 was used to calculate the volume of groundwater discharge to the Bronkhorstspuit and Koffiespruit surface water bodies. *Surfer 8* was used to calculate the mined volumes of each individual opencast pit, after which hand calculations were used to calculate the time-to-decant and the expected decant volumes.

As mentioned before, the use of hand calculations to determine groundwater discharge into surface water bodies are restricted because of the heterogeneous nature of aquifer systems. By scrutinising **Equation 3.2-3**, the following restrictions are made clear:

- Aquifer transmissivity is a highly heterogeneous aquifer parameter, due to the fact that aquifers may be composed of highly transmissive fractures and a low transmissivity matrix. Fracture transmissivity may vary significantly within only a few centimetres because of varying fracture aperture and areal extent. The nature of different types of sedimentary rocks may also cause significant variations in matrix transmissivity.

Therefore, the only solution to the immense heterogeneous nature of aquifer transmissivity is to establish an average aquifer transmissivity as discussed and calculated in **Section 5.4** of the thesis,

- The hydraulic gradient between the aquifer and the surface water body vary along the length of the surface water body as a result of varying aquifer transmissivity. In order to overcome this problem, an average hydraulic gradient must be calculated for the entire length of the streams.

Because of the restrictions related to hand calculations, as discussed above, calculations are merely estimates and are only as accurate as the field data they are based upon, and the techniques used for calculating the necessary parameters.

By keeping the above mentioned restrictions in mind, groundwater discharge to the **Bronkhorstspuit** was calculated to be **130 m³/d**, while a discharge of **140 m³/d** was calculated for the **Koffiespruit**.

Effective porosity, as used in the calculations (**Table 7-2**), refers to the percentage of voids (relative to the percentage of solid material) that are interconnected to each other so that water can freely pass through it. The percentages that are used thus refer to the total porosity of the backfill material as a whole.

Section 8 of the thesis provides a full discussion of the results of both the numerical groundwater flow model simulations and analytical calculations.

Table 7-1: Volume calculations

	Total mined volume m ³ (below decant elevation)	Void volume m ³ (15% effective porosity)	Void volume m ³ (20% effective porosity)	Void volume m ³ (25% effective porosity)
Pit01	15133981	2270097	3026796	3783495
Pit02	20477335	3071600	4095467	5119334
Pit03	10081722	1512258	2016344	2520431
Pit04	4781012	717152	956202	1195253
Pit05	8257523	1238628	1651505	2064381
Pit06	27473238	4120986	5494648	6868310
Pit07	62270485	9340573	12454097	15567621
Pit08	1730623	259593	346125	432656
Pit09	732790	109919	146558	183198
Pit10	2009342	301401	401868	502336
Pit11	5908957	886344	1181791	1477239
Pit12	1916507	287476	383301	479127
Pit13	2333344	350002	466669	583336
Pit14	46315608	6947341	9263122	11578902
Pit15	4349713	652457	869943	1087428
Pit16	8251366	1237705	1650273	2062842
Pit17	18034147	2705122	3606829	4508537
Pit18	5949936	892490	1189987	1487484
Pit19	4218364	632755	843673	1054591
Pit20	6063285	909493	1212657	1515821
Pit21	63499513	9524927	12699903	15874878
Pit22	3829728	574459	765946	957432
Pit23	17412794	2611919	3482559	4353199
Pit24	3465026	519754	693005	866257

Table 7-2: Time-to-decant calculations (years)

	Worst case scenario	Average	Best case scenario
	Effective porosity (15%)	Effective porosity (20%)	Effective porosity (25%)
	Recharge (16%)	Recharge (13%)	Recharge (10%)
Pit01	34	55	90
Pit02	35	58	94
Pit03	13	21	34
Pit04	33	54	88
Pit05	37	61	100
Pit06	28	46	75
Pit07	64	104	170
Pit08	19	31	51
Pit09	22	36	58
Pit10	40	66	108
Pit11	49	81	132
Pit12	42	69	112
Pit13	44	72	118
Pit14	55	91	148
Pit15	56	92	150
Pit16	75	123	200
Pit17	28	47	76
Pit18	35	57	93
Pit19	61	100	163
Pit20	38	62	100
Pit21	49	80	131
Pit22	21	35	56
Pit23	55	91	148
Pit24	60	98	159

Table 7-3: Decant volume calculations (m³/d)

	Pit surface area (m ²)	Recharge (10%)	Recharge (13%)	Recharge (16%)
Pit01	601780	115	150	185
Pit02	779240	149	194	239
Pit03	1060450	203	264	325
Pit04	193650	37	48	59
Pit05	295750	57	74	91
Pit06	1313300	252	327	403
Pit07	1311010	251	327	402
Pit08	122270	23	30	38
Pit09	45180	9	11	14
Pit10	66700	13	17	20
Pit11	160500	31	40	49
Pit12	61030	12	15	19
Pit13	70860	14	18	22
Pit14	1118720	214	279	343
Pit15	103920	20	26	32
Pit16	147170	28	37	45
Pit17	850040	163	212	261
Pit18	229340	44	57	70
Pit19	92360	18	23	28
Pit20	215730	41	54	66
Pit21	1738080	333	433	533
Pit22	243000	47	61	75
Pit23	420550	81	105	129
Pit24	77740	15	19	24

8. Discussion

In short, the objectives of the study are as follow:

- To determine decant volumes with varying recharge percentages,
- To determine the time of decant with varying degrees of backfill material porosity and recharge percentages,
- To determine the volume of groundwater discharge to both the Bronkhorstspuit and Koffiespruit.

The above mentioned objectives were completed by means of numerical groundwater flow model simulations and analytical hand calculations. A summary as well as a correlation of the results of the two methods will follow:

8.1 Numerical groundwater flow model results

As discussed in **Section 6** of the thesis, two flow models were constructed, namely:

- A **pre-mining numerical groundwater flow model** which was used to determine the **steady state groundwater discharge** to both the Bronkhorstspuit and Koffiespruit, and
- A **post-closure numerical groundwater flow model** during which the effects of the increased transmissivity, specific yield, storage coefficient, and recharge of the rehabilitated opencast pits were simulated during 9 different model simulations. **Groundwater discharge** to the Bronkhorstspuit and Koffiespruit, **time-to-decant**, as well as **decant volumes** were determined during post-closure model simulations.

To provide structure to the findings of both the pre-mining numerical groundwater flow model simulations as well as the post-closure model simulations, the results of the pre-mining model simulations are discussed in **Subsection 8.1.1**, whereas the results of the post-closure simulations are discussed in **Subsection 8.1.2**.

8.1.1 Pre-mining numerical groundwater flow model results

During **steady state** model simulations groundwater discharge to the **Bronkhorstspuit** was estimated to be **90 m³/d**, while discharge to the **Koffiespruit** was estimated at **130 m³/d**. As evident from **Figure 5.2-4**, greater groundwater gradients occur to the east of the Koffiespruit, which may be the reason for the slightly higher groundwater discharge.

At the **end of active mining**, groundwater discharge to the **Bronkhorstspuit** was estimated to be **30 m³/d**, while discharge to the **Koffiespruit** was estimated at **20 m³/d**.

The decrease in groundwater discharge to both surface water streams is a direct result of mine dewatering, which ultimately leads to a decrease in the local groundwater levels.

8.1.2 Post-closure numerical groundwater flow model results

Post-closure groundwater discharge to both surface water streams was estimated and the results are provided in **Table 6.2-2**. During the model simulations an effective aquifer recharge of 13% of the mean annual precipitation was used, while the backfilled opencast pits were simulated with a transmissivity of 25 m²/d, a specific yield (layer 1) of 0.12, and a storage coefficient (layer 2) of 0.01.

Post-closure groundwater discharge to both the Bronkhorstspuit and Koffiespruit was estimated according to post-closure model Scenario 5 (**Table 6.2-1**), as discussed above. Groundwater discharge to the **Bronkhorstspuit** increased significantly from **140 m³/d** at five years post-closure to **700 m³/d** at 50 years post-closure.

Similar trends were observed for groundwater discharge to the **Koffiespruit**. Discharge increased from **50 m³/d** at five years post-closure to **570 m³/d** at 50 years post-closure. The steady increase in groundwater discharge to both surface water streams is the result of recovering groundwater levels.

The post-closure model simulations clearly indicate that post-closure groundwater discharge to the Bronkhorstspruit and Koffiespruit far exceed the pre-mining groundwater discharge, which is the direct result of increased transmissivity and recharge to the rehabilitated opencast pits.

The results of the nine post-closure model scenarios, as explained in **Table 6.2-1**, are provided in **Tables 6.2-3 to 6.2-7**. To provide structure to the findings of the model scenarios, the results of each model scenario will be discussed independently and will be compared to the results of the analytical calculations. The opencast pits were also divided into two groups according to their sizes to further promote the structure of the findings. The groups into which the opencast pits were divided are illustrated in **Figure 8.1.2-1**.

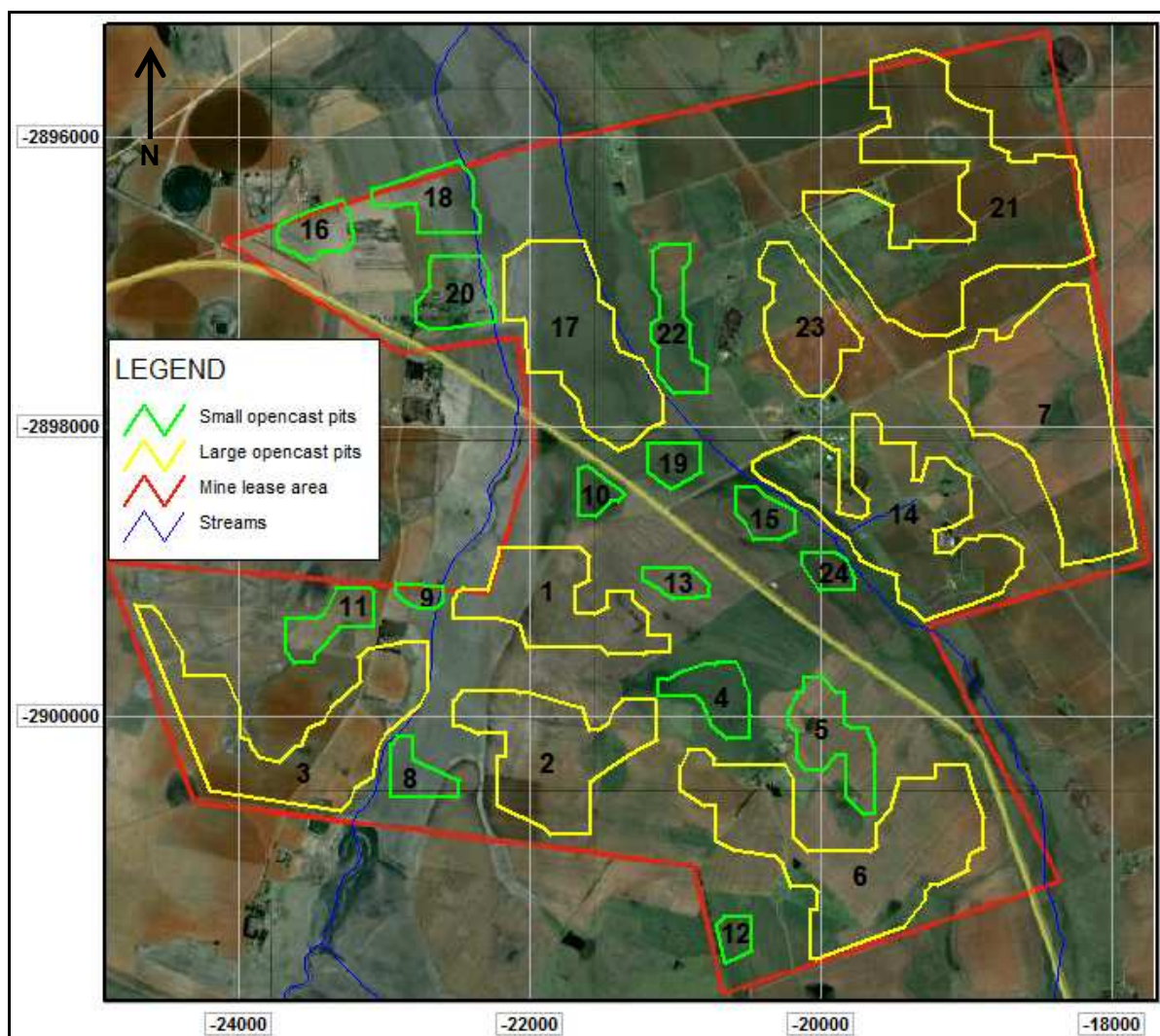


Figure 8.1.2-1: Subdivision of opencast pits

Post-closure model Scenario 1

Model **Scenario 1** represents pre-mining aquifer conditions with an effective aquifer recharge of **10%** of the mean annual rainfall. Layer 1 was assigned a **specific yield** of **0.06**, while a **storage coefficient** of **0.008** was assigned to layer 2. Aquifer **transmissivity** remained unchanged, as illustrated in **Figure 6.1-2**.

According to the model simulation the **time-to-decant** of the 15 **smaller opencast pits** (as illustrated in **Figure 8.1.2-1**) vary between **5 and 120** years post-closure, with an average of **52** years. Simulated **decant volumes** vary between **0 and 55 m³/d**, with an average of **22 m³/d**.

For the 9 **larger opencast pits** the **time-to-decant** was simulated to vary between **20 and 82** years post closure, with an average of **48** years. Simulated **decant volumes** vary between **52 and 252 m³/d**, with an average of **145 m³/d**.

From Scenario 1 it is clear that the time-to-decant is not purely dependant on the size of the opencast pit, as the longest time-to-decant was simulated for pit 12, which is one of the smaller pits. Factors affecting the time-to-decant of an opencast pit are discussed in **Section 6.2** of the thesis. Decant volumes are however highly dependant on the size of the opencast pit, as recharge to the backfilled opencast pits are affected by the size of the disturbed surface area. Decant volumes simulated for the larger opencast pits far exceed the volumes of the smaller pits.

No decant was simulated for opencast pit 12, as the groundwater level is below the decant elevation of the pit, which is at 1 580 mamsl.

Post-closure model Scenario 2

Model **Scenario 2** represents post-mining aquifer conditions with an effective aquifer recharge of **10%** of the mean annual rainfall. **Transmissivity** of the backfilled opencast pits was increased to **25 m²/d**, while the **specific yield** of layer 1 was increased to **0.12** and the **storage coefficient** of layer 2 was increased to **0.01**.

According to the model simulation the **time-to-decant** of the 15 **smaller opencast pits** (as illustrated in **Figure 8.1.2-1**) vary between **5 and 237** years post-closure, with an average of **70** years. Simulated **decant volumes** vary between **0 and 50 m³/d**, with an average of **21 m³/d**.

For the 9 **larger opencast pits** the **time-to-decant** was simulated to vary between **22 and 122** years post closure, with an average of **69** years. Simulated **decant volumes** vary between **46 and 254 m³/d**, with an average of **155 m³/d**.

The most noticeable difference between model Scenario 1 and 2 is the simulated time-to-decant. For both the smaller and larger opencast pits the model simulated time-to-decant is longer for Scenario 2 when compared to Scenario 1. Simulated decant volumes of both Scenario 1 and 2 are however very similar.

The longer time-to-decant that was simulated for Scenario 2 is the direct result of an increased specific yield and storage coefficient of the backfilled opencast pits. By increasing the above mentioned aquifer parameters, the volumes of groundwater the aquifer is capable of storing is increased. The end result is that more water is required before the water level within the backfilled opencast pit reach the decant elevation, which will lead to an increased time-to-decant.

Once again pit 12 did not show any decant during model simulations, and is caused by its decant elevation which is situated higher than the local groundwater level.

Post-closure model Scenario 3

Model **Scenario 3** represents post-mining aquifer conditions with an effective aquifer recharge of **10%** of the mean annual rainfall. **Transmissivity** of the backfilled opencast pits was increased to **50 m²/d**, while the **specific yield** of layer 1 was increased to **0.18** and the **storage coefficient** of layer 2 was increased to **0.012**

According to the model simulation the **time-to-decant** of the 15 **smaller opencast pits** (as illustrated in **Figure 8.1.2-1**) vary between **5 and 137** years post-closure, with an average of **65** years. Simulated **decant volumes** vary between **0 and 81 m³/d**, with an average of **22 m³/d**.

For the 9 **larger opencast pits** the **time-to-decant** was simulated to vary between **25 and 162** years post closure, with an average of **83** years. Simulated **decant volumes** vary between **47 and 271 m³/d**, with an average of **164 m³/d**.

Once again, time-to-decant of the 9 larger pits increased from Scenario 1, due to the increased specific yield and storage coefficient. According to the model simulations both pits 12 and 16 do not show any worthwhile decant, because the local groundwater level do not rise above their decant elevations. When comparing the decant volumes of Scenario 2 and 3, it becomes clear that there is no significant difference or change from Scenario 2 to 3.

The following conclusions can be drawn from model Scenarios 1, 2, and 3:

- The time-to-decant increase steadily from Scenario 1 through to Scenario 3,
- The increase in time-to-decant is the direct result of an increase in specific yield and storage coefficient, which ultimately leads to an increased volume of water that is required to fill the backfilled opencast pits to their decant elevations,
- No significant change in the decant volumes occurred from Scenario 1 through to Scenario 3,
- The unchanged aquifer recharge of 10% of the mean annual rainfall that was simulated for Scenarios 1, 2, and 3 is the reason for the relatively unaffected decant volumes.

Post-closure model Scenario 4

Model **Scenario 4** represents pre-mining aquifer conditions with an effective aquifer recharge of **13%** of the mean annual rainfall. Layer 1 was assigned a **specific yield** of **0.06**, while a **storage coefficient** of **0.008** was assigned to layer 2. Aquifer **transmissivity** remained unchanged, as illustrated in **Figure 6.1-2**.

According to the model simulation the **time-to-decant** of the 15 **smaller opencast pits** (as illustrated in **Figure 8.1.2-1**) vary between **5 and 80** years post-closure, with an average of **39** years. Simulated **decant volumes** vary between **0 and 70 m³/d**, with an average of **29 m³/d**.

For the 9 **larger opencast pits** the **time-to-decant** was simulated to vary between **15 and 70** years post closure, with an average of **39** years. Simulated **decant volumes** vary between **76 and 343 m³/d**, with an average of **199 m³/d**.

The increase in aquifer recharge from 10% in Scenario 1 to 13% in Scenario 4 caused a significant increase in decant volumes from an average of 145 m³/d to 199 m³/d respectively for the 9 larger opencast pits. Simulated time-to-decant decreased from Scenario 1 to Scenario 4, which is the result of the increased recharge to the backfilled opencast pits. An increase in the available volumes of water cause a decrease in the amount of time it takes a backfilled opencast pit to fill with water to its decant elevation.

Post-closure model Scenario 5

Model **Scenario 5** represents post-mining aquifer conditions with an effective aquifer recharge of **13%** of the mean annual rainfall. **Transmissivity** of the backfilled opencast pits was increased to **25 m²/d**, while the **specific yield** of layer 1 was increased to **0.12** and the **storage coefficient** of layer 2 was increased to **0.01**.

According to the model simulation the **time-to-decant** of the 15 **smaller opencast pits** (as illustrated in **Figure 8.1.2-1**) vary between **5 and 172** years post-closure, with an average of **61** years. Simulated **decant volumes** vary between **0 and 89 m³/d**, with an average of **30 m³/d**.

For the 9 **larger opencast pits** the **time-to-decant** was simulated to vary between **17 and 97** years post closure, with an average of **54** years. Simulated **decant volumes** vary between **67 and 335 m³/d**, with an average of **208 m³/d**.

Once again the increase in recharge from 10% of the mean annual precipitation in Scenario 2 to 13% in Scenario 5 caused a significant decrease in the time-to-decant. The average time-to-decant decreased from 69 years post closure in Scenario 2 to 54 years in Scenario 5 for the larger opencast pits. Decant volumes increased significantly from Scenario 2 to Scenario 5 from 155 m³/d to 208 m³/d for the larger pits.

Post-closure model Scenario 6

Model **Scenario 6** represents post-mining aquifer conditions with an effective aquifer recharge of **13%** of the mean annual rainfall. **Transmissivity** of the backfilled opencast pits was increased to **50 m²/d**, while the **specific yield** of layer 1 was increased to **0.18** and the **storage coefficient** of layer 2 was increased to **0.012**

According to the model simulation the **time-to-decant** of the 15 **smaller opencast pits** (as illustrated in **Figure 8.1.2-1**) vary between **5 and 217** years post-closure, with an average of **76** years. Simulated **decant volumes** vary between **0 and 95 m³/d**, with an average of **30 m³/d**.

For the 9 **larger opencast pits** the **time-to-decant** was simulated to vary between **20 and 122** years post closure, with an average of **66** years. Simulated **decant volumes** vary between **69 and 360 m³/d**, with an average of **218 m³/d**.

As with Scenario 4 and 5, the increase in recharge from 10% in Scenario 3 to 13% in Scenario 6 caused decrease in the time-to-decant. The average time-to-decant of the larger opencast pits decreased from 83 years post closure in Scenario 3 to 66 years in Scenario 6. As expected, average decant volumes increased from 164 m³/d to 218 m³/d.

The following conclusions can be drawn from model Scenarios 1, 2, 3, 4, 5, and 6:

- The increase in aquifer recharge from 10% in Scenarios 1, 2, and 3 to 13% in Scenarios 4, 5, and 6 caused a significant decrease in the time-to-decant, while a major increase in the decant volumes were observed,
- The effective recharge to the backfilled opencast pits is a more sensitive aquifer parameter than both the specific yield and storage coefficient, as is evident in the significantly decreased time-to-decant and increased decant volumes.

Post-closure model Scenario 7

Model **Scenario 7** represents pre-mining aquifer conditions with an effective aquifer recharge of **16%** of the mean annual rainfall. Layer 1 was assigned a **specific yield** of **0.06**, while a **storage coefficient** of **0.008** was assigned to layer 2. Aquifer **transmissivity** remained unchanged, as illustrated in **Figure 6.1-2**.

According to the model simulation the **time-to-decant** of the 15 **smaller opencast pits** (as illustrated in **Figure 8.1.2-1**) vary between **2 and 60** years post-closure, with an average of **30** years. Simulated **decant volumes** vary between **0 and 90 m³/d**, with an average of **38 m³/d**.

For the 9 **larger opencast pits** the **time-to-decant** was simulated to vary between **10 and 60** years post closure, with an average of **31** years. Simulated **decant volumes** vary between **103 and 455 m³/d**, with an average of **263 m³/d**.

The increase in effective aquifer recharge from 13% in Scenario 4 to 16% in Scenario 7 caused a significant decrease in the average time-to-decant from 39 years post-closure to 31 years for the larger opencast pits. The average decant volumes increased from 199 m³/d in Scenario 4 to 263 m³/d for the larger pits in Scenario 7.

Post-closure model Scenario 8

Model **Scenario 8** represents post-mining aquifer conditions with an effective aquifer recharge of **16%** of the mean annual rainfall. **Transmissivity** of the backfilled opencast pits was increased to **25 m²/d**, while the **specific yield** of layer 1 was increased to **0.12** and the **storage coefficient** of layer 2 was increased to **0.01**.

According to the model simulation the **time-to-decant** of the 15 **smaller opencast pits** (as illustrated in **Figure 8.1.2-1**) vary between **7 and 127** years post-closure, with an average of **48** years. Simulated **decant volumes** vary between **0 and 103 m³/d**, with an average of **38 m³/d**.

For the 9 **larger opencast pits** the **time-to-decant** was simulated to vary between **12 and 85** years post closure, with an average of **44** years. Simulated **decant volumes** vary between **91 and 418 m³/d**, with an average of **264 m³/d**.

As expected the increase in recharge from 13% of the mean annual rainfall in Scenario 5 to 16% in Scenario 8 caused a decrease in the time-to-decant from 54 years post-closure to 44 years for the larger opencast. Decant volumes increased significantly from 208 m³/d to 264 m³/d for the larger pits.

Post-closure model Scenario 9

Model **Scenario 9** represents post-mining aquifer conditions with an effective aquifer recharge of **16%** of the mean annual rainfall. **Transmissivity** of the backfilled opencast pits was increased to **50 m²/d**, while the **specific yield** of layer 1 was increased to **0.18** and the **storage coefficient** of layer 2 was increased to **0.012**

According to the model simulation the **time-to-decant** of the 15 **smaller opencast pits** (as illustrated in **Figure 8.1.2-1**) vary between **7 and 162** years post-closure, with an average of **58** years. Simulated **decant volumes** vary between **0 and 109 m³/d**, with an average of **38 m³/d**.

For the 9 **larger opencast pits** the **time-to-decant** was simulated to vary between **15 and 100** years post closure, with an average of **54** years. Simulated **decant volumes** vary between **91 and 449 m³/d**, with an average of **274 m³/d**.

As with Scenarios 7 and 8 the increase in effective aquifer recharge from 13% of the mean annual rainfall in Scenario 6 to 16% in Scenario 9 caused a decrease in the time-to-decant from 66 years post-closure to 54 years for the larger opencast pits. The average decant volume of the larger opencast pits increased from 218 m³/d to 274 m³/d.

The following conclusions can be drawn from all 9 the model simulations:

- The effective aquifer recharge is a very sensitive parameter (more so than specific yield and storage coefficient), as significant decreases in the time-to-decant were simulated with an increase in the aquifer recharge,
- Major increases in the decant volumes followed after each increase in the effective recharge to the backfilled opencast pits.

A transmissivity sensitivity analysis was conducted with the use of the numerical groundwater flow model in order to determine to what extent decant volumes are affected by changes in both pit transmissivities and the transmissivity of the surrounding, undisturbed aquifer/s. The results of 8 numerical groundwater flow model simulations are provided in **Tables 8.1.2-1** and **8.1.2-2**.

In theory, the transmissivity of the backfilled opencast pits are not supposed to have an influence on the volumes of groundwater moving through, and subsequently decanting from the pits, as the structure of the surrounding aquifer/s remain undisturbed by the mining activities. Increases in the transmissivity of the backfilled opencast pits are however expected to cause an increase in recharge (*Hodgson et al, 2005*). The expected increase in recharge to the backfilled opencast pits was addressed in the construction of the post closure numerical groundwater flow model, as recharge to the pits increased from $\pm 3\%$ to a maximum of 16% of the mean annual precipitation.

According to the sensitivity analysis (**Tables 8.1.2-1** and **8.1.2-2**) the transmissivity of the backfilled opencast pits do not play a major role in the numerical decant volume estimations. A 100% increase in the transmissivity of the opencast pits merely lead to a 2 - 3% increase in the estimated decant volumes.

The transmissivity of the surrounding, undisturbed aquifer/s (**Tables 8.1.2-1** and **8.1.2-2**) play a more significant role in the numerical decant volume calculations. An increase in the transmissivity of the surrounding aquifer/s lead to overall lower decant volumes, however, a 100% increase in the transmissivity of the opencast pits now lead to a 6 - 10% increase in the estimated decant volumes.

Table 8.1.2-1: Transmissivity sensitivity analysis ($T = 2 \text{ m}^2/\text{d}$)

Surrounding aquifer $T = 2 \text{ m}^2/\text{d}$							
Pit	PT = 25	% Increase	PT = 50	% Increase	PT = 100	% Increase	PT = 150
1	181		188		198		206
2	250		249		248		251
3	249		291		334		361
4	57		58		55		50
5	95		90		84		81
6	346		360		375		382
7	240		207		181		164
8	54		56		57		57
9	10		13		15		16
10	15		14		13		12
11	35		28		21		16
12	0		0		0		0
13	22		21		19		16
14	444		476		497		508
15	24		24		25		25
16	38		38		37		36
17	185		191		201		207
18	58		58		61		62
19	24		23		21		20
20	55		55		55		55
21	325		357		400		436
22	138		143		147		151
23	70		71		70		67
24	16		17		18		19
Total	2931	3	3028	3	3132	2	3198

Notes:

T - Transmissivity

PT - Pit Transmissivity

Table 8.1.2-2: Transmissivity sensitivity analysis ($T = 4 \text{ m}^2/\text{d}$)

Surrounding aquifer $T = 4 \text{ m}^2/\text{d}$							
Pit	PT = 25	% Increase	PT = 50	% Increase	PT = 100	% Increase	PT = 150
1	192		205		222		236
2	251		250		250		253
3	190		234		285		322
4	52		53		50		42
5	87		79		71		68
6	196		313		334		344
7	67		29		2		0
8	75		80		82		82
9	11		15		17		17
10	18		17		15		14
11	0		0		0		0
12	0		0		0		0
13	24		23		21		16
14	477		538		583		602
15	33		33		33		34
16	1		0		0		0
17	176		185		201		212
18	58		59		62		65
19	28		26		23		21
20	48		49		49		49
21	194		223		263		286
22	188		200		210		216
23	23		20		11		4
24	18		21		24		25
Total	2407	10	2652	6	2808	4	2908

Notes:

T - Transmissivity

PT - Pit Transmissivity

What is of interest is the fact that the estimated decant volumes decrease with an increase in the transmissivity of the surrounding aquifer. A possible explanation for the phenomenon is the fact that an increase in the transmissivity of the surrounding aquifer leads to smoother groundwater hydraulic gradients, which subsequently leads to a decrease in groundwater discharge to the rehabilitated pits. The same phenomenon was also encountered in a study that was conducted by the IGS in 2005 (**Section 3.4**). In theory, an increase in transmissivity should lead to an increase in groundwater moving into the void, with a subsequent increase in groundwater decanting from the pit – the numerical groundwater flow model did however simulate the opposite. The theory is half true, as the rate at which water flows from the void also increases, resulting in more water leaving the pit than entering it (*Hodgson et al, 2005*).

The conclusion that is therefore drawn from the sensitivity analysis is that pit transmissivity is a less sensitive parameter compared to the transmissivity of the surrounding aquifer/s – in the context of groundwater decant volumes. A pit transmissivity of 50 m²/d is therefore considered to be sufficient to comply with the objectives of the thesis. Furthermore, the values assigned to the model parameters compare well with an earlier study conducted by professor Frank Hodgson in 2005 (*Hodgson et al, 2005*). The groundwater contribution to pit water was also found to be far less compared to the recharge component.

8.2 Analytical and volume calculations results

Groundwater discharge to both the Bronkhorstspruit and Koffiespruit was calculated with the use of **Equation 3.2-3**. Discharge to the **Bronkhorstspruit** was calculated to be **130 m³/d**, while discharge to the **Koffiespruit** was calculated at **140 m³/d**.

Surfer 8 was used to calculate the total-mined-volume for each individual opencast pit and the results are provided in **Table 7-1**. According to the calculations the following five pits (high to low) have the largest mined-volume: pit 21, 07, 14, 06, and 02; while pits (low to high) 09, 08, 12, 10, and 13 have the smallest mined-volumes.

Due to the uncertainty regarding the effective recharge to the rehabilitated opencast pits and transmissivity of the backfill material, sensitivity analyses were conducted to determine the time-to-decant and decant volumes of each individual opencast pit. The results of the analyses are provided in **Tables 7-2 and 7-3**.

Worst case scenario

During the worst case scenario the backfilled opencast pits were assigned an effective porosity of 15%, while an effective recharge 16% of the mean annual rainfall was assigned to the aquifer.

According to the worst case scenario calculations the **time-to-decant** of the 15 **smaller opencast pits** (as illustrated in **Figure 8.1.2-1**) vary between **19 and 75** years post-closure, with an average of **42** years. Simulated **decant volumes** vary between **14 and 91 m³/d**, with an average of **43 m³/d**.

For the 9 **larger opencast pits** the **time-to-decant** was calculated to vary between **13 and 64** years post closure, with an average of **40** years. Simulated **decant volumes** vary between **129 and 533 m³/d**, with an average of **313 m³/d**.

Average scenario

During the average scenario the backfilled opencast pits were assigned an effective porosity of 20%, while an effective recharge 13% of the mean annual rainfall was assigned to the aquifer.

According to the average scenario calculations the **time-to-decant** of the 15 **smaller opencast pits** (as illustrated in **Figure 8.1.2-1**) vary between **31 and 123** years post-closure, with an average of **69** years. Simulated **decant volumes** vary between **11 and 74 m³/d**, with an average of **35 m³/d**.

For the 9 **larger opencast pits** the **time-to-decant** was calculated to vary between **21 and 104** years post closure, with an average of **66** years. Simulated **decant volumes** vary between **105 and 433 m³/d**, with an average of **255 m³/d**.

Best case scenario

During the best case scenario the backfilled opencast pits were assigned an effective porosity of 25%, while an effective recharge 10% of the mean annual rainfall was assigned to the aquifer.

According to the average scenario calculations the **time-to-decant** of the 15 **smaller opencast pits** (as illustrated in **Figure 8.1.2-1**) vary between **51 and 200** years post-closure, with an average of **112** years. Simulated **decant volumes** vary between **9 and 57 m³/d**, with an average of **27 m³/d**.

For the 9 **larger opencast pits** the **time-to-decant** was calculated to vary between **34 and 170** years post closure, with an average of **107** years. Simulated **decant volumes** vary between **81 and 333 m³/d**, with an average of **196 m³/d**.

The following conclusions can be drawn from the three scenarios:

- An increase in the effective porosity of the backfilled opencast pits cause an increase in the time-to-decant, as more water is required to fill the pits to their decant elevations,
- An increase in the effective aquifer recharge cause an increase in the decant volumes and a decrease in the time-to-decant, because more water is available to fill the pits to their decant elevations.

8.3 Numerical and analytical correlation

In order to determine the relationship between the numerical groundwater flow model simulations and analytical calculations, statistical analyses were conducted for all **nine numerical groundwater flow model simulations** during which the results were compared to those of the **analytical average scenario calculations**. A short summary of each analysis is provided.

Post-closure model Scenario 1

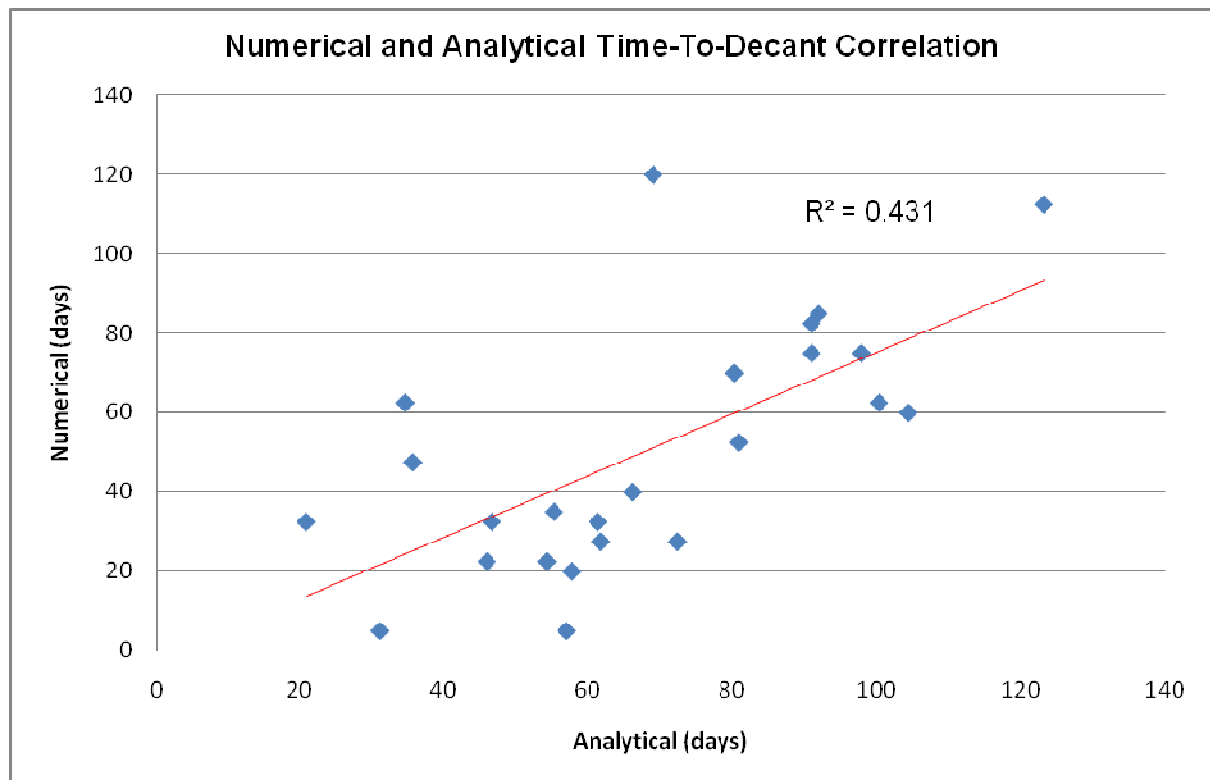


Figure 8.3-1: Time-to-decant correlation graph – Scenario 1

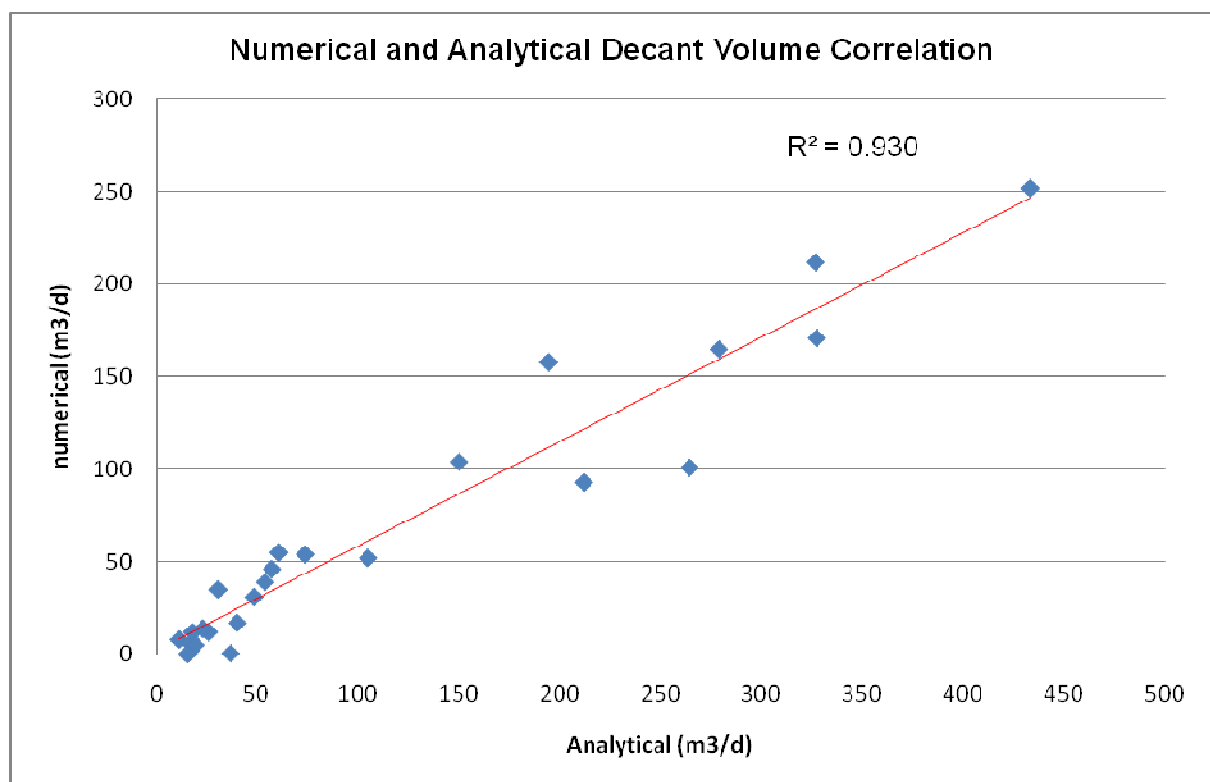


Figure 8.3-2: Decant volume correlation graph – Scenario 1

The following conclusions can be drawn from **Figures 8.3-1** and **8.3-2**:

- There exist no significant correlation between the results of the numerical post-closure Scenario 1 and the analytical average scenario time-to-decant calculations. A correlation of $\pm 43\%$ was calculated,
- Overall longer time-to-decant values were simulated with the numerical post-closure model when compared to the analytical calculations,
- A very good correlation exists between the results of the numerical post-closure Scenario 1 and the analytical average scenario decant volume calculations. A correlation of $\pm 93\%$ was calculated.

Post-closure model Scenario 2

The following conclusions can be drawn from **Figures 8.3-3** and **8.3-4**:

- There exists a better correlation between the numerical post-closure Scenario 2 and analytical average scenario time-to-decant calculations,
- The time-to-decant correlation increased from $\pm 43\%$ in Scenario 1 to approximately 69% in Scenario 2,
- There still exists a very good correlation between the numerical and analytical decant volume calculations,
- The correlation did however decrease slightly from 93% in Scenario 1 to approximately 90% in Scenario 2.

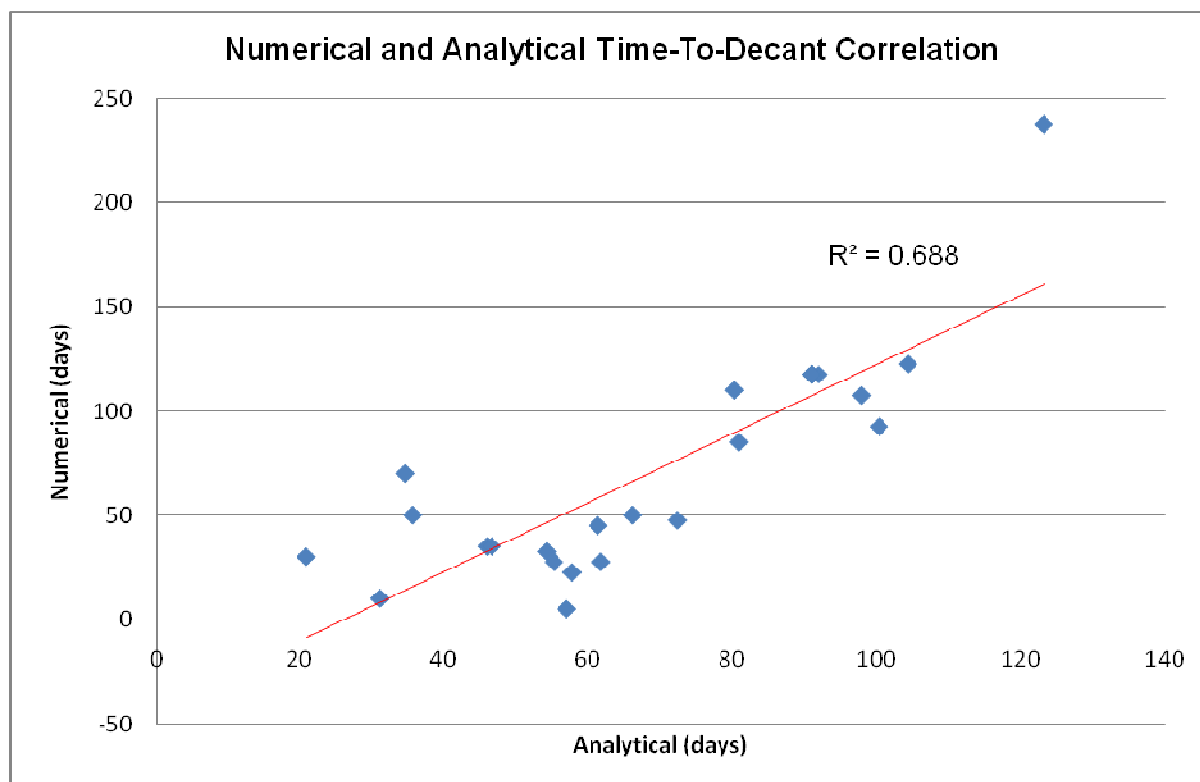


Figure 8.3-3: Time-to-decant correlation graph – Scenario 2

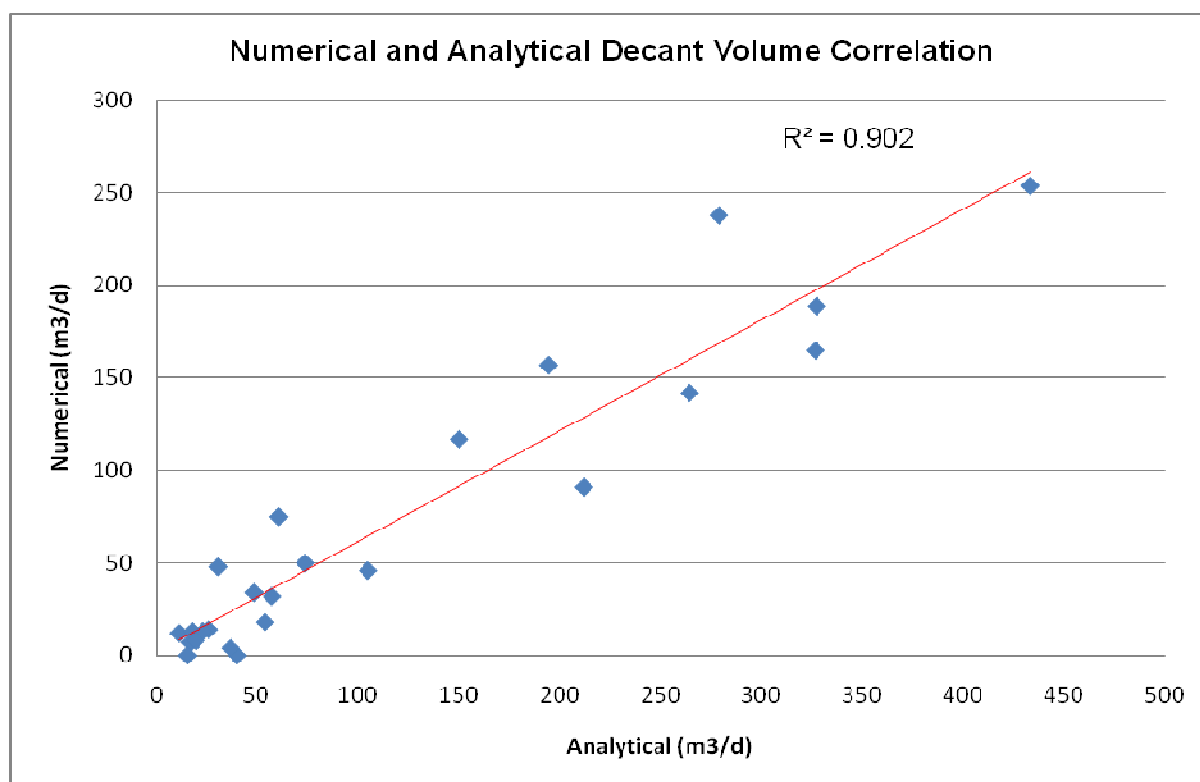


Figure 8.3-4: Decant volume correlation graph – Scenario 2

Post-closure model Scenario 3

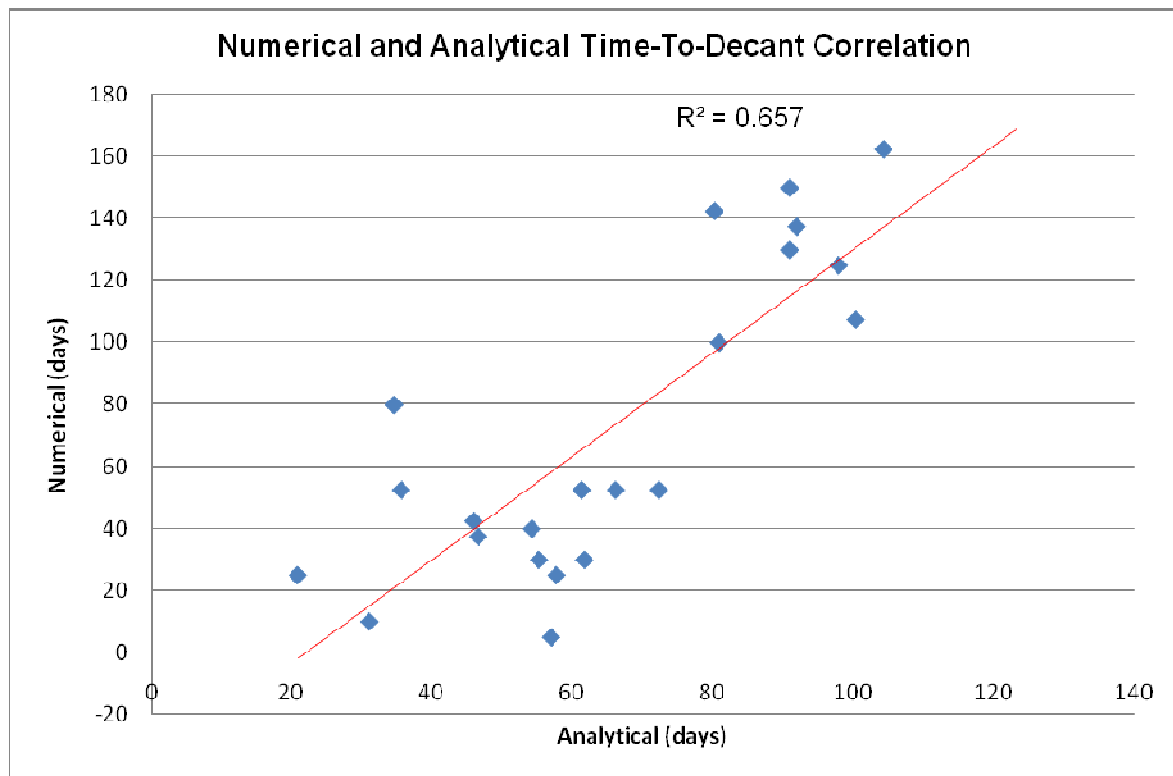


Figure 8.3-5: Time-to-decant correlation graph – Scenario 3

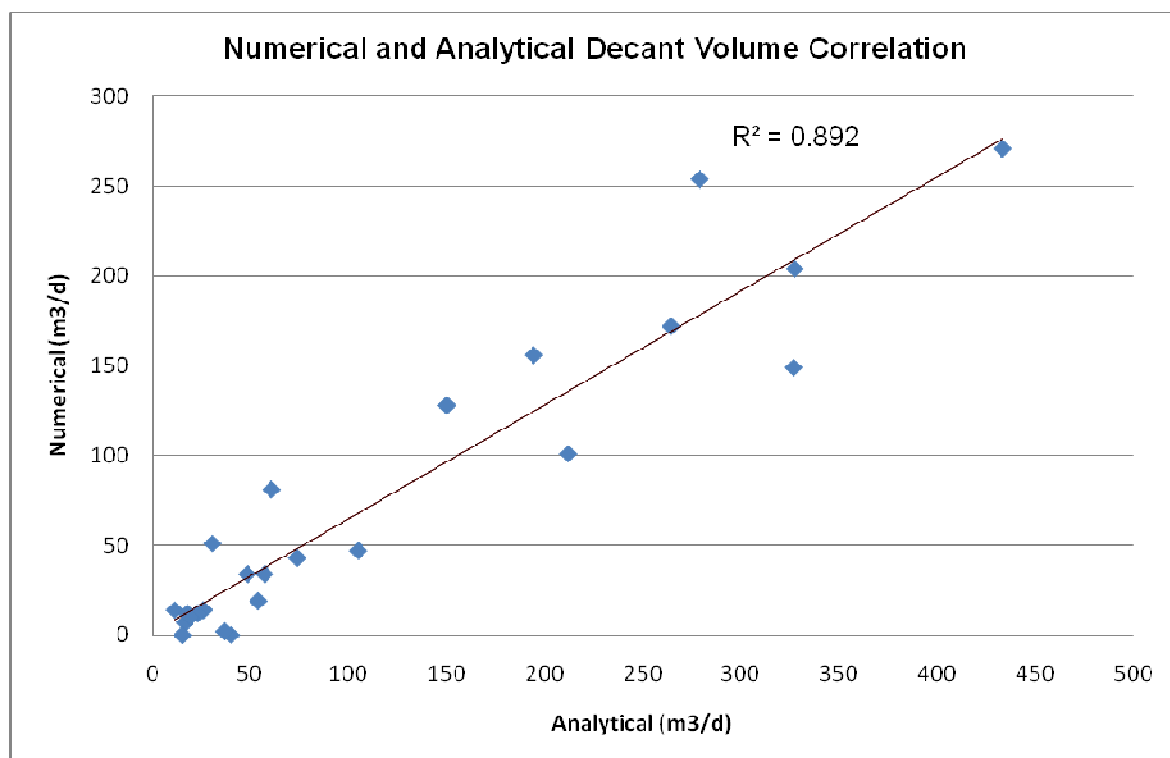


Figure 8.3-6: Decant volume correlation graph – Scenario 3

The following conclusions can be drawn from **Figures 8.3-5** and **8.3-6**:

- The correlation of both the time-to-decant and the decant volume of Scenario 3 decreased slightly from Scenario 2,
- A correlation of $\pm 66\%$ was calculated for the time-to-decant, while a correlation of approximately 89% was calculated for the decant volume calculations.

Post-closure model Scenario 4

The following conclusions can be drawn from **Figures 8.3-7** and **8.3-8**:

- The time-to-decant correlation increased from 43% in Scenario 1 to 46% in Scenario 4,
- The decant volume correlations also showed an increase from 93% in Scenario 1 to approximately 96% in Scenario 4.

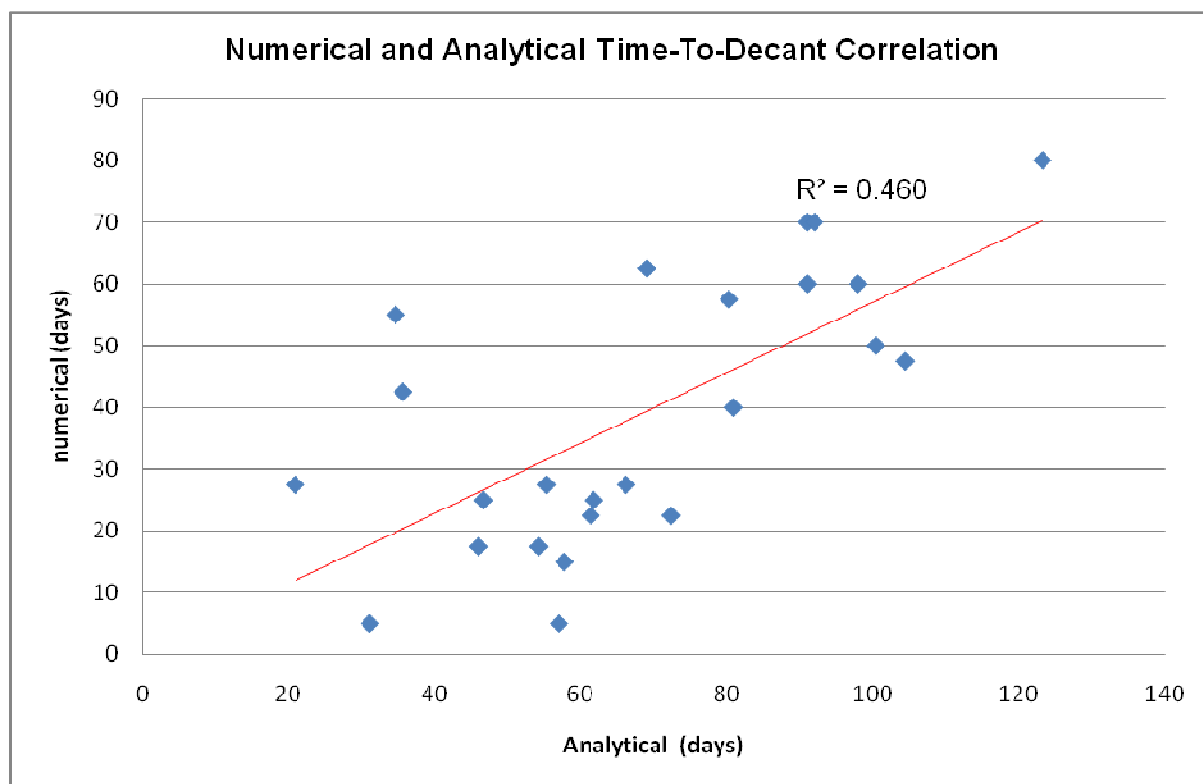


Figure 8.3-7: Time-to-decant correlation graph – Scenario 4

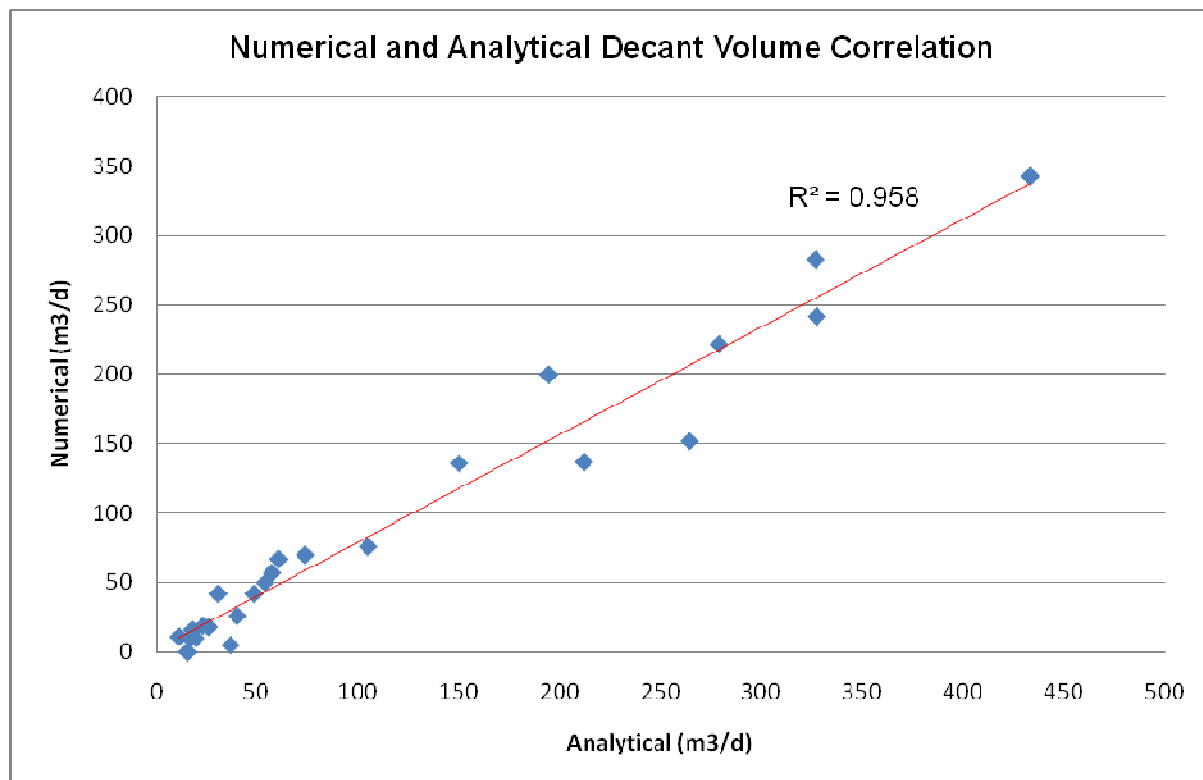


Figure 8.3-8: Decant volume correlation graph – Scenario 4

Post-closure model Scenario 5

The following conclusions can be drawn from **Figures 8.3-9** and **8.3-10**:

- The time-to-decant correlation decreased from 69% in Scenario 2 to 53% in Scenario 5,
- The decant volume correlation increased from 90% in Scenario 2 to approximately 94% in Scenario 5.

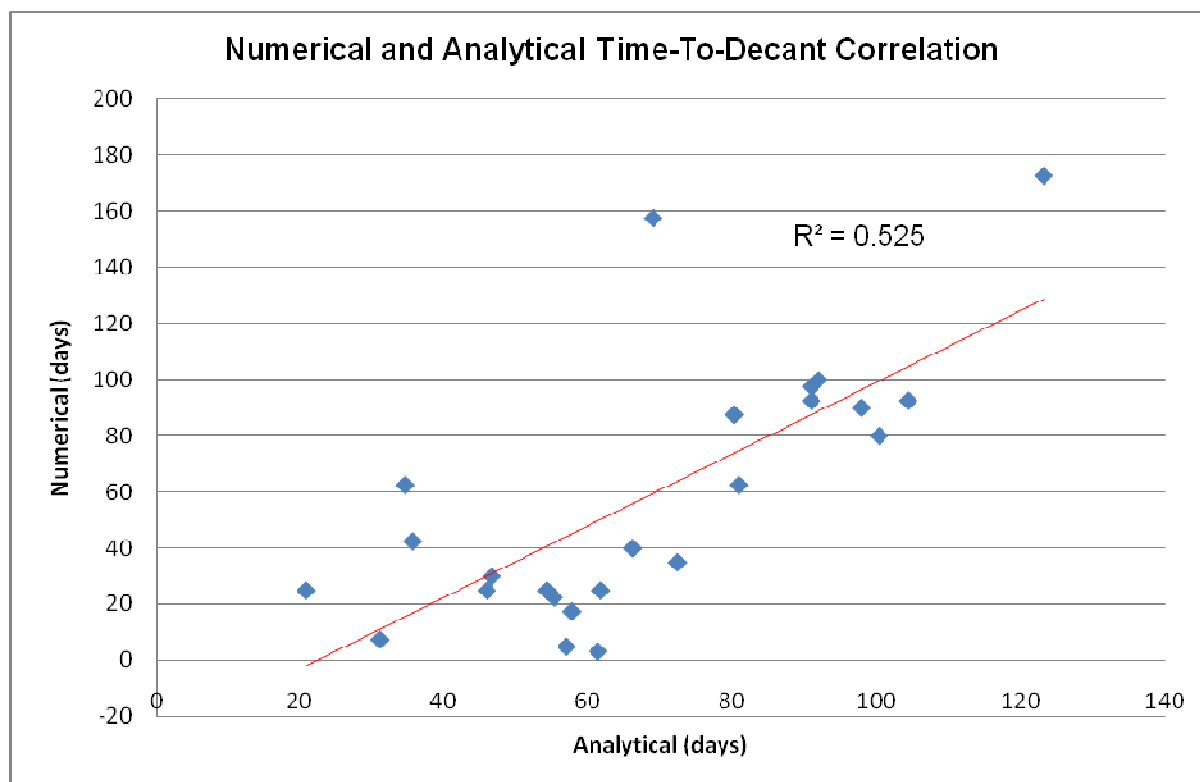


Figure 8.3-9: Time-to-decant correlation graph – Scenario 5

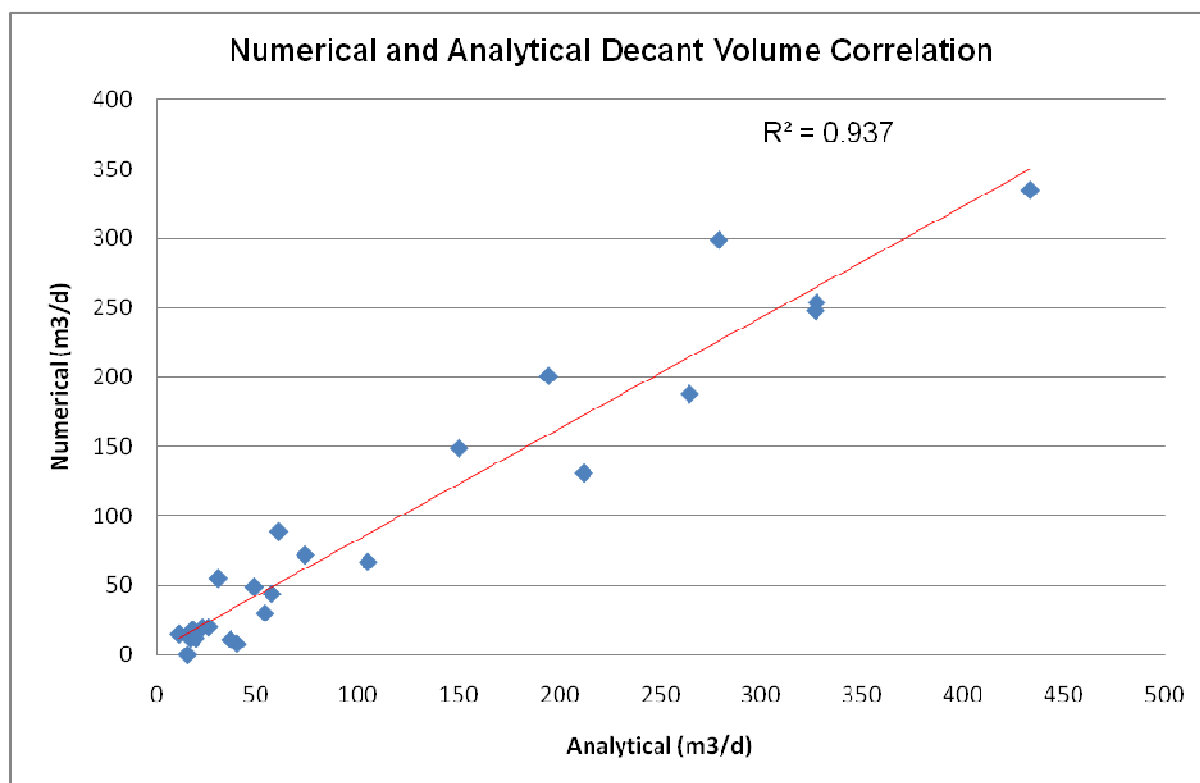


Figure 8.3-10: Decant volume correlation graph – Scenario 5

Post-closure model Scenario 6

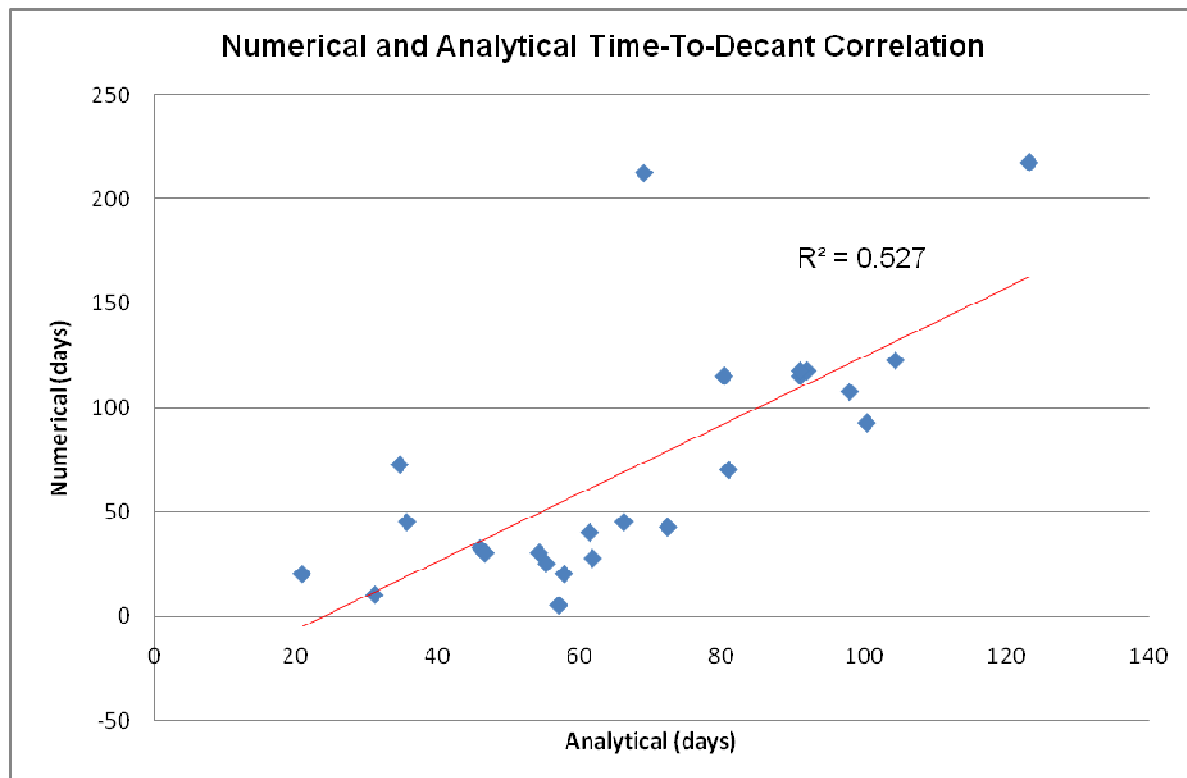


Figure 8.3-11: Time-to-decant correlation graph – Scenario 6

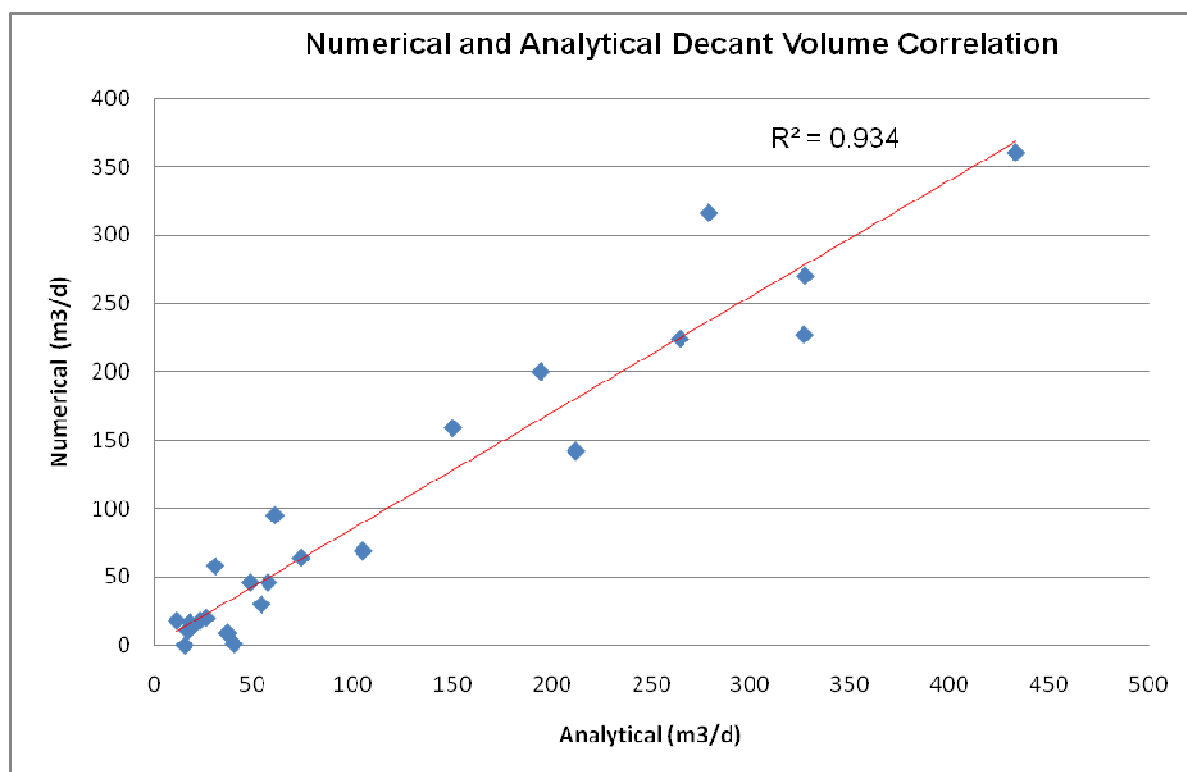


Figure 8.3-12: Decant volume correlation graph – Scenario 6

The following conclusions can be drawn from **Figures 8.3-11** and **8.3-12**:

- The time-to-decant correlation decreased from 66% in Scenario 3 to approximately 53% in Scenario 6,
- The decant volume correlation increased however from 89% in Scenario 3 to approximately 93% in Scenario 6.

Post-closure model Scenario 7

The following conclusions can be drawn from **Figures 8.3-13** and **8.3-14**:

- The time-to-decant correlation decreased from 46% in Scenario 4 to approximately 40% in Scenario 7,
- The decant volume correlation increased however from 96% in Scenario 4 to approximately 97% in Scenario 7.

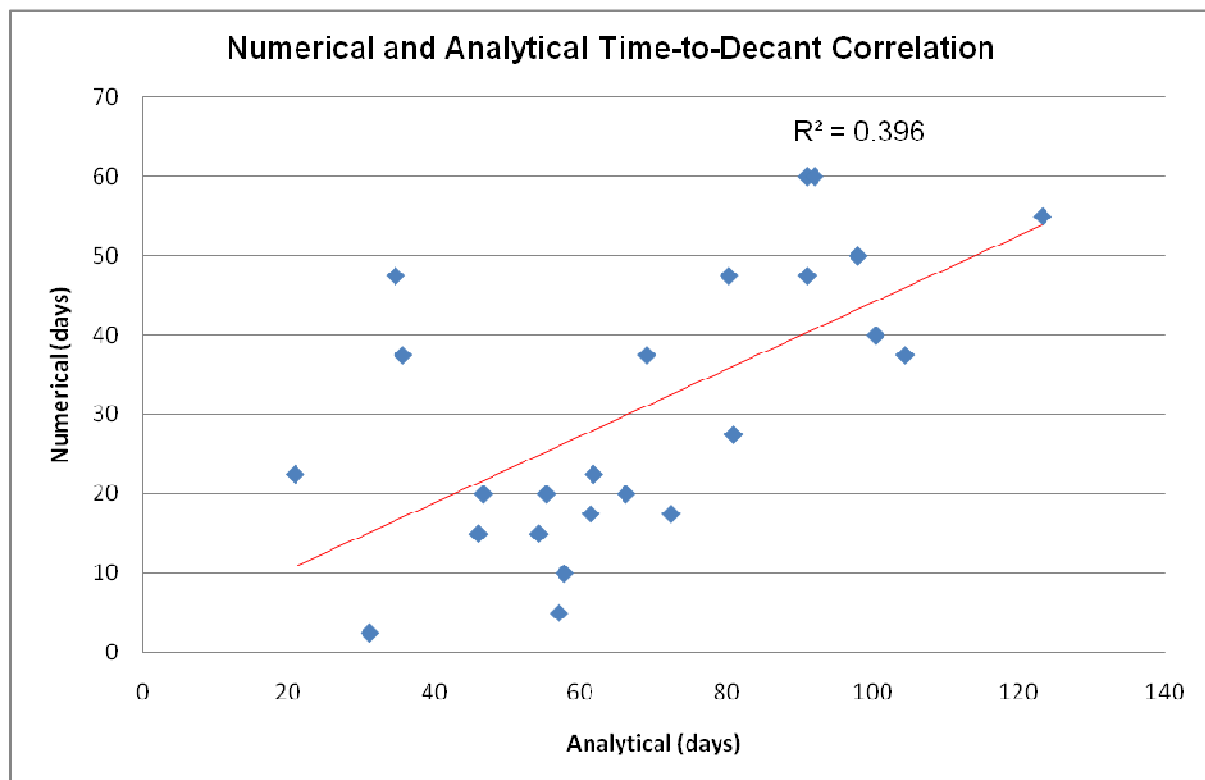


Figure 8.3-13: Time-to-decant correlation graph – Scenario 7

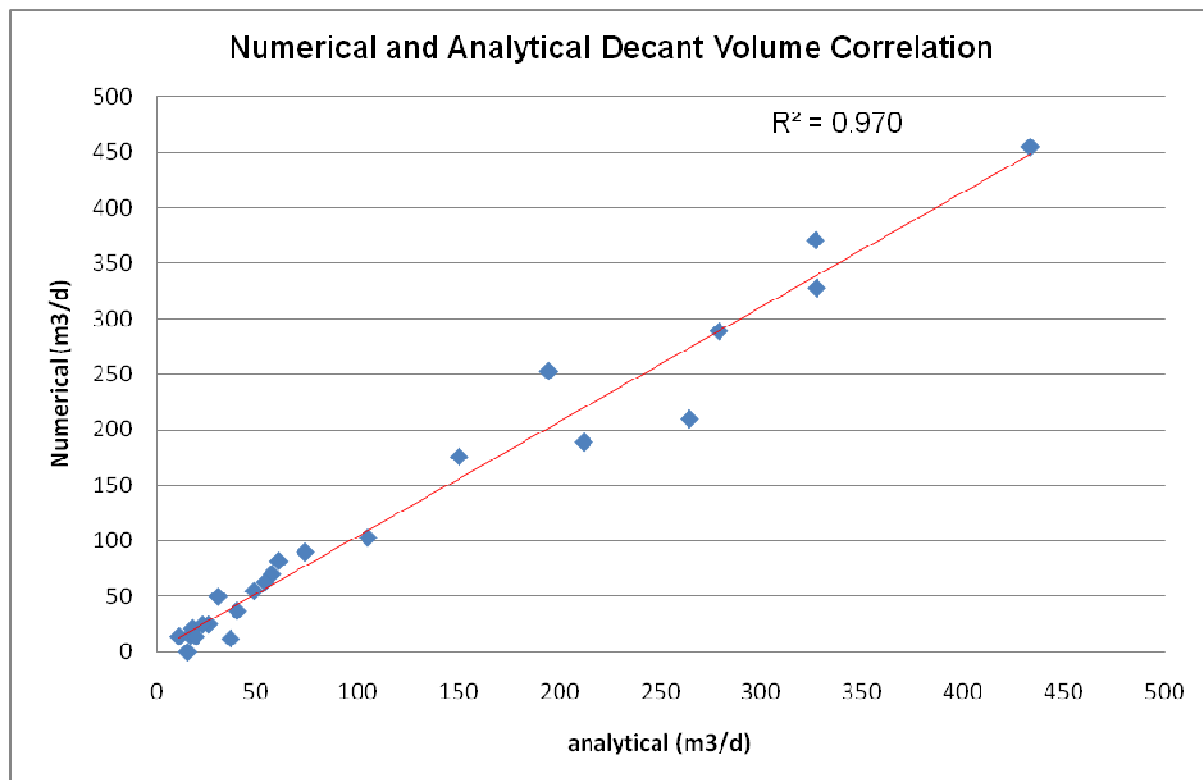


Figure 8.3-14: Decant volume correlation graph – Scenario 7

Post-closure model Scenario 8

The following conclusions can be drawn from **Figures 8.3-15** and **8.3-16**:

- The time-to-decant correlation increased from 52% in Scenario 5 to approximately 62% in Scenario 8,
- The decant volume correlation once again increased from 94% in Scenario 5 to approximately 96% in Scenario 8.

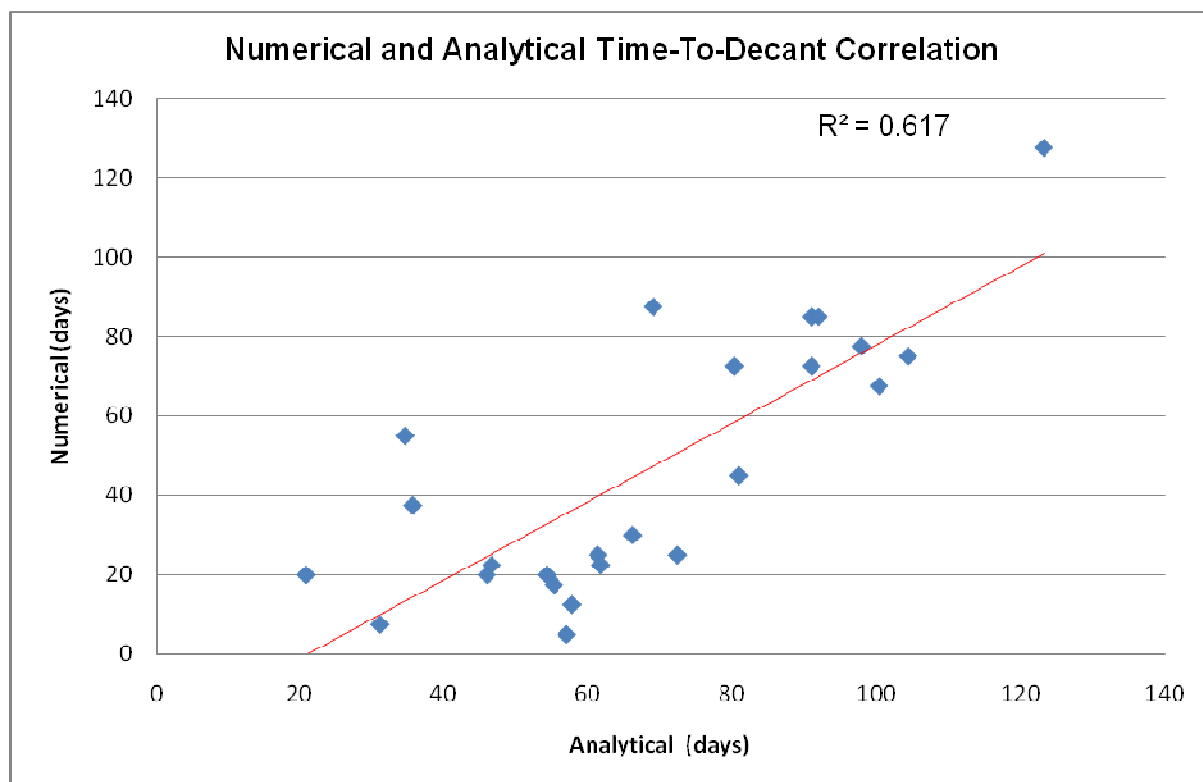


Figure 8.3-15: Time-to-decant correlation graph – Scenario 8

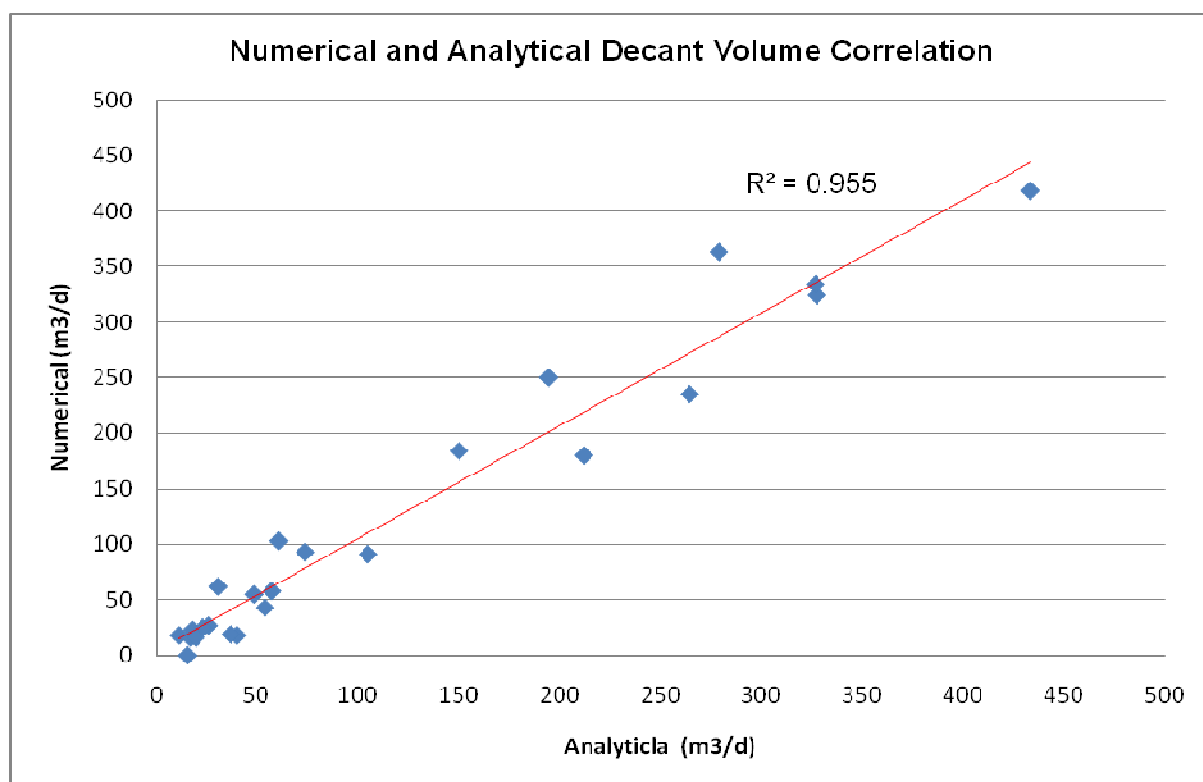


Figure 8.3-16: Decant volume correlation graph – Scenario 8

Post-closure model Scenario 9

The following conclusions can be drawn from **Figures 8.3-17** and **8.3-18**:

- The time-to-decant correlation increased from 53% in Scenario 6 to approximately 64% in Scenario 9,
- The decant volume correlation once again increased from 93% in Scenario 6 to approximately 96% in Scenario 9.

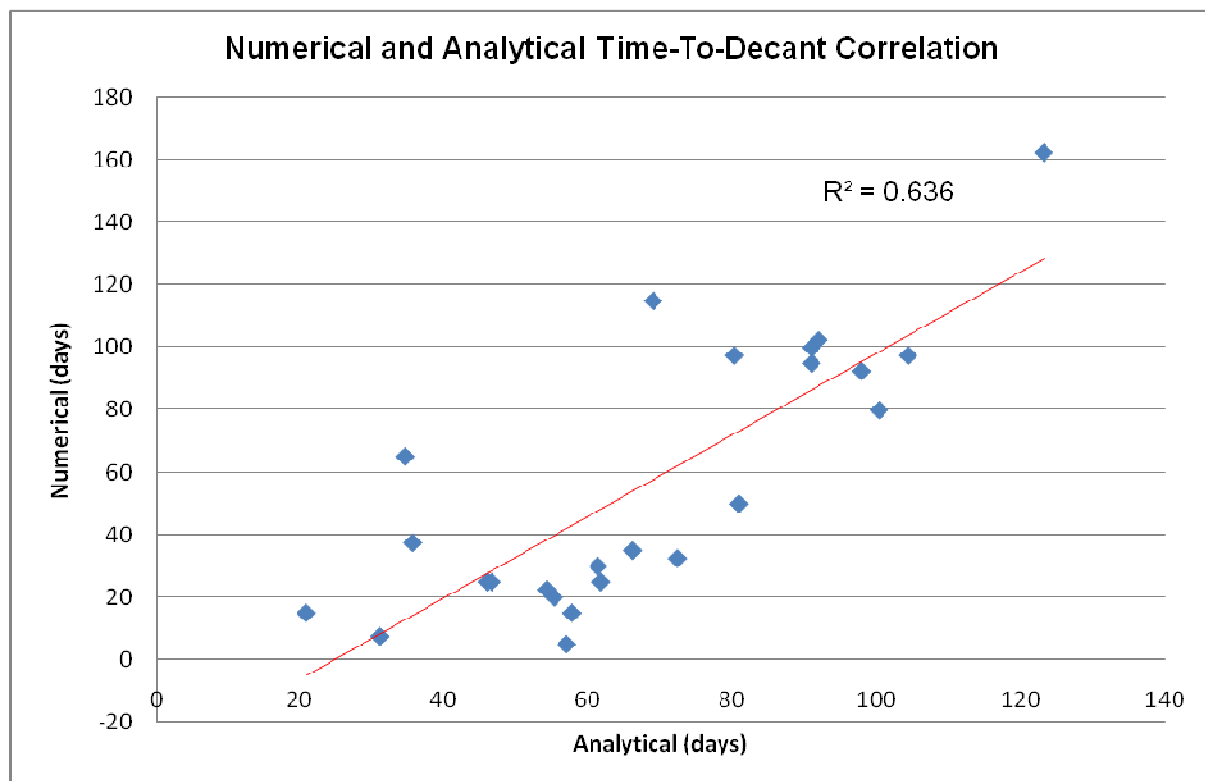


Figure 8.3-17: Time-to-decant correlation graph – Scenario 9

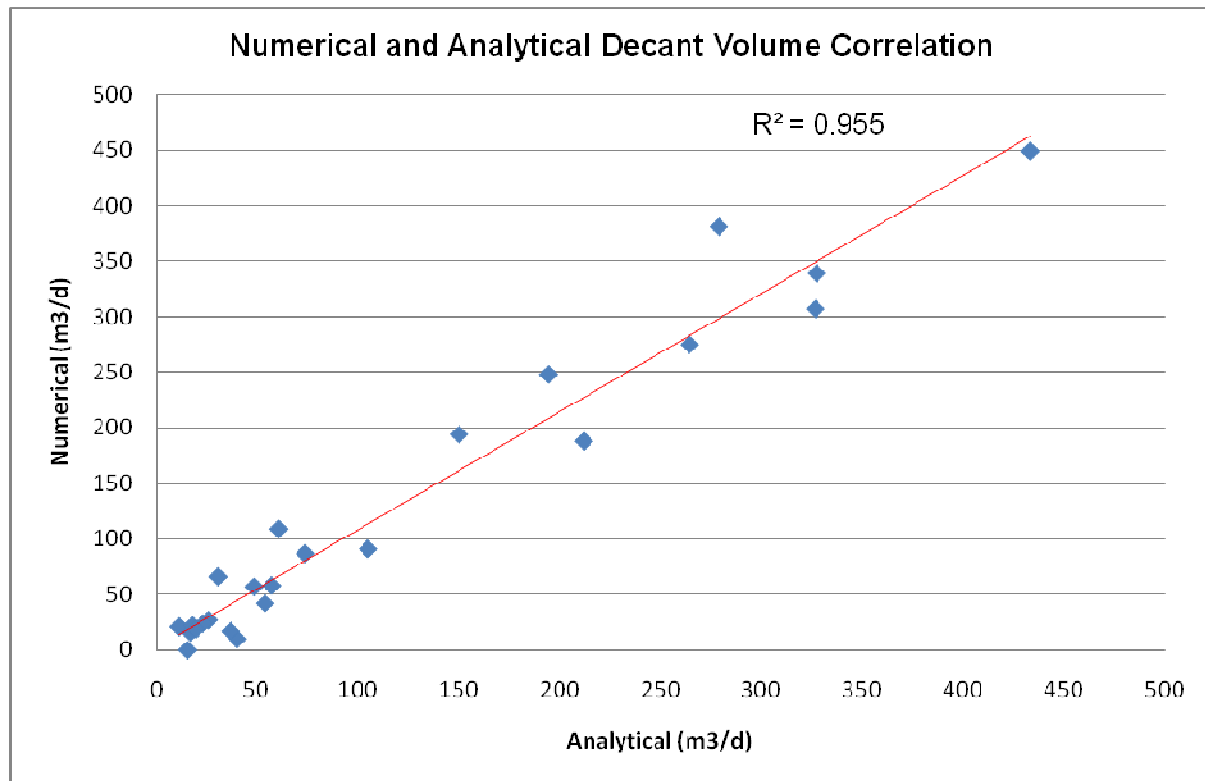


Figure 8.3-18: Decant volume correlation graph – Scenario 9

The following main conclusions can be drawn from both the time-to-decant and decant volume correlations:

- The **lowest time-to-decant** correlation of approximately **40%** was calculated for numerical model **Scenario 7** and the **analytical average scenario**,
- The **best**, or **highest time-to-decant** correlation of approximately **69%** was calculated for the numerical model **Scenario 2** and the **average analytical scenario**,
- All nine of the **decant volume** correlations were high with an average of 94%, while there exist a low correlation between the numerical and analytical **time-to-decant** calculations,
- The **lowest decant volume** correlation of **89%** was however calculated for numerical model **Simulation 3** and the **average analytical scenario**,
- The **highest decant volume** correlation of **97%** was calculated for numerical model **Simulation 7** and the **average analytical scenario**.

It is worth mentioning that the study conducted by the IGS in 2005 came to the same conclusion, namely that there exists a good correlation between numerical and analytical decant volume calculations, whereas there exists no correlation between the numerical and analytical filling times/time-to-decant estimations (*Hodgson et al, 2005*).

Given the amount of uncertainty regarding aquifer transmissivity and hydraulic gradient between the aquifer and surface water bodies, the numerical and analytical groundwater discharge estimations to the Bronkhorstspuit and Koffiespruit are also closely related. A difference of **40 m³/d** discharge to the **Bronkhorstspuit** and **10 m³/d** to the **Koffiespruit** is considered to be insignificant.

9. Conclusions

The results of the numerical and analytical estimations are discussed in detail in **Section 8** of the thesis. A short summary of the findings is given below:

- Given the amount of uncertainty regarding aquifer heterogeneity, there do exist a good correlation between the numerical and analytical groundwater decant volume estimations,
- According to numerical groundwater discharge calculations, a groundwater discharge of 90 m³/d into the Bronkhorstspuit and 130 m³/d into the Koffiespruit was estimated,
- Numerical groundwater flow model simulations indicated a significant decrease in groundwater discharge to both surface water streams as soon as mining begins. End-of-mine simulations indicated a groundwater discharge of 30 m³/d to the Bronkhorstspuit and 20 m³/d to the Koffiespruit,
- The decrease in groundwater discharge to both surface water streams is the direct result of mine dewatering, which ultimately leads to a decrease in the local groundwater levels,
- Post-closure model simulations indicated a significant increase in groundwater discharge after active mining has ceased to both surface water streams,
- Increased groundwater discharge to the surface water streams is the direct result of increased recharge to the backfilled opencast pits and transmissivity to a lesser extent,
- According to analytical groundwater discharge calculations, a discharge of 130 m³/d to the Bronkhorstspuit and 140 m³/d to the Koffiespruit was estimated,
- An increase in the effective porosity of the backfilled opencast pits cause an increase in the time-to-decant, as more water is required to fill the pits to their decant elevations,
- An increase in the effective porosity will also lead to an increase in the chemical reaction surface, which ultimately leads to an accelerated sulphate production and acidification of groundwater,

- An increase in the effective aquifer recharge cause an increase in the decant volumes and a decrease in the time-to-decant, because more water is available to fill the pits to their decant elevations,
- The effective aquifer recharge is a very sensitive parameter (more so than specific yield and storage coefficient), as significant decreases in the time-to-decant were simulated with an increase in the aquifer recharge,
- The volumes of groundwater decant are more sensitive to variations in the transmissivity of the surrounding aquifer/s compared to the transmissivity of the backfilled opencast pits,
- During the numerical groundwater flow model simulations it was found that the groundwater contribution to pit water is far less compared to the recharge component,
- Major increases in the decant volumes followed after each increase in the effective recharge to the backfilled opencast pits during post-closure numerical groundwater flow model simulations,
- The **lowest time-to-decant** correlation of approximately **40%** was calculated for numerical model **Scenario 7** and the **analytical average scenario**,
- The **best**, or **highest time-to-decant** correlation of approximately **69%** was calculated for the numerical model **Scenario 2** and the **average analytical scenario**,
- All nine of the **decant volume** correlations were high with an average of 94%, while there exist a low correlation between the numerical and analytical **time-to-decant** calculations,
- The **lowest decant volume** correlation of **89%** was however calculated for numerical model **Simulation 3** and the **average analytical scenario**,
- The **highest decant volume** correlation of **97%** was calculated for numerical model **Simulation 7** and the **average analytical scenario**.

The above summary and detailed discussion of both the numerical groundwater flow model simulations and analytical calculations in **Section 8** of the thesis prove that there are still applications for analytical calculations in modern day geohydrology, despite the continuous development of numerical groundwater flow models.

Based on experience in similar coal mining operations within the Mpumalanga coal fields, the results of both the analytical decant volume and time-to-decant estimations correspond well with actual figures. One must however understand and master the various equations and keep in mind that an aquifer is a highly heterogeneous system. The results of both numerical groundwater flow model simulations and analytical calculations are only as good as the understanding of the geohydrological environment and the data they are based on.

10. References

- Acocks, J.P.H. (1988). *Veld types of South Africa*, 3rd ed. Botanical Research Institute, Department of Agriculture and Water Supply, Pretoria.
- Adams, R. and Younger, P.L. (2002). A Physically Based Model of Rebound in South Crofty Tin Mine. *Cornwall Adams and Younger Geological Society*, **198**, 89-97.
- Ahmad, M.D., Love, D., Kinoti, J., Kongo, V., Magagula, T.F. and Mul, M.L. (2005). Estimating Actual Evapotranspiration through Remote Sensing Techniques to Improve Agricultural Water Management: A Case Study in the Transboundary Olifants Catchment in the Limpopo Basin, South Africa. In: *The 6th WaterNet/WARFSA/GWP Annual Symposium*, Ezulwini, Swaziland, November 1–4 2005.
- Akcil, A. and Koldas, S. (2006). Acid Mine Drainage (AMD): Causes, Treatment and Case Studies. *Journal of Cleaner Production*, **14**, 1139-1145.
- Banks, D., Younger, P.L., Arnesen, R.T., Iversen, E.R. and Banks, S.B. (1997). Mine Water Chemistry: The Good, the Bad and the Ugly. *Environmental Geology*, **32(3)**, 157-174.
- Braun, T. (2002). Introduction to Pit Lakes in the Southwest. *Southwest Hydrology*, **1(3)**, 12-13.
- Bredenkamp, D.B., Botha, L.J., Van Tonder, G.J. and Van Rensburg, H.J. (1995). Manual on Quantitative Estimation of Groundwater Recharge and Aquifer Storativity. *WRC Report TT218/03*, Water Research Commission, Pretoria.

Buck, B.W. and Winegar, B. (2003). Integration of Surface Water Management with Mitigation of Groundwater Impacts at a Proposed Phosphate Mine Overburden Facility. In: National Meeting of the American Society of Mining and Reclamation and the 9th Billings Land Reclamation Symposium, 3134 Montavesta Rd., Lexington, June 3-6, 2003.

Chevallier, L., and Woodford, A.C. (2002). Hydrogeology of the Main Karoo Basin: Current Knowledge and Future Research Needs. WRC Report No TT179/02, Water Research Commission, Pretoria.

Colvin, C.A. and Le Maitre, D.C. (2008). Assessment of the Contribution of Groundwater Discharges to Rivers Using Monthly Flow Statistics and Flow Seasonality. *Water SA*, **34(5)**, 549-564.

Conrad, J., Hughes, D. and Parsons, R. (2007). Quantification of the Groundwater Contribution to Baseflow. *WRC Report No 1498/1/07*, Water Research Commission, Pretoria.

Fox, R. and Rowntree, K. (2000). *The Geography of South Africa in a Changing World*. OXFORD University Press South Africa, Cape Town.

Freeze, R.Z. and Cherry, J.A. (1979). *Groundwater*. Prentice-Hall Inc. Englewood Cliffs.

Hodgson, F.D.I. and Krantz, R.M. (1998). Groundwater Quality Deterioration in the Olifants River Catchment above the Loskop Dam with Specialist Investigations in the Witbank Dam Sub-Catchment. *WRC Report No 291/1/98*, Water Research Commission, Pretoria.

Hodgson, F.D.I., Vermeulen, P.D., Cruywagen, L.M. and De Necker, E. (2007). Investigation of Water Decant from the Underground Collieries in Mpumalanga, with Special Emphasis on Predictive Tools and Long-Term Water Quality Management. *WRC Report No 1263/1/07*, Water Research Commission, Pretoria.

Hodgson, F.D.I., Van Tonder, G., Havenga, A. and Usher, B. (2005). The Use and Applicability of Flow Models to Quantify Intermine Flow in the Western Witbank Coalfields. *The Journal of the South African Institute of Mining and Metallurgy*, **105**, 687-694.

Kirchner, R., Van Tonder, G.J. and Lukas, E. (1991). Exploitation Potential of Karoo Aquifers. *WRC Report No 170/1/91*, Water Research Commission, Pretoria.

Kotze, J.C. (2001). *Modelling of Groundwater Flow in the Table Mountain Group Fractured Sandstone Aquifer*. Unpubl. Ph.D Thesis, Institute for Groundwater Studies, University of the Free State.

Low, A.B. and Rebelo, A.G. (1996). *Vegetation of South Africa, Lesotho and Swaziland*. Department of Environmental Affairs & Tourism, Pretoria.

Manahan, Stanley E. (1991). *Environmental Chemistry*, 5th ed. Lewis Publishers Inc., United States of America.

Maree, J.P., Hlabela, P., Nengovhela, A.J., Geldenhuys, A.J., Mbhele, N., Nevhulaudzi, T. and Waanders, F.B. (2004). Treatment of Mine Water for Sulphate and Metal Removal Using Barium Sulphide. *Mine Water and the Environment*, **23(4)**, 195-203.

Midgeley, D.C., Pitman, W.V. and Middleton, B.J. (1990). Surface Water Resources of South Africa. *WRC Report No 298/1.1/94*, Water Research Commission, Pretoria.

Nichols, G. (1999). *Sedimentology & Stratigraphy*. Blackwell Publishing Company, United States of America.

Parsons, R. (2004). Surface Water – Groundwater Interaction in a Southern African Context. *WRC Report No TT218/03*, Water Research Commission, Pretoria.

Paul, M., Baacke, D., Metschies, T. and Kuhn, W. (2009). Post-Flooding Water Management at the Ronneburg Uranium Mine: Lessons Learned and Remaining Challenges. In: *International Mine Water Conference*, Pretoria, South Africa, October 19 – 23, 2009.

Pulles, W., Banister, S. and Van Biljon, M. (2005). The Development of Appropriate Procedures towards and After Closure of Underground Gold Mines from a Water Management Perspective. *WRC Report No 1215/1/05*, Water Research Commission, Pretoria.

Scott, D.F. and Le Maitre, D.C. (1997). The Interaction between Vegetation and Groundwater – Research Priorities for South Africa. *WRC Report No K5/730*, Water Research Commission, Pretoria.

Straskraba, V. (1986). Groundwater Recovery Problems Associated with Open Pit Reclamation in the Western U.S.A. *International Journal of Mine Water*, **5(4)**, 49-56.

Susset, B. and Grathwohl, P. (2001). *Column Leaching Tests for Groundwater Risk Assessment: Concept, Interpretation of Results, and Reproducibility*. Centre for Applied Geoscience, Eberhard Karls University, Tübingen.

The South African Bureau of Standards (SABS), ISO 5667-1 to 5667-15, First Edition, 1999.

Van der Watt, H.V.H. and Van Rooyen, T.H. (1995). *A Glossary of Soil Science*. The Soil Science Society of South Africa, Pretoria.

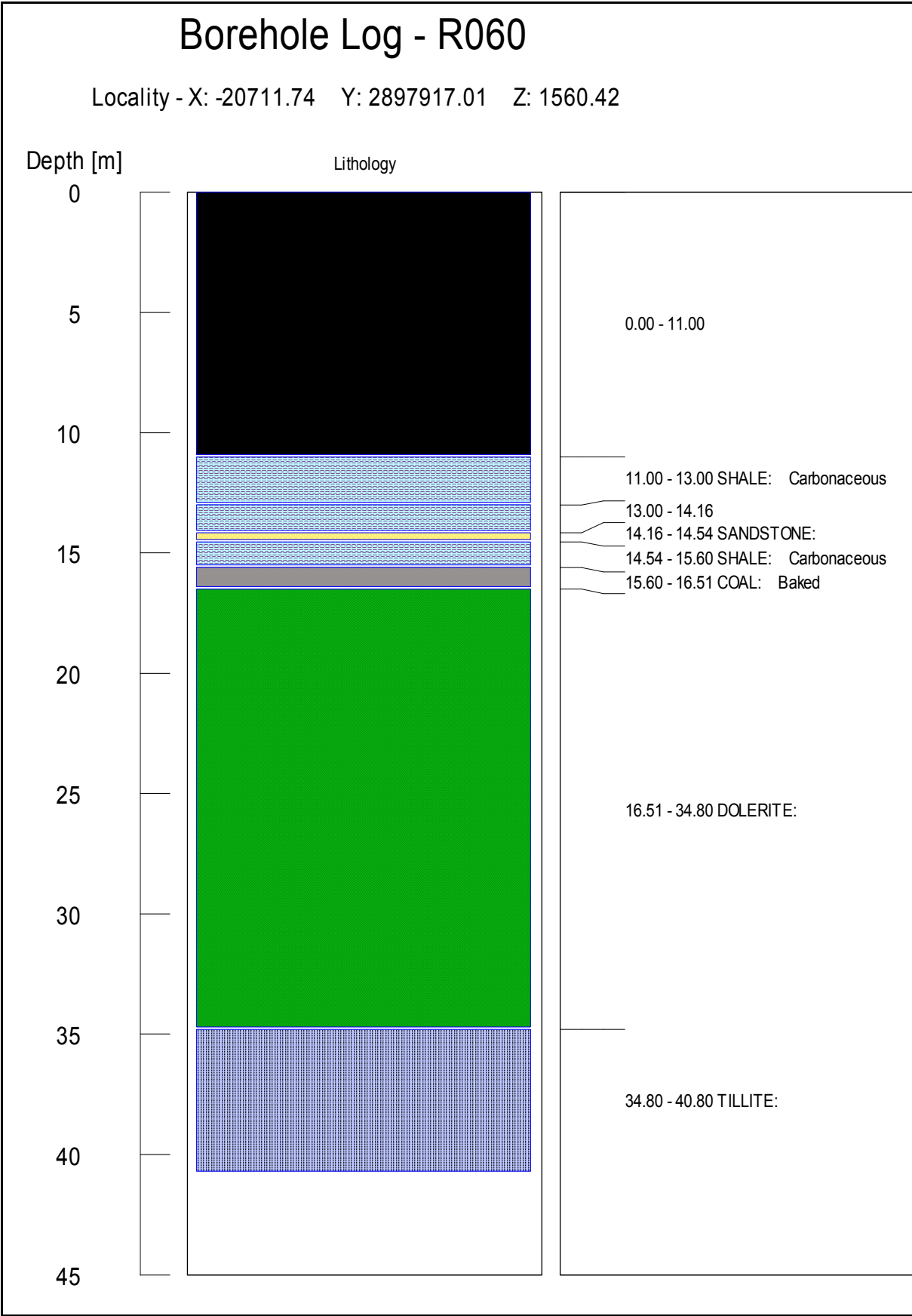
Van Tonder, G.J. and Bean, J. (2003). *Challenges in Estimating Groundwater Recharge*. Institute for Groundwater Studies, University of the Free State.

Van Tonder, G.J., Vermeulen, P.D. and Dennis, I. (2004). *The Errors Hydrogeologists make when assessing Groundwater Flow Systems and the Implications Thereof*. Institute for Groundwater Studies, University of the Free State.

Vegter, J.R. (2001). Groundwater Development in South Africa and an Introduction to the Geohydrology of Groundwater Regions. *WRC Report No TT134/00*, Water Research Commission, Pretoria.

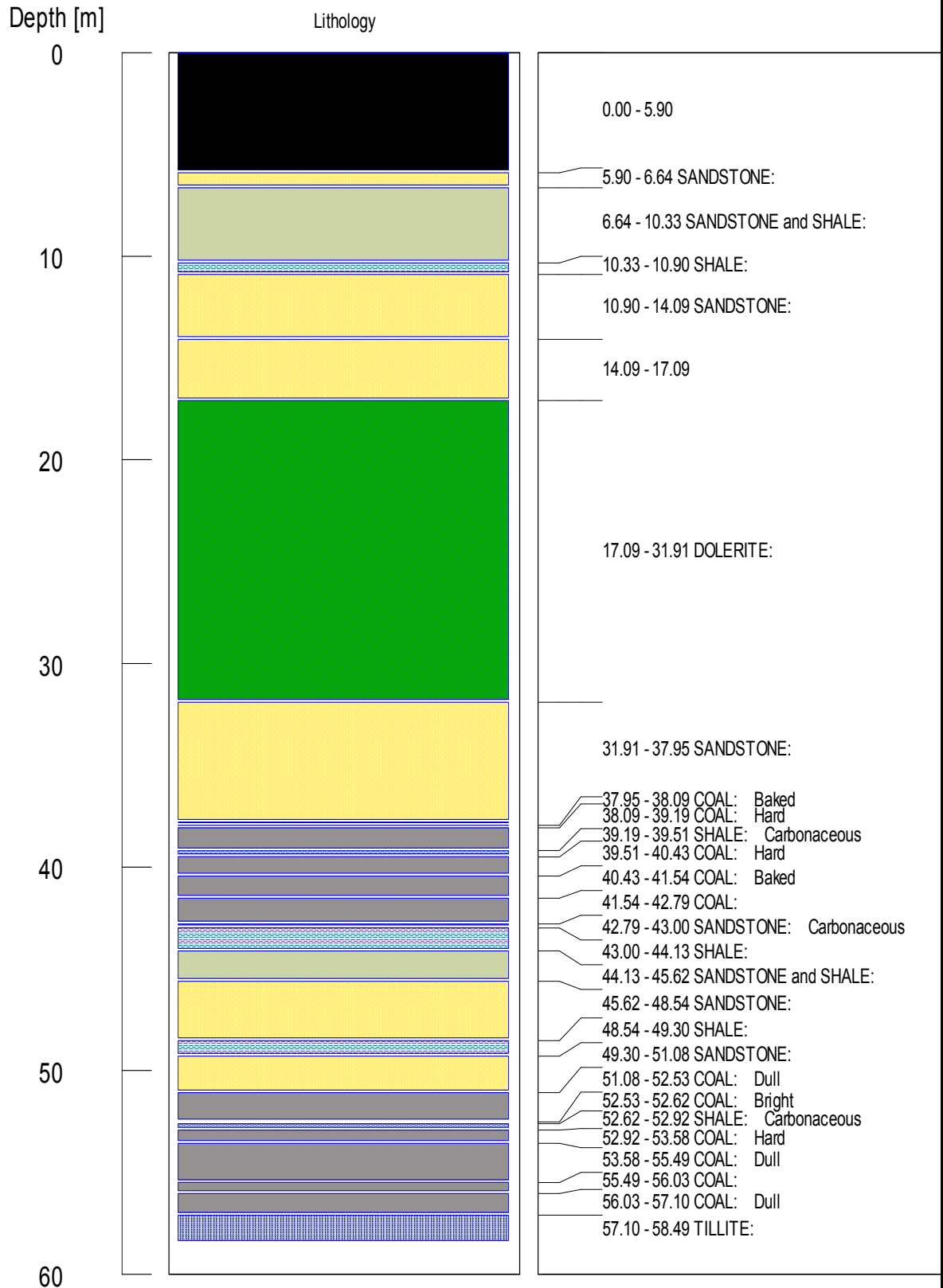
Younger, P.L. (1997). The Longevity of Mine Water Pollution: A Basis for Decision-Making. *The Science of the Total Environment*, **194/195**, 457-466.

11. **Appendix A: Monitoring Boreholes Logs**



Borehole Log - R133

Locality - X: -19610.22 Y: 2898860.35 Z: 1565.94



Borehole Log - R142

Locality - X: -20750.13 Y: 2898430.89 Z: 1561.72

Depth [m]

Lithology

0

0.00 - 1.00

5

1.00 - 7.30 CLAY:

10

15

20

7.30 - 33.36 DOLERITE:

25

30

33.36 - 33.71 SANDSTONE: Gritty

35

33.71 - 35.55 SHALE: Carbonaceous

40

Borehole Log - R149

Locality - X: -21428.41 Y: 2896547.61 Z: 1555.75

Depth [m]

Lithology

0

5

10

15

20

25

30

35

0.00 - 11.91

11.91 - 25.73 DOLERITE:

25.73 - 29.32 SANDSTONE:

29.32 - 29.60 COAL: Baked

29.60 - 30.25 SHALE:

30.25 - 30.53 COAL: Dull

30.53 - 30.70 COAL: Hard

30.70 - 31.09 COAL: Dull

31.09 - 31.58 MUDSTONE:

31.58 - 31.73 COAL: Dull

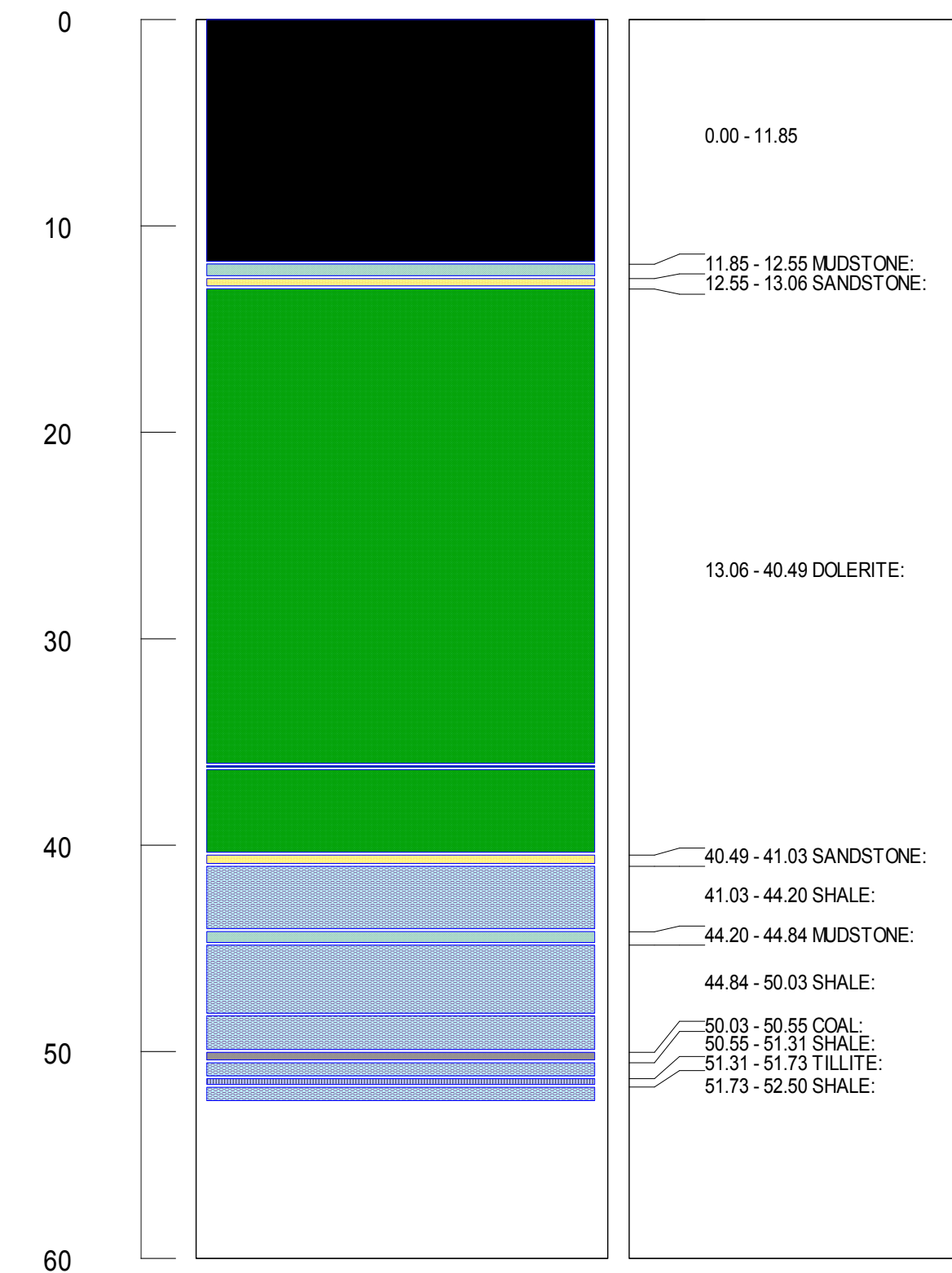
31.73 - 32.55 TILLITE:

Borehole Log - R171

Locality - X: -20348.35 Y: 2901166.33 Z: -1.00

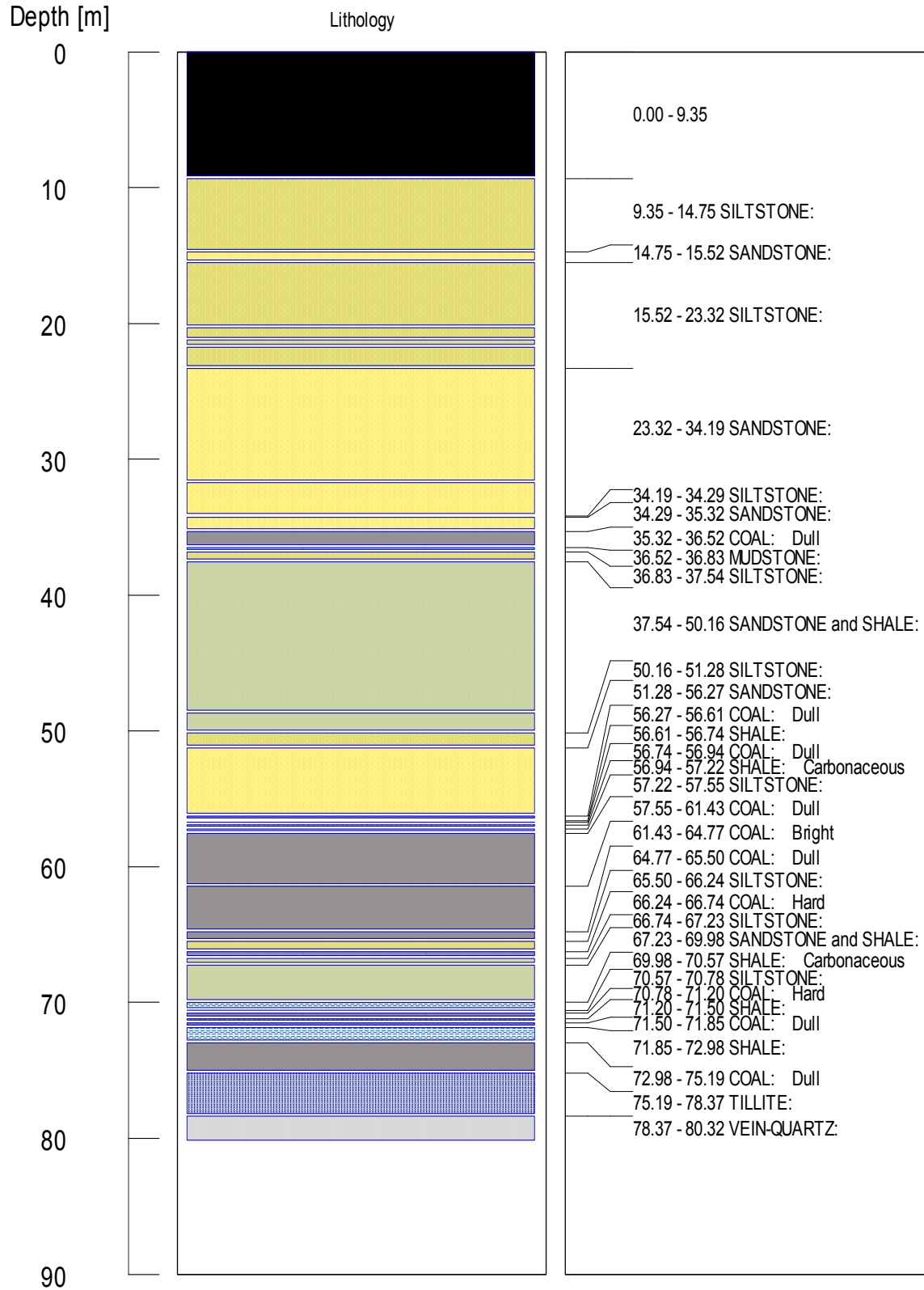
Depth [m]

Lithology



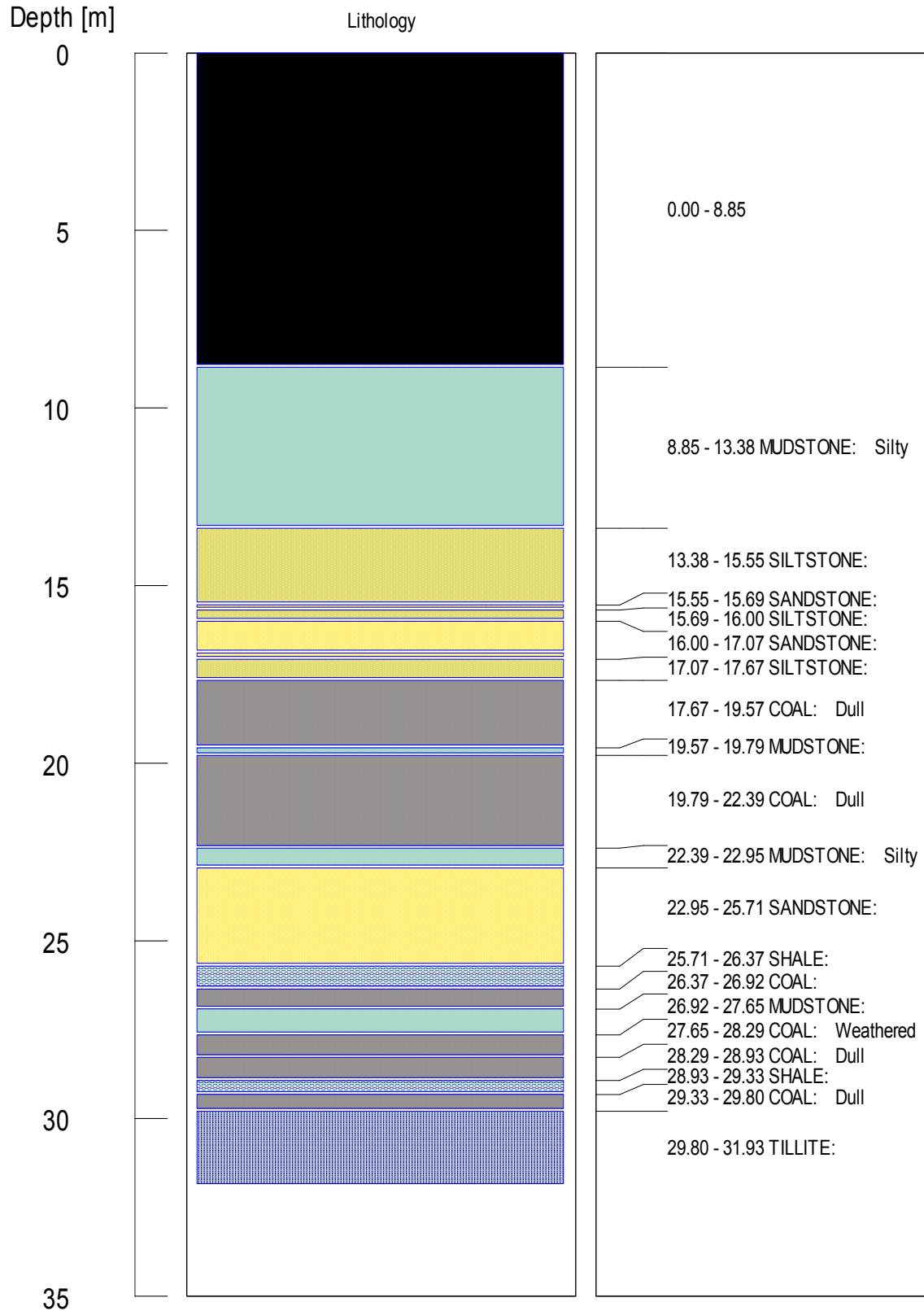
Borehole Log - R184

Locality - X: -18478.00 Y: 2897086.00 Z: 1604.00



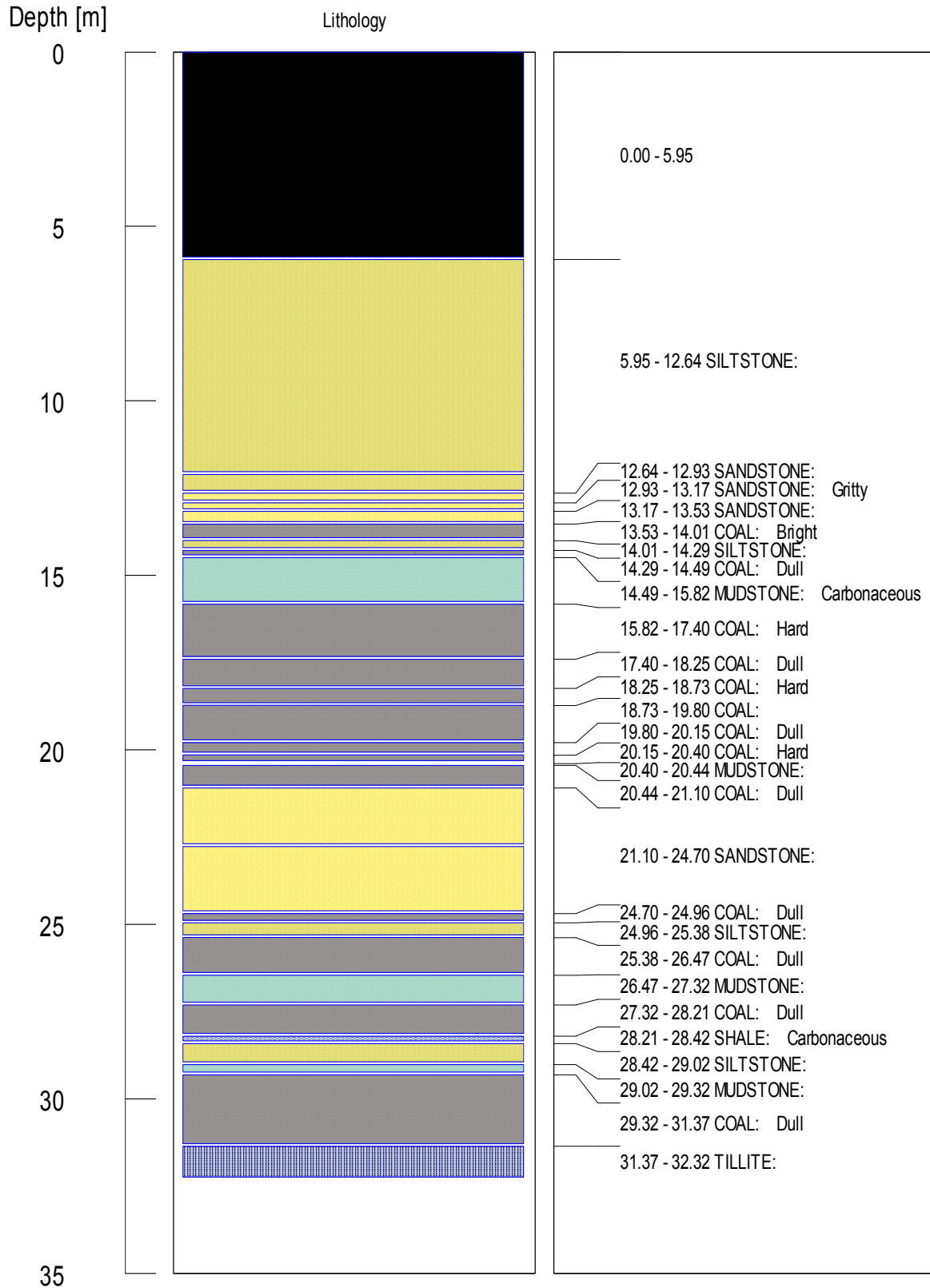
Borehole Log - R196

Locality - X: -22977.72 Y: 2896342.75 Z: -1.00



Borehole Log - R199

Locality - X: -21838.17 Y: 2896879.23 Z: -1.00

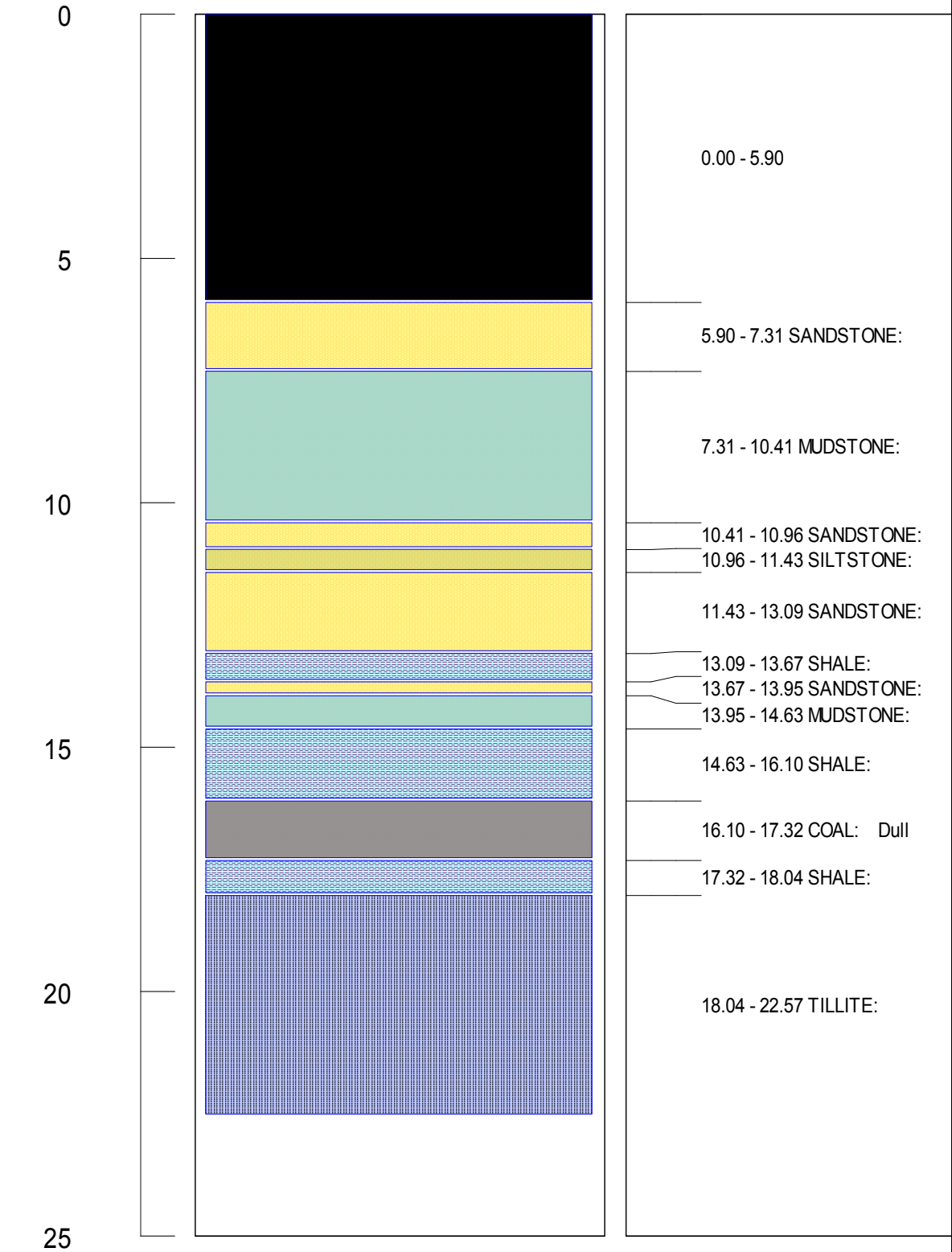


Borehole Log - R206

Locality - X: -21928.74 Y: 2898885.82 Z: -1.00

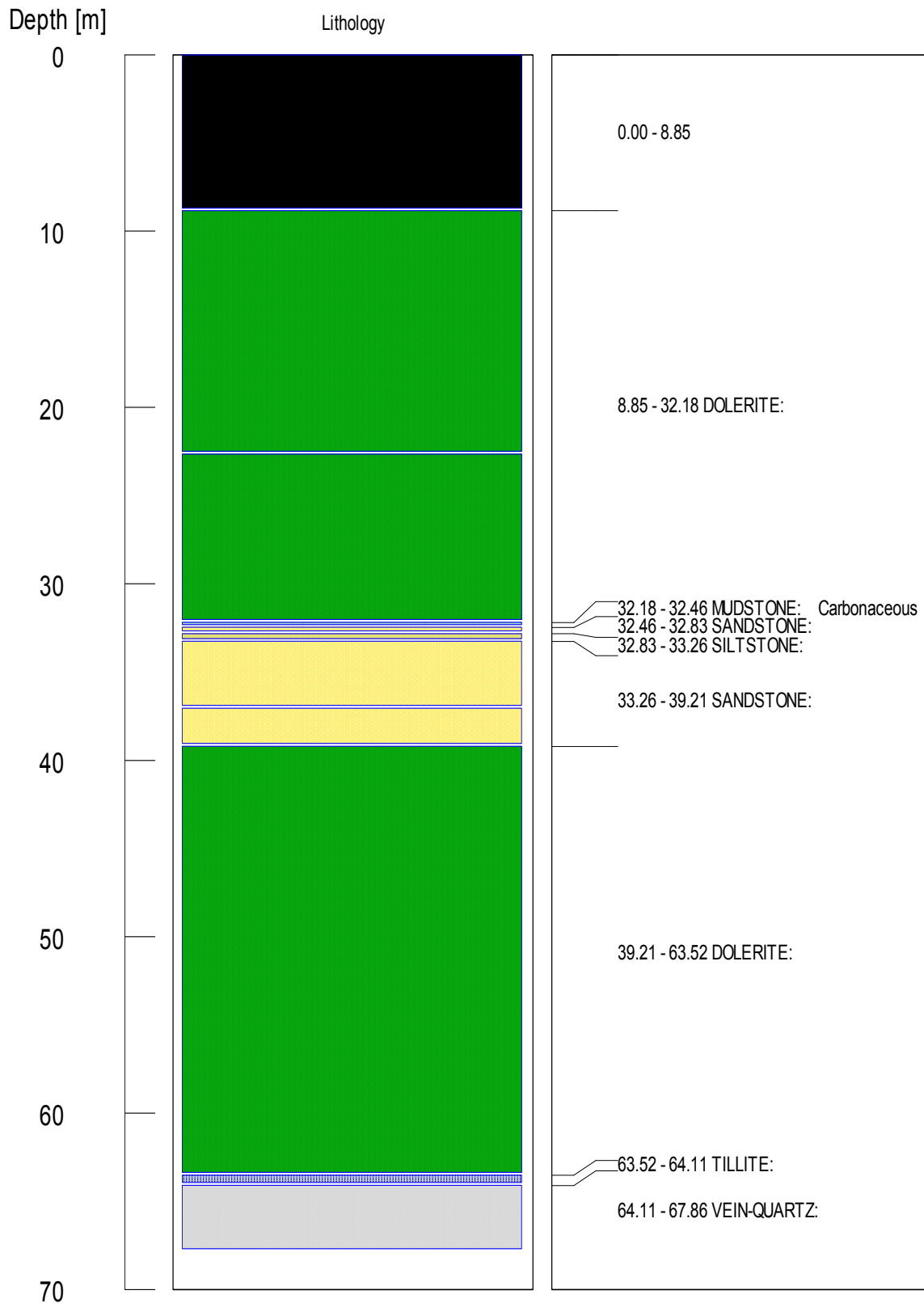
Depth [m]

Lithology



Borehole Log - R210

Locality - X: -18739.61 Y: 2900788.66 Z: -1.00

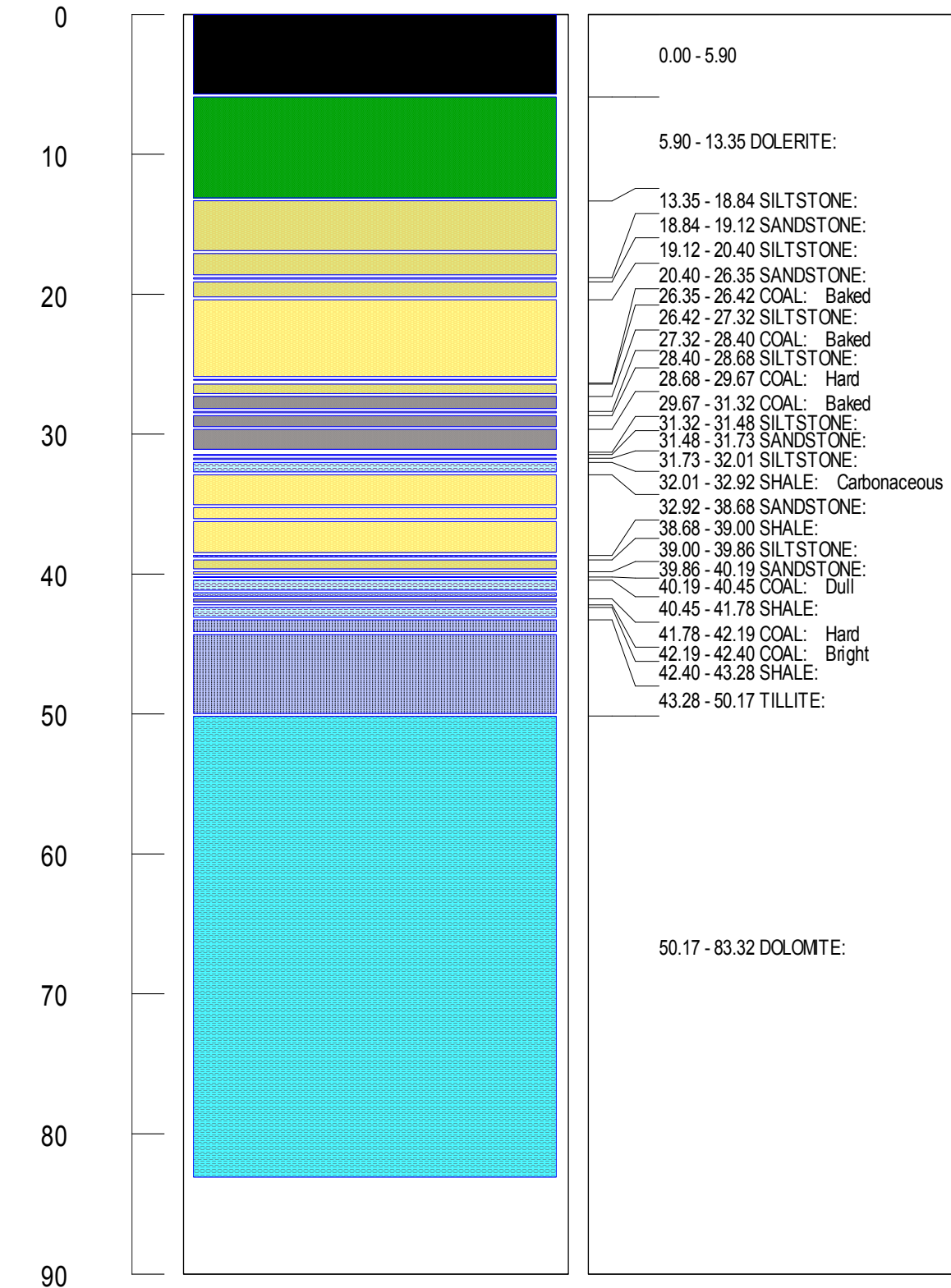


Borehole Log - R216

Locality - X: -20220.01 Y: 2899269.71 Z: -1.00

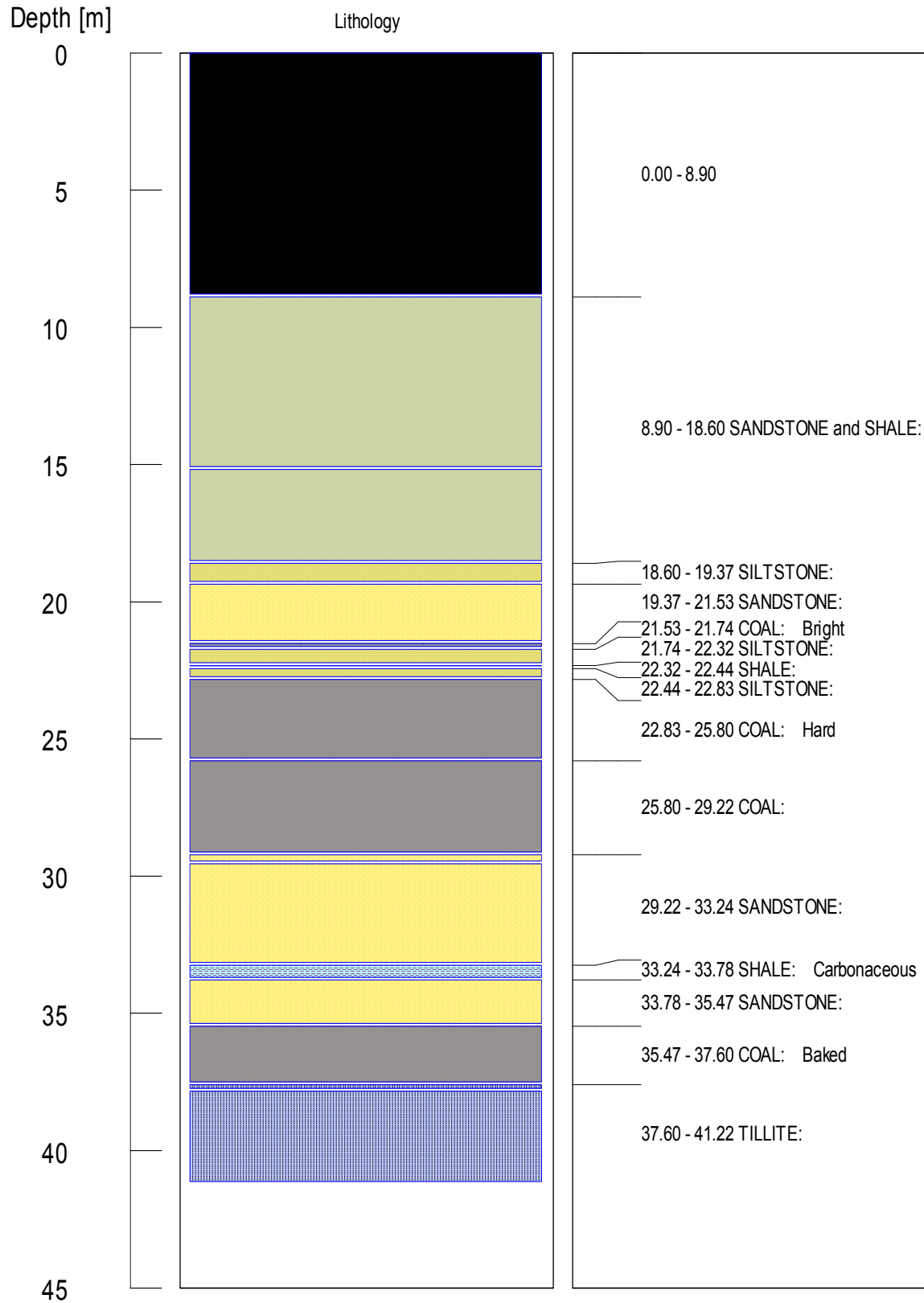
Depth [m]

Lithology



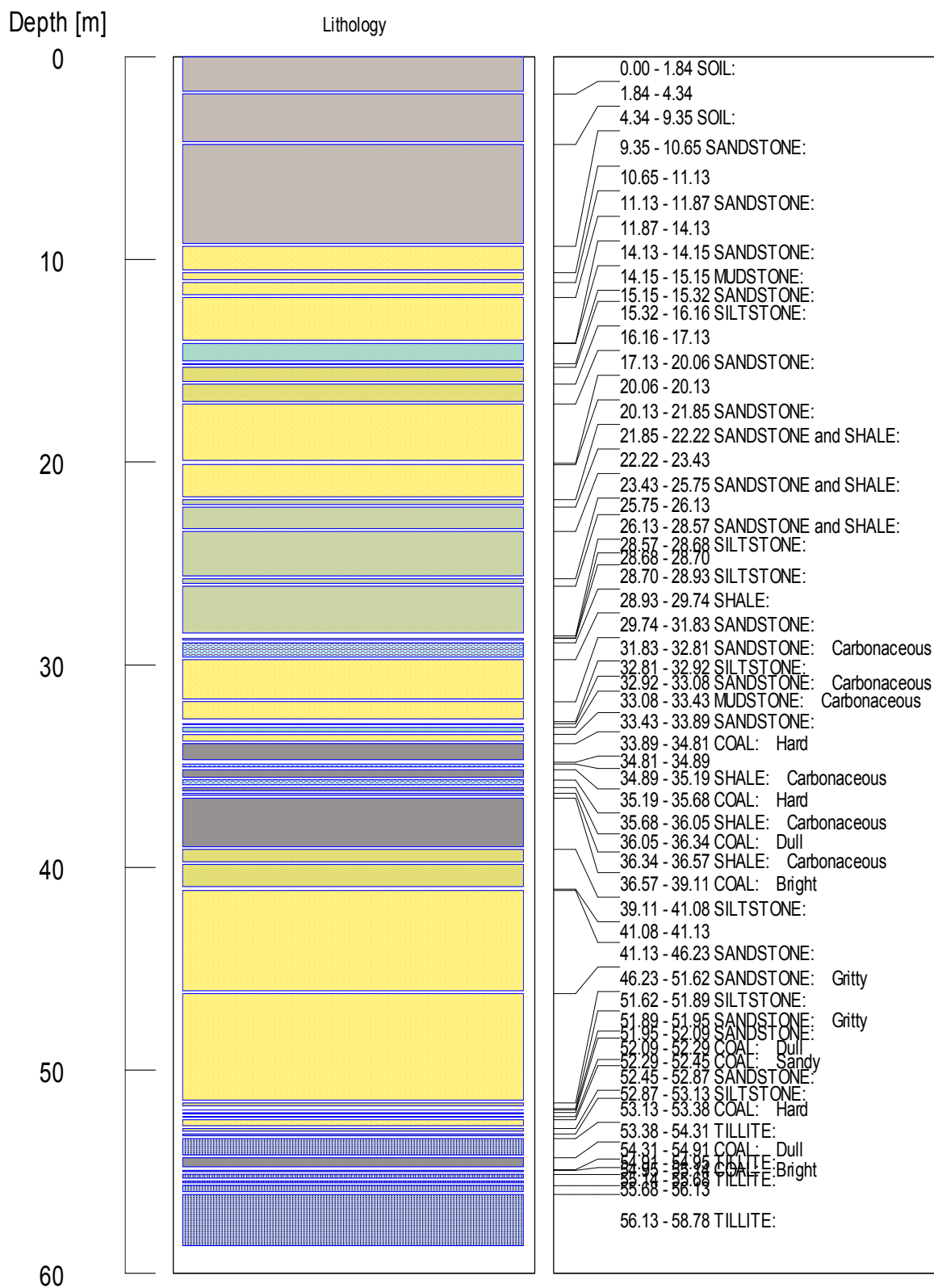
Borehole Log - R222

Locality - X: -23095.87 Y: 2899603.56 Z: -1.00



Borehole Log - R265

Locality - X: -19731.45 Y: 2900468.83 Z: -1.00

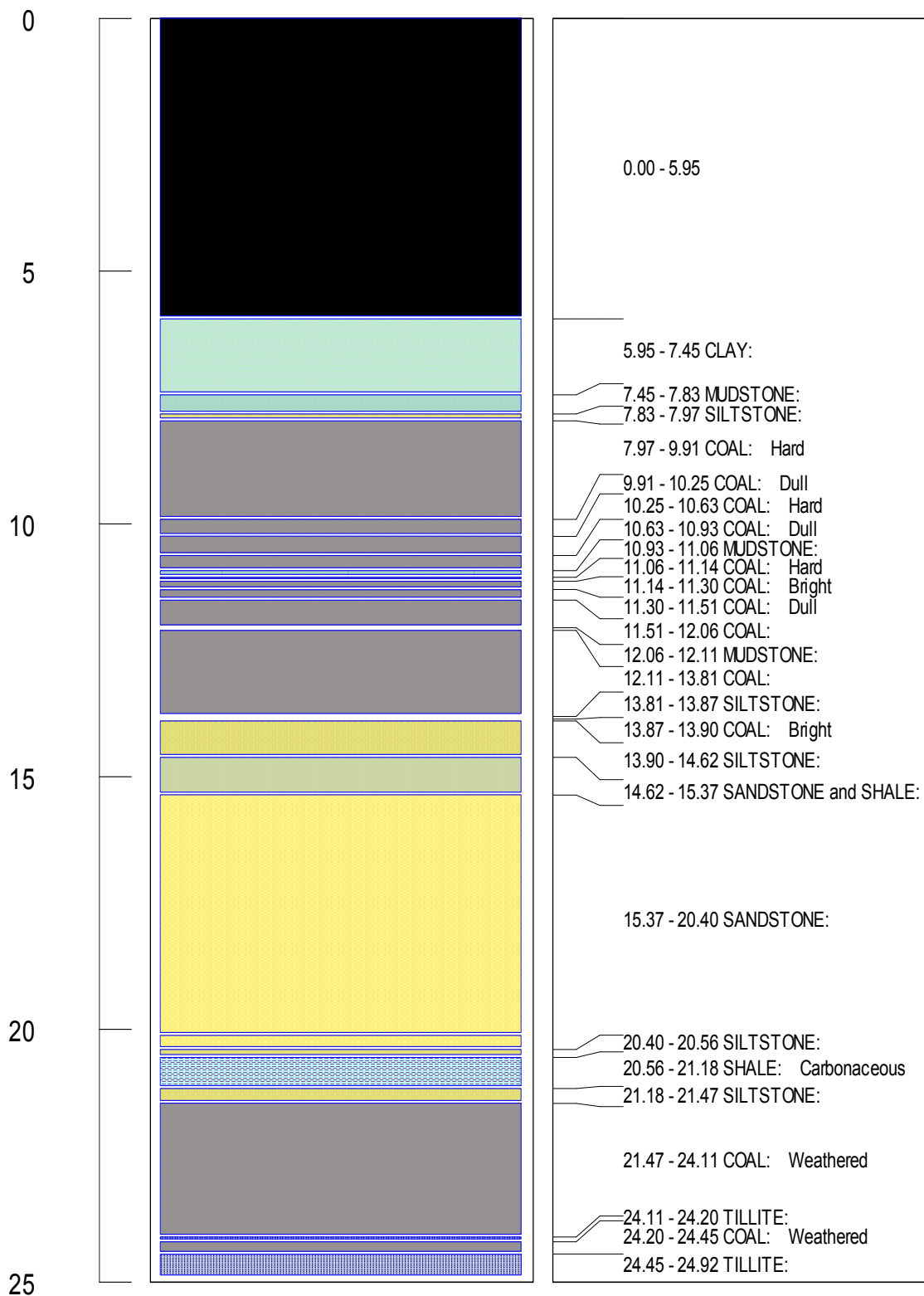


Borehole Log - R274

Locality - X: -22905.80 Y: 2900271.30 Z: -1.00

Depth [m]

Lithology



12. Appendix B: Pumptest Sheets

		DATE: 2009/05/28					
		BOREHOLE NUMBER: EX 02					
	(m)						
Hole depth	56.00m		Client				
Static depth	3.65m		Address				
Pump depth	30.00m						
Start Depth	3.15m						
Sart Time							
Coords			Contact no				
Pump Test		Flow	Control time	Recovery			
0.5	3.36	260 l/h		0.5	9.97		
1	3.52			1	9.75		
1.5	3.69			1.5	9.71		
2	3.77			2	9.68		
3	3.90			3	9.61		
5	4.37			5	9.47		
7.5	5.03			7.5	9.33		
10	5.51			10	9.18		
12.5	6.12			12.5	9.06		
15	6.69			15	8.95		
20	7.80			20	8.76		
25	8.82	260 l/h		25	8.59		
30	9.82			30	8.43		

DATE: 2009/05/28							
BOREHOLE NUMBER: EX 03							
	(m)						
Hole depth	62.50m		Client				
Static depth	3.49m		Address				
Pump depth	10.00m						
Start Depth	3.89m						
Sart Time							
Coords			Contact no				
Pump Test		Flow	Control time	Recovery			
0.5	4.00	260 l/h		0.5	7.68		
1	4.16			1	7.67		
1.5	4.33			1.5	7.66		
2	4.42			2	7.63		
3	4.71			3	7.60		
5	5.31			5	7.56		
7.5	5.98			7.5	7.52		
10	6.64			10	7.50		
12.5	6.91			12.5	7.45		
15	7.59	260 l/h		15	7.39		
20	7.72			20	7.32		
25				25	7.26		

DATE: 2009/05/28							
BOREHOLE NUMBER: EX 05							
	(m)						
Hole depth	57.50m		Client				
Static depth	5.38m		Address				
Pump depth	30.00m						
Start Depth	5.15m						
Sart Time							
Coords			Contact no				
Pump Test		Flow	Control time	Recovery			
0.5	5.24	260 l/h		0.5	8.82		
1	5.32			1	8.81		
1.5	5.41			1.5	8.80		
2	5.50			2	8.79		
3	5.66			3	8.77		
5	5.96			5	8.74		
7.5	6.30			7.5	8.66		
10	6.60			10	8.62		
12.5	6.90			12.5	8.58		
15	7.28	260 l/h		15	8.55		
20	7.74			20	8.51		
25	8.42			25	8.44		
30	8.82			30	8.37		

DATE: 2009/05/28							
BOREHOLE NUMBER: EX 12							
	(m)						
Hole depth	32.00m		Client				
Static depth	13.45m		Address				
Pump depth	25.00m						
Start Depth	16.04m						
Sart Time							
Coords			Contact no				
Pump Test		Flow	Control time	Recovery			
0.5	16.43	260 l/h		0.5	23.63		
1	16.76			1	23.63		
1.5	17.09			1.5	23.62		
2	17.44			2	23.60		
3	18.09			3	23.56		
5	19.28			5	23.45		
7.5	20.65			7.5	23.31		
10	21.66			10	23.19		
12.5	22.67			12.5	23.05		
15	23.63	260 l/h		15	22.93		

DATE: 2009/05/28							
BOREHOLE NUMBER: EX 13							
	(m)						
Hole depth	30.50m		Client				
Static depth	5.59m		Address				
Pump depth	25.00m						
Start Depth	4.91m						
Sart Time							
Coords			Contact no				
Pump Test		Flow	Control time	Recovery			
0.5	5.39	260 l/h		0.5	17.63		
1	5.81			1	17.43		
1.5	6.23			1.5	17.22		
2	6.64			2	17.02		
3	7.47			3	16.61		
5	8.97			5	15.76		
7.5	10.46			7.5	14.72		
10	11.65			10	13.65		
12.5	12.68			12.5	12.55		
15	13.64	260 l/h		15	11.58		
20	15.23			20	10.03		
25	16.62			25	8.85		
30	17.82	260 l/h		30	7.95		

DATE: 2009/05/21							
BOREHOLE NUMBER: EX 17							
	(m)						
Hole depth	32.00m		Client				
Static depth	1.97m		Address				
Pump depth	30.00m						
Start Depth	0.63m						
Sart Time							
Coords			Contact no				
Pump Test		Flow	Control time	Recovery			
0.5	3.60m	1600 l/h		0.5	27.89m		
1	5.80m			1	27.95m		
1.5	8.09m			1.5	27.94m		
2	10.49m	1600 l/h		2	27.94m		
3	16.13m			3	27.93m		
5	20.74m	1500 l/h		5	27.93m		
7.5	24.60m			7.5	27.92m		
10	28.35m			10	27.92m		
12.5				12.5	27.90m		
15				15	27.89m		
20				20	27.87m		

DATE: 2009/05/21							
BOREHOLE NUMBER: EX 21							
	(m)						
Hole depth	37.50m		Client				
Static depth	3.68m		Address				
Pump depth	30.00m						
Start Depth	2.85m						
Sart Time							
Coords			Contact no				
Pump Test		Flow	Control time	Recovery			
0.5	4.38m	1600 l/h		0.5			
1	4.82m			1			
1.5	5.57m			1.5			
2	6.15m			2			
3	7.01m	1500 l/h		3			
5	9.46m	1400 l/h		5			
7.5	11.80m	1150 l/h		7.5			
10	12.35m			10			
12.5	13.00m			12.5			
15	13.45m			15			
20	Pomp geblok			20			

DATE: 2009/05/21							
BOREHOLE NUMBER: EX 22							
	(m)						
Hole depth	16.50m		Client				
Static depth	2.75m		Address				
Pump depth	14.50m						
Start Depth	2.30m						
Sart Time							
Coords			Contact no				
Pump Test		Flow	Control time	Recovery			
0.5	3.10m	1550 l/h		0.5	14.30m		
1	3.75m			1	14.26m		
1.5	4.60m			1.5	14.24m		
2	5.15m	1450 l/h		2	14.20m		
3	6.05m			3	14.17m		
5	7.95m	1400 l/h		5	14.09m		
7.5	10.10m	1300 l/h		7.5	14.00m		
10	12.25m			10	13.87m		
12.5	14.35m	1250 l/h		12.5	13.77m		
15				15	13.67m		
20				20	13.49m		

DATE: 2009/05/21							
BOREHOLE NUMBER: EX 23							
	(m)						
Hole depth	9.40m		Client				
Static depth	1.41m		Address				
Pump depth	8.50m						
Start Depth	1.21m						
Sart Time							
Coords			Contact no				
Pump Test		Flow	Control time	Recovery			
0.5	1.75m	260 l/h		0.5	6.47m		
1	1.98m			1	6.47m		
1.5	2.35m			1.5	6.47m		
2	2.65m			2	6.47m		
3	2.25m			3	6.46m		
5	3.96m			5	6.46m		
7.5	4.61m			7.5	6.46m		
10	5.36m			10	6.45m		
12.5	5.98m			12.5	6.45m		
15	6.37m			15	6.44m		
20	6.47m	260 l/h		20			

DATE: 2009/05/21							
BOREHOLE NUMBER: EX 25							
	(m)						
Hole depth	24.00m		Client				
Static depth	2.27m		Address				
Pump depth	23.00m						
Start Depth	2.25m						
Sart Time							
Coords			Contact no				
Pump Test		Flow	Control time	Recovery			
0.5	3.21m	1600 l/h		0.5	3.94m		
1	3.46m			1	3.43m		
1.5	3.54m			1.5	3.20m		
2	3.64m			2	3.12m		
3	3.74m			3	3.01m		
5	3.90m			5	2.89m		
7.5	4.02m			7.5	2.80m		
10	4.12m			10	2.72m		
12.5	4.19m			12.5	2.67m		
15	4.24m			15	2.62m		
20	4.33m			20	2.57m		
25	4.40m			25			
30	4.45m	1600 l/h		30			

DATE: 2009/07/28							
BOREHOLE NUMBER: R60							
	(m)						
Hole depth	25		Client				
Static depth	7.85		Address				
Pump depth	17						
Start Depth	6.85						
Sart Time							
Coords			Contact no				
Pump Test		Flow	Control time	Recovery			
0.5	7.98			0.5			
1	9.12			1	14.73		
1.5	10.31			1.5	14.68		
2	11.27			2	14.59		
3	13.13			3	14.59		
5	16.02			5	14.58		
7.5				7.5	14.57		
10				10	14.56		
12.5				12.5	14.55		

DATE: 2009/07/24							
BOREHOLE NUMBER: R133							
	(m)						
Hole depth			Client				
Static depth	3.38		Address				
Pump depth	6.5						
Start Depth	3.32						
Sart Time							
Coords			Contact no				
Pump Test		Flow	Control time	Recovery			
0.5	3.32			0.5	3.54		
1	3.32			1	3.49		
1.5	3.32			1.5	3.46		
2	3.33			2	3.43		
3	3.36			3	3.41		
5	3.40			5	3.38		
7.5	3.47			7.5	3.35		
10	3.53			10	3.33		
12.5	3.56			12.5	3.32		
15	3.58			15			
20	3.60			20			
25	3.62			25			

DATE: 2009/07/24							
BOREHOLE NUMBER: R142							
	(m)						
Hole depth			Client				
Static depth	2.27		Address				
Pump depth	20						
Start Depth	1.29						
Sart Time							
Coords			Contact no				
Pump Test		Flow	Control time	Recovery			
0.5	2.03			0.5	8.52		
1	2.85			1	8.18		
1.5	3.55			1.5	7.95		
2	4.10			2	7.78		
3	4.96			3	7.38		
5	6.53			5	6.60		
7.5	8.32			7.5	5.82		
10	9.37			10	5.09		
12.5				12.5	4.47		
15				15	3.82		
20				20	3.30		
25				25	2.98		
30				30	2.80		

DATE: 2009/07/28							
BOREHOLE NUMBER: R149							
	(m)						
Hole depth	32		Client				
Static depth	6.13		Address				
Pump depth	25						
Start Depth	5.62						
Sart Time							
Coords			Contact no				
Pump Test		Flow	Control time	Recovery			
0.5	6.12			0.5	13.85		
1	6.57			1	13.51		
1.5	7.07			1.5	13.33		
2	7.40			2	13.12		
3	8.09			3	12.70		
5	9.38			5	11.81		
7.5	10.63			7.5	10.98		
10	11.69			10	10.19		
12.5	12.57			12.5	9.56		
15	13.31			15	8.99		
20	14.05			20			
25	14.40			25			

DATE: 2009/07/29							
BOREHOLE NUMBER: R171							
	(m)						
Hole depth	30m		Client				
Static depth	4.8		Address				
Pump depth	17m						
Start Depth	4.71						
Sart Time							
Coords			Contact no				
Pump Test		Flow	Control time	Recovery			
0.5	4.80			0.5	6.04		
1	4.88			1	5.95		
1.5	4.96			1.5	5.91		
2	5.03			2	5.88		
3	5.11			3	5.80		
5	5.30			5	5.68		
7.5	5.51			7.5	5.58		
8.5	5.60			10	5.46		
10	5.70			12.5	5.36		
12.5	5.84			15	5.30		
15	5.94			20	5.20		
20	6.13			25			

DATE: 2009/07/24							
BOREHOLE NUMBER: R184							
	(m)						
Hole depth			Client				
Static depth	5.65		Address				
Pump depth							
Start Depth	5.59						
Sart Time							
Coords			Contact no				
Pump Test		Flow	Control time	Recovery			
0.5	5.65			0.5	7.56		
1	5.70			1	7.54		
1.5	5.77			1.5	7.54		
2	5.84			2	7.53		
3	5.94			3	7.53		
5	6.16			5	7.51		
7.5	6.43			7.5	7.49		
10	6.67			10	7.47		
12.5	6.92			12.5	7.44		
15	7.18			15	7.42		
20	7.65			20			

DATE: 2009/07/29							
BOREHOLE NUMBER: R199							
	(m)						
Hole depth	31		Client				
Static depth	15.84		Address				
Pump depth	27						
Start Depth	15.46						
Sart Time							
Coords			Contact no				
Pump Test		Flow	Control time	Recovery			
0.5	15.73			0.5	25.85		
1	16.07			1	25.62		
1.5	16.62			1.5	25.60		
2	16.92			2	25.54		
3	17.70			3	25.46		
5	19.01			5	25.35		
7.5	20.45			7.5	25.21		
10	21.89			10	25.05		
12.5	22.97			12.5	24.90		
15	24.23			15	24.72		
20	26.33			20	24.46		

DATE: 2009/07/29							
BOREHOLE NUMBER: R216							
	(m)						
Hole depth	30		Client				
Static depth	2.3		Address				
Pump depth	10						
Start Depth	2.2						
Sart Time							
Coords			Contact no				
Pump Test		Flow	Control time	Recovery			
0.5	2.65			0.5	3.26		
1	2.86			1	2.88		
1.5	3.04			1.5	2.67		
2	3.19			2	2.58		
3	3.38			3	2.45		
5	3.60			5	2.35		
7.5	3.69			7.5	2.31		
10	3.73			10	2.30		
12.5	3.73			12.5			
15	3.73			15			
20	3.72			20			

DATE: 2009/07/29							
BOREHOLE NUMBER: R241							
	(m)						
Hole depth	30		Client				
Static depth	1.69		Address				
Pump depth	27						
Start Depth	1.29						
Sart Time							
Coords			Contact no				
Pump Test		Flow	Control time	Recovery			
0.5	1.98			0.5	4.58		
1	2.31			1	4.12		
1.5	2.72			1.5	3.83		
2	3.01			2	3.54		
3	3.62			3	3.19		
5	4.38			5	2.65		
7.5	4.78			7.5	2.39		
10	4.99			10	2.20		
12.5	5.03			12.5	2.01		
15	5.05			15			
20	5.08			20			

DATE: 2009/07/30							
BOREHOLE NUMBER: R265							
	(m)						
Hole depth	30m		Client				
Static depth	1.55m		Address				
Pump depth	10m						
Start Depth	1.35						
Sart Time							
Coords			Contact no				
Pump Test		Flow	Control time	Recovery			
0.5	1.56			0.5	4.75		
1	1.80			1	4.68		
1.5	2.02			1.5	4.63		
2	2.11			2	4.60		
3	2.29			3	4.59		
5	2.68			5	4.58		
7.5	3.09			7.5	4.55		
10	3.25			10	4.54		
12.5	3.45			12.5	4.50		
15	3.75			15	4.48		
20	4.75			17	4.46		

13. Appendix C: Hydrocensus Report

1. INTRODUCTION

A concentric radius of two (2) kilometers around the mining section was included for the hydrocensus study. Various water levels and water samples were taken on the site visits from 22 to 24 April 2009.

The proposed mining area as well as a buffer zone was surveyed. The potential surface and groundwater users in the area were identified. Although more than one borehole often exists for a user like a farmstead, all boreholes will be surveyed and water level (if access is obtainable to the water level), use and related info recorded but only the main used borehole will be sampled and analysed for groundwater quality.

2. SCOPE OF WORK

The goal of a hydrocensus field survey is as follows:

- Locating and informing all I&AP of the proposed development
- Gathering of personal information from the I&AP (Name, Telephone number, Address, etc.)
- Accurately logging representative boreholes on the I&AP properties
- Gathering of information of the logged boreholes (Water level, pump type, use, etc.)
- Analysing a representative groundwater sample from the I&AP property
- Establishing baseline groundwater quality before mining commences in the area
- Presenting all the surveyed localities on a GIS based map

3. INTERESTED AND AFFECTED PARTIES

Contact was made with 13 interested and affected parties, as shown in Table 3-1 below. Figure 3-1 indicates the position of all the surveyed localities as well as the exploration holes used to obtain water levels in the area. Various borehole localities were logged (40 localities were surveyed), and water levels were taken. Water quality data for 16 localities and water level data for 25 localities were gathered. Due to the restricted access to the majority of the landowner boreholes exploration boreholes were used to update the groundwater levels of the area. Table 3-1 is only a summarised version of the I&AP information gathered during the hydrocensus, for complete information, the hydrocensus forms in Appendix A can be viewed. As indicated by Table 3-1, the proposed Rietkuil project is surrounded by various landowners farming with cattle, sheep, and maize.

4. FIELD RESULTS & FINDINGS

Table 4-1 indicates the summarised geohydrological information gathered for the boreholes surveyed on the various farms. As indicated by Table 4.1, all landowner affiliated boreholes, are either used for domestic, irrigation, or livestock watering purposes. Table 4-2 indicates the percentage break-up of the total localities surveyed, in terms of water use.

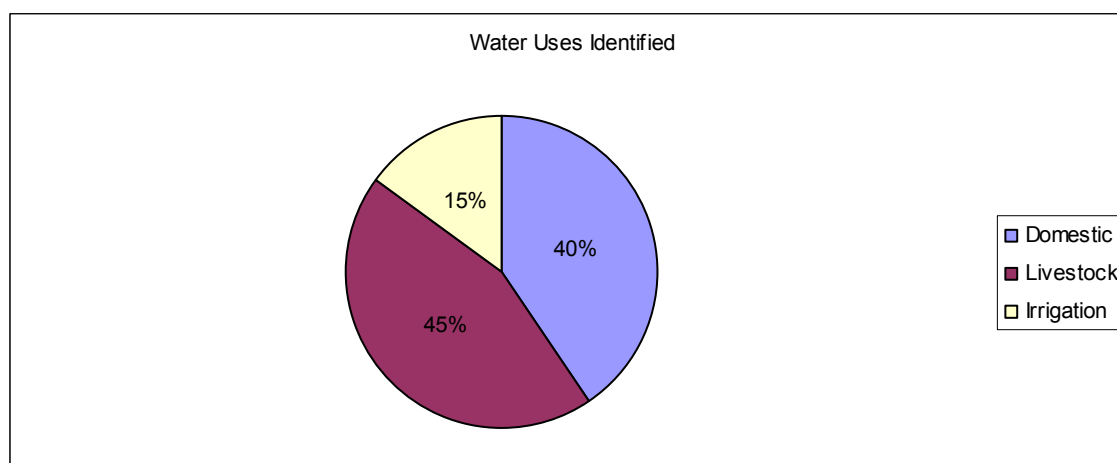


Table 4-2: Percentage break-up of the total localities surveyed, in terms of water use, for the Rietkuil Mine hydrocensus.

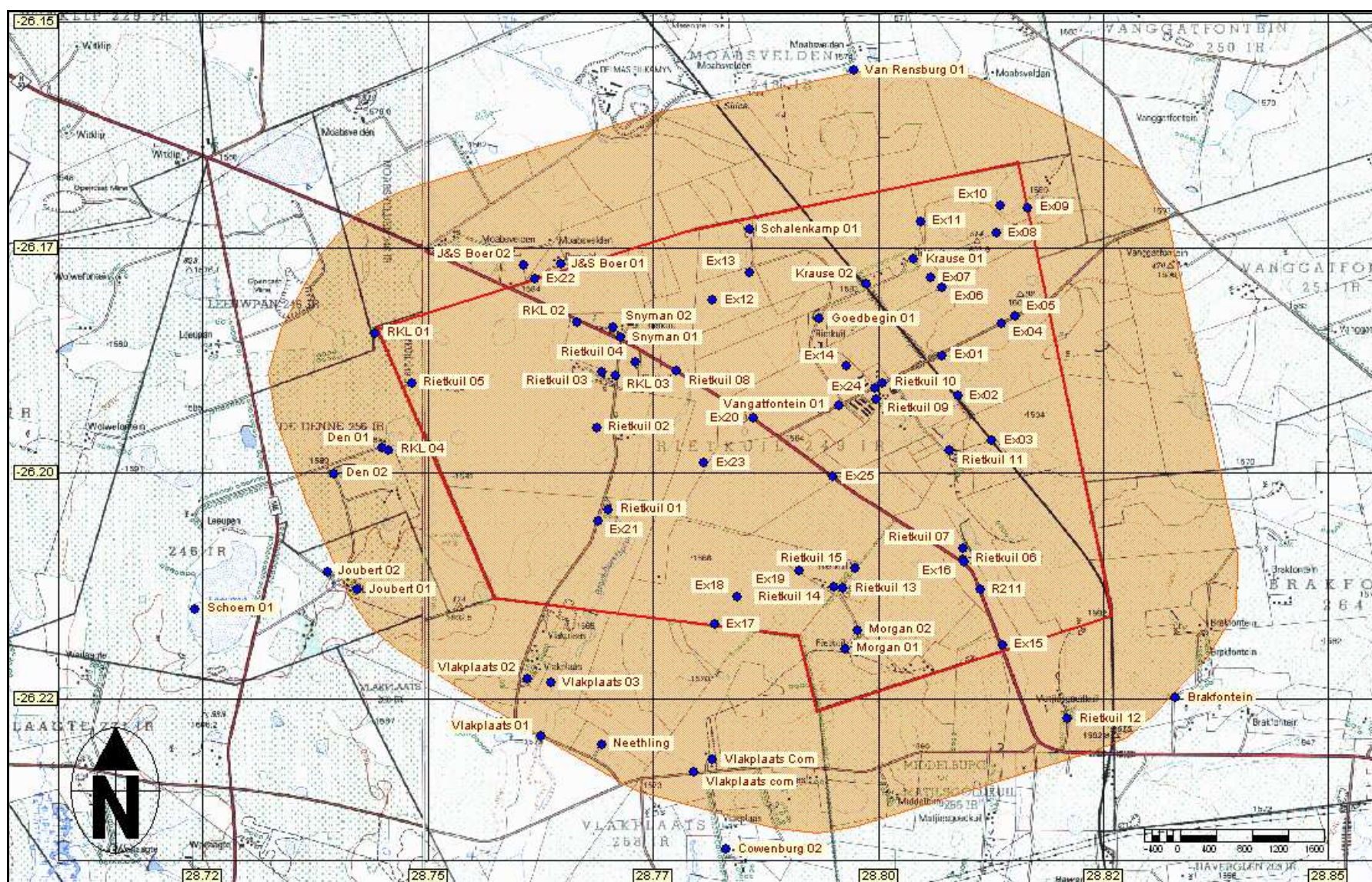


Figure 3-1: All localities surveyed during the Rietkuil hydrocensus.

DELTA MINING COMPANY - HYDROCENSUS INFO (APRIL 2009)					
Loc No		South Coordinates	East Coordinates	Elevation	Site Type
1	Brakfontein	-26.22487	28.83297	1589	Marsh
2	Cowenburg02	-26.24177	28.78304	1585	B - Drinking
3	Den01	-26.19722	28.74492	1600	B - Drinking
4	Den02	-26.20014	28.7396	1600	Dam - Livestock / Irrigation
5	J&S BOER01	-26.17684	28.76479	1579	B - Drinking
6	J&S BOER02	-26.177	28.76062	1582	Dam - Livestock / Irrigation
7	Joubert01	-26.21289	28.7421	1607	B - Livestock
8	Joubert02	-26.21107	28.73886	1605	B - Livestock
9	Morgan Beef	-26.26449	28.79366	1614	Marsh
10	Morgan01	-26.21949	28.79627	1593	B - Drinking
11	Morgan02	-26.2175	28.79771	1591	Dam - Livestock
12	Neethling	-26.23019	28.76926	1580	B - Drinking
13	Rietkuil01	-26.20408	28.76998	1583	B - Drinking
14	Rietkuil02	-26.19502	28.76881	1581	Dam - Livestock / Irrigation
15	Rietkuil03	-26.18876	28.76936	1581	B - Drinking
16	Rietkuil04	-26.18771	28.77308	1574	B - Drinking
17	Rietkuil05	-26.19012	28.74817	1602	B - Drinking
18	Rietkuil06	-26.20969	28.80946	1577	Marsh
19	Rietkuil07	-26.20845	28.80942	1577	Marsh
20	Rietkuil08	-26.18861	28.77753	1565	Stream
21	Rietkuil09	-26.19187	28.79974	1589	B - Drinking
22	Rietkuil10	-26.1901	28.80043	1593	Marsh
23	Rietkuil11	-26.19753	28.80792	1581	B - Drinking
24	Rietkuil12	-26.22722	28.82096	1588	Dam - Livestock / Irrigation
25	Rietkuil13	-26.21278	28.79606	1578	Dam - Livestock / Irrigation
26	Rietkuil14	-26.21268	28.7951	1578	B - Drinking
27	Rietkuil15	-26.2105	28.79749	1577	B - Drinking
28	Snyman01	-26.18501	28.77136	1577	B - Drinking
29	Snyman02	-26.18379	28.77059	1578	B - Drinking
30	Vangatfontein1	-26.1925	28.79563	1571	Marsh
31	Vlakplaats Com01	-26.23175	28.78164	1588	B - Drinking
32	Vlakplaats01	-26.22923	28.76258	1580	Dam - Livestock / Irrigation
33	Vlakplaats02	-26.22281	28.7611	1591	B - Drinking
34	Vlakplaats03	-26.22323	28.76373	1576	Dam - Livestock / Irrigation
35	VlakplaatsCom02	-26.23325	28.77956	1585	Marsh
36	Van Rensburg 01	-26.15537	28.79731	1583	B - Drinking
37	Vangatfontein 01	-26.19250	28.79563	1571	Marsh
38	Vlakplaats 01	-26.22923	28.76258	1580	Stream
39	Vlakplaats 02	-26.22281	28.76110	1591	B - Drinking
40	Vlakplaats 03	-26.22323	28.76373	1576	Dam - Livestock

Table 4-1: Summarised geohydrological information gathered for the boreholes on the Rietkuil survey

5. WATER QUALITY RESULTS

Water quality data for 16 hydrocensus and 10 exploration borehole localities was available for the study area. Clean Stream Scientific Services were responsible for the hydrochemical analysis and the water quality results are presented in Appendix A, under each landowner. Water qualities are discussed for selected pollution indicator parameters i.e. pH, EC (salinity), SO₄, and NO₃ concentration.

Water qualities are compared against the proposed SANS241:2006 drinking water standards.

Four main factors usually influence groundwater quality in the aquifer, namely:

- **annual recharge** to the groundwater system,
- **type of bedrock** where ion exchange may impact on the hydrogeochemistry,
- **flow dynamics** within the aquifer(s), determining the water age and
- **source(s) of pollution** with their associated leachates or contaminant streams.

Where no specific **source of groundwater pollution** is present upstream of the borehole, only the other three factors play a role.

Table 5-1 and Table 5-2 indicate the recorded water quality information for the hydrocensus and exploration borehole localities respectively. Water quality is measured against the SANS 241 drinking water guidelines, DWAF Targeted Water Quality Guideline Range (TWQGR) for large livestock watering and irrigation. Each locality is highlighted according to the relevant usage.

Potable Water Localities:

Localities Cowenburg01, Den01, J&SBoer01, Morgan01, Neethling, Rietkuil01, Rietkuil03, Rietkuil04, Rietkuil09, Rietkuil11, Rietkuil14, Rietkuil15, Snyman01, Snyman02, Vlakplaats02, and Vlakplaats com are all identified as drinking water localities in the hydrocensus. Localities non-compliant with the SANS 241 drinking water standards are Cowenburg01 (F), Rietkuil04 (NO₃_N), Snyman01 (F), Snyman02 (F), and Vlakplaat02 (F, Al, and Fe).

Possible health effects due to the recorded non-compliant variables are listed below:

- **Fluoride (F):** Insignificant to slight health risk posed to sensitive users may include brittling of bone structure, staining of teeth.
- **Nitrate (NO₃_N):** A slight chronic risk to some babies could be recorded. Health effects include tiredness, lack of energy, and in extreme cases cyanosis and breathing difficulty in infants.

- **Iron (Fe):** Increasing effects in sensitive users. Objectionable taste and color to water may be present.
- **Aluminium (Al):** No immediate health effects are expected. Long term exposure may include neurotoxic effects.

Livestock Watering Localities:

Locality Rietkuil05 was recorded as a livestock watering locality, and complies with the DWAF TWQGR for large livestock watering.

Delta Mining Rietkuil - Hydrocensus : Selected date - 2009/05/15												
Variable	SANS 241 Potable	DWAf Livestock	DWAf Irrigation	Monitoring localities								
				Cowenburg 01	Den 01	J&S Boer 01	Morgan 01	Neethling	Rietkuil 01	Rietkuil 03	Rietkuil 04	Rietkuil 05
pH ()	5.0 - 9.5	-	6.0 - 9.1	8.74	8.32	8.16	8.41	8.47	8.52	8.04	8.30	6.40
EC (mS/m)	150	500	40	75.10	40.00	71.00	36.60	53.40	42.70	42.90	84.00	6.14
TDS (mg/l)	1000	2000	260	444	210	401	187	289	231	212	350	-65
T hardness (mg/l)	-	-	-	69.0	128.0	306.0	139.0	185.0	108.0	117.0	377.0	20.0
Ca (mg/l)	150	1000	-	15	29	57	31	48	26	21	78	4
Mg (mg/l)	70	500	300	7	13	40	15	16	11	15	44	2
Na (mg/l)	200	2000	70	181	42	39	28	55	60	37	18	2
K (mg/l)	50	-	-	6	3	10	7	-1	3	9	7	1
M _{alk} (mg/l)	-	-	-	324	151	168	150	203	153	44	84	18
Cl (mg/l)	200	1500	100	37	17	57	10	40	24	60	119	-1
SO ₄ (mg/l)	400	1000	200	1	13	96	2	6	12	39	7	0.2
NO ₃ _N (mg/l)	10	100	-	-0.06	1.36	0.26	4.08	0.74	2.98	3.34	26.29	1.43
F (mg/l)	1	2	2	1.474	0.353	0.234	0.301	0.265	0.335	-0.183	-0.183	0.489
Al (mg/l)	0.3	5	5	-0.037	-0.037	-0.037	-0.037	-0.037	-0.037	-0.037	-0.037	-0.037
Fe (mg/l)	0.2	10	5	0.026	0.001	0.001	0.001	-0.001	0.001	0.003	-0.001	1.466
Mn (mg/l)	0.1	10	0.02	0.003	-0.001	-0.001	0.003	-0.001	0.007	-0.001	0.002	0.003
NH ₃ (mg/l)	1	-	-	-0.01	-0.01	0.01	-0.01	-0.01	-0.01	-0.01	-0.01	1.88
PO ₄ (mg/l)	-	-	-	0.04	0.17	0.04	0.05	0.03	0.03	0.03	0.03	0.63
SAR (ratio)	-	-	2	9.50	1.62	0.98	1.03	1.75	2.50	1.49	0.40	0.19

*negative values are indicative of values below the detection limits i.e <0.1 or <0.01

Table 5-1a: Water Quality information for the Rietkuil hydrocensus localities measured against the SANS 241 potable water standards as well as the DWAf TWQGR for large livestock watering and domestic use.

Delta Mining Rietkuil - Hydrocensus : Selected date - 2009/05/15											
Variable	SANS 241 Potable	DWAF Livestock	DWAF Irrigation	Monitoring localities							
				Rietkuil 09	Rietkuil 11	Rietkuil 14	Rietkuil 15	Snyman 01	Snyman 02	Vlakplaats 02	Vlakplaats com
pH ()	5.0 - 9.5	-	6.0 - 9.1	7.51	8.39	8.52	8.50	8.41	8.49	8.76	8.29
EC (mS/m)	150	500	40	5.21	31.03	50.30	48.60	56.80	57.90	69.50	44.00
TDS (mg/l)	1000	2000	260	-65	160	260	245	306	309	379	213
T hardness (mg/l)	-	-	-	7.0	114.0	189.0	177.0	85.0	90.0	33.0	163.0
Ca (mg/l)	150	1000	-	2	25	44	41	17	18	9	31
Mg (mg/l)	70	500	300	1	13	19	18	10	11	3	21
Na (mg/l)	200	2000	70	4	28	40	37	100	102	153	27
K (mg/l)	50	-	-	-1	3	6	6	3	3	3	5
M alk (mg/l)	-	-	-	15	124	157	164	170	167	276	170
Cl (mg/l)	200	1500	100	-1	10	44	35	57	58	35	10
SO4 (mg/l)	400	1000	200	1	4	9	7	16	16	9	13
NO3 (mg/l)	10	100	-	-0.06	2.97	4.53	3.26	0.12	-0.06	0.35	4.20
F (mg/l)	1	2	2	-0.183	-0.183	0.259	0.237	1.179	1.107	1.086	0.225
Al (mg/l)	0.3	5	5	-0.037	-0.037	-0.037	-0.037	-0.037	-0.037	7.039	-0.037
Fe (mg/l)	0.2	10	5	0.001	0.002	0.001	0.001	0.001	0.002	3.385	0.001
Mn (mg/l)	0.1	10	0.02	-0.001	0.005	-0.001	-0.001	-0.001	-0.001	0.011	-0.001
NH3_N (mg/l)	1	-	-	0.02	-0.01	-0.01	-0.01	-0.01	-0.01	-0.01	-0.01
PO4 (mg/l)	-	-	-	0.03	0.03	0.04	0.04	0.06	0.09	0.03	0.04
SAR (ratio)	-	-	2	0.70	1.14	1.25	1.20	4.74	4.66	11.68	0.92

*negative values are indicative of values below the detection limits i.e <0.1 or <0.01

Table 5-1b: Water Quality information for the Rietkuil hydrocensus localities measured against the SANS 241 potable water standards as well as the DWAF TWQGR for large livestock watering and domestic use.

Delta Rietkuil Exploration Boreholes : Selected date - 2009/05/13													
Variable	SANS 241 Potable	DWAF Livestock	DWAF Irrigation	Monitoring localities									
				EX02	EX03	EX05	EX12	EX13	EX17	EX21	EX22	EX23	EX25
pH ()	5.0 - 9.5	-	6.0 - 9.1	6.80	7.09	6.58	8.22	8.26	7.56	7.16	7.59	8.47	8.27
EC (mS/m)	150	500	40	21.38	46.60	27.05	86.70	53.60	38.50	29.83	43.60	46.20	43.90
TDS (mg/l)	1000	2000	260	91	200	99	378	257	199	118	140	243	211
T hardness (mg/l)	-	-	-	26.0	152.0	83.0	199.0	144.0	96.0	85.0	96.0	110.0	169.0
Ca (mg/l)	150	1000	-	6	30	17	43	28	21	17	18	30	42
Mg (mg/l)	70	500	300	3	19	10	22	18	10	10	12	8	15
Na (mg/l)	200	2000	70	35	23	11	93	51	43	19	34	45	24
K (mg/l)	50	-	-	2	5	8	3	4	9	4	8	1	3
M alk (mg/l)	-	-	-	64	34	56	167	170	158	42	16	246	191
Cl (mg/l)	200	1500	100	-1	22	10	116	42	12	8	26	9	2
SO4 (mg/l)	400	1000	200	-0.1	75	2	-0.1	12	2	27	9	-0.1	9
NO3_N (mg/l)	10	100	-	5.80	7.86	7.27	-0.06	0.20	5.04	7.19	23.08	-0.06	1.35
F (mg/l)	1	2	2	-0.183	-0.183	-0.183	0.748	0.211	0.791	-0.183	-0.183	0.840	-0.183
Al (mg/l)	0.3	5	5	0.236	-0.037	-0.037	-0.037	0.037	0.037	0.037	0.037	2.716	-0.037
Fe (mg/l)	0.2	10	5	0.142	0.002	0.023	0.002	0.344	4.165	0.022	0.002	4.646	0.005
Mn (mg/l)	0.1	10	0.02	0.027	0.031	0.347	-0.001	0.033	0.454	0.001	0.001	0.132	0.005
NH3 (mg/l)	1	-	-	0.09	0.05	0.38	0.09	0.10	0.14	0.06	0.05	0.07	0.05
PO4 (mg/l)	-	-	-	-0.03	-0.03	-0.03	-0.03	-0.03	-0.03	0.04	0.14	-0.03	-0.03
SAR (ratio)	-	-	2	2.98	0.80	0.51	2.86	1.84	1.91	0.90	1.49	1.88	0.80

*negative values are indicative of values below the detection limits i.e <0.1 or <0.01

Table 5-2: Water Quality information for the Rietkuil exploration borehole localities measured against the SANS 241 potable water standards as well as the DWAF TWQGR for livestock watering and domestic use.

For comparative purposes, the exploration borehole water qualities are compared with the SANS 241 potable water standards. It should be noted, that none of the exploration localities are presently being used for any domestic, livestock, or irrigation purposes. High nitrate concentrations are recorded for locality EX22, and high metal concentrations (Al and Fe) at locality EX23.

For the selected parameters, maps are included indicating the recorded parameter concentrations at each surveyed locality. In evaluating the data presented on the maps, it must be noted that the size of the circle indicating the concentration or value at a monitoring locality is in relation to the values of the other monitoring localities on the map. A large circle therefore does not necessarily imply water of a poor quality or very high concentration for the specified variable. Compliance to the SANS 241 drinking water guideline is coloured according to compliance (green=compliant/good water quality, yellow=Non-compliant/marginal water quality, red=Non-compliant/poor water quality).

5.1 pH

pH is the logarithmic expression of the hydrogen ion concentration in water which reflects the degree of acidity ($\text{pH} < 7.0$) or alkalinity ($\text{pH} > 7$) of the water. The pH levels of most unpolluted waters are between 6.5 – 8.5. pH levels below 6.5 may be found in areas where acidification processes have occurred, the most dramatic being that of acid mine drainage where pH levels may drop to 3.5. Health effects associated with pH can be direct or indirect. Direct causes include the irritation or burning of the mucous membranes with extreme acidic waters, and indirect causes are consequences of corrosion to cooking appliances and distribution pipes.

Figure 5.1-1 indicated the various recorded pH concentrations for the Rietkuil Project surveyed localities. As indicated by the Figure, all water qualities comply with the SANS241:2006 drinking water standards.

5.2 Salinity (EC)

Salinity (EC) is the measurement of ease with which water conducts electricity, or the sum of dissolved salts (Cl, SO₄, etc) in the water. Distilled water (no salinity) conducts electricity poorly, whilst sea water (high salinity) is a good conductor of electricity. Health effects associated with high salinity (>370 mS/m) values are:

- Disturbance in the salt balance of infants
- Adverse effects on sensitive users such as individuals with high blood pressure and heart diseases
- Adverse effects on individuals with renal/kidney disease

Figure 5.2-1 indicates the spatial variation of the EC concentration across the hydrocensus area. Low salinity concentrations are recorded throughout the hydrocensus area. Salinity concentrations range between 5.2 mS/m to 86 mS/m indicating non-saline water quality conditions.

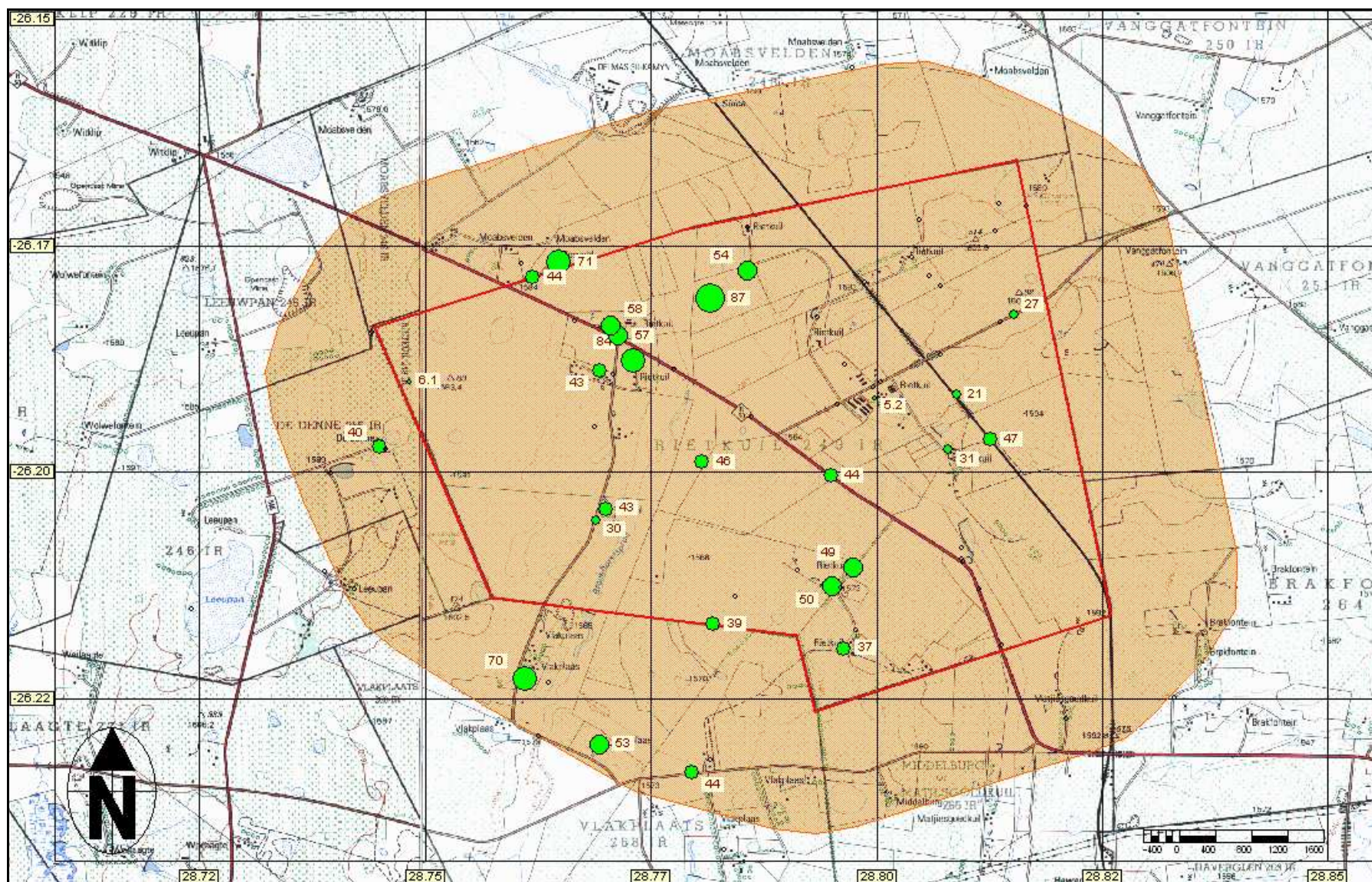


Figure 5.2-1: Recorded EC (Salinity) concentrations for the Rietkuil Mine surveyed localities.

5.3 Sulphate (SO₄)

Sulphate is the oxy-anion of sulphur and forms salts with various cations such as magnesium (Epsom Salt). Consumption of excessive amounts of sulphate, typically results in diarrhoea. However, adaptation to high sulphate tends to occur with prolonged use. Sulphate imparts a bitter or salty taste to water. Corrosion of the distribution system is also likely in cases of high sulphate concentrations.

Figure 5.3-1 indicates the spatial variation of the SO₄ concentration across the hydrocensus area. As with the EC concentrations, very low SO₄ concentrations are recorded for the hydrocensus area.

5.4 Nitrate (NO₃)

In fresh unpolluted water, the NO₃ concentration is often below 2mg/l (as N). Nitrate concentrations are produced by the decay of plant, animal, and human waste, and nitrate pollution is often found wherever intensive land use activities take place. Nitrate concentrations exceeding 20mg/l are common in groundwater where extensive land use takes place. Health effects associated with high NO₃ (>20mg/l) concentrations are impaired concentration, lack of energy, and the formation methaemoglobin in blood cells. Individuals at risk are specifically infants under the age of 1 year.

From Figure 5.4-1 it is evident that except for the NO₃ concentrations recorded at Rietkuil04 (23.08 mg/l) and Ex22 (26.29 mg/l) all other localities comply with the SANS drinking water guidelines. It is advised that caution be taken in using these localities as drinking water sources, especially with regards to infants.

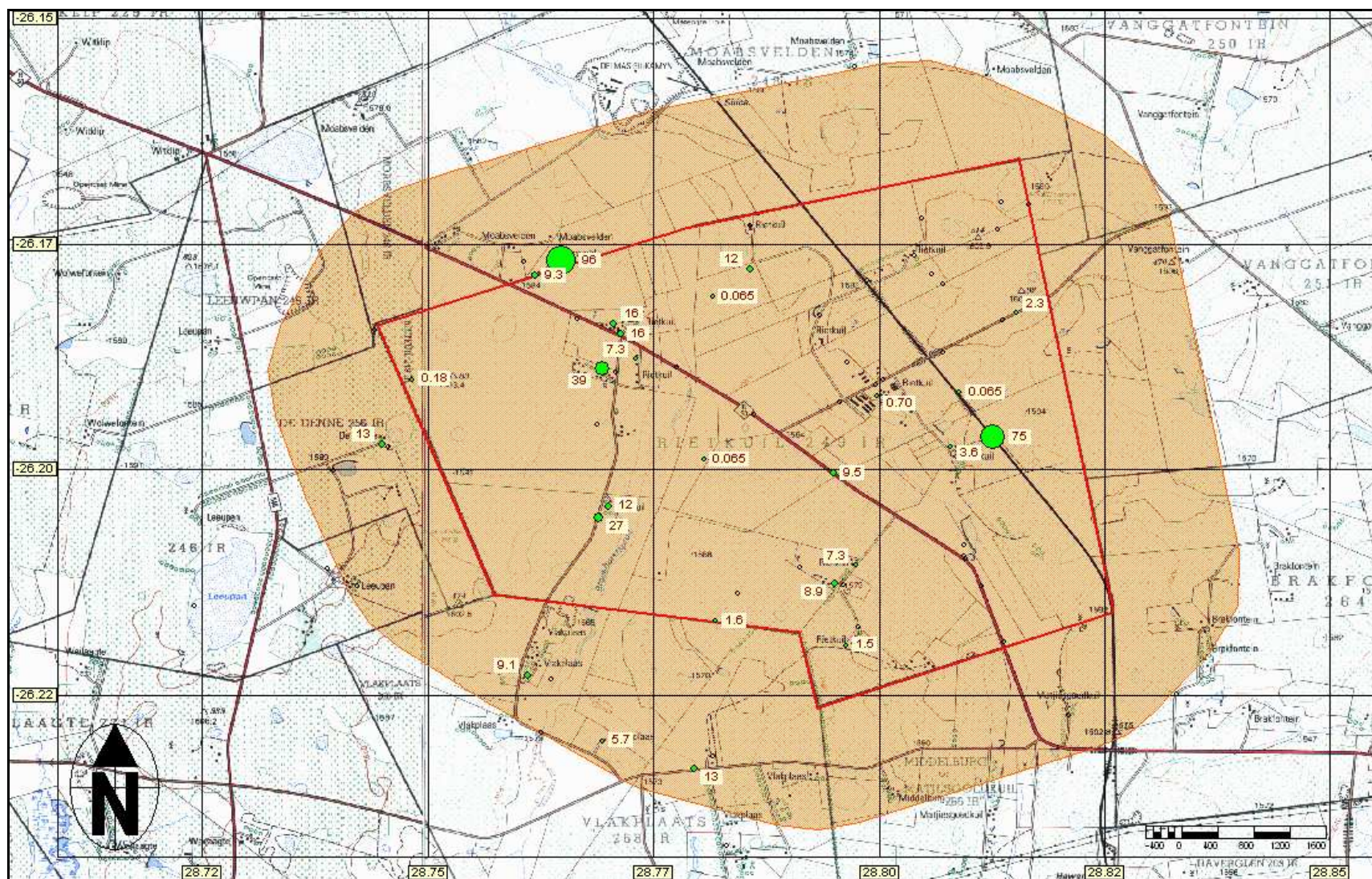


Figure 5.3-1: Recorded SO₄ (sulphate) concentrations for the Rietkuil Mine surveyed localities.

6. RECORDED WATER LEVEL

Recorded water levels for the exploration borehole localities are illustrated in Figure 6.1-1. Table 3-1 indicates the measured water levels, for the exploration localities where access to the water level were possible. All water levels are given as meters below ground (surface) level.

The static groundwater levels varied between 1.31m and 13.45m. As indicated by both Table 6-1 and Figure 6.1-1, lower groundwater levels (<5m) were recorded for most of the hydrocensus area, with the average ground water level at 3.9m. The deeper groundwater levels were recorded EX12 (13.45m) and at RKL01 (9.05m).

Table 6-1: Water Level information gathered from the exploration boreholes on the proposed Rietkuil project.

DELTA MINING COMPANY - WATER LEVELS (APRIL 2009)					
Loc No		South Coordinates	East Coordinates	Elevation	Water level (m)
1	RKL 01	-26.18500	28.74400	-	9.05
2	RKL 02	26.18300	28.76600	-	5.22
3	Ex01	-26.18696	28.80702	1581.0	4.87
4	Ex02	-26.19145	28.80890	1592.0	3.65
5	Ex03	-26.19639	28.81257	1593.0	3.49
6	Ex04	-26.18344	28.81365	1607.0	7.40
7	Ex05	-26.18265	28.81518	1610.0	5.38
8	Ex06	-26.17941	28.80715	1602.0	1.94
9	Ex08	-26.17336	28.81316	1608.0	4.34
10	Ex09	-26.17065	28.81657	1602.0	2.03
11	Ex10	-26.17038	28.81360	1602.0	1.98
12	Ex11	-26.17218	28.80470	1603.0	4.97
13	Ex12	-26.18077	28.78154	1561.0	13.45
14	Ex13	-26.17776	28.78571	1561.0	5.59
15	Ex14	-26.18818	28.79641	1579.0	2.60
16	Ex16	-26.20991	28.80953	1574.0	1.45
17	Ex17	-26.21679	28.78188	1576.0	1.97
18	Ex18	-26.21382	28.78430	1573.0	1.31
19	Ex20	-26.19387	28.78610	1566.0	2.40
20	Ex21	-26.20531	28.76895	1583.0	3.68
21	Ex22	-26.17853	28.76186	1579.0	2.75
22	Ex23	-26.19887	28.78060	1565.0	1.41
23	Ex24	-26.19055	28.79960	1581.0	2.71
24	Ex25	-26.20044	28.79498	1569.0	2.27
25	R211	-26.21297	28.81136	-	1.69
Maximum Water level					13.45
Minimum Water level					1.31
Average water level					3.90

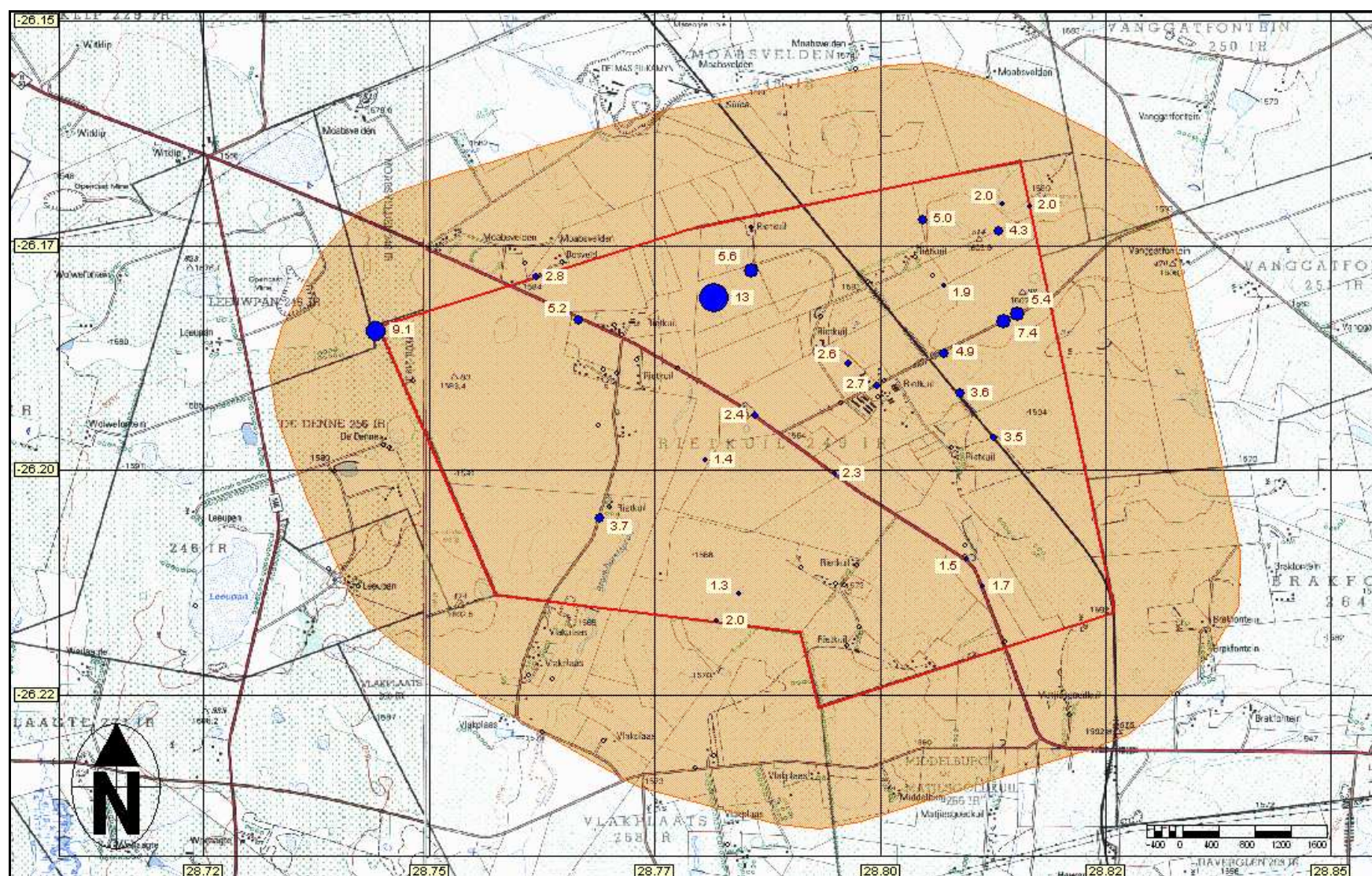


Figure 6.1-1: Recorded water levels for the Rietkuil Mine surveyed localities.

7. CONCLUSION

Clean Stream Scientific Services conducted a hydrocensus in April 2009 on the properties of landowners adjacent to the proposed Rietkuil mining area. The aim of the hydrocensus was to establish baseline water quality and water level data for the area for any future reference.

Contact was made with 13 interested and affected parties. Various borehole localities were logged (40 localities were surveyed), and water levels were taken. Water quality data for 16 localities and water level data for 25 localities were gathered.

The water quality can be summarised as follow:

- Regional pH, EC, and SO₄ concentrations were recorded as compliant with the SANS241 drinking water standards.
- Recorded NO₃ concentrations exceeded the proposed SANS 241 and DWAF domestic guidelines at two localities; Rietkuil04 and EX22.
- The general water quality of the area can be described as good for domestic, irrigation and livestock watering purposes.

Groundwater levels can be summarised as follow:

- Static groundwater level depths vary between 1.31 and 13.45 meters below surface over the entire area.
- Average water level was recorded at 3.9 meters below surface.

8. REFERENCES

Department of Water Affairs and Forestry (DWAF). Act N. 36 of 1998: National Water Act, 1998

Department of Minerals and Energy (DME). Act N 28 of 2002: Minerals and Petroleum Resources Development Act, 2002

The South African Bureau of Standards (SABS), ISO 5667-1 to 5667-15, First Edition, 1999

Department of Water Affairs and Forestry (DWAF). 2006: Best Practice Guideline N. G3. Water Monitoring Systems.

Department of Water Affairs and Forestry (DWAF). Targeted Water Quality Guidelines: Domestic Use (Volume 01), Livestock Watering (Volume 05), Irrigation (Volume 04). 1998.

14. Summary

Acid mine drainage is by far the most significant long term groundwater quality impact associated with both opencast and underground coal mining, in both a local and international context. The modern day geohydrologist has access to numerous tools, which can be used to determine important decant issues – issues ranging from **when** decanting will begin to occur, and the **volumes** of water that are expected to decant.

The continuous development and improvement of numerical groundwater flow models is steadily leading to an increasing dependence on them. The main aim of the thesis was to determine whether there exists any correlation between modern day numerical groundwater flow models and analytical calculations, and the presentation of a toolbox of tools that may be used for decant related issues. The following conclusions were drawn after numerous numerical and analytical scenarios and statistical correlations were performed:

- Given the amount of uncertainty regarding aquifer heterogeneity, there do exist a good correlation between the numerical and analytical groundwater decant volume estimations,
- An increase in the effective porosity of the backfilled opencast pits cause an increase in the time-to-decant, as more water is required to fill the pits to their decant elevations,
- An increase in the effective aquifer recharge cause an increase in the decant volumes and a decrease in the time-to-decant, because more water is available to fill the pits to their decant elevations,
- The effective aquifer recharge is a very sensitive parameter (more so than specific yield, storage coefficient, and transmissivity), as significant decreases in the time-to-decant were simulated with an increase in the aquifer recharge, as were significant increases in decant volumes simulated with an increase in recharge,
- The volumes of groundwater decant are more sensitive to variations in the transmissivity of the surrounding aquifer/s compared to the transmissivity of the backfilled opencast pits,

- During the numerous flow model scenarios it was found that the groundwater contribution to pit water is far less compared to the recharge component.

The above conclusions prove that there are still applications for analytical calculations in modern day geohydrology, despite the continuous development of numerical groundwater flow models.

Based on experience in similar coal mining operations within the Mpumalanga coal fields, the results of both the analytical decant volume and time-to-decant estimations correspond well with actual figures. One must however understand and master the various equations and keep in mind that an aquifer is a highly heterogeneous system. The results of both numerical groundwater flow model simulations and analytical calculations are only as good as the understanding of the geohydrological environment and the data they are based on.

15. Opsomming

Die dreinerings van suur myn water is by verre die belangrikste lang termyn grondwater kwaliteit impak wat geassosieer word met beide oopgroef en ondergrond steenkool myne – beide op nasionale en internasionale vlakke. Die moderne geohidroloog het toegang tot verskeie metodes om menige grondwater oorloop probleme op te los. Die belangrikste probleme sluit in die verwagte volumes van grondwater oorloop, asook die tyd wat dit gaan neem vir die myn om oor te loop.

Die aanhoudende ontwikkeling en verbetering van numeriese grondwater modelle is geleidelik besig om te lei tot 'n totale afhanklikheid van numeriese modelle. Die hoof doel van die tesis is om te bepaal of daar enige korrelasie is tussen numeriese en analitiese metodes, asook die akwifere toestande waarin die metodes gebruik kan word. Die resultate van 'n aantal numeriese en analitiese modelle het gelei tot die volgende gevolgtrekkings:

- Tensypte van die hoogs heterogene natuur van 'n akwifere sisteem, bestaan daar wel 'n goeie korrelasie tussen numeriese en analitiese oorloop-volume berekeninge,
- 'n Toename in die porositeit van die gerehabiliteerde oopgroewe lei tot 'n toename in die tyd wat dit neem vir die groewe om oor te loop, aangesien meer water nou benodig word om die groewe te vul,
- 'n Toename in akwifere aanvulling lei tot 'n toename in oorloop volumes asook 'n afname in die tyd wat dit neem vir die groewe om oor te loop, aangesien meer water beskikbaar is om die groewe te vul,
- Akwifere aanvulling is die sensitiefste parameter, aangesien 'n beduidende afname in oorloop tyd gesimuleer was tydens 'n toename in aanvulling, terwyl 'n beduidende toename in oorloop volumes ook gesimuleer was tydens 'n toename in aanvulling,
- Oorloop volumes word eerder deur die transmissiviteit van die omliggende akwifere beïnvloed as deur die transmissiviteit van die groewe self,
- Die numeriese model simulasies het getoon dat die grondwater bydrae tot groef water veel minder is as die akwifere aanvulling komponent.

Die bogenoemde gevolgtrekkings bewys dat analitiese metodes steeds gebruik kan word om akkurate resultate te lewer, tenspyte van die aanhoudende verbetering en ontwikkeling van numeriese modelle.

Gebasseer op ondervinding in soortgelyke steenkool myne in die Mpumalanga steenkool velde, die resultate van die analitiese oorloop volumes en tyd van oorloop berekeninge korreleer met bevestigde waardes. `n Persoon moet egter die vergelykings en berekeninge verstaan en baas raak, en in ag neem dat die akwifere sisteem hoogs heterogeen is. Die resultate van die analitiese berekeninge is dus net so goed as wat `n persoon se begrip van die akwifere sisteem is en die data waarop dit gebaseer is.